

This electronic thesis or dissertation has been downloaded from the King's Research Portal at <https://kclpure.kcl.ac.uk/portal/>



Computational Magnetic Resonance Image Analysis of Brain Development in the Preterm Infant

Ball, Gareth

Awarding institution:
Imperial College London

The copyright of this thesis rests with the author and no quotation from it or information derived from it may be published without proper acknowledgement.

END USER LICENCE AGREEMENT



Unless another licence is stated on the immediately following page this work is licensed

under a Creative Commons Attribution-NonCommercial-NoDerivatives 4.0 International

licence. <https://creativecommons.org/licenses/by-nc-nd/4.0/>

You are free to copy, distribute and transmit the work

Under the following conditions:

- Attribution: You must attribute the work in the manner specified by the author (but not in any way that suggests that they endorse you or your use of the work).
- Non Commercial: You may not use this work for commercial purposes.
- No Derivative Works - You may not alter, transform, or build upon this work.

Any of these conditions can be waived if you receive permission from the author. Your fair dealings and other rights are in no way affected by the above.

Take down policy

If you believe that this document breaches copyright please contact librarypure@kcl.ac.uk providing details, and we will remove access to the work immediately and investigate your claim.

September 2011
Imperial College London
MRC Clinical Sciences Centre

Computational Magnetic Resonance Image Analysis of Brain Development in the Preterm Infant

Gareth Ball

A dissertation submitted in partial fulfilment of the requirements for the degree of
Doctor of Philosophy
from
Imperial College London

Abstract

Currently 7-8% of all babies born in the UK are born preterm and the incidence has increased significantly over the past two decades. Improving medical care has led to increased survival in those born prematurely; however, preterm infants carry a profound risk of severe neurological disabilities along with a spectrum of major deficits across several domains including cognition, attention, coordination and behaviour. These wide-ranging and long-term consequences represent a significant burden to health and education services, yet the aetiology of the most prevalent cognitive and behavioural disorders remain unclear.

Magnetic resonance imaging provides the means to quantitatively assess cerebral growth and development and is being increasingly employed to study the developing preterm brain. Evidence from neonatal imaging studies has revealed a number of specific cerebral alterations present in the preterm population that appear to predict neurodevelopmental outcome in early childhood and include diffuse microstructural disturbances of the developing white matter and regional volumetric tissue losses. In addition, a number of perinatal risk factors have been identified that are associated with both preterm birth and altered cerebral development.

This thesis aims to test the hypothesis that connectivity and growth of developing neural systems are adversely affected by prematurity at birth and additionally influenced by specific perinatal risk factors. This is achieved through the application of multi-subject, multi-modal MRI analysis to quantify tissue microstructure and volume alongside novel methods for defining regional connectivity in the developing preterm brain.

Evidence is provided that suggests connected neural structures are disturbed in preterm infants resulting in a complex pattern of regional micro- and macrostructural alteration that is evident at term-equivalent age and potentiated by respiratory morbidity. This is convergent with current theories of the mechanisms underpinning preterm brain injury and provides further insight into the consequences of preterm birth on brain development.

Declaration

This thesis and the work presented herein are my own and were conducted at Imperial College London between October 2008 and September 2011, all sources are appropriately referenced.

This work has not been submitted for the purpose of obtaining any other degree at this University or any other institution.

Gareth Ball

Acknowledgements

I would like to thank my supervisors: James Boardman, Serena Counsell, Daniel Rueckert and David Edwards for their encouragement, insight and enthusiasm and for the time they have taken to provide discussion, feedback and support, it has been very much appreciated. I am particularly grateful for the opportunity and freedom I have been offered to follow a number of pathways (or cul-de-sacs, as has often been the case) during the course of this PhD; this has been a key factor in making the past three years so enjoyable. I would also like to thank Paul Aljabar, Mary Rutherford, Jo Hajnal, Rolf Heckemann, Ioannis Gousias and Ahmed Serag for their contributions and advice.

Thanks are also due to many, many people who have shared the office, and their computers, with me, to everyone at the ISD and to Lauren for her patience, support and packed lunches.

Contents

Abstract	3
Declaration	4
Acknowledgements	5
List of Figures	8
List of Abbreviations	10
Publications	12
1 Introduction	
1.1 Background and Motivation	15
1.2 Hypothesis and Aims	16
1.3 Thesis Outline	16
2 Magnetic Resonance and Diffusion Imaging	
2.1 Magnetic Resonance Imaging	19
2.2 Diffusion MRI	23
2.3 Image Registration	28
2.4 Structural MR Analysis	35
2.5 Diffusion MR Analysis	37
3 The Developing Brain and Preterm Birth	
3.1 Human Brain Development	41
3.2 Epidemiology of Preterm Birth	43
3.3 Neurodevelopmental Outcome Following Preterm Birth	43
3.4 Preterm Brain Injury	46
3.5 Quantitative Imaging of the Preterm Brain	49
4 Tract-Based Spatial Statistics in Preterm Neonates: Optimisation and Application	
4.1 Introduction	54

4.2	Materials and Methods	55
4.3	Results: Optimisation	58
4.4	Results: Investigating Respiratory Morbidity in Preterm Infants	63
4.5	Discussion	67
5	Thalamic and Cortical Development Following Preterm Birth	
5.1	Introduction	70
5.2	Materials and Methods	71
5.3	Results: Regional Brain Volume and Prematurity at Birth	76
5.4	Results: Thalamo-Cortical Development after Preterm Birth	78
5.5	Discussion	84
6	Tractography in Preterm Neonates: Exploring Connectivity	
6.1	Introduction	87
6.2	Material and Methods	90
6.3	Results: Comparison to Term-Born Controls	95
6.4	Results: Effect of Prematurity on Connectivity	98
6.5	Discussion	99
7	Summary	
7.1	Conclusions	104
7.2	Future Work	105
7.3	Summary	107
	References	106
	Appendices	
	Appendix A: MR Pulse Sequences	145
	Appendix B: Deformation-Based Morphometry: Analyses	147
	Appendix C: An Optimised Tract-Based Spatial Statistics Protocol for Neonates: Applications to Prematurity and Chronic Lung Disease	149
	Appendix D: The Effect of Preterm Birth on Thalamic and Cortical Development	159
	Appendix E: Automatic Segmentation and Parcellation of Subcortical White and Grey Matter using DTI in the Preterm Neonate	169

List of Figures

Figure 2.1: Spin precession in a magnetic field.	20
Figure 2.2: RF-excitation of precessing spins.	20
Figure 2.3: Isotropic and anisotropic diffusion in the brain.	24
Figure 2.4: Crossing fibres and the diffusion tensor.	28
Figure 2.5: Image registration between a source and target image.	29
Figure 2.6: A nonlinear transform can be modelled using a smooth approximation of deformations of regularly spaced control points.	30
Figure 2.7: Volume change induced by transformations.	37
Figure 2.8: Generating the FA skeleton in TBSS.	38
Figure 2.9: Comparison of deterministic and probabilistic tractography.	40
Figure 3.1: Laminar structure of the developing neocortex.	42
Figure 3.2: White matter injury in the preterm neonate.	47
Figure 3.3: Increasing cortical complexity with age.	50
Figure 4.1: Mean displacements after all-to-all registration of FA maps.	59
Figure 4.2: Example registrations between source and target FA maps using the original and modified registration protocols.	60
Figure 4.3: Volume difference between transformed images and intended target images following linear registration.	61
Figure 4.4: Standard deviation of FA after registration to an individual or population-average FA map.	62
Figure 4.5: Higher projected FA across the mean skeleton following registration to a mean FA map.	62
Figure 4.6: Revised processing pipeline for use in TBSS analysis of neonatal diffusion datasets.	63
Figure 4.7: Associations between white matter microstructure, age at scan and gestational age at birth.	64
Figure 4.8: Chronic lung disease is associated with increased RD and decreased FA.	65
Figure 4.9: Increased length of neonatal respiratory support is associated with altered white matter microstructure.	66
Figure 5.1: Final reference template and thalamic and cortical segmentations.	73
Figure 5.2: Decreasing regularisation of warp smoothness.	75
Figure 5.3: Deformation-based morphometry processing pipeline.	75
Figure 5. 4: Cortical grey matter volume is correlated with prematurity at birth and thalamic volume at term-equivalent age.	77
Figure 5.5: Regional associations between brain tissue volume and prematurity at birth.	78
Figure 5.6: Regional associations between brain tissue volume and thalamic volume at term- equivalent age.	79

Figure 5.7: Thalamic volume is associated with white matter microstructure.	80
Figure 5.8: Cortical volume is associated with white matter microstructure.	81
Figure 5.9: Significant associations between FA and tissue volume remain when correcting for chronic lung disease status.	82
Figure 5.10: Differential associations between tissue volume and FA in the internal capsule and corpus callosum.	83
Figure 5.11: Thalamic diffusivity is associated with thalamic volume and FA in the internal capsule.	83
Figure 6.1: Connectivity-based thalamic segmentation in preterm neonates.	88
Figure 6.2: Cortical parcellation using Poisson disk sampling.	93
Figure 6.3: Connectivity estimates after repeated parcellations.	94
Figure 6.4: Processing pipeline used for assessing thalamo-cortical connectivity in neonates.	95
Figure 6.5: Thalamo-cortical anisotropy is significantly lower in preterm infants.	96
Figure 6.6: Mean anisotropy extracted from four regions-of-interest.	97
Figure 6.7: Spatial extent of specific thalamo-cortical tracts that appear significantly affected in preterm infants.	98
Figure 6.8: Association between thalamo-cortical connectivity and prematurity at birth.	99
Figure A.1: Gradient-echo pulse sequence.	145
Figure A.2: Spin-echo pulse sequence.	146
Figure A.3: Pulsed gradient spin-echo sequence.	146
Figure B.1: DBM analysis is robust to target choice.	147
Figure B.2: Performing further iterations of nonlinear registration when constructing the final DBM template does not significantly alter the resulting statistical associations.	148

List of Abbreviations

AD	Axial diffusivity
ADC	Apparent diffusion coefficient
BET	Brain extraction tool
BSID-II/III	Bayley scales of infant development II/III
CC	Cross correlation
CLD	Chronic lung disease
CP	Cerebral palsy
cPAP	Continuous positive airway pressure
CSF	Cerebro-spinal fluid
DBM	Deformation-based morphometry
DEHSI	Diffuse excessive high signal intensity
DOF	Degrees-of-freedom
DQ	Development quotient
DTI	Diffusion tensor imaging
EPI	Echo-planar imaging
FA	Fractional anisotropy
FAST	FMRIB's automated segmentation tool
FDT	FMRIB's diffusion toolbox
FDR	False discovery rate
FFD	Free-form deformation
FLIRT	FMRIB's linear image registration tool
FMRIB	Functional magnetic resonance imaging of the brain analysis group
FNIRT	FMRIB's nonlinear image registration tool
FSL	FMRIB's software library
FWE	Familywise error
FWHM	Full-width-at-half-maximum
GA	Gestational age
GLH	Germinal layer haemorrhage
HPI	Haemorrhagic parenchymal infarction
ILF	Inferior longitudinal fasciculus
IRTK	Image registration toolkit
IQ	Intelligence quotient
IUGR	Intrauterine growth restriction
IVH	Intraventricular haemorrhage
K-ABC	Kaufman assessment battery for children

MD	Mean diffusivity
MI	Mutual information
MR	Magnetic resonance
MRI	Magnetic resonance imaging
NMI	Normalised mutual information
NMR	Nuclear magnetic resonance
ODF	Orientation distribution function
PFC	Prefrontal cortex
PLIC	Posterior limb of the internal capsule
PMA	Postmenstrual age
PPROM	Preterm premature rupture of membranes
PVL	Periventricular leucomalacia
QCCH	Queen Charlotte's and Chelsea Hospital
RA	Relative anisotropy
RD	Radial diffusivity
RF	Radio-frequency
ROI	Region-of-interest
ROP	Retinopathy of prematurity
SENSE	Sensitivity encoding
SMA	Supplementary motor area
SPSS	Statistical package for the social sciences
SSD	Sum of squared differences
SVZ	Subventricular zone
TBM	Tensor-based morphometry
TBSS	Tract-based spatial statistics
TE	Echo time
TFCE	Threshold-free cluster enhancement
TR	Repetition time
VBM	Voxel-based morphometry
VZ	Ventricular zone

Publications

Journal Papers

Ball G, Boardman JP, Rueckert D, Aljabar P, Arichi T, Merchant N, Gousias IS, Edwards AD, Counsell SJ. 2011. The effect of preterm birth on thalamic and cortical development. *Cereb Cortex* doi: 10.1093/cercor/bhr176

van Kooij BJM, Counsell SJ, **Ball G**, van Haastert IC, Benders M, de Vries LS, Groenendaal F. 2011. Neonatal tract-based spatial statistics findings and outcome in preterm infants. *Am J Neuroradiol* doi: 10.3174/ajnr.A2723

Bassi L, Chew A, Merchant N, **Ball G**, Ramenghi L, Boardman J, Allsop JM, Doria V, Arichi T, Mosca F, Edwards AD, Cowan FM, Rutherford MA, Counsell SJ. 2011. Diffusion tensor imaging in preterm infants with punctuate white matter lesions. *Pediatr Res* 69:561-566

Ball G, Counsell SJ, Anjari M, Merchant N, Arichi T, Doria V, Rutherford MA, Edwards AD, Rueckert D, Boardman JP. 2010. An optimised tract-based spatial statistics protocol for neonates: applications to prematurity and chronic lung disease. *Neuroimage* 53:93-102

Book Chapters

Ball G, Rutherford MA, Counsell SJ. Imaging the preterm brain. To appear in: Shevell M, Miller SP (Ed.). *Acquired Brain Injury in the Fetus and Newborn*. Mac Keith Press: London, UK.

Conference Abstracts

Ball G, Boardman JP, Rueckert D, Aljabar P, Arichi T, Merchant N, Gousias IS, Edwards AD, Counsell SJ. 2011. Diminished local brain growth and impaired microstructural development following preterm birth.

In *Pediatric Academic Societies and International Society for Magnetic Resonance in Medicine*

Ball G, Counsell SJ, Gousias IS, Aljabar P, Hajnal JV, Rueckert D, Edwards AD, Boardman JP. 2011. Automatic segmentation of subcortical white and grey matter using DTI in the preterm neonate.

In *Pediatric Academic Societies and International Society for Magnetic Resonance in Medicine*

- Rollins NK, Seo Y, Chalak L, Chia JM, **Ball G**, Wang ZJ. 2011. Comparison of DTI Metrics in Neonates Obtained with Manual ROI Analysis vs Modified TBSS
In *International Society for Magnetic Resonance in Medicine*
- Serag A, Aljabar P, **Ball G**, Counsell SJ, Boardman JP, Rueckert D, Hajnal JV. 2011. Longitudinal analysis of tissue property changes in multi-modal MRI of the developing preterm brain
In *International Society for Magnetic Resonance in Medicine*
- Roze E, Harris PA, **Ball G**, Braga R, Allsop JM, Merchant N, Porter E, Arichi T, Edwards AD, Rutherford MA, Cowan FM, Counsell SJ. 2011. Diffusion tractography of the corticospinal tracts in neonates with focal perinatal injury: Comparison with normal control infants and to motor development.
In *Pediatric Academic Societies*
- Serag A, Counsell SJ, Aljabar P, **Ball G**, Hajnal JV, Edwards AD, Rueckert D, Boardman JP. 2011. Spatio-temporal maps of T1 and T2 weighted signal intensity change in the developing brain.
In *Pediatric Academic Societies*
- Ball G**, Boardman JP, Rueckert D, Merchant N, Arichi T, Edwards AD, Counsell SJ. 2010. Population-mapped probabilistic tractography – a new tool for studying white matter architecture in neonates.
In *Pediatric Academic Societies*
- Bassi L, Chew A, Merchant M, **Ball G**, Ramenghi L, Boardman JP, Allsop JM, Doria V, Arichi T, Edwards AD, Cowan FM, Rutherford MA, Counsell SJ. 2010. Diffusion tensor imaging in preterm infants with punctate white matter lesions.
In *Pediatric Academic Societies*
- Counsell SJ, Chew A, Merchant N, **Ball G**, Allsop JM, Hughes-Carre L, Boardman JP, Rutherford MA, Cowan FM, Edwards AD. 2010. Perinatal clinical correlates of impaired white matter development in children who were born preterm.
In *Pediatric Academic Societies*
- van Kooij B, Counsell SJ, **Ball G**, Benders M, de Vries L, Groenendaal F. 2010. White matter microstructure in prematurely born neonates at term equivalent age is related to neurodevelopmental outcome at 15 months corrected age.
In *Pediatric Academic Societies*
- Serag A, Aljabar P, **Ball G**, Counsell SJ, Boardman JP, Hajnal JV, Rueckert D. 2010. Developmental signal intensity changes in subcortical structures of the perinatal brain detected using multi-modal MRI.
In *MICCAI: Workshop on spatio-temporal image analysis*
- Ball G**, Boardman JP, Anjari M, Merchant N, Edwards AD, Rueckert D, Counsell SJ. 2009. The effect of chronic lung disease on white matter anisotropy in preterm infants.
In *European Society for Paediatric Research*
Young Investigator Prize Nominee

Chapter 1

Introduction

1.1 Background and Motivation

Over the past two decades, the incidence of preterm birth has steadily risen (Beck et al. 2010). Currently 7-8% of all babies in the UK are born before 37 weeks of completed gestation and, with advancing medical care, survival rates in the most premature are improving (Horbar et al. 2002, Slattery and Morrison 2002, Wilson-Costello et al. 2007). However, the adverse consequences of preterm birth can be long-term and wide-reaching, encompassing a range of neurosensory and cognitive deficits that become evident during early infancy and can persist into adolescence and adulthood (Wood et al. 2000, Bhutta et al. 2002, Marlow et al. 2005, Hille et al. 2007). Although the incidence of severe neurological disorders, such as cerebral palsy, associated with preterm birth has decreased (Vohr et al. 2005, van Haastert et al. 2011), a concomitant increase in subtle impairments across several domains including language, learning, attention, memory, coordination and behaviour has been observed (Marlow et al. 2005, Delobel-Ayoub et al. 2009). These impairments are often complex and overlapping, imparting a significant morbidity on the preterm population.

The neural substrates that underlie these deficits are not known. A clear association has been identified between destructive cerebral tissue lesions and severe neurological outcomes (Rogers et al. 1994; de Vries et al. 1998, Sherlock et al. 2005) but, in line with improved survival, the incidence of such injuries has decreased significantly in recent years (Larroque et al. 2003). In contrast, the advent of magnetic resonance imaging (MRI) and its application in neonatal cohorts has revealed subtle alterations in the developing cerebral white matter that appears to affect up to 75% of all preterm infants (Maalouf et al. 1999, Dyet et al. 2006, Skiold et al. 2010). Advanced MRI techniques have since identified a number of structural and microstructural alterations in the preterm brain that appear to be associated with short term measures of neurodevelopmental outcome (Inder et al. 2005, Krishnan et al. 2007, Boardman et al. 2010). In addition, a number of perinatal risk factors that are associated with preterm birth and with altered cerebral development have been identified (Thompson et al. 2007). Of these, respiratory morbidity appears not to have declined significantly over the past decade (Groenendaal et al. 2010) and is itself independently associated with cerebral injury and poor outcome (Short et al. 2003, Inder et al. 2005, Anjari et al. 2007).

Current evidence suggests that preterm brain injury comprises a spectrum of white and grey matter abnormalities that includes system-wide disruption of connected neural structures occurring during a

critical window of development after preterm birth (Volpe 2009). Advanced imaging techniques, and the application of computational analysis tools, provide the means to test these hypotheses and quantitatively assess the growth and development of neural systems in the developing brain across a large cohort of preterm infants, while accounting for confounding factors such as chronic lung disease (CLD). Ultimately they have the potential to provide biomarkers for future outcome and prospective therapeutic strategies (Ment et al. 2009).

1.2 Hypothesis and Aims

This thesis aims to test the following hypotheses:

Connectivity and growth of developing neural systems are adversely affected by prematurity at birth.

Abnormal white matter connectivity and/or regional brain growth are associated with specific perinatal clinical risk factors.

This is conducted with the following aims:

1. Optimise and apply multi-subject diffusion tensor imaging (DTI) analysis and non-rigid registration of T_1 -weighted images in a large cohort of preterm infants at term-equivalent age to identify regions of abnormal microstructural and macrostructural growth and development associated with prematurity at birth and perinatal risk factors, specifically chronic lung disease.
2. Explore using a novel, probabilistic tractography algorithm, combined with tissue classification and segmentation techniques based on non-rigid registration, patterns of connectivity between specific structures that appear especially vulnerable following preterm birth.

1.3 Thesis Outline

The rest of the thesis is summarised below:

Chapter 2 reviews MRI and diffusion weighted imaging, before discussing the principal methods underlying quantitative, computational MRI analysis including image registration, morphometry and tractography.

Chapter 3 describes the incidence, epidemiology and neurodevelopmental outcome of preterm birth. The most common forms of preterm brain injury are described and an overview of quantitative imaging of the preterm brain is given. Computer-assisted processing tools are being increasingly utilised in neonatal MR analysis; the contribution of these techniques to current knowledge of preterm brain development and injury is discussed.

Chapter 4 describes the optimisation and application of the multi-subject DTI analysis tool Tract-Based Spatial Statistics (TBSS) to a cohort of preterm infants at term-equivalent age. Diffusion imaging in preterm neonates has revealed a number of microstructural alterations in the developing cerebral white matter but often depends on manual selection of regions-of-interest (ROI). TBSS provides the means to analyse DTI data in a whole-brain, automatic and exploratory manner, but has been developed and optimised for adult analyses. This Chapter describes key modifications to the standard TBSS processing pipeline that improve reliability and precision in neonatal DTI analysis. This method is applied to demonstrate that alongside prematurity at birth, respiratory morbidity due to chronic lung disease is associated with widespread microstructural alterations.

Chapter 5 combines high-dimensional image registration of structural T_1 -weighted MR images, and the optimised DTI protocol described in Chapter 4 to investigate the relationship between regional tissue volume and the microstructural integrity of connective neural pathways. The thalamus has been previously shown to be particularly vulnerable following preterm birth. Here, it is shown to be a central part of a wider pattern of altered cerebral development in the preterm brain that encompasses volume reductions in several cerebral structures and is dependent on prematurity at birth. Furthermore, an association between abnormal thalamic development and white matter microstructure suggests an underlying disturbance of thalamo-cortical connectivity.

Chapter 6 describes a novel method for determining thalamo-cortical connectivity in the neonate. Thalamo-cortical connections are established during the third trimester and the disruption of key developmental processes by preterm birth may result in maldevelopment of, or injury to, the thalamo-cortical system as a whole. There is currently no way to reliably quantify connectivity between remote regions in neonatal cohorts. By combining probabilistic tractography, image registration, tissue segmentation and parcellation, connectivity between the thalamus and every cortical voxel is mapped in a cohort of preterm infants. It is shown that thalamo-cortical connectivity is significantly lessened in preterm infants, when compared to term-born controls. In particular, connectivity to fronto-temporal regions appears to be affected, reflecting a possible neural substrate for the poor neurodevelopmental outcome commonly seen in this population.

Chapter 7 provides a summary of the work presented in this thesis and examines potential pathways for future study.

Chapter 2

Magnetic Resonance and Diffusion Imaging

2.1 Magnetic Resonance Imaging

Nuclear magnetic resonance

First identified over 70 years ago, nuclear magnetic resonance (NMR) describes a phenomenon based on the quantum mechanical spin properties of atomic nuclei within a magnetic field (Rabi et al. 1938, Bloch et al. 1946, Purcell et al. 1946). Nuclei with non-zero spin possess an angular momentum that induces a magnetic moment along the axis of their rotation. For the purposes of imaging organic structures, this property is most notable in the hydrogen protons (^1H) that exist abundantly in water. In general, the orientation of each moment is random but when an external magnetic field (B_0) is applied, the moments align with it in one of two states: parallel (low energy) or anti-parallel (high energy). At room temperature spins will preferentially align in the low energy state, resulting in a net magnetisation parallel to the applied field (Figure 2.1). In addition, the external magnetic field exerts a torque on the individual magnetic moments that induces a rotation about the axis of B_0 , termed *precession*. The spins precess about the external field with an angular frequency given by Equation 2.1:

$$\omega = \gamma B_0 \quad [2.1]$$

where ω is the Larmor, or resonant, frequency and γ is the gyromagnetic ratio – a constant for specific nuclei in a magnetic field ($\gamma = 42.57 \text{ MHz/T}$ for ^1H).

Applying a second external magnetic field (B_1), at 90° to B_0 and oscillating at the (^1H -specific) resonant frequency, simultaneously excites hydrogen protons into the higher energy state – reducing longitudinal (parallel to B_0) magnetisation – and induces phase coherence in the precessing spins – increasing transverse (parallel to B_1) magnetisation. The sum vector of net magnetisation can be represented in a rotating frame of reference as moving towards the transverse plane (Figure 2.2); the degree to which net magnetisation rotates is termed the *flip angle*. As the magnetisation vector rotates in the transverse plane it induces a current in a receiver coil placed perpendicular to B_0 , which is recorded as an oscillating MR signal.

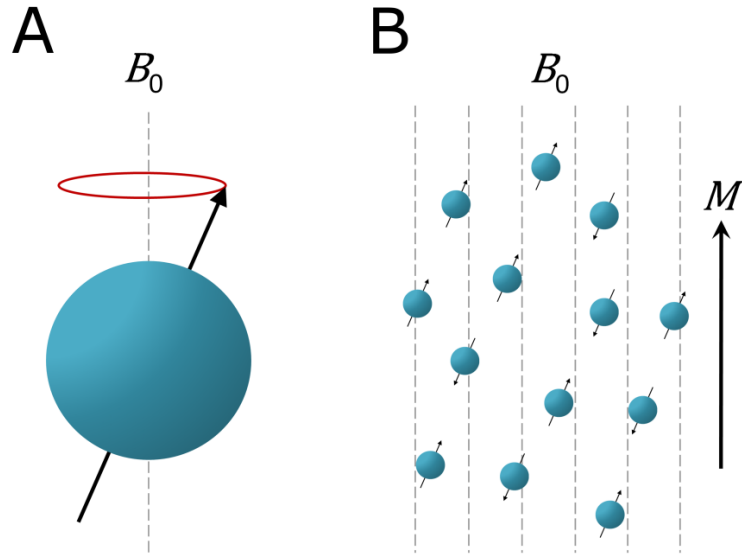


Figure 2.1: Spin precession in a magnetic field. Hydrogen protons possess spin, a quantum property that induces a molecular moment (A; black arrow) along the axis of rotation. When an external magnetic field is applied, spins precess about the field with frequency ω (A) and align parallel to it (B), producing a net magnetisation vector M .

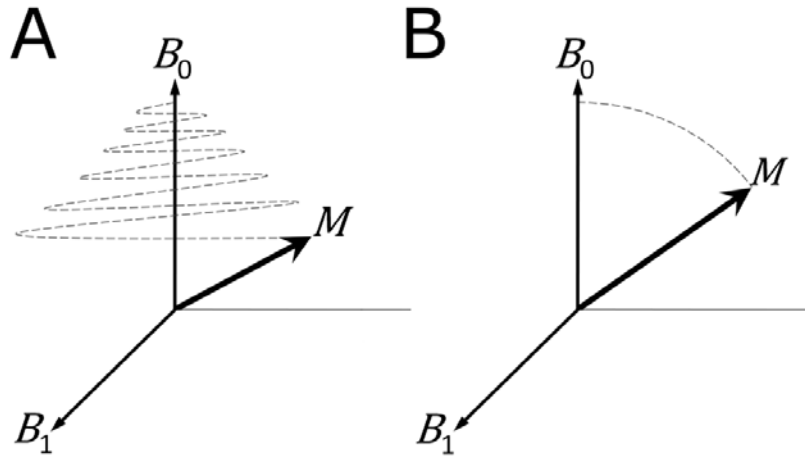


Figure 2.2: RF-excitation of precessing spins. The application of an RF-excitation field B_1 causes the net magnetisation vector to spiral towards the transverse plane at the angular frequency ω (A). In a rotating frame of reference (B) this can be represented as a rotation of the vector towards the xy -plane.

Cessation of the transverse radio-frequency (RF) pulse causes the spins to gradually revert to their original state. This reversion is characterised by two relaxation times, both of which can be modelled as exponential curves: T_1 , or spin-lattice relaxation (Equation 2.2), is the time taken for longitudinal magnetisation to recover to equilibrium as spins return to a low energy state; and T_2 , or spin-spin relaxation (Equation 2.3), which is the time taken for the received MR signal to decay due to a loss of coherence in the precessing spins and a decrease in transverse magnetisation.

$$M_z = M_{z0}(1 - e^{-t/T_1}) \quad [2.2]$$

$$M_{xy} = M_{xy0}e^{-t/T_2} \quad [2.3]$$

where M_z and M_{xy} represent the magnitude of longitudinal and transverse magnetisation before (M_{z0} and M_{xy0}) and after the RF pulse. In practice, signal decay due to dephasing (or free-induction decay) occurs faster than is suggested by T_2 due to local variations (inhomogeneity) of B_0 – this time is referred to as T_2^* .

Importantly, T_1 and T_2 are not constant and differ according to the medium in which they are measured. This provides the contrast mechanism necessary to image the soft tissues of the brain.

Magnetic resonance imaging

NMR provides the substrate for MRI but in order to construct an image it is necessary to spatially resolve the observed NMR signal. This can be achieved with the application of spatially-varying magnetic gradients (Lauterbur 1973). An additional magnetic gradient (G) applied over an axis (x) exerts a position-dependent shift in the precessional frequency (ω) of spins in the magnetic field, as shown in Equation 2.4:

$$\omega_x = \gamma(B_0 + G_x) \quad [2.4]$$

The resultant MR signal is a mixture of precessional frequencies that relate to the position of spins along the gradient axis – this process is termed frequency-encoding. Additionally, a gradient applied along the y axis (G_y) can be used to alter the *phase* of the precessing spins. Applying a gradient briefly and immediately after the RF-excitation pulse while the spins are phase-coherent induces position-dependent phase shifts that are retained once the gradient is turned off prior to signal read-out. By repeating this process across multiple read-outs using phase-encoding gradients of different magnitudes, precessing spins along the y -axis acquire a specific, and position-dependent, *rate of change* of phase – or frequency – in the y -axis. Therefore, position is encoded in a two-dimensional plane according to both the phase and frequency of the received signal. These data are stored in k -space, a two-dimensional matrix in the spatial frequency domain, where one row is filled after each phase-encoding step and from which the MR image can be calculated by two-dimensional Fourier transform.

In order to build a three-dimensional image, a third additional gradient is used. The slice-select gradient (G_z) is applied perpendicular to both G_x and G_y at the same time as the RF excitation pulse. As

shown in Equation 2.4, this induces a shift in resonant frequency along z as a function of gradient strength. The RF pulse is used to selectively excite spins at a specific point along z where its oscillatory frequency matches the resonant frequency of the spins. By altering the RF pulse frequency, consecutive ‘slices’ of z can be excited prior to two-dimensional phase- and frequency-encoding in the xy plane. The thickness of each slice is dependent on the strength of G_z and the bandwidth (or range of frequencies) of the applied RF pulse. It is also possible to avoid slice-selection and acquire a full three-dimensional image using a second set of phase-encoding gradients applied in the z direction followed by three-dimensional Fourier transform. The timing of each magnetic gradient and RF pulse is critical for MR acquisition, examples of some common pulse sequences used to acquire MR data are described in Appendix A.

As stated, the received MR signal is governed by two tissue-dependent properties (T_1 and T_2) that can be used to provide image contrast. T_1 - and T_2 -weighting is achieved by altering the time between consecutive RF excitations pulses (repetition time; TR) and between the RF excitation pulse and signal readout (echo time; TE). T_1 -weighted images are typically acquired with (or with variations of) a gradient-echo sequence, a rapid sequence that allows for smaller flip angles and shorter TR and TE times (shown in Appendix A; Figure A.1). A shorter TR does not allow for full recovery of longitudinal magnetisation before the next RF pulse. Consequently, in tissues with long T_1 , magnetisation does not recover fully before RF excitation, resulting in lower transverse magnetisation and less contribution to the MR signal after excitation.

T_2 -weighted images are typically acquired using spin-echo sequences (Appendix A; Figure A.2) with longer TR (greater than T_1) to allow full recovery of longitudinal magnetisation and a larger flip angle to maximise transverse magnetisation after RF excitation. A longer TE is also used to maximise the difference in time taken between tissue types for the transverse signal to decay due to dephasing. During a spin-echo sequence, signal attenuation due to spin dephasing is offset by the application of a 180° refocusing RF pulse at time t . This flips magnetisation in the xy plane and as the spins continue to precess at the frequency dictated by the local field variations about them, they rephase at time $2t$, producing a phase-coherent MR signal. This sequence can be extended to include multiple rephasing RF pulses – an echo train – continually flipping magnetisation and providing multiple signal readouts from a single 90° RF excitation pulse. As each echo fills a row of k -space, fast spin echo sequences greatly decrease scanning time.

Echo-planar imaging

In contrast to sequences that fill k -space one row at a time, techniques have been developed that fill k -space with a single acquisition. Echo-planar imaging (EPI; Mansfield 1977, Ordidge et al. 1981) is able to capture whole-brain images in under 100 ms through the rapid switching of gradients. Although many variants exist, the basic EPI sequence requires rapid oscillation of the frequency-encoding gradient to produce a train of gradient echoes, each one of which is phase encoded differently. Each

oscillation fills a row of k -space, with the next row indicated by the ‘blipped’ phase encode (Stehling et al. 1989).

EPI requires specific MR scanner hardware that is capable of producing large, fast gradient oscillations and is susceptible to signal artefacts and geometric distortions due to eddy current effects and local field inhomogeneities caused by the rapidly switching gradients (Jezzard et al. 1998). Also, single-shot EPI is commonly of poorer contrast and lower resolution than other forms of MRI, but it allows the capture of rapidly changing dynamic processes, most notably changes in blood oxygenation in functional MRI and the diffusion of water molecules in diffusion MRI, that have led to wide application as a clinical and research tool.

2.2 Diffusion MRI

Diffusion

Brownian motion describes the stochastic movement of particles imparted by thermal energy and underlies the process of molecular diffusion. Einstein formalised this process in 1905, demonstrating that the mean displacement of a set of freely-diffusing particles is dependent on both the time taken to diffuse and the diffusion coefficient, or diffusivity, of the medium in which they are in (Einstein 1905; Equation 2.5).

$$\lambda = \sqrt{6Dt} \quad [2.5]$$

where λ is the root mean square displacement of a molecule in three dimensions over time t , and D is the diffusion coefficient of the medium. In the case of water at room temperature, D equals 2.3×10^{-3} mm²/s.

Statistically, this ‘free’ diffusion process can be described as a Gaussian function, shown in Equation 2.6, such that over a given time, the probability P of a molecule arriving at a given point \mathbf{r} after time t is equal in all directions:

$$P(\mathbf{r}_0; \mathbf{r}, t) = \frac{e^{-(\mathbf{r}-\mathbf{r}_0)^2/4Dt}}{(4\pi Dt)^{\frac{3}{2}}} \quad [2.6]$$

Therefore, within a homogeneous medium (e.g. water), displacement due to diffusion can be described as isotropic (Figure 2.3). In contrast, the brain is clearly not a homogeneous medium and the presence of various cellular compartments within the parenchyma creates barriers to diffusing water molecules, reducing their mean displacement over time (Beaulieu 2002). Additionally, the coherent organisation of long neuronal axons into tracts within the cerebral white matter preferentially favours diffusion along, rather than across, the length of the axons. This diffusional anisotropy of water molecules (Figure 2.3), or more specifically, of water proton spins, within the brain was first demonstrated by Moseley et al. (Moseley et al. 1990) and forms the basis of clinical diffusion MRI.

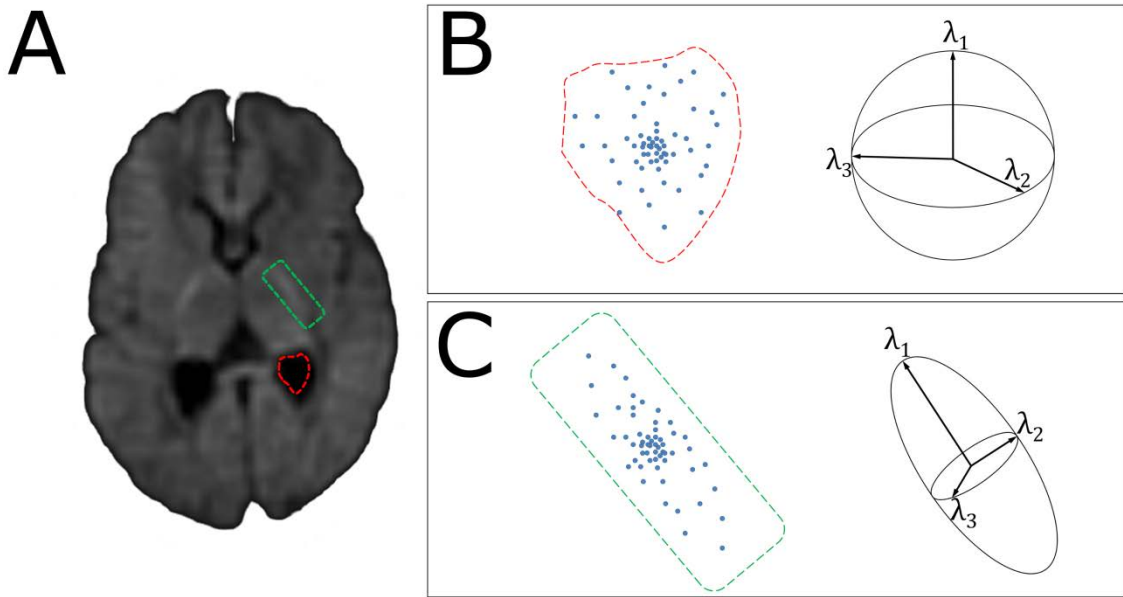


Figure 2.3: Isotropic and anisotropic diffusion in the brain. Diffusion-weighted imaging of a preterm infant at term-equivalent age reveals the nature of water diffusion within different brain tissue compartments (A). In the ventricular cerebro-spinal fluid (CSF; outlined in red), diffusion is unhindered and can be described as isotropic (see panel B). In white matter, diffusion occurs preferentially along the white matter tracts (outlined in green), resulting in anisotropic diffusion (panel C). Diffusion tensor ellipsoids representing isotropic and anisotropic diffusion are shown in panels (B) and (C) respectively. Each tensor is expressed by three eigenvectors with values λ_1 , λ_2 and λ_3 . In isotropic diffusion $\lambda_1 = \lambda_2 = \lambda_3$, whereas in anisotropic diffusion the long axis of the ellipsoid aligns with the underlying white matter and λ_1 is greater than λ_2 and λ_3 .

Diffusion-weighted imaging

To sensitise MR signal intensity to the magnitude of diffusion within the brain, a pulsed field gradient spin-echo sequence is commonly used. Initially developed by Stejskal and Tanner in 1965, this sequence, shown in a simplified format in Appendix A, induces diffusion weighting through two pulsed gradients applied either side of a 180° RF pulse (Stejskal and Tanner 1965).

During the first diffusion gradient, spins accumulate a position-dependent phase shift, the radio pulse inverts the spins before the second diffusion gradient, equal in amplitude and duration to the first, rephases the spins to bring them into coherence and produce the MR signal. Spins that remain

stationary between the application of the two gradients refocus completely; the two phase shifts cancelling each other out with no loss of signal. Conversely, the random motion of spins induced by water diffusion results in the application of unequal phase shifts, intravoxel spin dephasing and a loss in signal amplitude. This is most evident in the fluid-filled structures of the brain (e.g. the ventricles, outlined in red in Figure 2.3).

The difference in signal between CSF and the parenchyma shown in the diffusion-weighted image in Figure 2.3 is not due to differences in the self-diffusivity of water in each compartment (in both, this is around $2\text{-}3 \times 10^{-3} \text{ mm}^2/\text{s}$). Instead, the *apparent* difference in diffusivity is due to the effect of various cellular barriers in the parenchyma restricting water displacement and, consequently, reducing signal attenuation. As such, the apparent diffusion coefficient (ADC) is commonly used in diffusion MRI to describe the estimated extent of water diffusivity accounting for impedance due to cellular barriers. ADC can be calculated from Equation 2.7 (Le Bihan et al. 1986):

$$D = -\frac{1}{b} \ln \left(\frac{S}{S_0} \right) \quad [2.7]$$

where S and S_0 are the signal measured with and without diffusion weighting and b reflects the degree of diffusion-weighting applied. The b -value commonly ranges between 750 and 1500 s/mm^2 for clinical diffusion MRI and can be calculated from Equation 2.8 (Stejskal and Tanner 1965):

$$b = \gamma^2 G^2 \delta^2 \left(\Delta - \frac{\delta}{3} \right) \quad [2.8]$$

where γ is the gyromagnetic ratio for water protons and G , δ , and Δ are the strength, duration and time between diffusion gradients, as shown in Appendix A (Figure A.3).

Due to the coherent organisation of the cerebral white matter, ADC is dependent on the direction of the underlying alignment of axons *relative* to the applied diffusion gradients. ADC is therefore considered a rotationally variant measurement; it is maximally sensitive to diffusion occurring in the direction of the applied gradient. Often this problem is overcome by applying three diffusion gradients, in the left-right, inferior-superior and anterior-posterior directions, and averaging the resultant ADC values. Alternatively, through the application of several diffusion-weighted gradients, it is possible to produce rotationally-invariant estimates of tissue diffusivity.

Diffusion tensor imaging

DTI requires the application of a minimum of six linearly-independent diffusion gradients, although commonly 15, 32 or more directions are acquired to construct the diffusion tensor. The tensor is

represented by a 3 x 3 symmetric matrix that describes the diffusion profile in a given voxel, as shown in Equation 2.9:

$$D = \begin{bmatrix} D_{xx} & D_{xy} & D_{xz} \\ D_{xy} & D_{yy} & D_{yz} \\ D_{xz} & D_{yz} & D_{zz} \end{bmatrix} \quad [2.9]$$

where the diagonal elements (D_{xx} , D_{yy} and D_{zz}) correspond to diffusivity along three orthogonal axes of the tensor and the off-diagonal elements reflect the correlation between these displacements.

The diffusion tensor describes an ellipsoid iso-surface that represents the probability of diffusion from the origin, examples are shown in Figure 2.3. In the case of isotropic diffusion, this probability is equal in all directions and the diffusion tensor describes a sphere. In an anisotropic medium, e.g. cerebral white matter, the orientation of the tensor ellipsoid is assumed to align with the underlying, dominant fibre orientation and can be expressed by three orthogonal eigenvectors with values λ_1 , λ_2 and λ_3 (Basser et al. 1994, Basser and Pierpaoli 1996, Pierpaoli and Basser 1996).

λ_1 , λ_2 and λ_3 are rotationally-invariant, scalar metrics often used to summarise voxelwise diffusion properties without a frame of reference. Independent of the direction of the underlying tracts, λ_1 represents the estimated magnitude of diffusion parallel to fibre direction, described here as axial diffusivity (AD), λ_2 and λ_3 represent the magnitude of diffusion perpendicular to λ_1 and, when averaged, provide an estimate of diffusion across the direction of the fibres, or radial diffusivity (RD). Several additional indices can be derived from these values. Mean diffusivity (MD; Equation 2.10) is calculated from the trace of the tensor, or the sum of the three eigenvalues, and represents the directionally-averaged tissue diffusivity. Relative anisotropy (RA; Equation 2.11) and fractional anisotropy (FA; Equation 2.12) both describe the degree to which diffusion along one axis occurs preferentially over others (Basser and Pierpaoli 1996).

$$MD = \bar{\lambda} = \frac{\lambda_1 + \lambda_2 + \lambda_3}{3} \quad [2.10]$$

$$RA = \sqrt{\frac{1}{3} \frac{(\lambda_1 - \bar{\lambda})^2 + (\lambda_2 - \bar{\lambda})^2 + (\lambda_3 - \bar{\lambda})^2}{\bar{\lambda}}} \quad [2.11]$$

$$FA = \sqrt{\frac{3}{2} \frac{(\lambda_1 - \bar{\lambda})^2 + (\lambda_2 - \bar{\lambda})^2 + (\lambda_3 - \bar{\lambda})^2}{\sqrt{(\lambda_1)^2 + (\lambda_2)^2 + (\lambda_3)^2}}} \quad [2.12]$$

FA takes a value between 0 and 1, where 0 corresponds to a perfectly isotropic, spherical tensor ellipsoid and 1 corresponds to the limit of infinite anisotropy. Although lower than typical adult values, high FA (in the range of 0.35 – 0.50) in the neonatal brain is characteristic of well-developed white matter tracts.

Multi-fibre modelling

Image resolution in clinical DTI is typically in the range of 1 – 3 mm and a single voxel can contain many thousands of axons forming coherent fibre bundles. One major limitation of DTI is the inability to resolve the local diffusion profile of multiple fibre populations passing through a voxel with different orientations. In some cases of complex fibre organisation, modelling diffusion as a Gaussian process under the assumption of a single dominant orientation is not appropriate (see Figure 2.4); this ‘crossing-fibre problem’ can prove particularly troublesome when performing tractography (see Section 2.5). A number of methods have been proposed to more accurately model multiple-fibre populations (Alexander 2005), either by modelling the underlying diffusion profile to estimate distinct fibre orientations (Tuch et al. 2002, Behrens et al. 2003a, Assaf et al. 2004, Chen et al. 2004, Hosey et al. 2005) or by inferring the diffusion profile directly with a model-free approach (Jansons and Alexander 2003, Tournier et al. 2004, Tuch 2004, Wedeen et al. 2005). Although the latter approaches have been used to detect up to three distinct fibre populations per voxel in some brain regions (Tuch et al. 2003), they require datasets acquired with high b -values and a large number of directions that are not yet practically achievable in a clinical setting.

Of the model-based approaches, Behrens et al. demonstrated that a clinically feasible acquisition scheme (60 gradient directions with a b -value of 1000 s/mm²) is adequate to detect 2 fibre populations in up to one third of white matter voxels using a ‘ball and stick’ compartment model (Behrens et al. 2007). Here, the diffusion signal is modelled as a combination of two compartments: anisotropic diffusion along the axis of each fibre population and isotropic diffusion of free water otherwise unattributed to axonal diffusion (see Figure 2.4). Although a limitation of typical multi-tensor models is the need for prior information on the number of expected fibre populations per voxel, this technique allows the automatic detection of the number of fibre populations supported by the data using Bayesian inference (Behrens et al. 2007).

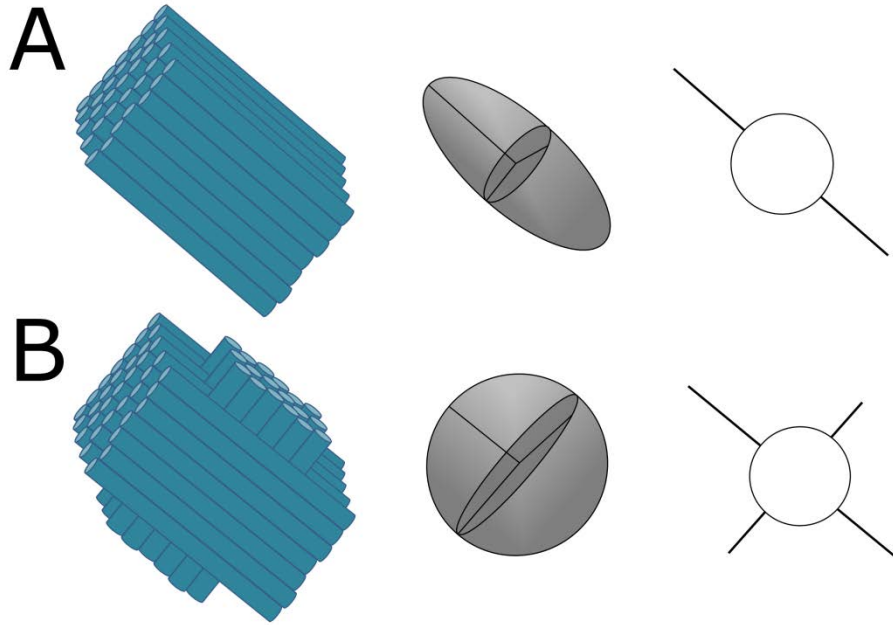


Figure 2.4: Crossing fibres and the diffusion tensor. Although single fibre populations can be modelled with a single diffusion tensor (A), more complex configurations, such as crossing fibres (B) can produce tensors that do not represent all fibre populations. Ball-and-stick models (A and B, right) are able to model the contribution of each fibre population to the anisotropic signal.

2.3 Image Registration

Computational MR analysis, driven by the increasing availability of modern, high-field clinical MR scanners coupled with powerful computers and the development of advanced post-acquisition processing pipelines, provides the means to quantify differences between MR images objectively, and often automatically, with robust, precise and reproducible measurements.

Image registration is a cornerstone of groupwise, quantitative MR analysis (Toga and Thompson 2001, Crum et al. 2004). The goal is to geometrically align, spatially normalise, or transform images acquired from different individuals, at different timepoints or with different modalities in order to achieve precise spatial correspondence in a common reference space for direct comparison. This process underlies many techniques that can provide insight into the subtle changes in cerebral volume, function and microstructure associated with development and aging (Thompson et al. 2000, Good et al. 2001, Aljabar et al. 2008, Giorgio et al. 2010a), disease progression (Thompson et al. 2003, Leow et al. 2009), post-operative changes (Ferrant et al. 2002) and task-related plasticity (Maguire et al. 2000, Scholz et al. 2009).

Registration can generally be separated into three components:

1. **Transformation:** to estimate the mapping between a given source (the image to be transformed) and a reference image.
2. **Similarity measurement:** to define the similarity between the transformed source and the intended reference.
3. **Optimisation:** to select, or improve upon, the transformation.

Image registration algorithms aim to maximise the similarity between the source and the target by optimising the parameters of the transformation model. Many transformation models exist but they can be broadly defined as one of two types: linear (rigid and affine) and nonlinear. Linear transformations can account for global differences in size and shape between two images; nonlinear transformations can additionally model local variations in anatomy, providing detailed and precise transformations (Hill et al. 2001; see Figure 2.5). This type of modelling is particularly useful when analysing MRI acquired from preterm infants due to the large variation in cerebral anatomy between subjects and the rapid cerebral development that occurs during the neonatal period.

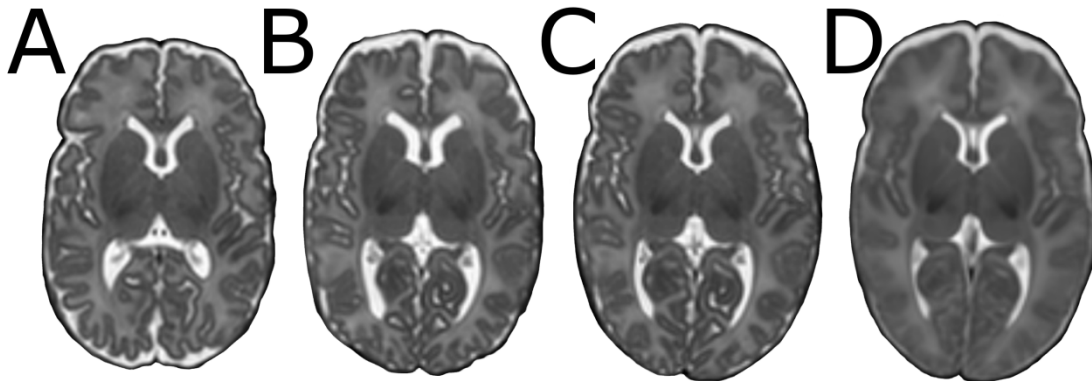


Figure 2.5: Image registration between a source and target image. A source image (A) is aligned to a target (D) with affine (B) and nonlinear transformations (C). The source image is a T_2 -weighted MRI from a preterm infant at term-equivalent age, the target is a population-average atlas as described in Kuklisova-Murgasova et al. (2011).

Linear registration

Transformation models are defined by the type and number of possible deformations that can be applied to align two images. Rigid transformations preserve shape, such that the distance between any given two points in an image remains the same after transformation. Rigid transformations are commonly used for intra-subject registration (i.e.: between a subject's T_1 and T_2 -weighted images), where the anatomy is matched but positional differences may exist due to movement in the scanner or altered field of view, or to provide a starting point for subsequent affine and nonlinear registration. The rigid transformation between two points in corresponding images is composed of a set of translations and rotations over three dimensions giving a total of six parameters, or degrees-of-freedom (DOF), to optimise during registration

Rigid transformations represent a subset of affine transformation that also includes scaling and shear parameters over three dimensions to give 12 DOF. Affine registration can be used to correct for scanner-induced geometric distortions – most commonly due to eddy current effects in EPI-acquired data – and for inter-subject registration to provide an approximate alignment of images from different subjects, able to model global changes in scales and shape but not local variations in anatomy. For more precise alignment, nonlinear registration is often required; an affine transformation can provide a starting estimate for these more computationally-demanding transformations.

Nonlinear registration

Several approaches to nonlinear registration exist: some model the image to be transformed as a deformable elastic material or fluid (Bajcsy and Kovačič 1989, Christensen et al. 1996), others model the deformation as a smooth combination of basis functions or splines (Bookstein 1989, Friston et al. 1995, Rueckert et al. 1999). Spline-based registrations require a set of landmarks, or control points, to be placed in each image – these may be anatomically informed or placed on a grid – with transformations represented by a smooth combination of the deformations at each control point (see Figure 2.6).

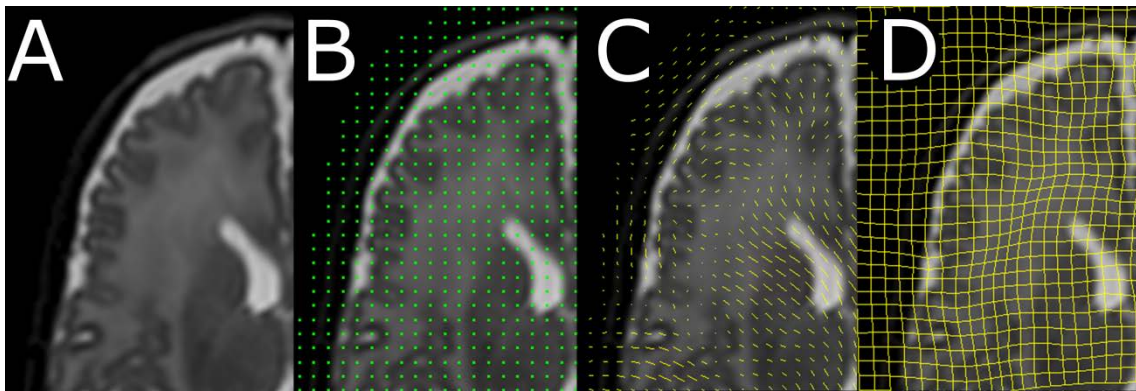


Figure 2.6: A nonlinear transform can be modelled using a smooth approximation of deformations of regularly spaced control points. A transformed image is shown in (A) with a regular grid of control points overlaid in (B). The vectors in (C) describe the deformation required in order for the control points to match their corresponding positions in the untransformed, source image. The smooth deformation field in (D) describes the final transformation.

The free-form deformation (FFD) model uses a regularly-spaced grid of control points, with the translation required of each to bring one image into the space of another described by a vector. Vectors at each control point are blended using a B -spline kernel to produce a smooth deformation field (Figure 2.6D). As B -splines are locally controlled, displacing a single control point will only directly affect neighbouring points and not the whole grid; this makes B -spline based registration computationally efficient and able to cope with locally varying structure (Rueckert et al. 1999).

Deformations estimated with FFD are calculated as a combination of local and global transformations, where the global estimate is provided by affine registration. The local transformation ($T_{local}(x)$) is

estimated as a three-dimensional tensor product of one-dimensional cubic B -splines, as shown in Equation 2.13:

$$T_{local}(x) = \sum_{l=0}^3 \sum_{m=0}^3 \sum_{n=0}^3 B_l(u)B_m(v)B_n(w)\Phi_{i+l,j+m,k+n} \quad [2.13]$$

where $\Phi_{i,j,k}$ represents a set of vectors on a $n_x \times n_y \times n_z$ lattice of control points; B_0, \dots, B_3 are the cubic B -spline basis functions; i, j and k are the control point indices; and u, v and w are fractional lattice coordinates corresponding to the position of x . The local displacement of x is given by the B -spline tensor product over the control point vectors.

The degree of achievable deformation depends on the resolution of the control point grid. Large control point spacings can model global deformations, whereas small spacings model local variations and fine anatomical detail. This means that many studies using FFD tend to optimise the transformation over several resolution levels, with the number of control points increasing at each level (Schnabel et al. 2001). This allows the capture of nonlinear deformations at increasingly more local scales, as shown in Equation 2.14:

$$T_{local}(x) = \sum_{l=1}^L T_{local}^l(x) \quad [2.14]$$

where the transformation $T_{local}(x)$ is given by the sum of prior local transformations $T_{local}^l(x)$ at increasing control point resolution levels l , where control point resolution increases from Φ^l to Φ^L .

In this thesis, unless otherwise stated, nonlinear registration between structural MR images is performed using IRTK (Image Registration Toolkit; <http://www.doc.ic.ac.uk/~dr/software/>; Rueckert et al. 1999). IRTK uses the FFD model and has been shown to perform consistently well in comparison to other registration software (Klein et al. 2009), and has been optimised for use in neonatal MR (Boardman et al. 2006). For registration of FA maps in Chapters 5 and 6, the FNIRT software is used (FSL's Nonlinear Registration Tool; <http://www.fmrib.ox.ac.uk/fsl/fnirt/>; Andersson et al. 2007). In FNIRT, deformations are constructed according to the same principles as IRTK (i.e.: linear combinations of basis functions) but the software has been specifically configured for use in the TBSS pipeline (see Section 3.3 below).

Measuring similarity

The goal of registration is to maximise the similarity between two images. Similarity can be defined in terms of geometric or intensity-based correspondence (Hajnal et al. 2001). By identifying reliable (i.e.:

anatomically consistent) landmarks it is possible to map the transformation between pairs of corresponding points in each image (Bookstein 1989, Rohr et al. 2001, Johnson and Christensen 2002), although the manual placement of each landmark must be precise to avoid introducing error or bias into the transformation. Other approaches use anatomical surfaces, such as the ventricular borders or cortical surfaces (Thompson and Toga 1996, Yeo et al. 2010) extracted automatically and used to define many points across the whole surface or anatomical features such as sulcal and gyral ridges that are used to drive the registration process (Subsol et al. 1997, Joshi et al. 2010). Although reliant on relatively sparse data, these surface-based techniques are particularly proficient when aligning the cortical surface between subjects – typically very difficult to achieve using intensity-based methods due to the highly complex and variable convolutions of the cortex across subjects (Rademacher et al. 1993). Despite increasingly sophisticated methods, the use of surface-based registration in neonatal population remains limited due to the technical difficulties in accurately extracting and aligning neonatal cortical surfaces (Xue et al. 2007, Hill et al. 2010).

Intensity-based similarity metrics measure the difference in voxel intensities at corresponding locations across the whole image. The simplest forms: sum of squared differences (SSD) and cross correlation (CC) are best suited to intramodal registration between images with similar intensities (i.e.: between two T_1 -weighted images). SSD is based on the assumption that, once transformed, the image intensities differ only due to Gaussian noise, the intensity range of each tissue class must therefore be identical in both images. When using CC, image intensity may differ but a linear relationship is assumed to exist between the intensities of corresponding points in each image at registration (Hill et al. 2001).

When performing registrations between different image modalities, or between images with different contrasts, entropy-based metrics are generally more suitable (Pluim et al. 2003). In information theory, entropy is a measure of uncertainty associated with a variable; in terms of image registration, entropy describes the probabilistic relationship between voxel intensities, as shown in Equation 2.15, and describes the expected uncertainty or information content of the image.

$$H_x = - \sum_i p(i) \log p(i) \quad [2.15]$$

where $p(i)$ represents the probability of voxels with intensity i occurring in an image x .

Entropy-based metrics such as mutual information (MI; Equation 2.17) and normalised mutual information (NMI; Equation 2.18) require an estimation of the probability density functions of image intensities in the target and source images. This is achieved by constructing a joint histogram of the intensities across the whole of each image into discrete bins of fixed width and calculating the joint probability that a voxel intensity lies within a specific intensity range in both images, shown in Equation 2.16:

$$H_{AB} = - \sum_a \sum_b p(a, b) \log p(a, b) \quad [2.16]$$

where $p(a, b)$ represents the joint probability of intensities a and b occurring in corresponding voxels of images A and B .

$$MI = H_A + H_B - H_{AB} \quad [2.17]$$

$$NMI = \frac{H_A + H_B}{H_{AB}} \quad [2.18]$$

where H_A and H_B represent the marginal entropies of images A and B as given by Equation 2.15, and H_{AB} represents the joint entropy of both A and B , shown in Equation 2.16. The more similar A and B are, the lower the joint entropy – maximising MI requires a balance between maximising each image's marginal entropy while minimising their joint entropy (Wells et al. 1996, Maes et al. 1997). In practice MI can be influenced by overlap of background, or low intensity regions, even if the main focus of the image is not well aligned, therefore NMI is more typically used for image registration as it is overlap-invariant (Studholme et al. 1999).

Optimisation and interpolation

Optimisation describes the process of finding the global minimum (or maximum) of a function of a set of parameters as determined by the choice of transformation model, for instance minimising SSD, or maximising MI. The large number of parameters required to describe a transformation model can make an exhaustive search for the optimum values of each impractical. A common approach in both linear and nonlinear registration is to adopt a multi-resolution approach with local optimisation (Woods et al. 1993, Studholme et al. 1996, Rueckert et al. 1999, Jenkinson and Smith 2001). This involves estimating an initial set of parameters and perturbing each by a given step size, chosen empirically, before re-evaluating the similarity metric. The transformation is updated according to the parameter change that results in the largest increase in similarity and the process continues stepping along the direction of maximum increase until no more increases are achieved, or a convergence criterion is reached. By altering the step size to become progressively smaller and sub-sampling the data onto lower resolution voxel grids, it is possible to perform registration in a coarse-to-fine manner through several resolution levels, optimising the alignment first according to gross image features and progressing to finer anatomical details. An advantage of this approach is that the initial transformations, at low resolution, can be calculated relatively quickly and used to inform higher resolution transformations. Occasionally, local optimisation strategies may fail due to the presence of local minima, possibly as a result of large differences in scale or extreme transformations between

images, which do not reflect the optimum global solution and can cause the registration process to fail, resulting in misaligned images (Jenkinson and Smith 2001).

Optimising intensity-based similarity metrics requires comparison of equivalent points in the target and transformed source images. Due to the discrete nature of MR images, data are sampled in a grid of voxels and it is unlikely that the corresponding points lie on the same voxel grid after transformation. To compare the images it is necessary to interpolate between points, resampling the transformed source image onto the same grid as the intended target (Lehmann et al. 1999, Hill et al. 2001). A number of interpolation methods exist, the choice of each depending on a trade-off between speed and accuracy. Nearest-neighbour interpolation simply assigns any given point the intensity of the geometrically-nearest voxel centre; it is quick to calculate and is often used when transforming binary or integer-labeled masks as it preserves the original voxel values without blurring. Trilinear interpolation is a commonly used method where intensity is calculated as the weighted average of neighbouring voxels, with the closest voxel centres weighted higher (Lehmann et al. 1999). More sophisticated interpolators, including *B*-spline and sinc interpolation, are more accurate but also more computationally demanding to calculate (Hajnal et al. 1995, Unser 1999).

Regularisation

Nonlinear registration can result in precise image alignment. Although this results in high similarity it may also produce implausible transformations containing sharp warps, folds or tears of the transformed image that are anatomically invalid (Crum et al. 2004). In general, it is assumed that similar structures are present in both images to be registered (although variability in their size and shape is expected); this is reflected in a one-to-one transformation, represented by a smooth and invertible deformation field, or diffeomorphism (Trouvé 1998). Diffeomorphic transformations are desirable when the output of the registration is required for analysis, for instance in deformation-based morphometry (DBM; Ashburner et al. 1998, Leow et al. 2007) and a number of nonlinear registration algorithms are diffeomorphic by design (Christensen et al. 1996, Marsland and Twining 2004, Beg et al. 2005, Ashburner 2007). Although FFD-based algorithms do not necessarily produce diffeomorphisms, invertible warps can be constructed by composing multiple FFD, each with a strong smoothness constraint, or by imposing sufficient regularisation on a single FFD (Rueckert et al. 2006).

Regularisation functions often reflect the nature of the deformation fields, for example bending energy (Rueckert et al. 1999) or membrane energy (Ashburner and Friston 1999), and can easily be incorporated into the registration. As shown in Equation 2.19, if C_{sim} represents the similarity metric and C_{reg} the regularisation term, the overall cost function to be optimised by the transformation is given by C . The contribution of the regularisation to the overall function is given by λ , which can be set heuristically to achieve the required level of constraint.

$$C = C_{sim} + \lambda C_{reg}$$

[2.19]

Defining correspondence

A major difficulty in image registration for the purpose of MR image analysis is establishing, and validating, image correspondence (Crum et al. 2003). A number of possible solutions exist for any given registration problem, and often the decision to use a particular transformation is a qualitative one based on visual inspection (Good et al. 2002). Studies have shown that for specific structures, automatic morphometry based on nonlinear registration is consistent with manual volumetry (Holden et al. 2002) and intensity-based nonlinear algorithms have been shown to accurately align 70% of a set of 128 anatomical landmarks placed across the brain with an error of less than 3 mm (Grachev et al. 1999). Indeed, when performing registration based on image intensity, borders between tissues with distinctly different contrasts (i.e.: the deep grey/white matter border) are often well-aligned but, in regions of similar tissue intensity, there is no way to guarantee that homologous regions are aligned to each other accurately, or reproducibly. This is of particular importance in the cortex where significant inter-individual variability exists (Rademacher et al. 1993). Care must therefore be taken to consider these limitations when interpreting statistical analyses based on image registration.

2.4 Structural MR Analysis

Morphometric analysis of structural MR is widely used in neuroimaging to detect alterations in structural shape, volume and tissue density without the need to select regions-of-interest *a priori*. Many different methods have been described; two of the most common are voxel-based morphometry (VBM; Wright et al. 1995, Ashburner and Friston 2000) and deformation (or tensor)-based morphometry (Ashburner et al. 1998, Chung et al. 2001, Rueckert et al. 2003).

Voxel-based morphometry

VBM combines the spatial normalisation of all images to a common space with a relatively low DOF nonlinear registration, tissue segmentation to extract voxels containing grey matter (or white matter), kernel-based smoothing and statistical analysis to determine regional tissue distribution on a voxelwise basis (Ashburner and Friston 2000). VBM is traditionally implemented with a low-dimensional registration for spatial normalisation that has been the source of some controversy regarding the possible confounding effects of misregistration on analyses (Ashburner and Friston 2001, Bookstein 2001). Good et al. introduced an ‘optimised’ VBM pipeline that takes into account the effect of volume change on tissue segmentations in template space and allows for more precise nonlinear registration (Good et al. 2001). Using the optimised pipeline, results obtained using VBM have been compared to manual volumetry and have demonstrated generally good correspondence (Good et al. 2002, Douaud et al. 2006, Bergouignan et al. 2009, Kennedy et al. 2009). A further complication of VBM analysis is the

choice of smoothing kernel and care must be taken when making this arbitrary decision as the width of the kernel used has been shown to alter the results of VBM-style analyses (Jones et al. 2005).

Although VBM has been used to study neonatal populations previously (Lodygensky et al. 2008), the difficulty in automatically segmenting tissue classes in the newborn brain, due to low contrast, intensity inhomogeneity and rapidly developing anatomical structures preclude the use of the standard pipeline (Weisenfeld and Warfield 2009). Additionally, due to the highly variable range of cerebral size and shape present in preterm populations, the use of low-dimensional warping in VBM may not sufficiently align all images in a cohort, making the process difficult to implement and interpret.

Deformation-based morphometry

In DBM, statistical analysis is performed directly on the nonlinear transformations, rather than the properties of the subsequently transformed images (Ashburner et al. 1998, Chung et al. 2001, Rueckert et al. 2003). As such, DBM relies on achieving precise spatial correspondence so that any difference between two images is encoded as fully as possible in the deformation field. In addition, DBM does not rely on tissue segmentation.

Although the terms are often used interchangeably, deformation-based and tensor-based morphometry (TBM) can refer to distinct analytical processes. In the literature, DBM refers to multivariate statistical analysis of parameters associated with the deformations, such as voxelwise displacement vectors (Ashburner et al. 1998, Gaser et al. 1999, Shi et al. 2009), whereas TBM tends to refer to the analysis of a derivative of the deformations, most commonly local volume change as described by the Jacobian determinant (Ceccarelli et al. 2009, Shi et al. 2009, Lu et al. 2011). This is not always the case, however, and DBM is often used to describe both types of analysis (Gaser et al. 2004, Rohlfing et al. 2006, Cardenas et al. 2007, Tosun et al. 2011). For the purposes of this thesis, and to be consistent with previous literature in the field (Boardman et al. 2006, Aljabar et al. 2008), statistical analysis of the Jacobian determinant, derived from the deformation fields, will be referred to as DBM.

To derive local volume change from a nonlinear deformation, the Jacobian operator D can be applied to any transformation T between two images (Equation 2.20). Volume change at a point x is then given by the determinant of the Jacobian operator $J(x)$ at that point (Equation 2.21).

$$DT = \begin{pmatrix} \frac{\partial T_x}{\partial x} & \frac{\partial T_x}{\partial y} & \frac{\partial T_x}{\partial z} \\ \frac{\partial T_y}{\partial x} & \frac{\partial T_y}{\partial y} & \frac{\partial T_y}{\partial z} \\ \frac{\partial T_z}{\partial x} & \frac{\partial T_z}{\partial y} & \frac{\partial T_z}{\partial z} \end{pmatrix} \quad [2.20]$$

where T_x , T_y and T_z represent the displacements in the x , y and z directions.

$$J(x) = \det(DT(x)) = \det(DT_{global}(x) + DT_{local}(x))$$

[2.21]

Figure 2.7 shows how volume change is induced by different types of transformation. Jacobian values are calculated in the space of the target image and values greater than 1 represent local tissue expansion whereas values less than 1 represent tissue contraction relative to the target. By calculating voxelwise volume change relative to a common target across a range of individuals, statistical analysis can test volumetric differences, or correlations within a study population.

As with VBM, the validity of DBM is dependent on the accuracy of the nonlinear registration. Gaser et al. demonstrated a high correlation ($r = 0.96$) between manual volumetry of the lateral ventricles and the mean Jacobian determinant calculated within a ventricular mask drawn in the space of the target image, using a multi-resolution nonlinear registration approach (Kjems et al. 1999, Gaser et al. 2001). Similar comparisons have been made with FFD registration (Holden et al. 2002). In addition, Han et al. demonstrated that FFD-based registration, implemented by IRTK, performs well detecting volume change in simulated deformation fields constructed from paediatric MRI (Han et al. 2011).

As DBM does not require tissue segmentation and uses high-dimensional registration techniques that are able to model large variations in size and shape, it represents an appropriate technique for structural MR analysis in the preterm neonate (Boardman et al. 2006, Boardman et al. 2007).

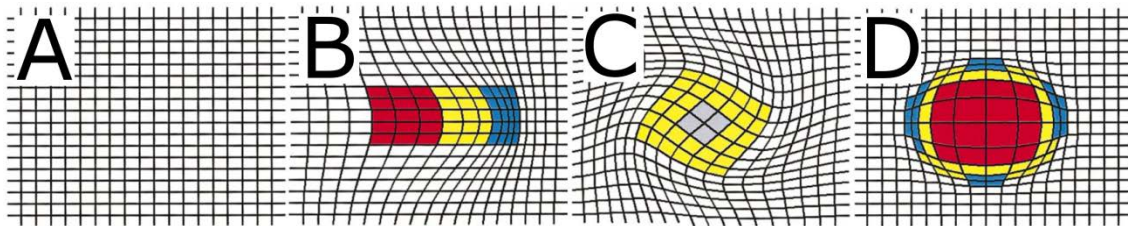


Figure 2.7: Volume change induced by transformations. Three different transformations are applied to the grid in (A). Translation caused by volume increase on the left side (B), clockwise rotation of 45° (C) and central volume expansion (D). The colour of each square represents the volume change induced by each transformation. Red = volume increase; blue = volume decrease; yellow = no overall volume change. Figure modified from Figure 2 in Chung et al. (2001).

2.5 Diffusion MR Analysis

Voxel-based analysis

As with standard VBM, scalar images derived from diffusion datasets – most commonly FA maps – can be aligned with nonlinear registration to a common target space, smoothed and analysed with mass-univariate statistics. As such, similar concerns about the interpretability of this style of analysis have

been raised, given the possible confounding effects of misregistration, smoothing and partial voluming (Jones and Cercignani 2010).

Partial volume effects can prove problematic when transformed FA maps are analysed directly. In voxels that contain more than one type of tissue, a change in the ratio of tissue type can result in a change in intensity and interpretation as a microstructural change reflected by altered FA. Therefore, it can be difficult to separate changes in contrast due to altered FA from those caused by mis-registered or altered anatomical borders (i.e.: enlarged ventricles), a problem that is exacerbated in clinical populations with known structural alterations (Simon et al. 2005, Smith et al. 2006). Although smoothing can mitigate the effects of residual misalignment after registration, it does not do so in a controlled manner, making it difficult to determine how much to apply without performing multiple repeated tests (Jones et al. 2005, Jones and Cercignani 2010).

TBSS was introduced by Smith et al. as a method of voxelwise DTI analysis that is not dependent on precise spatial alignment and does not require smoothing (Smith et al. 2006). The key step is the generation of a skeletonised dataset that represents the centre of all white matter tracts common to the group and over which statistical analysis is performed. After nonlinear alignment, an intensity-averaged image of the co-registered FA maps is created and thinned using non-maximum suppression perpendicular to the local tract direction. This process identifies voxels of the highest intensity, or FA, which are assumed to represent the centre of each tract, or contiguous group of tracts, and creates a set of curved sheets, or tubes (see Figure 2.8).

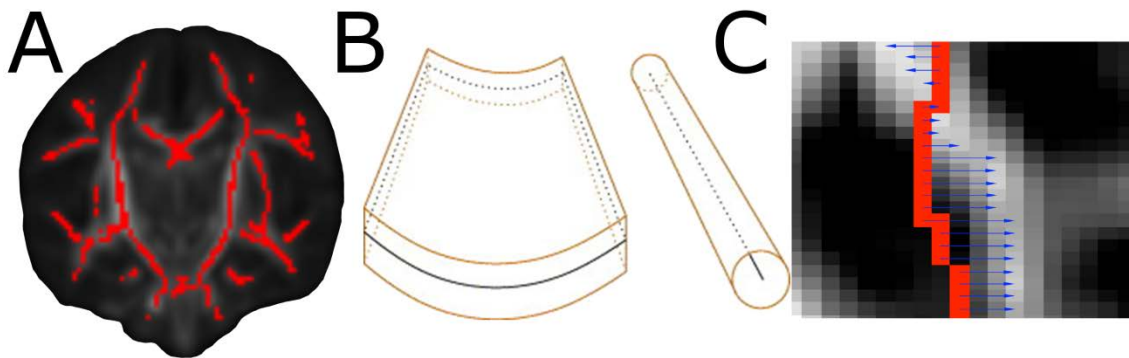


Figure 2.8: Generating the FA skeleton in TBSS. White matter tracts are thinned to form a FA skeleton (A) comprising a set of sheets or tubes that represent the topology of the white matter and contain voxels from the centre of the tracts (B). Individual FA values are then projected from transformed maps onto the group skeleton, in order to reduce the effect of mis-registration (C). Modified from Figure 2 in Smith et al. (2006).

Following skeletonisation, individual FA values are projected onto the group FA skeleton. Precise spatial alignment is not required at this point; a local search method is employed to find the highest intensity voxel nearby (assumed to represent the centre of the relevant tract in each individual) and project its value onto the appropriate skeleton voxel (see Figure 2.8). This process aims to align the core of the white matter across individuals for analysis and ensures that TBSS is robust to small alignment errors. As sub-optimal registration and misalignment can result from high anatomical variability

within a study population, TBSS is particularly suitable for voxel-based neonatal DTI analysis (Anjari et al. 2007).

Tractography

Tractography represents an alternative method for diffusion analysis. By exploiting directionally coherent diffusivity in the cerebral white matter it is also possible to infer the path taken by specific white matter tracts through the brain (Mori et al. 1999). These methods can be used as *in vivo* dissection tools, extracting 3-dimensional representations of specific tracts for anatomical comparison on a macro- or microstructural scale (Wakana et al. 2004) or to infer structural connectivity between remote cortical or subcortical regions (Behrens et al. 2003b).

The earliest tractographic algorithms propagate pathways, tracks, or streamlines, from an initial starting point – the ‘seed’ region – through the diffusion data with the direction of the principal eigenvector λ_1 at each point defining the direction of the next step (Conturo et al. 1999, Mori et al. 1999, Jones et al. 1999). This process, termed deterministic or streamline tractography, continues until the streamline enters a region of low anisotropy, usually set as a hard threshold to ensure that streamlines remain in the white matter where directional diffusivity is well-defined, or makes a change in direction that exceeds a preset curvature limit, beyond which the pathway is deemed biologically implausible.

Streamline techniques, constrained by anatomically informed ROI, are able to delineate the major white matter fasciculi in a manner that is both reliable and consistent with known neuroanatomy (see Figure 2.9; Catani et al. 2002, Mori et al. 2002, Wakana et al. 2004, Wakana et al. 2007). In addition, tract-related indices including streamline length, tract volume and diffusivity appear sensitive to psychiatric, neurological and neurodegenerative disease states (Ciccarelli et al. 2008).

However, deterministic tractography is reliant on the clear determination of the direction of maximal diffusion in each voxel, a measurement that can be confounded by a number of factors. Low spatial resolution, poor signal-to-noise ratio and the presence of multiple fibre populations that cannot be modelled by the diffusion tensor can all introduce error into tract propagation (Mori and van Zijl 2002, Le Bihan et al. 2006, Ciccarelli et al. 2008). Reliance on relatively high anisotropy for accurate tracking also limits the application of these techniques in neonatal populations, where cerebral white matter is characterised by generally lower anisotropy, and precludes tracking into cortical or subcortical grey matter – essential for assessing thalamo-cortical connectivity.

Alternative approaches operate within a probabilistic framework, accounting for the uncertainty in voxelwise diffusion estimates, and often utilising multi-fibre models of diffusion to allow tracking through more complex fibre configurations (Figure 2.9; Behrens et al. 2003a, Parker and Alexander 2005, Behrens et al. 2007). A probabilistic model provides a distribution on the direction of maximal diffusion at each voxel rather than a single point estimate, with a broad distribution reflecting increased uncertainty in the estimation. Multiple streamlines are propagated from each voxel in a given seed region and the direction of each is drawn at random from the distribution of directions available, meaning that any given streamline need not follow the path of another. As each streamline

steps through the diffusion data, a connectivity distribution of all possible pathways is built up, with the intensity at a given voxel representing the number of streamlines that have passed through it and reflecting the confidence of a connection existing between the voxel and seed region. Few termination criteria or constraints are required, although often a curvature threshold is applied (Behrens et al. 2003a).

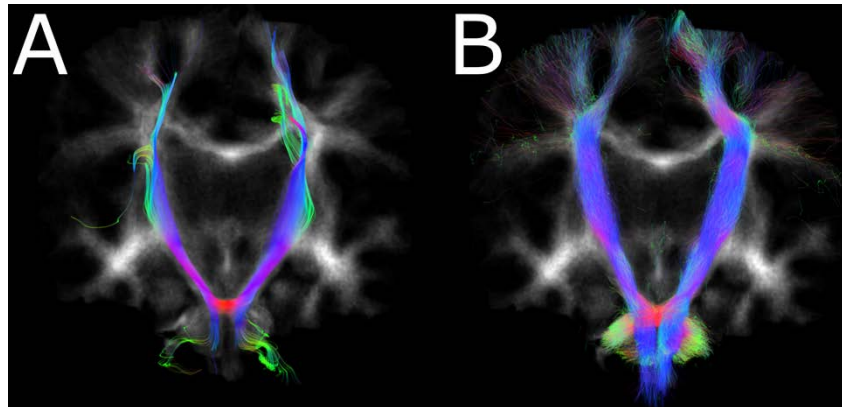


Figure 2.9: Comparison of deterministic and probabilistic tractography. The cortico-spinal tract is delineated in a preterm infant at term-equivalent age with deterministic (A) and probabilistic (B) tractography. Diffusion is modelled voxelwise with the diffusion tensor in (A), and with constrained spherical deconvolution (Tournier et al. 2004), to account for multiple fibre directions, in (B). Note how probabilistic tractography captures the lateral projections of the cortico-spinal tract more fully than deterministic tracking.

Probabilistic tractography allows pathways to be traced in the presence of uncertainty, through multi-fibre populations and into regions of low anisotropy and has proved suitable for neonatal DTI analysis (Bassi et al. 2008, Liu et al. 2010). Importantly, it also provides a measure of connectivity, in terms of pathway probability, that has been used to reliably quantify connections between remote structures in both adult and paediatric populations (Behrens et al. 2003b, Johansen-Berg et al. 2005, Counsell et al. 2007, Traynor et al. 2010). In contrast to voxel-based analysis, tractography generally requires a prior hypothesis on the regions to be tested, with assumptions made on the position and path of the tracts-of-interest but a number of techniques based on the same principles have been developed to investigate whole-brain connectivity in an exploratory manner (Sporns et al. 2005, Hagmann et al. 2008, Gong et al. 2009, Robinson et al. 2010). These techniques can be used to map structural connectivity across the brain as complex networks, analysed with computational methods often drawn from graph theory, attributes of which appear to reflect normal development and are altered in disease states (Strogatz 2001, Stam et al. 2007, Bullmore and Sporns 2009, Rubinov et al. 2009).

Chapter 3

The Developing Brain and Preterm Birth

3.1 Human Brain Development

The period between 24 and 40 weeks of gestation is a critical time in human brain development; the formation of cerebral pathways through axonal growth, neuronal differentiation and synaptogenesis in the cortex that occurs during this time is essential for normal brain development and function (Kostovic and Jovanov-Milosevic 2006, Kostovic and Judas 2010).

In early gestation, brain development is characterised by proliferative processes. Dividing neuroepithelial cells in the wall of the closing neural tube form the ventricular zone (VZ), the cells of which extend radial processes toward the pial surface (Rakic 1988). As the VZ increases in size and surface area, neurogenesis begins and postmitotic cells migrate along the radial scaffold forming transient, laminar structures in the developing neocortex (Hatten 1999). By gestational week 14, six cellular zones are present, as shown in Figure 3.1: the VZ; the subventricular zone (SVZ), which forms the principal site of neuronal and glial proliferation during the second half of gestation; the intermediate zone; the subplate, a transient structure essential for establishing thalamo-cortical and cortico-cortical connections; the cortical plate, formed from the pre-plate and which, along with the marginal zone, will eventually form the six layers of the neocortex (Bystron et al. 2008).

By mid-gestation, the subplate is the thickest of these zones, containing postmitotic and migratory neurons, glial cells and serving as a prominent site for neuronal differentiation and synaptogenesis (Kostovic and Rakic 1990, Kostovic and Judas 2010). In addition, the subplate serves as a major target for growing afferent axons, and a front of afferent fibres originating from the brainstem, thalamus and other cortical regions accumulate within the subplate, forming transient, functional circuits before penetrating the cortical plate between 24 and 26 weeks gestational age (GA) (Kostovic and Goldman-Rakic 1983, Allendoerfer and Shatz 1994, Herrmann et al. 1994, Kostovic and Judas 2002). At this point, the subplate is clearly visible with MRI in both early preterm infants and fetuses *in utero* (Maas et al. 2004, Perkins et al. 2008, Dudink et al. 2010). The coincident timing of subplate development and the highest incidence of major brain pathologies associated with preterm birth indicates that during this period the subplate is specifically vulnerable to injury in these infants (Volpe 2009). From around 26 weeks, the subplate begins to diminish and thalamo-cortical afferents begin to synapse in the deep layers of the cortical plate, before progressing into layers III and IV (Kostovic and Judas 2010). Dendritic differentiation, synaptic formation and glial proliferation increases within the cortical plate,

further demarcating the cortical layers and forming a complex multi-directional fibre arrangement and a change in cortical cytoarchitecture that can be detected with DTI (McKinstry et al. 2002).

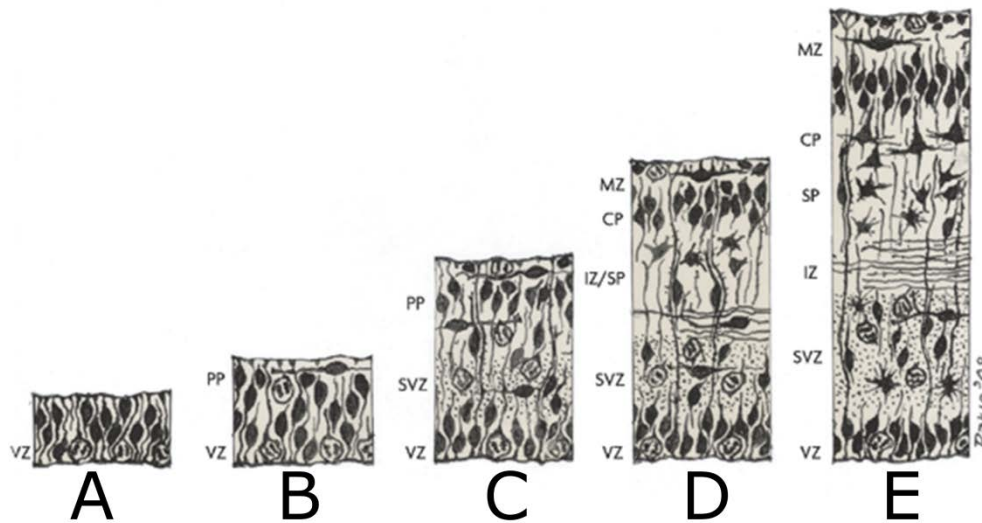


Figure 3.1: Laminar structure of the developing neocortex. Illustration of the sequence of development of the six major transient zones of the developing cortex, shown after approximately 30 (A), 32 (B), 45 (C), 55 (D) and 90 (E) embryonic days. Each zone has a distinct cytoarchitecture and role during development. VZ=ventricular zone, PP=preplate, SVZ=subventricular zone, IZ=intermediate zone, SP=subplate, CP=cortical plate and MZ=marginal zone. Image modified from Figure 1 in Bystron et al. (2008).

From around 30 weeks gestation, the primary cortical gyri and sulci begin to form according to a specific spatiotemporal schedule (Chi et al. 1977) and interhemispheric callosal fibres begin to spread throughout the subplate (Judas et al. 2005, Kostovic and Jovanov-Milosevic 2006). An initial over-production of interhemispheric connections means that the number of axons passing through the corpus callosum is maximal prenatally, prior to postnatal pruning and retraction (LaMantia and Rakic 1990). The continued proliferation of cortico-cortical association and commissural fibres and diminution of the subplate continues towards term.

Myelination

Although essential for normal brain function, the process of myelination predominantly occurs postnatally, progressing in a posterior-to-anterior and medial-to-lateral direction and continuing into adolescence and adulthood (Yakovlev and Lecours 1967, Gilles et al. 1983, Benes 1989). Histological evidence indicates that myelinated fibres are only present in the vestibular and cochlear systems, cerebral peduncles and the inferior sections of the posterior limb of the internal capsule (PLIC) by term (Yakovlev and Lecours 1967). Myelinating oligodendrocytes develop from around mid-gestation according to a well-established lineage with successful stages marked by specific cell-surface antibodies and morphology (Pfeiffer et al. 1993, Back et al. 2007). Oligodendrocyte progenitors originate from the VZ and migrate along radial projections to distribute through the developing cerebral parenchyma, before forming premyelinating, differentiating oligodendrocytes (Miller 2002). Pre-oligodendrocytes account for 90% of all oligodendroglial cells at 28 weeks gestation, reducing to 50% at term as they form

mature myelinating oligodendrocytes, and as a population have a selective vulnerability to the injurious mechanisms associated with preterm brain injury (Back et al. 2001, Volpe et al. 2011).

3.2 Epidemiology of Preterm Birth

Currently, 7-8% of all babies born in the UK are born preterm, typically defined as birth after less than 37 weeks of completed gestation (Health and Social Care Information Centre 2010, Petrou et al. 2011) and the rate of preterm birth in industrialised countries has increased steadily over the past two decades (Beck et al. 2010). The adverse consequences of preterm birth are far-reaching and represent a significant burden to health and education services, as well as to the individual and their family. In the USA alone, where the incidence of preterm birth is significantly greater at 12.5%, the annual societal cost in 2005 was estimated to be at least \$26.2 billion – over \$51 000 per infant (Behrman and Butler 2007).

Some 65-70% of preterm births occur following spontaneous labour or preterm premature rupture of membranes (PPROM; Goldenberg et al. 2008). The aetiology of spontaneous preterm birth is unclear but is unlikely to depend on a single pathologic process. Epidemiological studies have identified a number of factors that confer additional risk for preterm birth (Slattery and Morrison 2002). These include: multiple pregnancies, due in part to the increased use of *in vitro* fertilisation techniques (Gardner et al. 1995, Blondel and Kaminski 2002); low socioeconomic status (Olsen et al. 1995); ethnic origin (Ananth et al. 2001, Steer 2005); substance abuse (Offidani et al. 1995); and maternal infection during pregnancy (Romero et al. 2001). In addition, studies have identified a multitude of underlying biological pathways and possible genetic and epigenetic mechanisms that influence birth timing (Vadillo-Ortega et al. 2002, Vuadens et al. 2003, Lockwood et al. 2005, Roizen et al. 2008, Tobi et al. 2011). However, effective prediction of preterm birth remains difficult, relying on a combination of clinical history, measurements of cervical length and biochemical markers such as foetal fibronectin, thereby limiting the effectiveness of targeted interventional strategies (Lockwood et al. 1991, Hassan et al. 2000, Chandiramani and Shennan 2006).

3.3 Neurodevelopmental Outcome Following Preterm Birth

Preterm birth is the most frequent cause of infant death in the USA, and almost a third of all early neonatal deaths can be attributed to prematurity (Callaghan et al. 2006, Lawn et al. 2006). With advances in perinatal care and specific interventions, including prophylactic antenatal steroids and early surfactant administration, mortality amongst preterm infants and the incidence of major

destructive cerebral lesions have decreased such that survival rates for infants born after more than 32 weeks completed gestation are approaching 100% (Horbar et al. 2002, Slattery and Morrison 2002, Wilson-Costello et al. 2007). However, the overall decrease in preterm neonatal mortality has been accompanied by a rise in morbidity and a high prevalence of cognitive and behavioural deficits in surviving preterm infants (Marlow et al. 2005, Delobel-Ayoub et al. 2009). Evidence from large, population-based studies demonstrate that over half of all infants born at less than twenty-six weeks gestational age suffer some form of developmental impairment by thirty months of age (Wood et al. 2000), with adverse functional and behavioural consequences that may persist into adolescence and early adulthood (Rushe et al. 2001, Hille et al. 2007, Aarnoudse-Moens et al. 2009). These impairments comprise complex and overlapping deficits across motor, sensory and cognitive domains that often occur simultaneously and confer a significant morbidity load on the preterm population.

Motor and sensory outcomes

Cerebral palsy (CP) represents one of the most severe adverse motor outcomes in surviving preterm infants. CP results from perinatal brain injury that disrupts movement and postural control with symptoms that can range from mild to severe and can affect balance, walking, and fine motor tasks with associated disturbances in sensory perception, cognition and behaviour (Bax 1964, Rosenbaum 2006). The risk of developing CP increases proportionally with decreasing gestational age, with 20% of preterm survivors born at less than 26 weeks gestational age diagnosed with CP by age 6 (Hagberg et al. 1996, Marlow et al. 2005, Vohr et al. 2005). Improving medical treatment, most notably the use of antenatal magnesium sulphate, has reduced the risk of cerebral palsy in preterm cohorts (Crowther et al. 2003, Rouse et al. 2008) and a recent study has demonstrated that in those born at less than 34 weeks gestation, the incidence and severity of CP has decreased significantly over the past twenty years (van Haastert et al. 2011).

In the absence of CP, fine motor and coordination impairments are prevalent in preterm populations, with developmental coordination disorders described in up to 30% of preterm children born at less than 32 weeks gestation (Goyen et al. 1998, Huddy et al. 2001, Bracewell and Marlow 2002, Foulder-Hughes and Cooke 2003, Goyen and Lui 2009). In an extremely preterm cohort, after excluding children with CP and/or severe cognitive deficits, Marlow et al. demonstrated that children born extremely preterm performed poorly compared to their term-born peers on a battery of tests designed to measure performance in motor control (i.e.: heel walking), visuospatial integration (i.e.: route finding) and sensorimotor function (i.e.: finger tapping) (Marlow et al. 2007). Although the impact of these deficits to an individual is less than that of CP, it is likely that they contribute to the poor performance at school commonly seen in this population (Marlow et al. 2007).

Sensory morbidity is also highly prevalent following preterm birth. Retinopathy of prematurity (ROP) is a neurovascular retinal disorder that becomes more common and severe with increasing prematurity at birth and can result in significant visual impairment (Repka 2002, Austeng et al. 2009). Prematurity and ROP are associated with visual deficits in childhood and mild visual impairment, defined as squint and/or the need for vision correction, are present in 28% of extremely preterm infants at 6 years, and

44% by 11 years (Marlow et al. 2005, Johnson et al. 2009); a similar prevalence has also been reported in gestationally older cohorts (Holmstrom et al. 1999, Hard et al. 2000, Cooke et al. 2004).

Cognitive outcomes

Adverse neurocognitive outcome is common in preterm survivors and encompasses a wide range of often subtle disorders across several domains including language, learning, attention, memory and behaviour. In a meta-analysis of several case-controlled studies, general cognitive function – defined by intelligence quotient (IQ) – was found to be significantly lower in preterm cohorts compared to their term counterparts when assessed in childhood and early adolescence (Bhutta et al. 2002). Bhutta et al. also demonstrated a linear relationship between IQ and gestational age at birth, and many studies have identified a trend towards lower cognitive scores with increasing prematurity (Breslau et al. 1994, McCarton et al. 1997, Saigal et al. 2000, Taylor et al. 2000, Saigal et al. 2003, Marlow et al. 2005).

However, IQ does not fully capture the range of cognitive dysfunction in this population (Aylward 2002). Often studies employ tests of multiple cognitive processes including memory, reasoning, language processing and attention (Lichtenberger 2005). These test batteries provide a fuller description of cognitive development and are applicable to younger pre-school cohorts, allowing neurodevelopmental assessment at a younger age. Using the Bayley Scales of Infant Development (Bayley 1993; BSID-II), Wood et al. found that extremely preterm infants at thirty months of age performed significantly worse in tests of both mental and psychomotor development compared to term-born controls (Wood et al. 2000). At six years, extremely preterm children without severe neurological impairment from the same cohort performed significantly worse in tests involving sequential and simultaneous mental processing, knowledge of facts, language concepts and other school-related skills as assessed by the Kaufman Assessment Battery for Children (K-ABC) (Kaufman and Kaufman 1983; Marlow et al. 2005). Similarly, significant deficits in memory (Rose and Feldman 1996, de Haan et al. 2000), composite executive functions (Harvey et al. 1999, Anderson et al. 2004) and language development (Breslau et al. 1996, Luoma et al. 1998) have been described in other preterm cohorts. Preterm children are also at much greater risk of developing behavioural problems such as attention deficit/hyperactivity disorder (Botting et al. 1997, Bhutta et al. 2002) and evidence suggests that the prevalence of psychiatric symptoms that may underlie disorders ranging from schizophrenia to autism are also increased in preterm adolescents (Indredavik et al. 2004).

Importantly, various cognitive deficits evident during childhood in this population appear to persist through adolescence and into adulthood. Mean IQ is significantly lower in preterm adults compared to controls (Hack et al. 2002, Lefebvre et al. 2005, Allin et al. 2008), and even after controlling for IQ, Nosarti et al. reported significant deficits in tasks of executive function including response inhibition and mental flexibility (Nosarti et al. 2007). Of note is the fact that these studies are reporting adult outcome in cohorts born when survival rates for extremely preterm infants – those with the worst prognosis in later life – were significantly lower than they are at present, and it is uncertain how improvements in mortality in this vulnerable population will affect outcome in more recently born cohorts (Doyle and Anderson 2010).

3.4 Preterm Brain Injury

The immaturity of the preterm brain renders it specifically vulnerable to perinatal injury and associations between major cerebral tissue lesions and serious neurological disorders such as CP are well documented in preterm populations (Stewart et al. 1999, Dyet et al. 2006). With increasingly advanced imaging techniques, a spectrum of cerebral injuries incorporating both white and grey matter have been identified that may predict later developmental outcome in preterm infants (Volpe 2009).

White matter injury

Periventricular white matter and the highly-vascularised germinal matrix, the neurogenetic layer of cells bordering the lateral ventricles and containing the VZ and SVZ, appear particularly vulnerable to haemorrhage and/or hypoxic-ischaemic insult and the most common indications of severe perinatal cerebral injury are bleeding into the germinal matrix and cystic lesions of the surrounding parenchyma (de Vries et al. 1993, de Vries et al. 1998, de Vries et al. 2001).

Germinal layer haemorrhage (GLH) predominantly occurs within the first 48 hours of life, following rupture of the germinal matrix vasculature (Hambleton and Wigglesworth 1976, Vohr and Ment 1996). Intraventricular haemorrhage (IVH) is a progression of GLH, occurring once the bleeding is substantial enough to penetrate the ventricular wall, filling the cerebral ventricles. IVH is associated with ventricular dilatation, due to altered CSF flow, and in around 5-10% of GLH/IVH cases, venous infarcts form in the periventricular white matter that often evolve to form porencephalic cysts by term-equivalent age (see Figure 3.2; de Vries et al. 2001). The pathogenesis of IVH is multifactorial and includes disturbances to cerebral blood flow (Bada et al. 1990), increases in venous pressure (Nakamura et al. 1990), sepsis (Linder et al. 2003) and the fragile microvasculature of the germinal matrix (Takashima and Tanaka 1978, Ballabh 2010).

Around 40% of infants born before 30 weeks gestation develop GLH/IVH, with the incidence and severity increasing with prematurity at birth (Dyet et al. 2006, Sarkar et al. 2009). The severity of IVH can be graded according to Papile et al. (1978); GLH and low-grade IVH may resolve by term and do not necessarily increase the risk of adverse outcome, but moderate to severe IVH (grades III and IV) is associated with high incidences of neurodevelopmental disabilities in surviving infants (Guzzetta et al. 1986, de Vries et al. 1998, de Vries et al. 2004, Sherlock et al. 2005), although the nature and extent of this disability varies according to the size and location of the haemorrhage (de Vries et al. 1999, Bassan et al. 2007).

Periventricular leucomalacia (PVL) represents a second pattern of cerebral injury predominantly affecting preterm infants born between 23 and 32 weeks gestation (Banker and Larroche 1962, Volpe 2001). The aetiology of PVL has been well described, and involves maturation-dependent contributions from a number of injurious processes: cerebral ischaemia, due to disturbances in cerebrovascular regulation; maternal-foetal infection and systemic inflammation; and the selective vulnerability of

precursor oligodendrocytes to glutamate-induced excitotoxicity, inflammatory cytokine release and free radical attack (Volpe 2001, Back et al. 2007, Deng 2010).

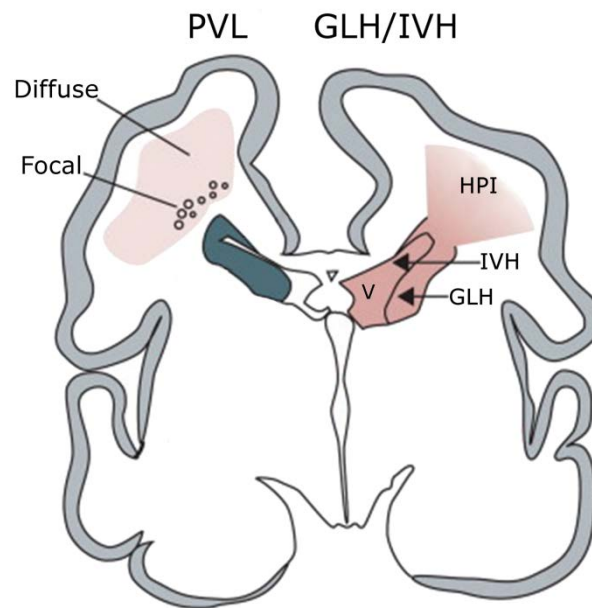


Figure 3.2: White matter injury in the preterm neonate. Common sites of white matter injury are shown on an illustrated coronal section from the brain of a 28-week-old premature infant. White matter surrounding the lateral ventricles (V) is susceptible to ischaemic and haemorrhagic insult resulting in focal and diffuse periventricular leucomalacia (PVL; left) and/or germinal layer/intraventricular haemorrhage (GLH/IVH; right). In extreme cases of GLH/IVH, haemorrhagic parenchymal infarctions (HPI) can form. Image modified from Figure 1 in Volpe (2009).

PVL consists of two principal components: focal, or cystic, PVL characterised by localised necrotic lesions and subsequent formation of cysts in the developing periventricular white matter; and diffuse PVL, a less severe, relatively non-specific white matter lesion (see Figure 3.2; Volpe 2001). In modern neonatal intensive care units, cystic PVL is less common than GLH/IVH – occurring in less than 5% of preterm infants (Larroque et al. 2003, Dyet et al. 2006) – but the neurodevelopmental outcomes are no less severe (Fazzi et al. 1994, Cioni et al. 1997, Resch et al. 2000, van Haastert et al. 2008). Neurodevelopmental disabilities are prevalent in surviving infants and dependent on the extent of the cystic lesions, becoming increasingly worse in cases of extensive, bilateral PVL where a 100% incidence of CP has been reported (Rogers et al. 1994).

Although clinical diagnosis of haemorrhagic infarctions and the cystic components of PVL are readily made with cranial ultrasonography, the increasing availability of early MRI allows better definition of lesions in terms of size and position, and detailed characterisation of deep structures, such as the basal ganglia, and the cortex that correlate well to post-mortem findings (Maalouf et al. 2001, Roelants-van Rijn et al. 2001, Leijser et al. 2009). Moreover, MRI can reveal subtle alterations not visible to ultrasound: Inder et al. demonstrated that early diffusion-weighted imaging can detect altered diffusivity in the periventricular white matter that appears to preface, and extend beyond, the

subsequent appearance of cysts in PVL (Inder et al. 1999). The most common MR-visible abnormality at term-equivalent age is diffuse and excessive high signal intensity (DEHSI) on T_2 -weighted images, present in up to 75% of preterm infants (Maalouf et al. 1999, Dyet et al. 2006, Skiold et al. 2010). Diffuse abnormal signal intensity can also be seen as a loss of T_1 -weighted signal and is commonly associated with ventricular dilatation and increased extracerebral CSF suggestive of white matter injury, and may represent the diffuse component of PVL (Inder et al. 2003). Indeed, Counsell et al. found that diffusivity within regions of abnormal signal intensity is comparable to that observed in more overt white matter pathology, including cystic PVL, and significantly higher than in corresponding regions of preterm infants without white matter abnormality (Counsell et al. 2003). Although the neurobiological basis of abnormal signal intensity is unclear, it occurs with a similar prevalence to the subsequent cognitive and behavioural impairments seen in this population, and altered diffusivity in the developing white matter is associated with short term measures of neurodevelopmental outcome in infants without focal cerebral lesions (Krishnan et al. 2007). These observations are indicative of subtle microstructural alterations that may reflect disturbance of normal maturational processes with long-term consequences (Volpe 2001, Back and Rivkees 2004, Back 2006).

Grey matter injury

Historically, the grey matter abnormalities associated with preterm brain injury have been overlooked in comparison to white matter pathology (Banker and Larroche 1962, Volpe 2005). Earlier neuropathological studies described progressive alterations of neural structure and circuitry in primarily undamaged cortical grey matter that overlaid extensive haemorrhagic or ischaemic white matter injuries (Marin-Padilla 1997, Marin-Padilla 1999). Using volumetric MRI analysis, Inder et al. demonstrated that cortical grey matter at term-equivalent age was reduced by 28% as a consequence of PVL; importantly this loss was seen in infants with both cystic and non-cystic injury when compared to term-born controls (Inder et al. 1999). Since then a number of quantitative MRI studies have demonstrated that the cortical and deep grey matter are specifically vulnerable following preterm birth (see Section 3.5). These observations agree with post-mortem studies that demonstrate neuronal loss and gliosis in the thalamus and cortical grey matter often accompany cystic lesions of the white matter (Pierson et al. 2007, Ligam et al. 2009). That preterm brain injury includes neuronal disturbances is perhaps not surprising given the cognitive deficits commonly observed in ex-preterm children and adolescents.

The ‘encephalopathy of prematurity’

Volpe recently reviewed the constellation of cerebral abnormalities observed in preterm infants, using the term ‘encephalopathy of prematurity’ to capture the spectrum of tissue loss and altered development of white and grey matter of the developing preterm brain (Volpe 2009). This spectrum includes PVL – both cystic and diffuse – neuronal disturbances characterised by tissue loss in the cortex, basal ganglia and brainstem, and axonal disturbance in the connective white matter. Diffuse axonal injury, typified by increased levels of the apoptotic marker fractin and distal to cystic lesions have been recorded in cases of PVL in association with neuronal loss in the thalamus and cortex (Haynes et al. 2008). Coupled with quantitative MRI and DTI studies that have revealed altered white matter

diffusivity and regional tissue losses, even in the absence of severe cerebral injuries (Huppi et al. 1998a, Huppi et al. 1998b, Counsell et al. 2003, Inder et al. 2005, Boardman et al. 2006, Counsell et al. 2006, Kapellou et al. 2006, Boardman et al. 2010), this indicates that preterm brain injury is not limited to single structures or tissue classes, but affects the shared developmental trajectories of connected regions, most notably the thalamo-cortical unit (Volpe 2005, Volpe 2009). It is not yet clear whether these abnormalities represent primary acquired insults or secondary events in a common injurious pathway. Primary neuronal loss in the thalamus or cortex, or axonal disturbance with loss of precursor oligodendrocytes in the white matter could promote anterograde and retrograde degeneration and loss of trophic support between connected regions. Interestingly, subplate neurones that are critical for cortical and thalamic neural development and the establishment of functional neuronal connections have been shown to be specifically vulnerable to hypoxic-ischaemic injury and represent a likely target for primary insult in the preterm period accompanied by widespread secondary effects in both the white and grey matter (Ghosh et al. 1990, Volpe 1996, McQuillen et al. 2003, Kostovic and Judas 2010).

3.5 Quantitative Imaging of the Preterm Brain

Computer-assisted processing tools are increasingly being employed in the analysis of neonatal MRI and can provide the means to perform objective and quantitative investigations of cerebral growth and development that are not available to conventional, qualitative MRI analysis. Volumetric and diffusion analyses, using techniques such as image segmentation and registration, morphometry, TBSS and tractography have the capacity to identify subtle developmental alterations to the preterm brain on a macro- and microstructural scale. Such approaches can be used to identify possible neuroanatomical correlates of the various functional impairments commonly seen in this population.

Volumetry

In preterm neonates, total cerebral volume increases linearly with postmenstrual age (PMA) but appears to be reduced compared to term-born controls by term-equivalent age (Huppi et al. 1998b, Inder et al. 2005, Thompson et al. 2007). This volumetric loss is principally due to significant reductions in cortical and subcortical grey matter and significantly increased ventricular volume (Inder et al. 2005). Regionally, Thompson et al. showed that the greatest relative reduction in tissue volume occurs in the orbito-frontal lobe, with other significant reductions in parieto-occipital, sensori-motor and premotor regions (Thompson et al. 2007). However, in infants with moderate to severe white matter injury, volumetric losses are particularly pronounced, even when compared to other preterm infants (Inder et al. 1999, Lin et al. 2001, Inder et al. 2005, Thompson et al. 2007, Nagasunder et al. 2011), indicating that reduced cerebral volume at term may be exacerbated by earlier injury. Indeed, in a serial MRI study of a small cohort of preterm infants without white matter pathology, Zacharia et al. found that cerebral tissue volumes are similar to those of term-born controls by term-equivalent age (Zacharia et al. 2006). Using nonlinear image registration in a larger cohort, Boardman et al. also found that total

cerebral tissue volume was not significantly reduced in the majority of preterm infants (Boardman et al. 2007). This suggests that global brain growth failure is not an inevitable consequence of preterm birth in the absence of cerebral injury and systemic illness. Similarly, the cerebellum is significantly smaller in preterm infants with PVL but cerebellar volume is not significantly different from term-born controls in the absence of supratentorial lesions (Argyropoulou et al. 2003, Shah et al. 2006, Srinivasan et al. 2006).

Cerebral growth in the neonatal period is characterised by pronounced increases in grey matter and, in particular, cortical grey matter, where a three-fold increase in absolute volume between 29 and 41 weeks postmenstrual age has been reported (Huppi et al. 1998b). The rapid increase in cortical volume during the neonatal period is primarily driven by sulcation and gyrification processes, resulting in an increasingly complex cortical surface as shown in Figure 3.3 (Kapellou et al. 2006, Dubois et al. 2008a). Compared to term-born controls, cortical volume and complexity in preterm infants without white matter injury are significantly reduced by term-equivalent age and are associated with systemic illness severity in the neonatal period and neurodevelopmental outcome in childhood (Ajayi-Obe et al. 2000, Inder et al. 2005, Kapellou et al. 2006, Dubois et al. 2008b, Kaukola et al. 2009b, Rathbone et al. 2011).

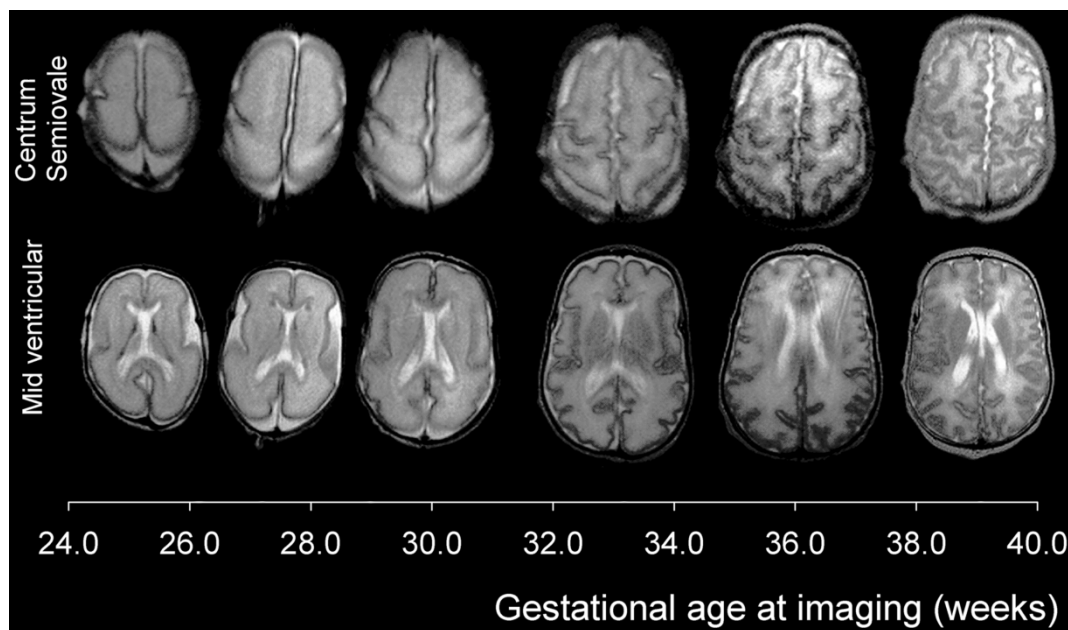


Figure 3.3: Increasing cortical complexity with age. Serial T_2 -weighted MRI acquired from a preterm infant born at 25 weeks gestation. Axial slices are shown at the mid-ventricular level (bottom row) and the level of the centrum semiovale (top row) between birth and term-equivalent age. Image modified from Figure 2 in Kapellou et al. (2006).

Subcortical grey matter growth is also adversely affected by preterm birth. Thalamic atrophy is present in preterm infants with PVL (Nagasunder et al. 2011) but even in the absence of cerebral injury, specific losses are observed. Boardman et al. used DBM to perform a whole-brain survey of tissue volume in a cohort of preterm infants at term-equivalent age without cerebral injury and found discrete tissue loss in the subcortical grey matter, specifically in the lentiform nucleus and thalamus when compared to controls (Boardman et al. 2006). This pattern of subcortical tissue loss was confirmed

using manual segmentation (Srinivasan et al. 2007) and is significantly worse in infants with microstructural alterations of the central white matter, as determined with diffusion imaging (Boardman et al. 2006). Recently, an anatomical phenotype comprising focal tissue loss in the thalamus and globus pallidus and altered diffusivity in the centrum semiovale was found to be strongly associated with development quotient (DQ), a general score assessed with the Griffiths Mental Development Scales (Huntley 1996) and including performance on a number of tests of social, motor-sensory and coordination skills at 2 years of age (Boardman et al. 2010). This suggests that the parallel growth and development of connected cerebral regions has important functional consequences in later life.

Similar associations have been reported between neurodevelopmental outcome and volume in mid-temporal, frontal, ventricular and cerebellar regions at term (Peterson et al. 2003, Inder et al. 2005, Lind et al. 2011, Maunu et al. 2011), although it is difficult to determine if these associations are independent of white matter injury or other confounding perinatal factors. Smaller hippocampal volumes have also been reported in preterm infants and, although these effects fail to reach significance after accounting for cerebral injury, a significant association was found between hippocampal volume and later memory deficits (Beauchamp et al. 2008, Thompson et al. 2008).

Extending beyond childhood, the structural correlates of preterm birth have been well-described. Cerebral tissue loss appears relatively widespread, encompassing grey and white matter in frontal, temporal, and parietal lobes and subcortical grey matter, including the basal ganglia and hippocampus and appears to contribute to cognitive and behavioural outcome (Nosarti et al. 2002, Gimenez et al. 2004, Gimenez et al. 2006a, Gimenez et al. 2006b, Nosarti et al. 2008, Martinussen et al. 2009, Nagy et al. 2009).

Diffusivity

Diffusion-weighted imaging provides a quantitative means to investigate microstructural changes in the developing neonatal brain. Diffusivity in the preterm brain is closely associated with age: between 28 and 30 weeks postmenstrual age, ADC in the central white matter approaches 2 mm²/s and relative anisotropy is around 10% (Huppi et al. 1998a). With increasing maturity, ADC decreases and approaches that of a normal newborn brain by term-equivalent age (around 1 – 1.5 mm²/s) while anisotropy remains considerably lower (Huppi et al. 1998a, Neil et al. 1998, Tanner et al. 2000, Miller et al. 2002, Mukherjee et al. 2002, Dudink et al. 2007). Maturation changes in diffusivity and anisotropy are not uniform across the brain. Early myelinating structures such as the PLIC demonstrate higher anisotropy and lower diffusivity from around 30 weeks gestational age. In contrast, diffusivity in some association tracts can remain relatively high up to term-equivalent age (Huppi et al. 1998a, Partridge et al. 2004). In the cortex, anisotropy peaks at 26 weeks gestational age and decreases with maturity, reaching zero by around 36 weeks (McKinstry et al. 2002, Gupta et al. 2005). Cortical anisotropy changes during this period occur first in the sensori-motor cortex followed by the occipital, frontal and temporal regions (Deipolyi et al. 2005, Gupta et al. 2005, Trivedi et al. 2009).

By term equivalent age, clear differences exist between the cerebral microstructure of a preterm and term-born neonate. By placing anatomically-informed ROI, Huppi et al. demonstrated significantly

decreased anisotropy in the PLIC and the corona radiata in preterm infants at term-equivalent age and without severe focal cerebral tissue lesions, when compared to term born controls (Huppi et al. 1998a). Similar techniques have subsequently revealed decreased FA and/or increased diffusivity in the corpus callosum that appears to be dependent on gestational age at birth (Skiold et al. 2010, Hasegawa et al. 2011, Thompson et al. 2011). Using TBSS to perform whole-brain analyses without the need to place ROI, widespread regions of reduced FA have been reported that include the internal capsule, corpus callosum, frontal white matter, the external capsule, the sagittal stratum and cerebral peduncle and that appear most widespread in the most immature infants, born below 28 weeks gestation (Anjari et al. 2007, Rose et al. 2008). It has also been suggested that certain regions of the preterm brain may have elevated FA by term-equivalent age, although this may reflect altered tissue water content in the full-term neonatal brain (Gimenez et al. 2008, Rose et al. 2008).

Diffusion tractography exploits the directional information captured with DTI to infer likely neural pathways through the brain. Several studies have performed diffusion tractography in preterm infants at term-equivalent age and have shown that developmental changes in tract-specific measurements of FA and diffusivity mirror those obtained with standard DTI analysis in the cortico-spinal tracts, thalamic radiations and corpus callosum (Berman et al. 2005, Partridge et al. 2005, Aeby et al. 2009, de Bruine et al. 2011, Hasegawa et al. 2011). In comparison to term-born controls, the volume of tracts passing through the corpus callosum are also significantly lower in preterm infants (Thompson et al. 2011). Bassi et al. were able to dissect the developing optic radiations using probabilistic tractography and found that FA within the tracts correlates with visual function at term-equivalent age, demonstrating the utility of this technique in quantifying early brain development in neonates (Bassi et al. 2008).

As with structure, diffusivity metrics at term-equivalent age have been shown to predict neurodevelopmental outcome in later childhood. Low FA in the PLIC at term (more than one standard deviation lower than a control group mean) was shown to be significantly associated with poor performance in tests of gross motor function and gait deficits at one and four years, with 6 out of 10 'low FA' infants diagnosed with CP (Rose et al. 2007). In the absence of severe neurological disorders, higher mean diffusivity in the centrum semiovale at term is associated with lower DQ at 2 years of age (Krishnan et al. 2007). More recently, van Kooij et al. used TBSS to reveal a number of associations between cognitive and motor outcome at 2 years – assessed with the BSID-III (Bayley 2006) – and FA in regions including the corpus callosum, fornix, the external capsule and PLIC at term (van Kooij et al. 2011), which mirror the microstructural associations seen in preterm children when imaged at 2 years (Counsell et al. 2008). Beyond infancy, microstructural correlates of preterm birth have been identified throughout the white matter and appear, at least in part, to contribute to the various cognitive deficits commonly seen in ex-preterm adolescents and adults (Nagy et al. 2003, Nagy et al. 2009, Skranes et al. 2009, Eikenes et al. 2011).

Confounding factors

Alongside prematurity at birth, a number of perinatal factors have been identified that impact negatively on cerebral growth and development, are associated with poor neurodevelopmental outcome and may confound studies of brain development in the preterm population. Principally, postnatal sepsis and necrotising enterocolitis are associated with white matter abnormalities and altered cortical development (Krishnan et al. 2007, Kaukola et al. 2009b, Shah et al. 2008); intrauterine growth restriction (IUGR; defined as birth weight less than 2 standard deviations below the age-appropriate mean) is associated with lower cerebral volume and reduced cortical volume and complexity (Inder et al. 2005, Thompson et al. 2007, Dubois et al. 2008b, Esteban et al. 2010); and prolonged respiratory support during neonatal intensive care is associated with poor outcome, global cerebral volume reductions, tissue loss in the deep grey matter, and microstructural alterations in developing white matter (Short et al. 2003, Inder et al. 2005, Boardman et al. 2007, Thompson et al. 2007, Anjari et al. 2009).

In preterm infants the immature lung is also particularly vulnerable to injury and almost 30% of infants born before 29 weeks gestation develop chronic lung disease (Smith et al. 2005). The definition of CLD, widely used in clinical practice in the UK, is the need for respiratory support of any form at 36 weeks postmenstrual age. Chronic lung disease results from inflammation and scarring of the alveoli and is associated with cerebral injury at term and poor neurodevelopmental outcome in childhood (Short et al. 2003, Inder et al. 2005, Baraldi and Filippone 2007, Boardman et al. 2007, Anjari et al. 2009). In these infants, respiratory support in the form of mechanical ventilation and nasal continuous positive airway pressure (cPAP) are necessary for survival but are also associated with adverse outcome and injury. Experimental studies in a primate model of preterm birth and neonatal care have demonstrated that mechanical ventilation after birth is associated with decreased brain growth and subtle neuropathologies that are mitigated only slightly by the use of cPAP instead (Dieni et al. 2004, Loeliger et al. 2006, Verney et al. 2010). These observations are mirrored by *in vivo* demonstrations of altered white matter microstructure, independent of prematurity, in infants who required more than 2 days of mechanical ventilation, and in those that later developed CLD (Anjari et al. 2009). Some evidence also suggests that CLD is one of a few complications of preterm birth that has not declined in incidence in recent years (Groenendaal et al. 2010). This thesis will, in part, focus on the association between CLD and brain development in preterm infants as respiratory morbidity represents a potentially modifiable perinatal factor in this population.

Chapter 4

Tract-Based Spatial Statistics in Preterm Neonates: Optimisation and Application

The data presented in this Chapter have been previously published in Ball et al. (2010); see Appendix C.

4.1 Introduction

Diffuse white matter injury is common among preterm infants at term-equivalent age and DTI has revealed diffuse microstructural disturbances in the developing white matter that are dependent on the degree of prematurity at birth and correlated to short term measures of neurodevelopmental outcome (Huppi et al. 1998a, Counsell et al. 2006, Anjari et al. 2007, Krishnan et al. 2007). In addition, early systemic illness, in the form of chronic lung disease, has been shown to be independently associated with cerebral tissue alterations and impact negatively on outcome (Short et al. 2003, Hansen et al. 2004, Anjari et al. 2009, Westby Wold et al. 2009). Specifically, it has been previously reported that CLD, defined by the need for respiratory support at 36 weeks postmenstrual age, is associated with reduced FA in the left inferior longitudinal fasciculus (ILF), independent of prematurity (Anjari et al. 2009). However, given the significant global reductions in cerebral volume seen in preterm infants requiring prolonged respiratory support (Boardman et al. 2007, Thompson et al. 2007), it is not clear why these microstructural associations should be regionally localised.

Many analyses of neonatal DTI have employed ROI selected *a priori* to measure diffusion parameters directly in native diffusion tensor images (Partridge et al. 2004, Counsell et al. 2006, Cheong et al. 2009, Kaukola et al. 2009a). Although this avoids computationally-demanding image registration and offers a valid method to infer groupwise variation in white matter development, it remains subjective and manually intensive and does not easily allow for comparisons across many subjects. As described in Chapter 2, TBSS is a tool for multi-subject DTI analysis designed to overcome partial volume effects and residual misalignment after registration by projecting data onto a skeletonised representation of major white matter tracts common to the group for voxelwise analysis (Smith et al. 2006).

Neonatal DTI data are often of lower resolution and contrast compared to adult data, and these differences, together with relatively wide variations in brain size and complexity within neonatal populations, pose technical challenges to DTI processing tools, including TBSS. In previous work, some

of these challenges have been partially overcome by using a representative, individual FA map as a study-specific template (Anjari et al. 2007, Anjari et al. 2009), however registration between neonatal FA maps can still fail (Bassi et al. 2008). In addition, registration within TBSS has been empirically optimised for accurate alignment to a group-average map that is distinctly different in both contrast and smoothness to an individual FA map.

Aims

The primary aim of this study is to improve the reliability of TBSS in neonates by implementing two modifications: the inclusion of an initial low DOF linear registration to improve global alignment between neonatal FA maps and a second registration to a population-average FA map to produce accurate projection of individual data on a skeleton for subsequent multi-subject analysis of white matter diffusivity and anisotropy.

As a secondary aim, using the optimised TBSS protocol, the association between prematurity, respiratory morbidity and white matter microstructure is investigated in a cohort of preterm infants imaged at term-equivalent age.

4.2 Materials and Methods

Ethical permission for this study was granted by the Hammersmith and Queen Charlotte's and Chelsea Hospital (QCCH) Research Ethics Committee. Written parental consent was obtained for each infant.

Subjects

Infants were recruited from the Neonatal Intensive Care Unit at QCCH. All infants born at less than 36 weeks gestational age (as defined by the last menstrual period) and who successfully underwent 15-direction DTI at term-equivalent age between March 2005 and October 2008 were eligible for inclusion. Infants were excluded if cystic PVL or HPI was apparent on the term-equivalent MRI. Forty-seven infants were included in a previously reported study of CLD (Anjari et al. 2009).

Ninety-three preterm infants (48 male) underwent successful DTI. The cohort had a median (range) gestational age of 28^{+5} (23^{+4} – 35^{+2}) weeks, median (range) birth weight of 1.10 (0.63 – 3.71) kg and a median (range) postmenstrual age at scan of 41^{+4} (38^{+1} – 46^{+6}) weeks. No infants received postnatal steroids, twenty-nine infants (31%) received mechanical ventilation for a median (range) 2 (1 – 33) days and additional ventilatory support was provided with nasal cPAP and oxygen supplementation. Across the whole cohort, the median (range) time spent receiving any form of respiratory support was 18 (0 – 116) days. According to standard practice at QCCH, prophylactic surfactant was administered to all infants born at less than 30 weeks gestational age. Nineteen infants had CLD, defined by the need for respiratory support at 36 weeks postmenstrual age.

Imaging

MRI was performed on a Philips 3-Tesla system (Philips Medical Systems, Netherlands) using an 8-channel phased array head coil. Single shot EPI DTI was acquired in the transverse plane in 15 non-collinear directions using the following parameters: TR: 8000 ms; TE: 49 ms; slice thickness: 2 mm; field of view: 224 mm; matrix: 128×128 (voxel size: $1.75 \times 1.75 \times 2$ mm); b -value: 750 seconds/mm²; SENSE factor of 2.

All examinations were supervised by a paediatrician experienced in MRI procedures. Infants were sedated with oral chloral hydrate (25 – 50 mg/kg) prior to scanning and pulse oximetry, temperature and electrocardiography data were monitored throughout. Ear protection was used for each infant, comprising earplugs moulded from a silicone-based putty (President Putty, Coltene Whaledent, Mahwah, NJ) placed in the external ear and neonatal earmuffs (MiniMuffs, Natus Medical Inc, San Carlos, CA).

Data analysis

DTI analysis was performed using FMRIB's Diffusion Toolbox (FDT v2.0) and TBSS v1.2 as implemented in FMRIB's Software Library (FSL v4.1; www.fmrib.ox.ac.uk/fsl; Smith et al. 2004). Each infant's diffusion weighted images were affine-registered to the respective non-diffusion weighted image to correct for subject motion and geometric distortions due to eddy currents. Images were brain extracted using Brain Extraction Tool (BET v2.1) and diffusion tensors calculated voxelwise, using a simple least squares fit of the tensor model to the diffusion data. From this, maps of the tensor eigenvalues, λ_1 , λ_2 and λ_3 , describing the diffusion strength in the primary, secondary and tertiary diffusion directions, and FA were calculated.

Image registration

The default TBSS pipeline is optimised for the nonlinear registration of FA maps to the population-average FMRIB58 FA template, constructed by iterative registration of fifty-eight FA maps acquired from healthy adults aged 20-50 years (http://www.fmrib.ox.ac.uk/fsl/data/FMRIB58_FA.html). Alternatively, prior to alignment in standard space, individual FA maps can be aligned to the single subject's FA map that is deemed to be most representative of the population, selected by one-to-one registration of every map to every other. The most typical FA map is affinely-aligned to the FMRIB58 FA template and this transformation is applied to each of the nonlinearly-aligned images to bring the whole population into a standard space (Smith et al. 2006). Study-specific templates, produced using similar approaches, are known to be particularly useful when studying populations that violate assumptions needed for registration to standard space, such as atrophic patient groups, and many paediatric populations (Good et al. 2001, Wilke et al. 2008). However, large differences in size, as are clearly present between neonatal FA maps and the FMRIB58 FA template, have previously been identified as a cause of registration failure when performing affine registration (Jenkinson and Smith 2001). Therefore, previous neonatal TBSS studies have not been performed in FMRIB58 standard space but in the space of the 'most typical' subject (Anjari et al. 2007, Anjari et al. 2009).

To identify an appropriate individual FA map to act as a study-specific target, every subject's FA map was registered to the map of every other subject using FMRIB's Linear Registration Tool (FLIRT v5.5; 12 DOF; default parameters) followed by FNIRT v1.0 (parameters as defined in FA_2_FMRIB58_1mm configuration file). FNIRT models each transformation field as a linear combination of cubic *B*-splines placed on a regular grid, with regularisation based on membrane energy. Registration is performed in a coarse-to-fine manner, beginning with low resolution, sub-sampled images and progressing until the required warp resolution is acquired (Andersson et al. 2007). Each warp field (final resolution: $8.75 \times 8.75 \times 10$ mm) was summarised by a score representing the mean square spline coefficients of displacement across 3 dimensions and the target image was chosen as the one with the minimum mean displacement score from all other subjects in the group, thus deemed to be the most 'typical' image of the group. Using the optimised registration method, the chosen target image was from an infant born at 33^{+2} weeks gestation and imaged at 38^{+2} postmenstrual weeks. The summary mean displacement score (\pm SD) between the target and all other images was $0.76 (\pm 0.32)$.

Registration optimisation

Co-registration of neonatal FA maps using tools optimised for analysis of adult datasets can result in poorly aligned images that prevent meaningful statistical analysis and may result in individual datasets being removed from studies (Bassi et al. 2008). This problem was evident in the current cohort, with a number of co-registrations resulting in gross misalignments (Figure 4.1). The global misalignment resulting from nonlinear registration was shown to be secondary to failed linear registration. To counteract this, an additional 6 DOF linear registration (FLIRT; default parameters) was performed prior to 12 DOF affine registration and nonlinear warping. Following the initial linear registration, the image was resampled according to the estimated 6 DOF transformation matrix, and affine registration performed between the transformed image and the intended target. Both the 6 and 12 DOF registration matrices were then concatenated and entered as an initial estimate for nonlinear registration. To compare both linear registration protocols, every subject's FA map was linearly registered to the map of every other subject using both protocols, resulting in 8556 transformations (after excluding self-to-self registrations). As a measure of similarity, the volumetric difference between every linearly transformed FA map and the intended target FA map was calculated. Successful linear registration should result in more similar volumes between the target and the transformed image.

Secondly, to parallel a typical adult TBSS analysis, where individual FA maps are aligned to a population-based template with smoothness and contrast distinct from an individual FA map, a second set of registrations were performed. After nonlinear registration of all images to the selected subject's FA map, estimated warps, including both the linear and nonlinear transform, were applied to every image to bring them into spatial correspondence. The aligned maps were intensity-averaged to form a mean FA map in the target space. A second iteration of linear (6 and 12 DOF) and nonlinear registrations was performed between the original FA maps and the mean FA map; a second mean FA map was then produced for statistical analysis.

Voxelwise analysis

Using the optimised TBSS pipeline, individual FA maps were aligned into the target space and upsampled to $1 \times 1 \times 1$ mm voxel size using the previously estimated warps. An average FA map was created and thinned by perpendicular non-maximum-suppression to generate a mean FA skeleton to represent the centre of all white matter tracts common to the group. This skeleton was thresholded at $FA > 0.15$ and manually cleaned to include the major white matter pathways but exclude cerebral sinuses and cerebrospinal fluid represented in the skeleton as artefact. Individual FA, AD – the magnitude of the principle vector of the diffusion tensor, λ_1 – and RD – the mean magnitude of the transverse vectors, λ_2 and λ_3 – data were then projected onto this skeleton prior to statistical analysis.

Voxelwise cross-subject statistical analysis was performed with Randomise v2.1 (Nichols and Holmes 2002) using univariate linear modelling in the form of a general linear model. The effect of chronic lung disease on RD, AD and FA was investigated. Infants with CLD had a significantly lower mean gestational age at birth (CLD: 26.26 ± 1.62 weeks; No CLD: 29.74 ± 2.84 weeks; t -test, $p < 0.001$) and significantly higher postmenstrual age at scan (CLD: 42.13 ± 1.98 weeks; No CLD: 41.33 ± 1.42 weeks; t -test, $p < 0.05$) than infants without CLD. Both gestational age at birth and postmenstrual age at scan were widely associated with altered diffusivity, therefore both were included as covariates. Linear regression was also performed to investigate the relationship between length of respiratory support and white matter diffusion metrics, correcting for gestational age at birth and postmenstrual age at scan. All images were subject to Familywise Error (FWE)-correction for multiple comparisons following threshold-free cluster enhancement (TFCE; Smith and Nichols 2009) and are shown at $p < 0.05$.

Where stated, further statistical analysis was performed using SPSS 16.0 (SPSS Inc., Chicago, IL, USA).

4.3 Results: Optimisation

Introducing an additional linear registration

Figure 4.1A shows the summary mean warp displacement scores from transformations between each subject's FA map ($n = 93$) and the map of every other subject using a 12 DOF affine registration followed by nonlinear registration. For each target, a column of scores summarises transformations to every other FA map.

Using the original protocol, mean displacement scores greater than 10 (mean = 1.42, range = 0 – 19.52) were present after registration to 29 out of 93 targets (31.2%). Figure 4.1C demonstrates how summary displacement scores of different magnitudes are represented in transformed FA maps. Large displacement scores represent registrations that have globally failed to align the image to the intended target. Applying a 6 DOF linear registration prior to affine registration significantly reduced mean displacement scores across the whole group (mean = 1.11, range = 0 – 9.30; Figure 4.1B). The

symmetric nature of the matrix in figure 4.1B indicates that two FA maps in particular (from subject 29 and subject 81) required large displacements to bring them into alignment with several other images. Visual inspection of the original datasets revealed that both infants were plagiocephalic, a condition characterised by an asymmetric lateral distortion of the skull.

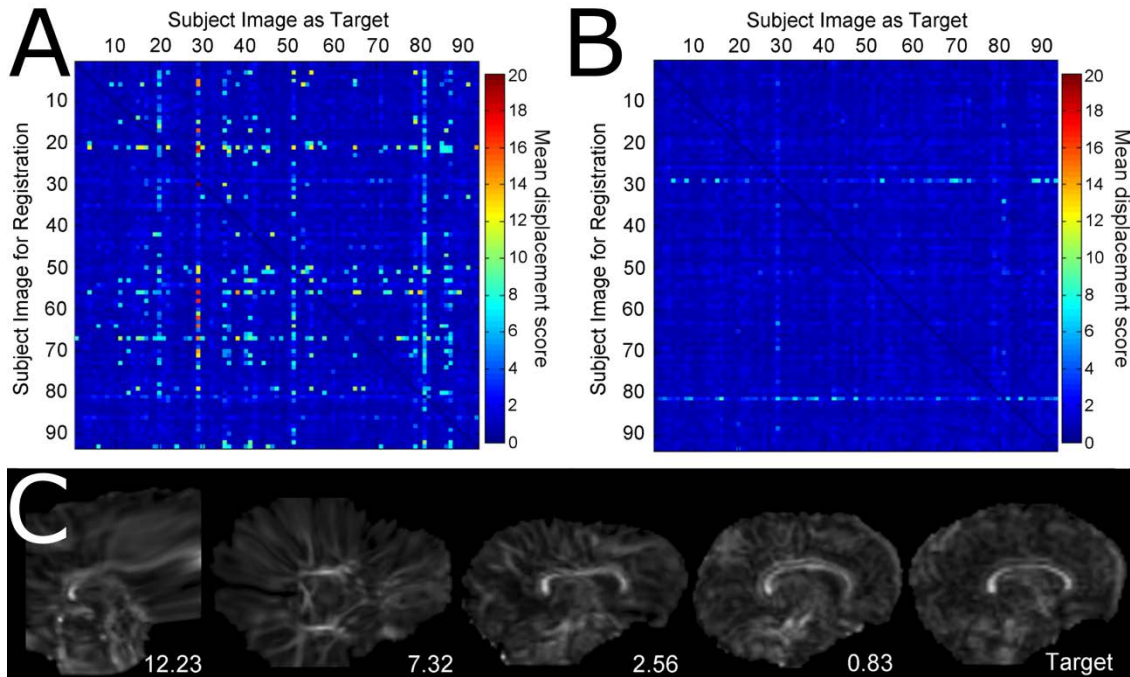


Figure 4.1: Mean displacements after all-to-all registration of FA maps. Matrices showing mean warp displacement scores as a summary of linear and nonlinear transformations between every subject's FA map, using the original registration parameters (A) of a 12 DOF affine registration followed by nonlinear registration and (B) with an additional 6 DOF linear registration. Examples in (C) were obtained by registering four FA maps to a target (right) and are displayed with the summary displacement scores of each transformation.

Additionally, applying an additional 6 DOF linear registration improved alignment in registrations that failed, but was not detrimental to registrations that were successful using the original protocol. Figure 4.2 shows two example registrations to the same target (right column) using the original protocol; one that failed (top row; mean displacement score = 6.41) and one that was successful (bottom row; mean displacement score = 0.65). Registration with the modified protocol resulted in accurate anatomical alignment in both cases, improving the registration that failed initially (top row; modified mean displacement score = 0.61) but with a similar outcome to the successful registration (bottom row; modified mean displacement score = 0.52).

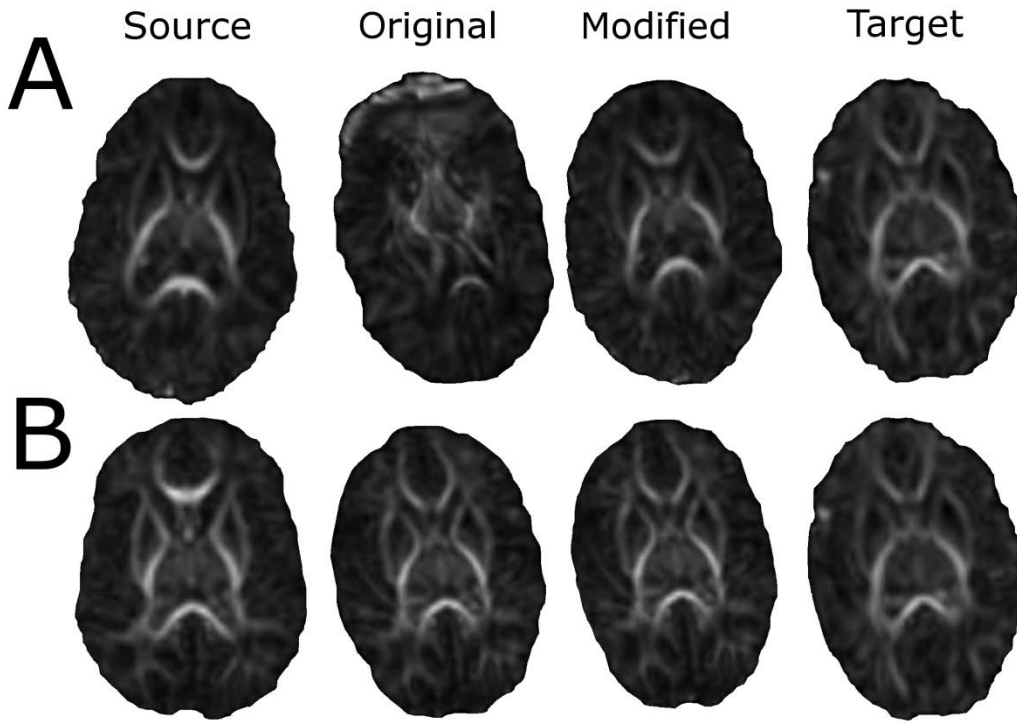


Figure 4.2: Example registrations between source and target FA maps using the original and modified registration protocols. Transformed FA maps following failed (A) and successful (B) registrations between source (left column) and target (right column) maps using the original (second column) and modified (third column) protocol.

Global misalignment prior to nonlinear registration was hypothesised to be the source of large mean displacement scores, as the relatively small local deformations normally performed during nonlinear registration would not be expected to result in such large warps. To test this, each FA map was registered to every other map with linear registration *only*. 8556 linear registrations (excluding self-to-self registrations) were performed with a single 12 DOF step resulting in a median difference in volume between transformed images and their intended targets of 28.4 cm^3 (interquartile range $8.6 - 51.4 \text{ cm}^3$). With an additional 6 DOF registration, the median difference in volume was 12.7 cm^3 (interquartile range: $8.0 - 17.7 \text{ cm}^3$). Figure 4.3 shows the distribution of volume differences in cm^3 between each transformed FA map and their intended target following a 12 DOF registration and both 6 and 12 DOF registrations. 2327 (27.2%) of the 12 DOF transformations produced transformed images that differed in volume from the target image by more than the maximum difference produced through the two-step process, indicating large scaling errors in the single 12 DOF linear transformation.

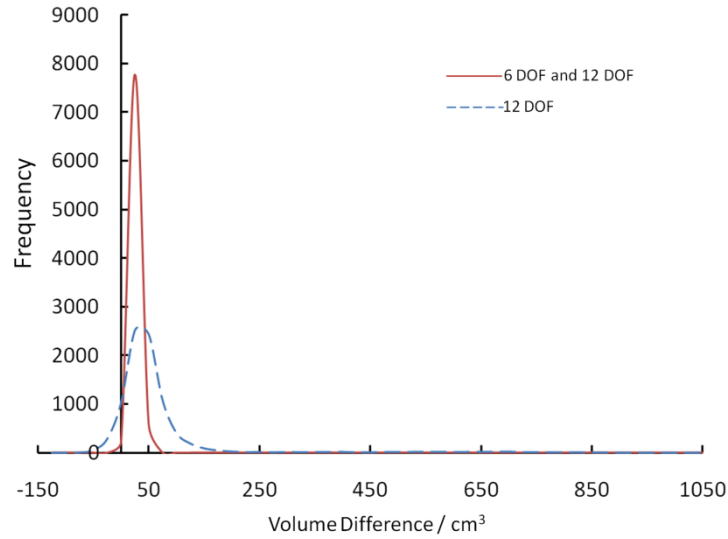


Figure 4.3: Volume difference between transformed images and intended target images following linear registration. Linear registration comprised a single 12 DOF affine registration (dashed line, range: $-112.8 - 1027.4 \text{ cm}^3$) or 6 followed by 12 DOF linear registration (solid line, range: $-15.2 - 48.7 \text{ cm}^3$).

Using an average FA map as a target

In order to more closely reproduce typical TBSS analyses, the effect of registration and projection of individual neonatal FA data onto a population-average FA map instead of an individual FA map was investigated. Figure 4.4 shows voxelwise standard deviation of FA across the group calculated after co-registration of all images to the chosen target and registration to the subsequently calculated mean FA map. Higher standard deviation is visible in several regions including the genu and splenium of the corpus callosum and cortico-spinal tracts (Figure 4.4A; black arrows) after registration to the individual FA map. To quantify the effect of the increased variance on the skeletonisation and projection step of the TBSS protocol, Figure 4.5 shows a Bland-Altman plot of FA extracted from the intersection of both skeletonised datasets. Projected FA was significantly higher across the whole skeleton after registration to the mean FA map (paired t -test: $p < 0.01$).

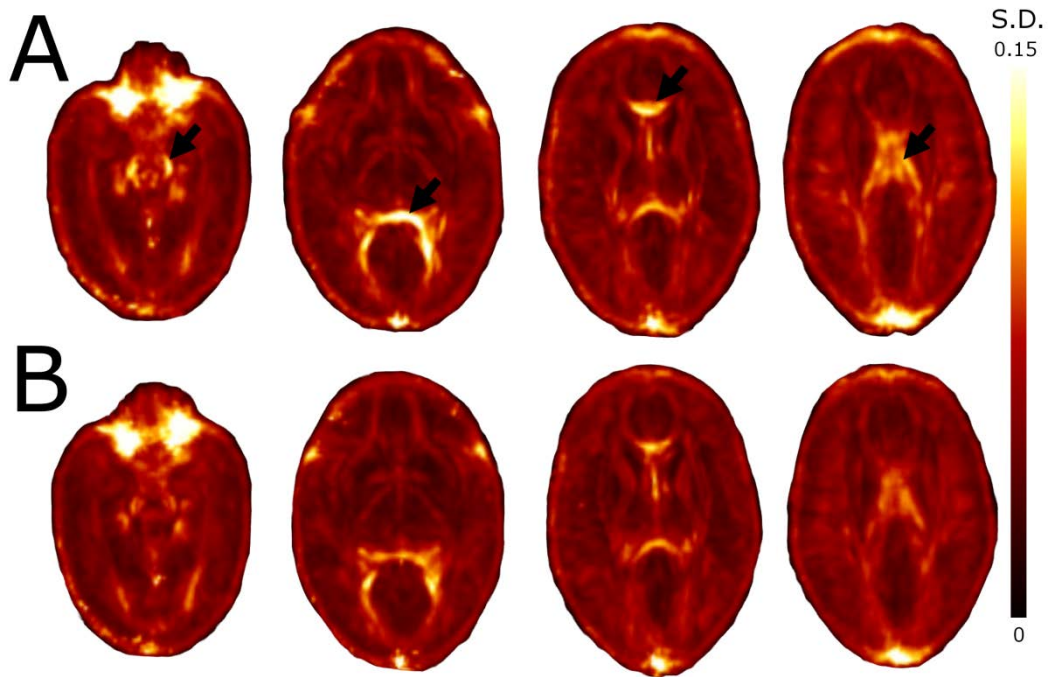


Figure 4.4: Standard deviation of FA after registration to an individual or population-average FA map. Black arrowheads indicate where standard deviation (SD) was greater after registration of all FA maps to an individual target map (A) compared to the population-average map (B). Colour bar indicates SD.

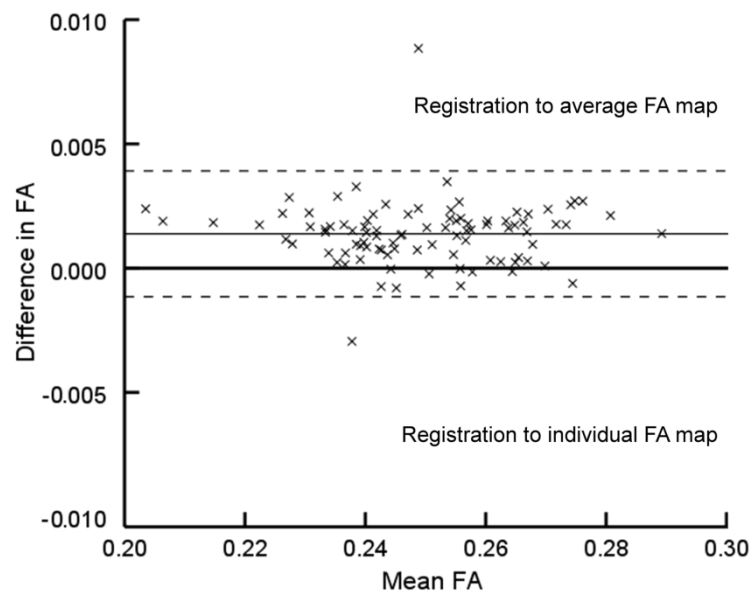


Figure 4.5: Higher projected FA across the mean skeleton following registration to a mean FA map. A Bland-Altman plot shows FA across the skeleton after registration to an individual target FA map and the population-average map. Median difference in FA and 95% confidence intervals are shown with solid and dotted lines.

Optimised registration pipeline

Figure 4.6 shows the optimised pipeline for TBSS preprocessing of neonatal DTI data. After the registration of every subject's FA map to each other, using two linear registration steps prior to nonlinear registration, the target described with minimum mean warp displacement score is chosen as the most 'typical' image, the chosen target. The estimated transformations are then applied to each image to align them in the target space and an average FA map is created, the mean FA map. A second set of registrations is completed to register every individual FA map to the mean FA map. The aligned images are then used to create another mean FA map and a mean FA skeleton that are passed into voxelwise statistical analysis.

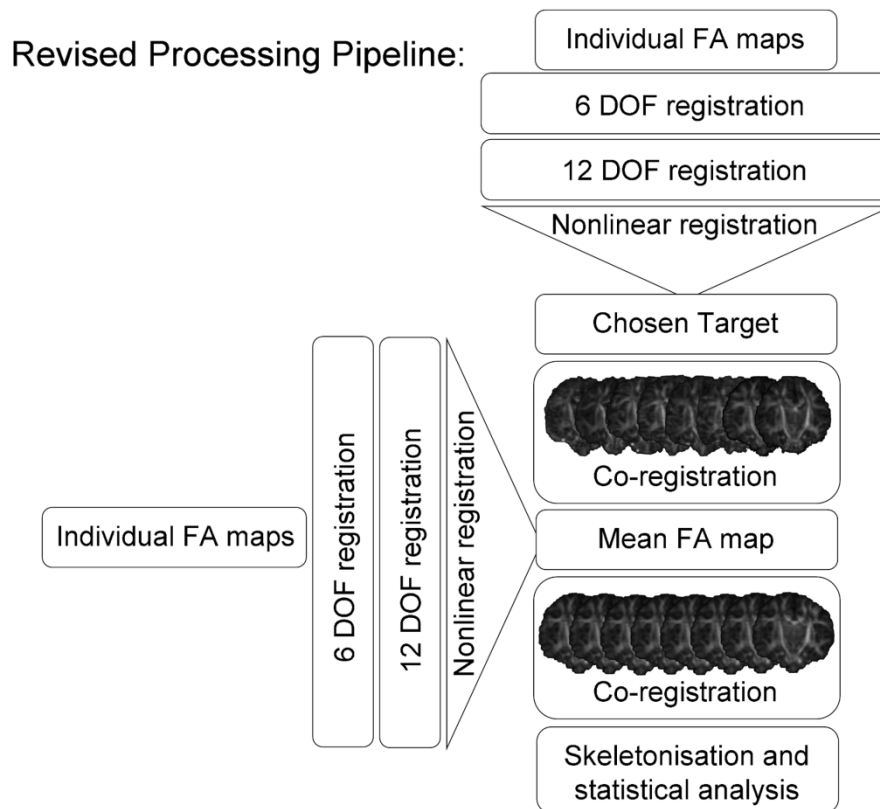


Figure 4.6: Revised processing pipeline for use in TBSS analysis of neonatal diffusion datasets.

4.4 Results: Investigating Respiratory Morbidity in Preterm Infants

Prematurity and age at imaging

To better characterise microstructural development of this population, prior to investigating associations with chronic lung disease, relationships between gestational age at birth, age at scan and white matter diffusivity were determined with the optimised TBSS protocol. Increasing age at scan was associated with globally increased FA (FWE-corrected for multiple comparisons, $p < 0.05$; Figure 4.7A).

Figure 4.7B shows widespread linear associations between FA and gestational age at birth, after correcting for the age of each infant at imaging (FWE-corrected, $p < 0.05$). Within these regions, linear regression showed that increasing prematurity was independently associated with increasing radial (partial $r = -0.45$, $p < 0.001$; full model: $R^2 = 0.35$, $p < 0.001$) and, to a lesser extent, axial (partial $r = -0.24$, $p < 0.05$; full model: $R^2 = 0.12$, $p < 0.005$) diffusivity at term, when entered into a model with age at scan as a covariate.

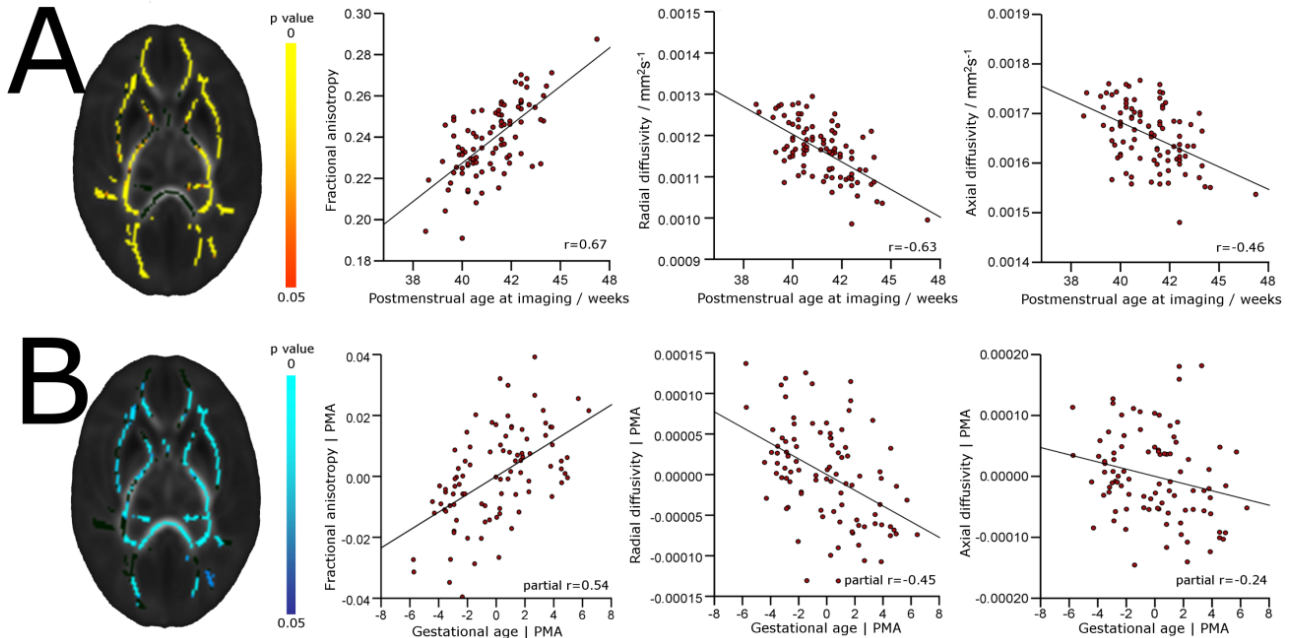


Figure 4.7: Associations between white matter microstructure, age at scan and gestational age at birth. FA was significantly associated with age at scan (row A; first column), correlations between mean FA (second column), RD (third column) and AD (last column) extracted from significant voxels and postmenstrual age at scan are shown. Row (B) shows where FA was significantly associated with GA at birth, after correcting for age at scan (first column). Partial regression plots show the relationship between GA and mean FA (second column), RD (third column) and AD (last column) extracted from significant voxels and corrected for age at scan (PMA). Images are FWE-corrected at $p < 0.05$ (colour bars indicate p-value).

Chronic lung disease

RD was significantly increased (Figure 4.8A) and FA significantly decreased (Figure 4.9B) in infants with chronic lung disease (FWE-corrected, $p < 0.05$), correcting for both gestational age and the postmenstrual age of each infant at scan. Increases in AD failed to reach significance after correction for multiple comparisons. RD was significantly increased bilaterally in the ILF, internal capsule and centrum semiovale and in the left external capsule and corpus callosum, including the genu and the splenium. Increased RD corresponded to regions of significantly decreased FA, seen in the ILF, left external capsule, centrum semiovale and corpus callosum. RD and FA values were extracted from significant voxels in Figure 4.8A and 4.8B, respectively. Mean RD was increased by around 6.0% in infants with chronic lung disease (CLD: mean RD = $0.00124 \text{ mm}^2/\text{s}$, SD = $0.00006 \text{ mm}^2/\text{s}$; No CLD:

mean RD = 0.00117 mm²/s, SD = 0.00008 mm²/s) whereas mean FA was decreased by around 6.4% (CLD: mean FA = 0.264, SD = 0.027; no CLD: mean FA = 0.282, SD = 0.019).

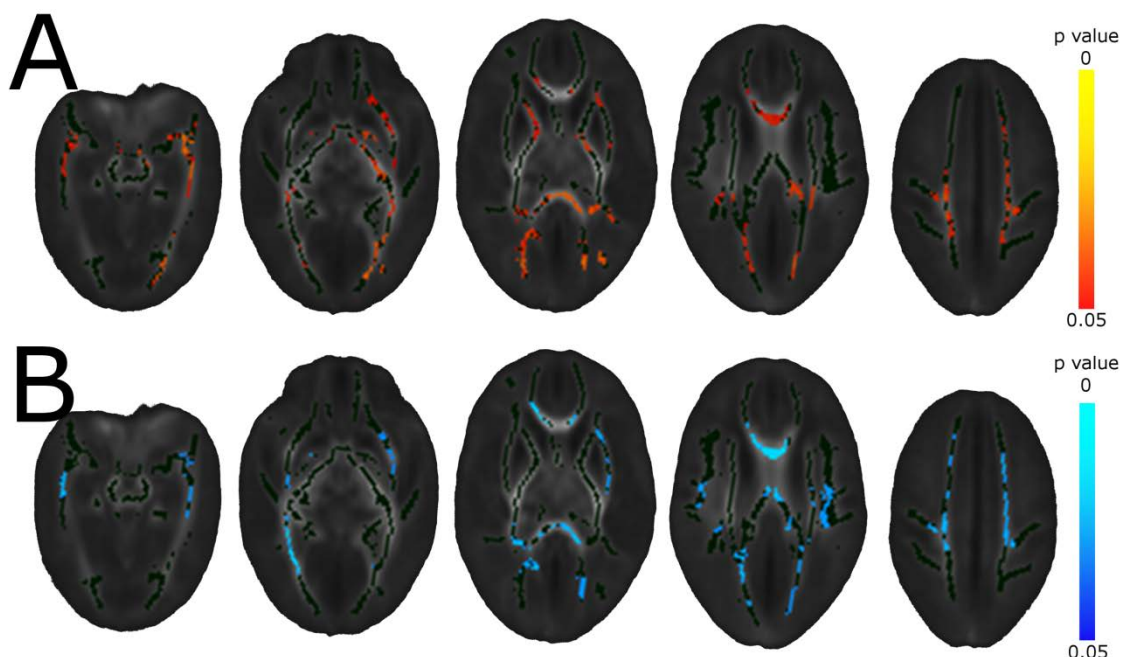


Figure 4.8: Chronic lung disease is associated with increased RD and decreased FA. Significant associations between CLD and RD (A), and FA (B) are shown FWE-corrected at $p < 0.05$, independent of both GA at birth and PMA at scan (colour bars indicate p-value).

Length of respiratory support

Seventy-eight infants (83.9%) required some form of respiratory support postnatally for a median 18 days (range: 0 – 116 days). Figure 4.9 shows regions where AD, RD and FA were linearly associated with the length of respiratory support received across the whole cohort (FWE-corrected for multiple comparisons, $p < 0.05$), after correcting for both gestational age at birth and the age of each infant at scan. Increasing AD was found in the centrum semiovale, corpus callosum and internal and external capsules. Increases in RD appeared more widespread, incorporating most of the white matter skeleton and, in many regions, surviving at a threshold of $p < 0.01$ corrected. Decreasing FA was observed across the skeleton and corresponded to regions of increasing RD and, to a lesser extent, increasing AD. To demonstrate these relationships, individual data were extracted from significant voxels in each image and plotted in partial correlation plots showing the associations between respiratory support and AD (partial $r = 0.48$, $p < 0.001$; full model: $R^2 = 0.34$, $p < 0.001$), RD (partial $r = 0.45$, $p < 0.001$; full model: $R^2 = 0.49$, $p < 0.001$) and FA (partial $r = -0.44$, $p < 0.001$; full model: $R^2 = 0.48$, $p < 0.001$) independent of gestational age at birth and age at scan.

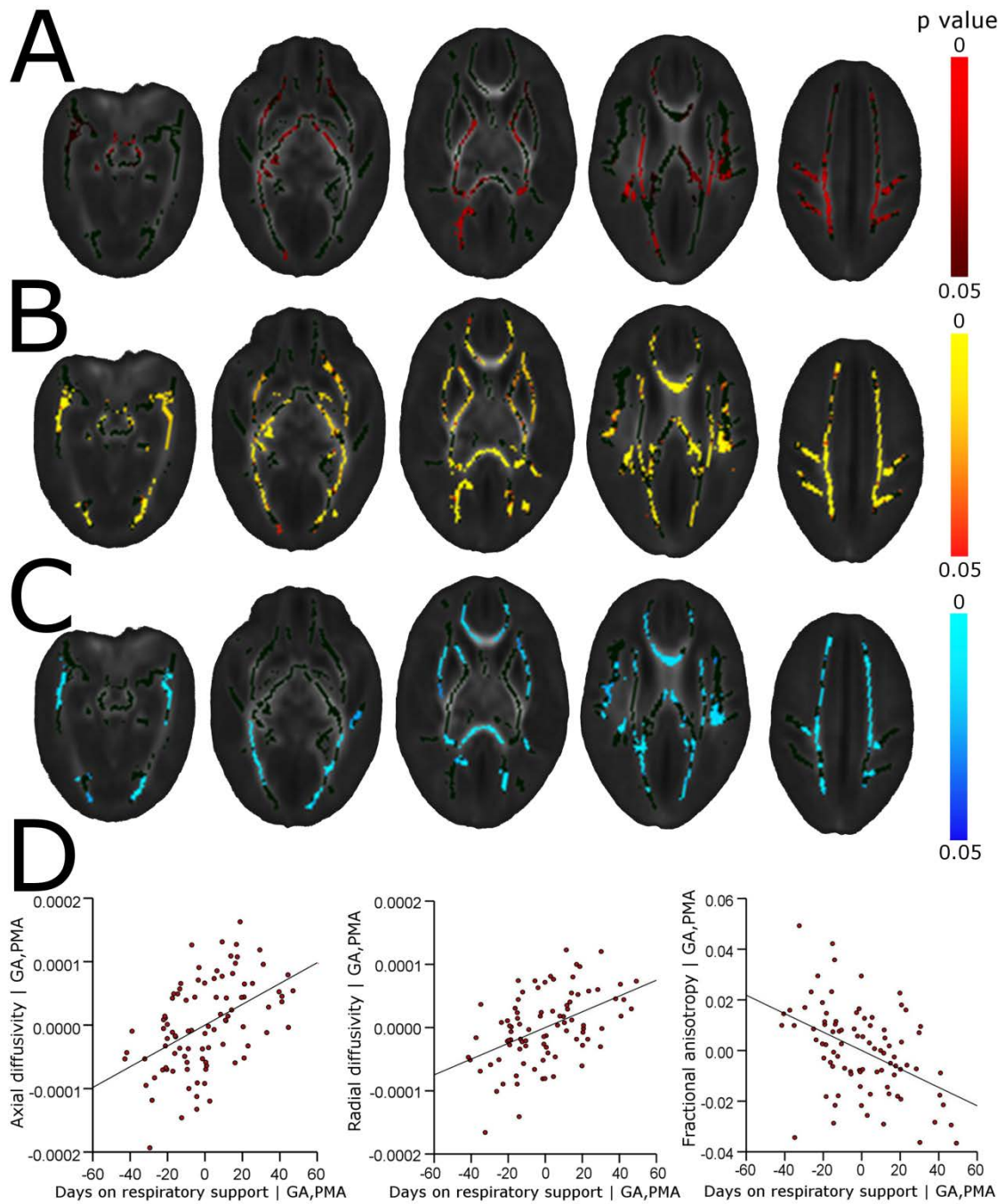


Figure 4.9: Increased length of neonatal respiratory support is associated with altered white matter microstructure. Increasing axial (A) and radial (B) diffusivity and decreasing FA (C) is associated with increasing respiratory support requirements, independent of GA at birth and PMA at scan (FWE-corrected, $p < 0.05$; colour bars indicate p-value). AD, RD and FA were extracted from each significant voxel in (A), (B) and (C), respectively, and entered into linear regression with length of respiratory support, GA at birth and PMA at scan. Partial regression plots showing the relationship between respiratory support and AD, RD, and FA are shown in (D).

4.5 Discussion

This study demonstrates that the existing TBSS pipeline developed for adult data is suboptimal for neonatal studies and through key modifications steps it can be optimised to reliably and precisely co-register neonatal DTI data. This method has been used to demonstrate strong, widespread associations between white matter anisotropy and diffusivity and both increasing prematurity at birth and respiratory morbidity in preterm infants.

The advantages of using TBSS for analysis of diffusion data are that it provides an objective method for multi-subject, whole-brain diffusion data analysis. Central to the method is the need for accurate spatial alignment of individual datasets through linear and nonlinear registration. Neonatal diffusion datasets are frequently of lower resolution and contrast compared with adult data, and neonates are substantially more diverse in terms of both brain volume and complexity as a population. Here, the introduction of an additional low DOF registration step prior to nonlinear registration has been shown to improve global alignment between neonatal FA maps. This method requires minimal extra processing time, it does not require alterations to the default parameters of the nonlinear registration tool FNIRT, which has been optimised specifically for DTI data, and does not adversely affect registrations that were successful using the default protocol.

Improving the reliability of neonatal registration removes the need to exclude datasets based solely on the inability to register them. To demonstrate, two FA maps proved particularly problematic for the registration procedure. Both of these were from plagiocephalic infants – a condition likely to have had an adverse outcome on image registration – and transformations between these maps and others were summarised by relatively large mean displacement scores (maximum = 9.03) using the optimised protocol. However, large displacements were not readily detected by visual inspection of the transformed images after registration to the chosen target for subsequent analysis.

The second modification required a second set of registrations between each FA map and a mean FA map created from the initial transformations into the space of the chosen target. Although registration to the individual and mean maps produced very similar mean FA maps and skeletons, there was greater variance in voxelwise FA after registration to the individual target, indicating that the co-registration of data was more variable. Subsequently, significantly higher projected FA from individual datasets onto the group skeleton was observed after registration to the mean FA target. The skeletonisation process within TBSS is designed to overcome some residual misalignment between subjects after the initial nonlinear registration (Smith et al. 2006) but this may signify that less precise registration to the individual FA map had an adverse effect on the subsequent data projection. As noted by Good et al., it is typically advantageous in structural MRI studies to use a population-specific target rather than a generic template or individual image (Good et al. 2001). Indeed, the benefits of population-average targets in volumetric studies of paediatric cohorts have been well described elsewhere (Aljabar et al. 2008, Altaye et al. 2008, Wilke et al. 2008). In previous studies where FNIRT has been used as part of the TBSS pipeline and a study-specific template was required, the precedent

has been to select a subject from the group and use their individual FA map as the target (Odegard et al. 2009, Roosendaal et al. 2009, Barrick et al. 2010, Giorgio et al. 2010b). This is the first study that demonstrates quantifiable improvements in DTI analysis through the use of an average, study-specific template in TBSS. Although the increase in mean FA proved to be small and the computational time required for data processing was effectively doubled, this is an important step to incorporate into studies requiring a subject-specific target, particularly those involving paediatric or neonatal cohorts. TBSS is designed to project data from the centre of white matter tracts onto the mean skeleton and due to the nature of the relationship between FA and tissue microstructure, it is likely that the higher skeleton FA better represents the tract centre in these individuals (Basser and Pierpaoli 1996). Other studies have recently used two sets of registrations to produce study-specific TBSS templates (Douaud et al. 2011) or employed the optimised TBSS pipeline for neonatal TBSS analysis (Bassi et al. 2011, van Kooij et al. 2011).

The secondary aim of this study was to use the modified TBSS pipeline to further investigate the association between white matter microstructural development, prematurity and respiratory morbidity in preterm neonates. Recently, TBSS has been used successfully to demonstrate the association between prematurity and chronic lung disease on FA in preterm infants (Anjari et al. 2007, Anjari et al. 2009). Here, widespread associations between increasing prematurity at birth and altered white matter microstructure at term-equivalent age were observed. After regressing out the strong effect of prematurity, a more widespread association of CLD with both FA and RD, incorporating not just the ILF bilaterally but also the corpus callosum and centrum semiovale, was observed.

Diffuse white matter changes in the absence of more obvious focal lesions are now the most common abnormality detected by conventional MRI (Dyet et al. 2006). Defining normal white matter in preterm infants with conventional MRI is a subjective process, however by using diffusion metrics such as FA and RD it is possible to perform an objective analysis of white matter integrity and capture more fully the spectrum of abnormality present in this population. DTI has revealed diffuse microstructural disturbances in the form of altered diffusivity and anisotropy in the developing white matter in preterm infants (Huppi et al. 1998a, Miller et al. 2002, Partridge et al. 2004, Counsell et al. 2006, Anjari et al. 2007, Cheong et al. 2009). Experimental evidence suggests that FA is primarily dependent on axonal thickness, density and myelination (Sakuma et al. 1991, Takagi et al. 2009). At term-equivalent age, within the telencephalon, only the PLIC displays histological evidence of myelination (Yakovlev and Lecours 1967). Most regions with observed alterations in this study are likely to be at a stage of premyelination, characterised by various processes including axonal widening and packing and association with immature oligodendroglia (Jessen and Mirsky 1991, Wimberger et al. 1995). Experimentally, the appearance and association of precursor oligodendroglia are enough to induce anisotropy in white matter in a process primarily driven by changes in RD (Drobyshevsky et al. 2005). This suggests that the diffuse and gestation-dependent alterations to white matter microstructure may represent a delay in normal maturational processes of the developing white matter.

Additionally, converging evidence suggests that systemic illness in the neonatal period increases the risk of injury and adverse neurodevelopmental outcome (Miller and Ferriero 2009) and early systemic illness, in the form of chronic lung disease, impacts negatively on white matter microstructure and neurocognitive outcome (Short et al. 2003, Anjari et al. 2009). In a primate model of premature birth prolonged exposure to ventilation is associated with adverse cerebral outcomes including reduced oligodendroglia number, volume loss and white matter injury, regardless of the type of ventilation used (Loeliger et al. 2006), and others have found that CLD is a risk factor for global reductions in brain size at term equivalent age (Boardman et al. 2007, Thompson et al. 2007). These findings are consistent with clinical, imaging, and experimental data that suggest an association between respiratory disease and abnormal brain development (Short et al. 2003, Anjari et al. 2009, Chahboune et al. 2009). This indicates that numerous injurious processes associated with preterm birth and systemic illness and mediated through inflammatory or excitotoxic pathways (Arai et al. 1995, Back et al. 2005, Bell et al. 2005, Robinson et al. 2006, Ligam et al. 2009) may potentiate the observed gestation-dependent microstructural alterations in this population. Importantly, a linear relationship between white matter microstructural development by term-equivalent age and the length of respiratory support required during the neonatal period was demonstrated. This association has recently been shown to persist into adolescence (Eikenes et al. 2011) confirming that the clinical care window for this population represents a critical period for vulnerability following preterm birth (Allendoerfer and Shatz 1994, Kostovic and Judas 2010).

In conclusion, the modified protocol improves the robustness of TBSS preprocessing in the analysis of neonatal DTI datasets. Respiratory morbidity is a potentially modifiable factor that appears to be associated with adverse brain development in preterm infants.

Chapter 5

Thalamic and Cortical Development Following Preterm Birth

The data presented in this Chapter have been previously published in Ball et al. (2011b); see Appendix D.

5.1 Introduction

In addition to the diffuse microstructural alterations to the cerebral white matter described in Chapter 4, morphometric MR studies have identified macro-scale alterations to cerebral tissue structure in preterm populations, which taken together are thought to reflect disturbances of key developmental processes during the neonatal period.

Using tissue segmentation methods, significant reductions in cerebral volume have been reported in preterm infants at term-equivalent age when compared to term-born controls (Inder et al. 2005). However, global reduction of brain growth does not appear to be an inevitable consequence of preterm birth, particularly in the absence of severe white matter injury or systemic illness (Zacharia et al. 2006, Boardman et al. 2007). Instead, current evidence suggests that tissue loss may occur in a more localised manner. Global cerebral loss appears in the most part driven by reduced tissue volume in the cortical and subcortical grey matter (Inder et al. 2005) and cortical disturbances arising before term, reported in terms of both volume and complexity, have also been shown to predict neurocognitive abilities at 1, 2 and 6 years (Inder et al. 2005, Kapellou et al. 2006, Rathbone et al. 2011). Regional tissue loss has also been observed in the hippocampus (Thompson et al. 2008), in a manner that predicts performance in later cognitive tests (Beauchamp et al. 2008).

In particular, and in the absence of severe white matter pathology, the subcortical grey matter and, specifically, the thalamus appears distinctively vulnerable following preterm birth (Boardman et al. 2006, Srinivasan et al. 2007). Volumetric deficits in the thalamus appear to be dependent on prematurity at birth (Inder et al. 2005) and a pattern of injury that includes thalamic volume loss and microstructural change in white matter is associated with neurodevelopmental outcome in early childhood (Boardman et al. 2010).

Observations of altered cerebral development that extend beyond white matter injury support the concept of an ‘encephalopathy of prematurity’, a complex of white and grey matter abnormalities that includes disruptions to the thalamo-cortical system with linked disturbances in the development and function of thalamic nuclei, topographically-related cortical regions and connecting white matter tracts (Volpe 2009). Transient developmental processes that underlie thalamo-cortical connectivity occur during a critical window for vulnerability following preterm birth and disruption of these processes may result in complex cerebral abnormalities (Allendoerfer and Shatz 1994, Kostovic and Judas 2010).

Aim

The aim of this study is to examine the thalamo-cortical system of preterm infants at term-equivalent age, testing the hypothesis that tissue loss in the thalamus is associated with changes in the associated cortical grey matter and alterations in the cerebral white matter containing thalamo-cortical tracts.

5.2 Materials and Methods

Ethical permission for this study was granted by the Hammersmith and QCCH Research Ethics Committee. Written parental consent was obtained for each infant.

Subjects

All infants born at less than 36 weeks gestational age (as defined by the last menstrual period) between March 2005 and October 2008 who successfully underwent T_1 - and T_2 -weighted MRI and 15-direction DTI acquisition at term-equivalent age were eligible for inclusion. Infants were excluded if cystic PVL or HPI was apparent on the term-equivalent MRI. All infants were included in the study described in Chapter 4.

Seventy-four preterm infants (42 male) underwent successful imaging; three infants were removed prior to statistical analysis due to unsatisfactory alignment to the reference template. The final cohort of seventy-one did not differ from the original cohort in gestational age, postmenstrual age at scan, birth weight or gender. The final cohort (41 male) had a median gestational age of 28^{+5} (range: $23^{+4} - 35^{+2}$) weeks, a median postmenstrual age at scan of 41^{+5} ($38^{+1} - 44^{+4}$) weeks and median birth weight of 1.11 (0.63 – 2.87) kg. No infants received postnatal steroids. Across the whole cohort, the median (range) time spent receiving any form of respiratory support was 17 (0 – 116) days. Fifteen infants had CLD, defined by the need for respiratory support at 36 weeks postmenstrual age.

Imaging

MRI was performed on a Philips 3-Tesla system (Philips Medical Systems, Netherlands) using an 8-channel phased array head coil. T_1 -weighted MRI was acquired using: TR: 17 ms; TE: 4.6 ms; flip angle 13° ; slice thickness: 1.6 mm; field-of-view: 210 mm; matrix: 256×256 (voxel size: $0.82 \times 0.82 \times 0.8$ mm). T_2 -weighted fast-spin echo MRI was acquired using: TR: 8670 ms; TE: 160 ms; flip angle 90° ; slice

thickness 2 mm; field-of-view: 220 mm; matrix: 256×256 (voxel size: $0.86 \times 0.86 \times 1$ mm). Single-shot EPI DTI was acquired as described in Chapter 4.

All examinations were supervised by a paediatrician experienced in MRI procedures. Infants were sedated with oral chloral hydrate (25 – 50 mg/kg) prior to scanning and pulse oximetry, temperature and electrocardiography data were monitored throughout. Ear protection was used for each infant, comprising earplugs moulded from a silicone-based putty (President Putty, Coltene Whaledent, Mahwah, NJ) placed in the external ear and neonatal earmuffs (MiniMuffs, Natus Medical Inc, San Carlos, CA).

Thalamic segmentation

The manual placement of ROI on individual MR images can be subjective and manually-intensive and does not easily allow for comparisons across large groups. To avoid this, a single bilateral thalamic mask was manually drawn on the final reference template according to anatomical borders previously described (Srinivasan et al. 2007) and with the aid of an age-appropriate histological atlas (Bayer and Altman 2004; Figure 5.1B; see *Deformation-Based Morphometry* for details of template construction). The head of the caudate formed the anterior border, the third ventricle formed the medial border and the PLIC formed the lateral border; the lateral ventricle formed the posterior border, and the subthalamic nuclei along with the geniculate bodies formed the inferior border. The high spatial correspondence between each T_1 -weighted image and the reference template following nonlinear registration precluded the need to manually place thalamic masks on individual T_1 images. Individual thalamic volume can be estimated by scaling the reference mask volume by the mean Jacobian determinant (a voxelwise measure of volume change between each image and the template, described below) calculated within the mask. To validate this assertion, manual thalamic segmentation was performed on T_1 images from ten randomly selected infants, thalamic volumes measured manually and volumes estimated from the mean Jacobian were consistent (Mean difference and limits of agreement = 0.29 ± 1.43 ml; Intraclass coefficient = 0.89, $p < 0.001$).

Cortical segmentation

Cortical tissue segmentation was performed on individual T_2 images using methods specifically optimised for neonatal tissue segmentation (for example segmentation see Figure 5.1C). Images were initially segmented using an expectation-maximisation segmentation method driven by age-specific, co-registered tissue probability priors obtained from a 4-dimensional, probabilistic neonatal atlas (Kuklisova-Murgasova et al. 2011). In addition, an automatic three-step segmentation algorithm was used to remove mislabeled partial volume voxels at the interface of the grey matter and CSF (Xue et al. 2007).

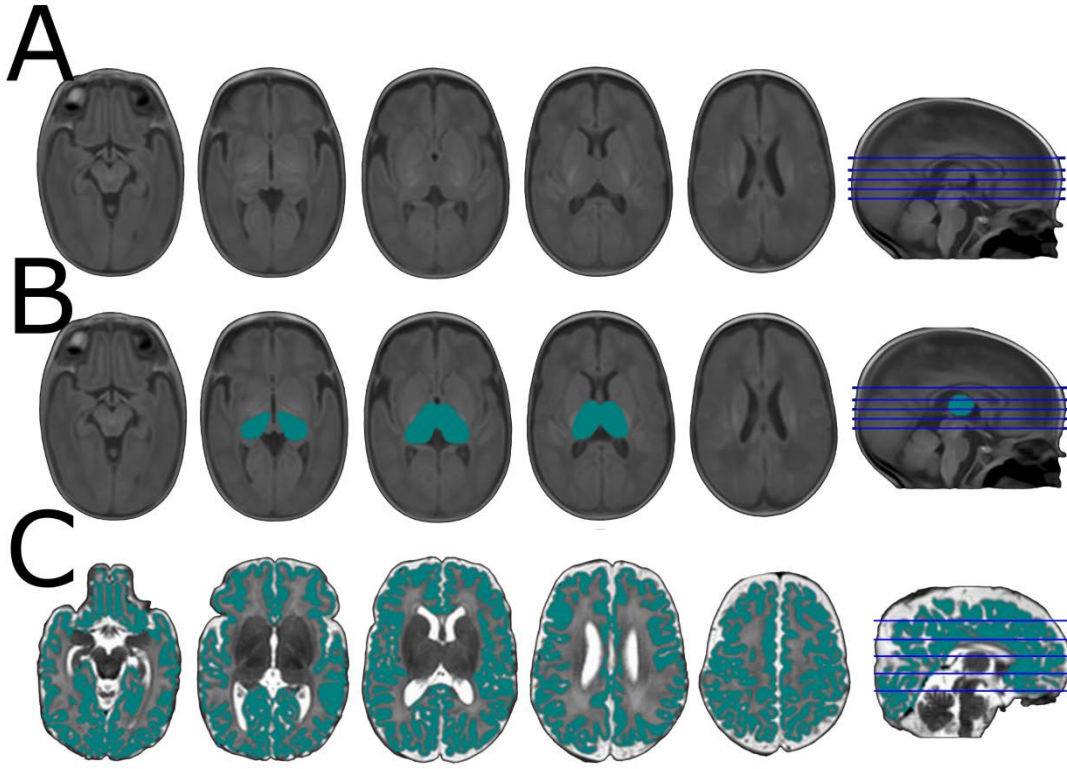


Figure 5.1: Final reference template and thalamic and cortical segmentations. The final average intensity template is shown in (A), the clarity of the subcortical structures and cortical differentiation indicate the accurate alignment of individual images. The mean Jacobian determinant within the mask shown in (B) represents the relative volume change between the template and each image and was used to represent thalamic volume across the cohort. A representative example of cortical grey matter segmentation is shown in (C).

Deformation-based morphometry

DBM does not require tissue segmentation or classification and can be used to localise regional variations in tissue volume (Ashburner et al. 1998, Chung et al. 2001, Rueckert et al. 2003). The key step is to achieve precise spatial correspondence between each subject's image and a reference template through image registration. The output of each registration is a three-dimensional deformation field representing transformations between each image and the final template (see Chapter 2, Section 2.3). At any given point x in the template image, the transformation $T(x)$ required to map the location of x in the source image is a combination of a global, 6 DOF rigid and 12 DOF affine transformation $T_{global}(x)$, represented by an affine matrix $M(x)$ encoding scales, shears and skews and a translation vector d , and a local transformation $T_{local}(x)$ modelled using FFD based on cubic B -splines (Equations 6.1 and 6.2; Rueckert et al. 1999, Rueckert et al. 2003).

$$T(x) = T_{global}(x) + T_{local}(x) = M(x) + d + T_{local}(x)$$

[6.1]

$$T_{local}(x) = \sum_{l=0}^3 \sum_{m=0}^3 \sum_{n=0}^3 B_l(u)B_m(v)B_n(w)\Phi_{i+l,j+m,k+n}$$

[6.2]

The Jacobian operator D can be applied to the transformation T between two images and volume change at x is given by the determinant of the Jacobian operator $J(x)$ (Equation 6.3).

$$J(x) = \det(DT(x)) = \det(DT_{global}(x) + DT_{local}(x))$$

[6.3]

Statistical groupwise analysis of the Jacobian reveals structural volume relative to the group template in an objective, voxelwise manner (see Chapter 2, Section 2.3; Ashburner et al. 1998, Rueckert et al. 2003).

After bias correction (FMRIB's Automated Segmentation Tool; FAST v4.1), each T_1 image was aligned to a chosen target image (GA = 28⁺⁵ weeks; PMA at scan = 42⁺⁰ weeks) using 6 DOF linear registration, followed by 12 DOF affine registration (rreg and areg; <http://www.doc.ic.ac.uk/~dr/software>). Each image was transformed into the reference space using sinc interpolation and a reference template was created by taking an intensity-average of the aligned images. Each MR image was then aligned to the reference template using linear, affine and high dimensional nonlinear registration based on cubic B -splines and averaged to form a second reference template. Nonlinear registration was carried out with successive control point spacing of 20, 10, 5 and 2.5 mm, the similarity metric was NMI and the smoothness penalty was represented by the bending energy associated with the deformation. Weighting of the regularisation (λ) was empirically set to 1×10^{-6} to ensure that the estimated warps were plausible (i.e.: there were no folds or tears in the deformation field) while still allowing for accurate alignment of the images. To demonstrate, a single T_1 image was registered to the reference template using decreasing values of λ . Figure 5.2 shows the effect of decreasing regularisation weighting on image alignment and the resultant deformation field. The value of $\lambda = 1 \times 10^{-6}$ was chosen to minimise the difference between the source and target image without sharp, implausible deformations.

A final set of registrations was performed with the second reference template as the target (Figure 5.3). A qualitative evaluation of the alignment accuracy of the transformed images with the template was made before individual deformation fields were used to calculate volume changes. The average-intensity template generated from the final set of registrations is shown in Figure 5.1A.

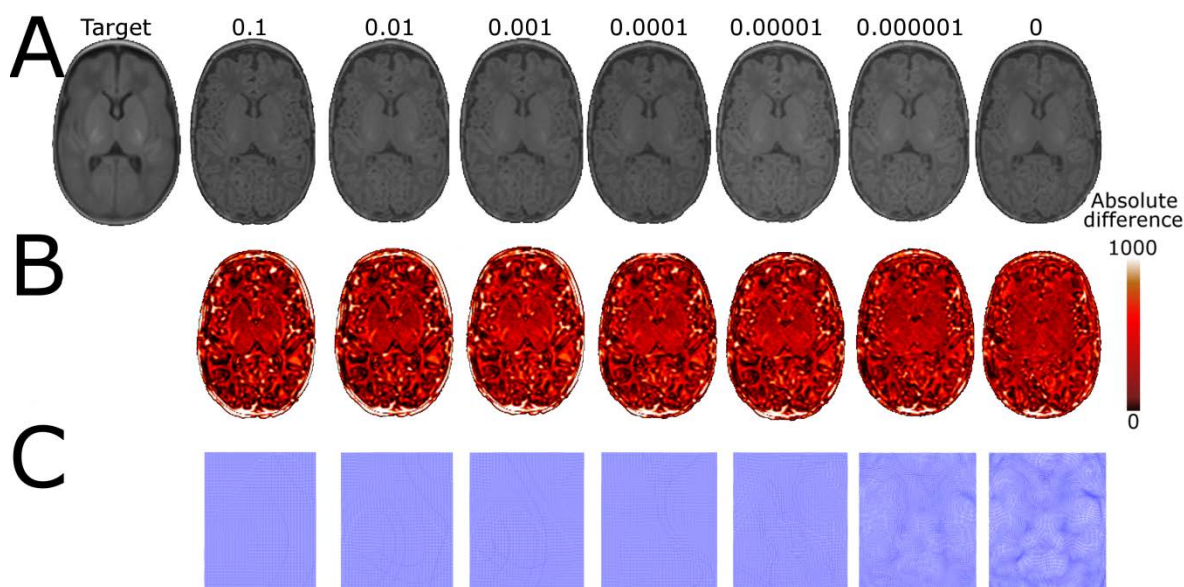


Figure 5.2: Decreasing regularisation of warp smoothness. A single T_1 image was registered to the template (A; left) using decreasing warp regularisation. The transformed images are shown in (A), the absolute difference between the transformed source and target images in (B) and the respective deformation fields in (C). Removing the regularisation term results in a better alignment, but produces a highly-deformed, non-invertible warp that is not appropriate for DBM analysis (Leow et al. 2007, Yanovsky et al. 2009).

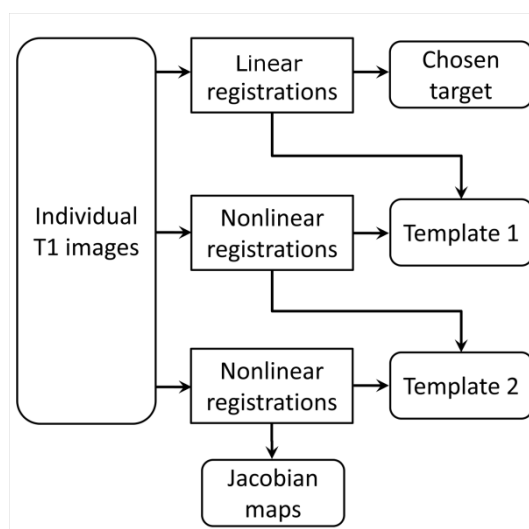


Figure 5.3: Deformation-based morphometry processing pipeline. After preprocessing, T_1 images are linearly aligned to an arbitrarily chosen target MR image and averaged to produce a reference template. Two subsequent iterations of nonlinear registration and template construction produce the final transformations used for analysis.

As discussed in Chapter 4, the use of an appropriate population-based template is essential for voxel-based analyses in populations with abnormal or altered anatomy (Good et al. 2001). Due to the inherent bias that can be introduced when selecting an image as a target for registration – particularly

if the image is not representative of the cohort as a whole—a number of methods have been published that describe techniques to create unbiased, population-average templates for volumetric analysis (Kochunov et al. 2001, Lepore et al. 2007, Lyttelton et al. 2007), some of which are applicable to pediatric images (Bhatia et al. 2007, Wilke et al. 2008, Fonov et al. 2011). The pipeline shown in Figure 5.3 provides a relatively quick and simple method to produce a population-based template that, although not technically unbiased, proves robust to alternative target selections. Appendix B (Section B.1) shows that effect of target choice on the results presented in Figure 5.5. Similarly, Appendix B (Section B.2) shows how performing one, two or three iterations of nonlinear registration alters the results shown in Figure 5.5.

Voxelwise cross-subject statistical analysis of volume relative to the template, represented by the Jacobian, was performed with Randomise (v2.5) as implemented in FSL (Smith et al. 2004). All statistical images were subject to false discovery rate (FDR) correction for multiple comparisons.

Tract-based spatial statistics

DTI analysis was performed using FDT v2.0 and the TBSS method optimised for neonatal DTI analysis in Chapter 4. Non-parametric, permutation-based statistical analysis was performed with Randomise. All diffusion statistics were subject to FWE-correction for multiple comparisons following TFCE and are shown at $p < 0.05$.

Statistical analysis

Further statistical analysis with multiple linear regression was performed with SPSS 17.0 (SPSS Inc., Chicago, IL, USA). In addition to explanatory variables of interest, gestational age at birth, postmenstrual age at scan, CLD status and total brain volume were entered into the regression models where stated, partial r values are reported.

5.3 Results: Regional Brain Volume and Prematurity at Birth

Mean (\pm SD) total cortical grey matter volume was 158 (\pm 26.6) ml. Both cortical grey matter volume and mean thalamic Jacobian (representing thalamic volume) were significantly associated with gestational age at birth, entered into the regression model with the age of each infant at scan (Cortical volume: partial $r = 0.37$, $p < 0.005$; full model: $R^2 = 0.59$, $p < 0.001$; Thalamic: partial $r = 0.40$, $p < 0.001$; full model: $R^2 = 0.61$, $p < 0.001$; Figure 5.4).

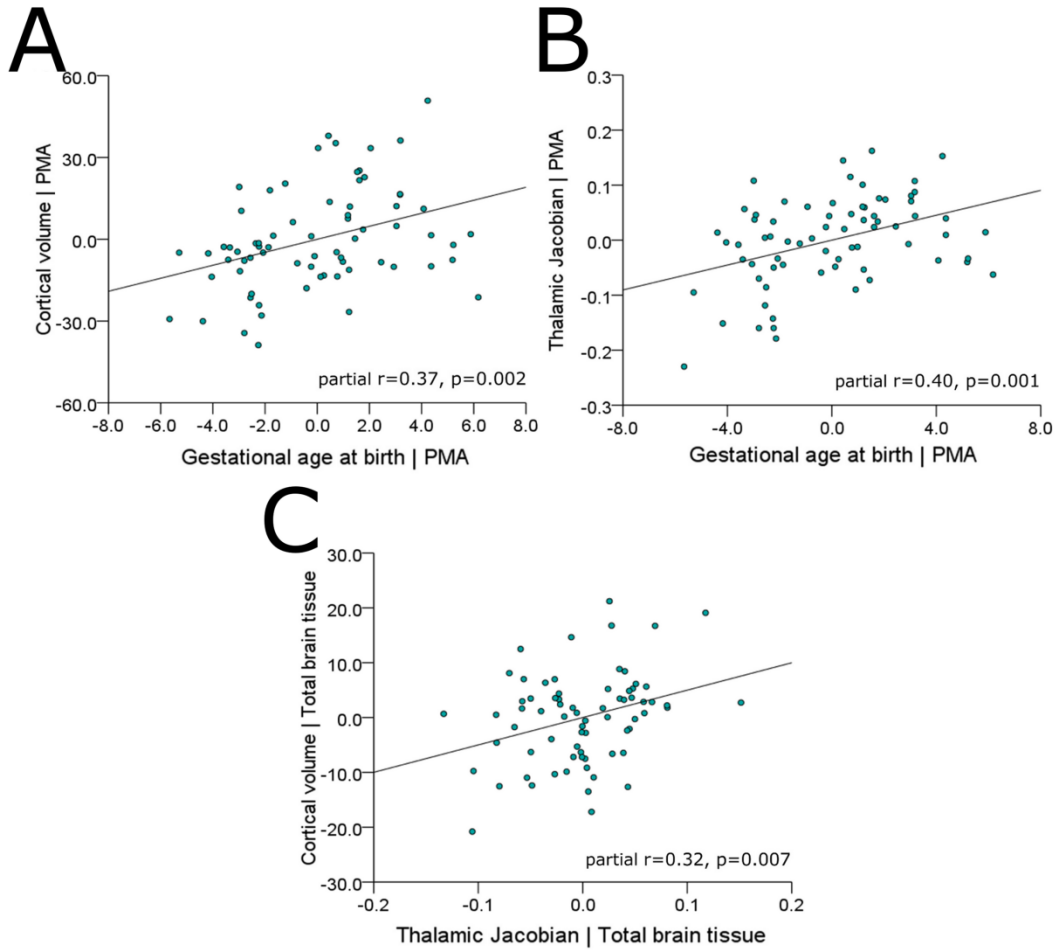


Figure 5. 4: Cortical grey matter volume is correlated with prematurity at birth and thalamic volume at term-equivalent age. Partial regression plots show significant associations between cortical grey matter volume and gestational age at birth (A) and mean thalamic Jacobian (representing thalamic volume) and GA (B), after correction of each measure for the age of each infant at scan (PMA). Shown in (C) is the significant association between cortical volume and thalamic Jacobian, after correction of each for total cerebral tissue volume.

DBM was used to locate other brain regions where tissue volume was associated with degree of prematurity at birth. Linear regression revealed significant localised associations between tissue volume (represented voxelwise by the Jacobian) and gestational age at birth (Figure 5.5; FDR-corrected for multiple comparisons at $p < 0.01$; minimum t-statistic = 2.98). Increasing prematurity was associated with a bilateral pattern of reduced volume present at term-equivalent age and encompassing the anterior temporal lobes, including the hippocampus, the orbitofrontal lobe and posterior cingulate cortex and extending into the centrum semiovale. Within the deep grey matter, the relationship was most prominent in the thalamus. In addition, discrete clusters were observed in the midbrain and cerebellum. DBM also revealed that increasing prematurity was associated with increasing extra-cerebral CSF, but this did not pass correction for multiple comparisons.

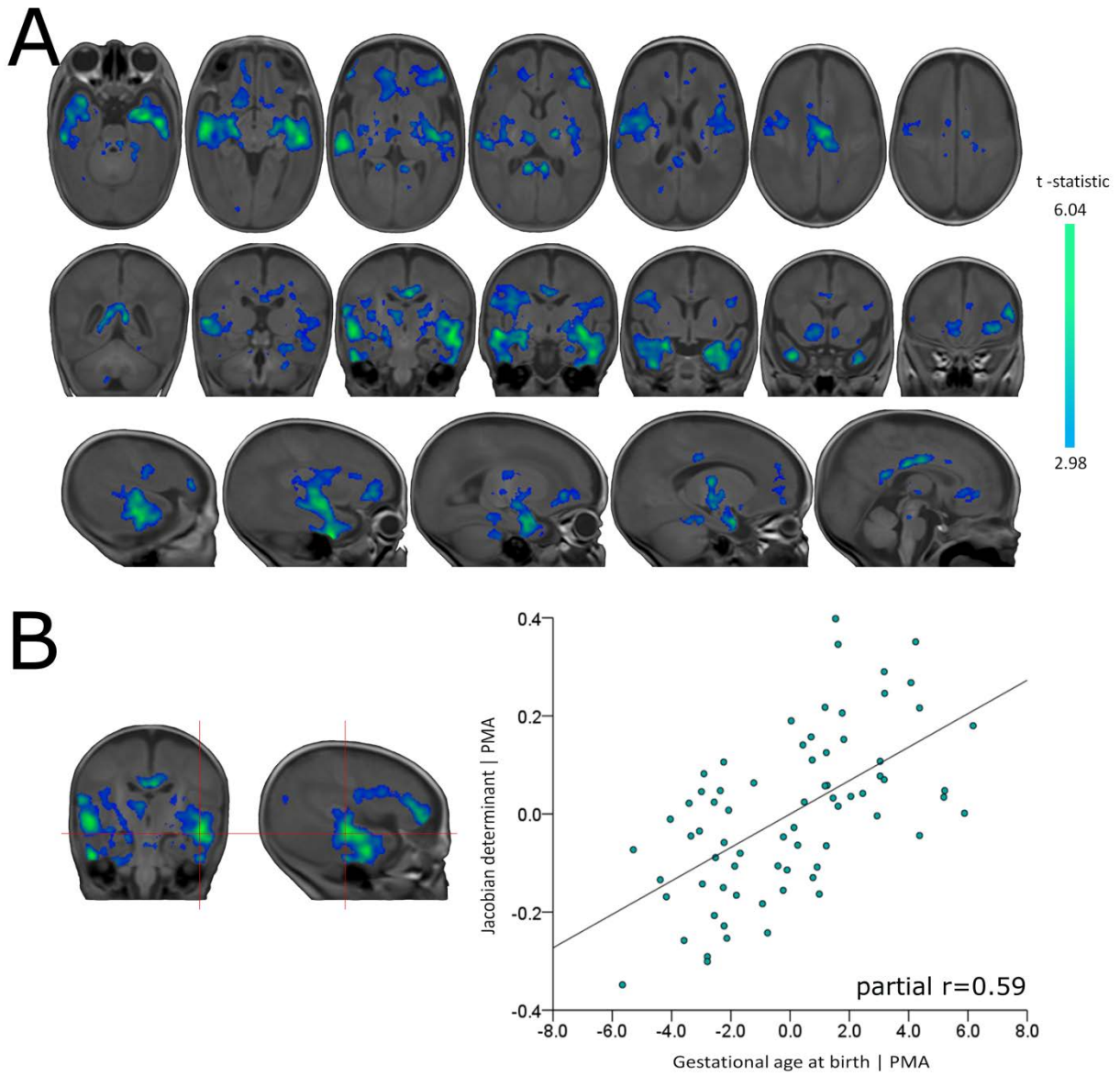


Figure 5.5: Regional associations between brain tissue volume and prematurity at birth. Regions where tissue volume was significantly associated with GA at birth after correcting for the age of each infant at scan (PMA) are shown in (A). Statistical images are corrected for multiple comparisons at $p < 0.01$ FDR-corrected (colour bar indicates t -statistic). To illustrate this relationship the Jacobian determinant at the site of the maximum t -statistic (red crosshairs; $t = 6.04$), was entered into a multiple linear regression with GA at birth and PMA at scan. The partial regression plot (B) shows the relationship between Jacobian and GA at birth.

5.4 Results: Thalamo-Cortical Development after Preterm Birth

When entered into a regression model with total brain tissue volume, cortical volume was significantly associated with mean thalamic Jacobian (partial $r = 0.32$, $p < 0.01$; full model: $R^2 = 0.91$; Figure 5.4C).

This association remained significant when also including gestational age at birth (partial $r = 0.31$, $p < 0.01$; full model: $R^2 = 0.91$, $p < 0.001$).

After correcting for the effects of prematurity and removing volume change due to individual differences in global brain scaling, DBM revealed significant volumetric covariance between the thalamus and other subcortical cerebral tissue (Figure 5.6; FDR-corrected $p < 0.001$, minimum t-statistic = 3.25). A bilateral pattern was observed comprising white and grey matter proximal to the thalamus and extending into the frontal and temporal lobes, including the hippocampus, through the centrum semiovale into the parietal lobe and, to a lesser extent, into periventricular white matter in the occipital lobes. This pattern remained highly significant when also co-varying for total cortical volume.

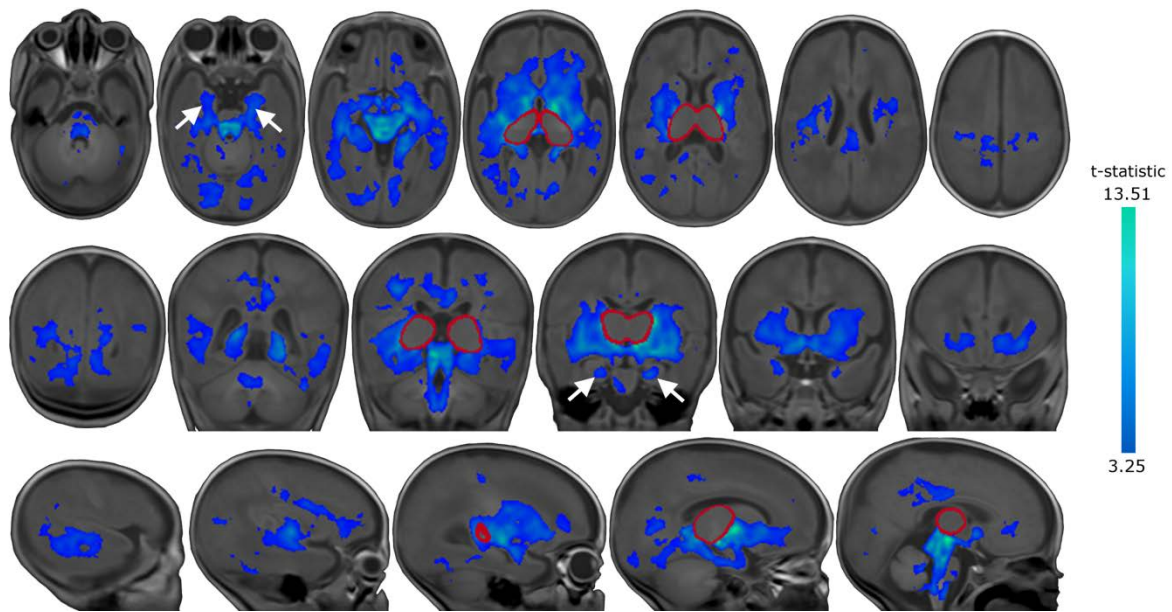


Figure 5.6: Regional associations between brain tissue volume and thalamic volume at term-equivalent age. Regions where cerebral tissue volume significantly co-varied with mean thalamic Jacobian (calculated within the region circled in red). Arrows indicate the hippocampus in each hemisphere, statistical images are corrected for multiple comparisons at $p < 0.001$ FDR-corrected (colour bar indicates t-statistic).

In addition to the observed structural associations, TBSS was used to identify where white matter microstructure was associated with thalamic and cortical volume. Increasing thalamic volume at term-equivalent age was significantly associated with FA in the PLIC and corpus callosum (including the splenium) after correction for degree of prematurity at birth and the age of each infant when scanned (FWE-corrected for multiple comparison, $p < 0.05$; Figure 5.7). Within these regions, linear regression showed that decreasing thalamic volume was independently associated with increasing RD (partial $r = -0.34$, $p < 0.005$; full model: $R^2 = 0.28$, $p < 0.001$) but not with AD (partial $r = 0.008$; full model: $R^2 = 0.05$, ns) when entered into a model with gestational age at birth and age at scan.

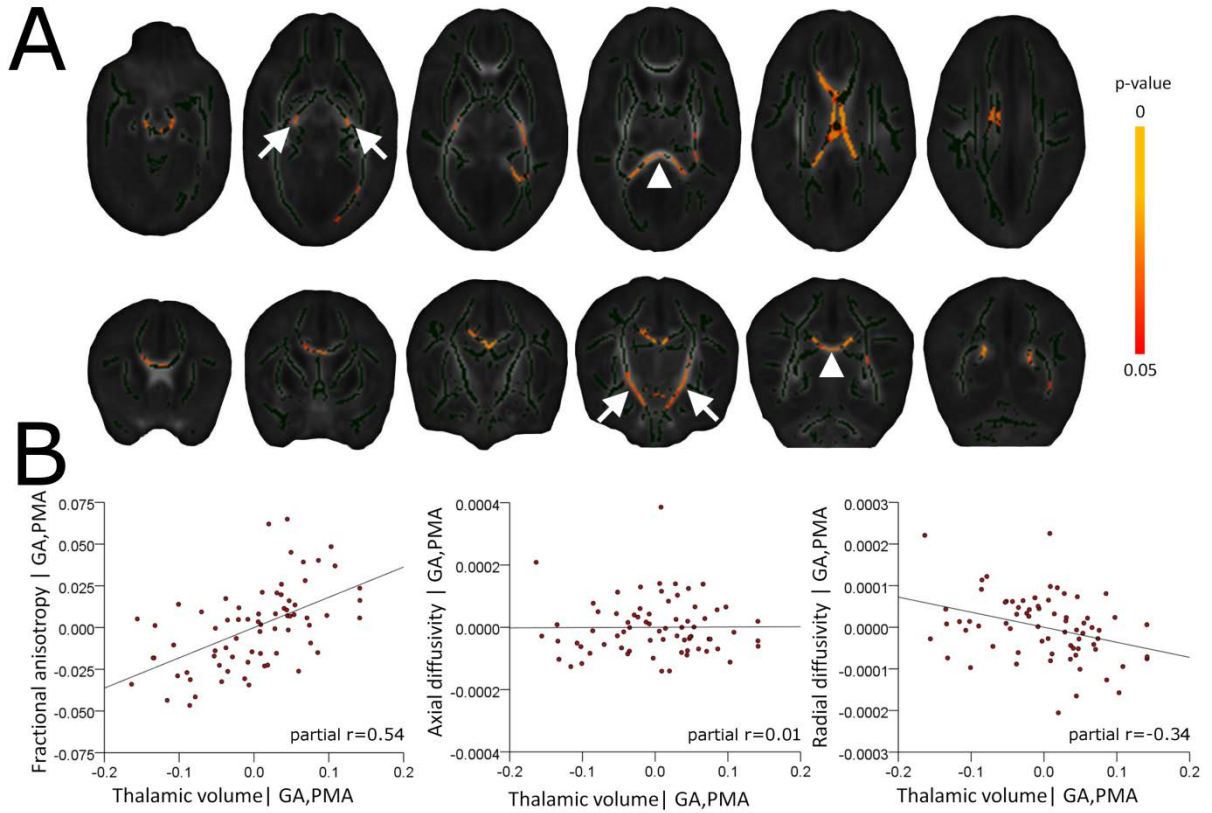


Figure 5.7: Thalamic volume is associated with white matter microstructure. TBSS reveals regions where FA is significantly associated with thalamic volume, beyond any common association with prematurity at birth and age at imaging, shown in (A). These regions include the PLIC (arrows) and the corpus callosum (arrowheads). Images are FWE-corrected at $p < 0.05$ (colour bar indicates p value); the mean FA skeleton is shown in dark green. Partial regression plots of the relationship between thalamic volume and mean FA, AD and RD extracted from each significant voxel identified in (A) and entered into linear regression with GA and age at scan (PMA) are shown in (B).

Cortical volume was significantly associated with FA in the posterior corpus callosum after correction for degree of prematurity at birth and age at scan (FWE-corrected, $p < 0.05$, Figure 5.8). In these regions, RD was associated with cortical volume (partial $r = 0.29$, $p < 0.05$; full model: $R^2 = 0.26$, $p < 0.001$) independent of gestational age and age at scan. AD was not significantly associated with cortical volume (partial $r = 0.16$, ns; full model: $R^2 = 0.12$, $p < 0.05$).

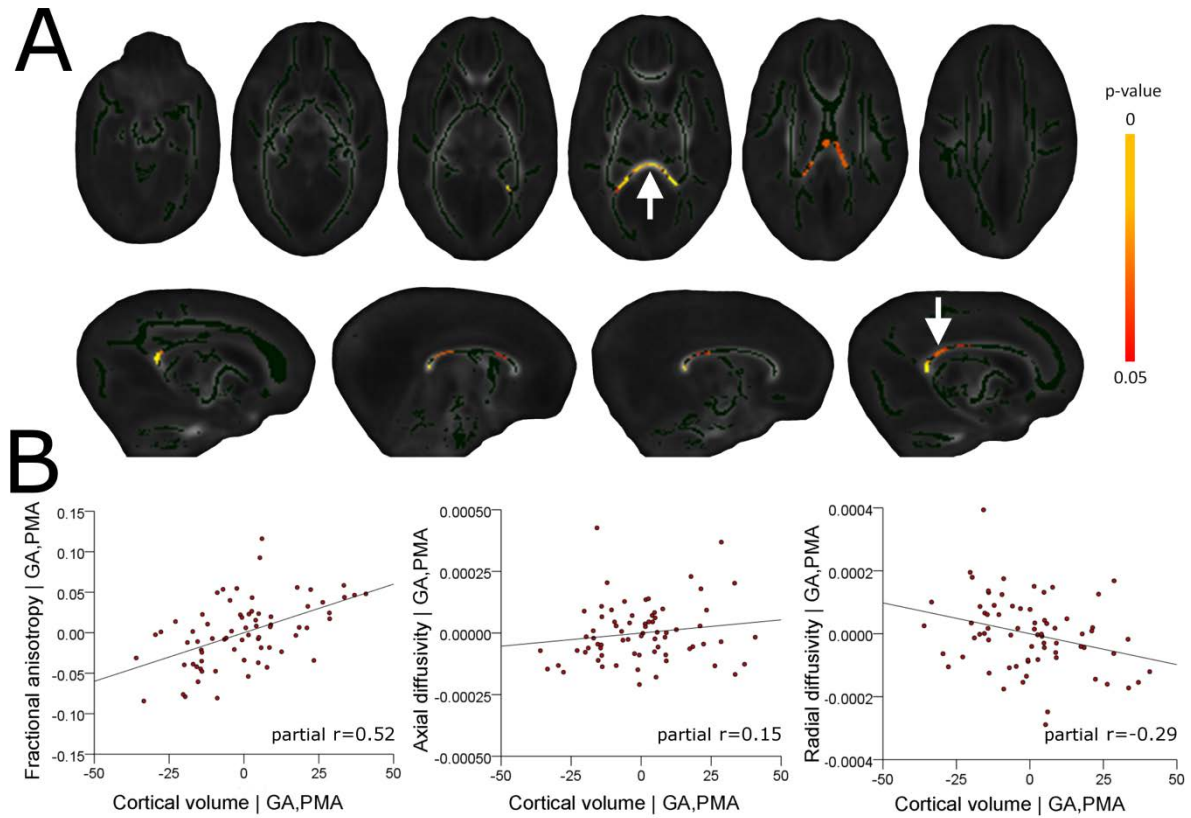


Figure 5.8: Cortical volume is associated with white matter microstructure. TBSS analysis reveals that FA in the posterior corpus callosum (A; arrow, bottom row) including the splenium (A; arrow, top row) is significantly associated with cortical volume, after correction for prematurity at birth and age at imaging. Images are shown as in Figure 5.7. Cortical volume and mean FA, AD and RD extracted from each significant voxel identified in (A) were entered into linear regression with GA and PMA at scan. Partial regression plots of the relationship between cortical volume and FA, AD and RD are shown in (B).

Additionally, in Chapter 4 it was shown that both FA and RD are significantly altered in infants with chronic lung disease; therefore this analysis was repeated including chronic lung disease status as a covariate. Both thalamic and cortical associations were diminished but remained significant (Figure 5.9). Additional DBM analyses did not reveal any significant associations between CLD and cerebral tissue volume after correction for gestational age at birth and age at scan.

To investigate the interaction of thalamic and cortical associations with white matter microstructure, a secondary ROI analysis was performed. FA values were extracted from masks in the PLIC and posterior corpus callosum (Figure 5.10). In the PLIC (Figure 5.10A), FA was significantly associated with thalamic (partial $r = 0.35$, $p < 0.01$) but not cortical volume (partial $r = -0.13$, ns) when both metrics were entered into linear regression alongside gestational age and age at scan (Full model: $R^2 = 0.43$, $p < 0.001$). Conversely, FA in the posterior corpus callosum (Figure 6.10B) was significantly associated with cortical volume (partial $r = 0.26$, $p < 0.05$) but not with thalamic volume (partial $r = 0.07$, ns; full model: $R^2 = 0.31$, $p < 0.001$).

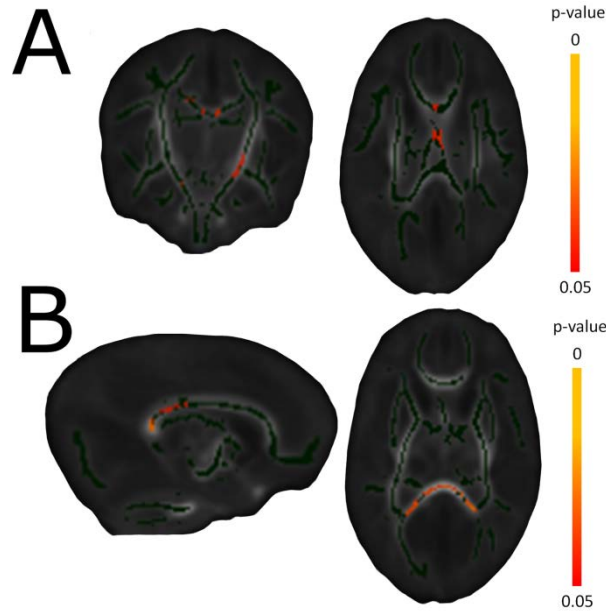


Figure 5.9: Significant associations between FA and tissue volume remain when correcting for chronic lung disease status. Regions where FA was significantly associated with thalamic (A) and cortical (B) volume, after correction for GA at birth, PMA at scan and CLD status are shown. Images are FWE-corrected at $p < 0.05$, the mean FA skeleton is shown in dark green.

Finally, to determine how reduced thalamic volume is reflected by the underlying tissue microstructure, mean diffusivity (mean magnitude of λ_1 , λ_2 and λ_3) was extracted from each infant's DTI dataset using a thalamic mask transformed onto the DTI reference template. Linear regression revealed that thalamic diffusivity was significantly associated with gestational age at birth, after correcting for age at scan (partial $r = -0.29$, $p < 0.05$; full model: $R^2 = 0.19$, $p < 0.05$) and significantly lower in infants with chronic lung disease, after correcting for both gestation and age at scan (general linear model: $F_{(1,67)} = 4.6$, $p < 0.05$). Smaller thalamic volume was significantly associated with increased mean thalamic diffusivity when entered into linear regression with gestational age at birth, total brain and total cortical volume (Figure 5.11; partial $r = -0.40$, $p < 0.001$; full model: $R^2 = 0.85$, $p < 0.001$). This association remained significant when also including CLD status and age at scan (partial $r = -0.32$, $p < 0.01$; full model: $R^2 = 0.87$, $p < 0.001$). TBSS analysis revealed that mean thalamic diffusivity was significantly associated with FA in the internal capsule, after correction for degree of prematurity, age at scan, cortical volume and CLD status (Figure 5.11B; FWE-corrected $p < 0.05$).

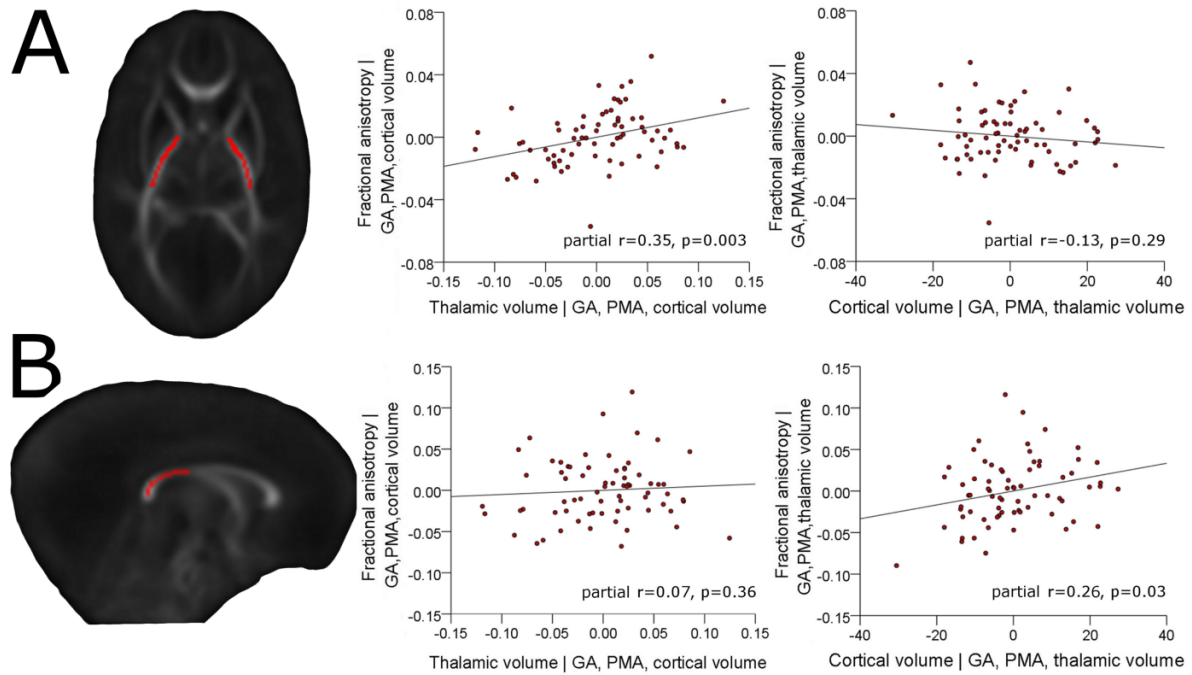


Figure 5.10: Differential associations between tissue volume and FA in the internal capsule and corpus callosum. FA in the posterior limb of the internal capsule (A) and the posterior corpus callosum (B), thalamic volume, cortical volume, GA at birth and age at scan (PMA) were entered into multiple linear regression. FA in the internal capsule was independently associated with thalamic volume (middle column), but not with cortical volume (right column). The opposite relationship was seen in the corpus callosum.

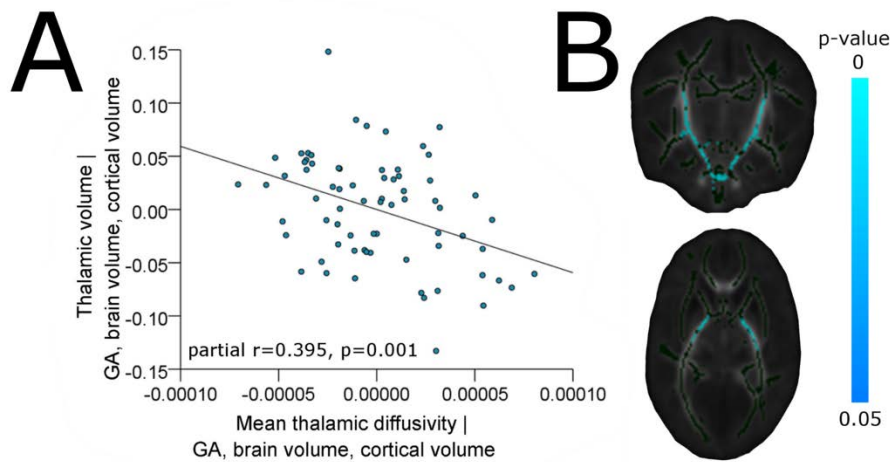


Figure 5.11: Thalamic diffusivity is associated with thalamic volume and FA in the internal capsule. Thalamic volume (estimated from the mean Jacobian) and mean thalamic diffusivity (estimated from a thalamic mask placed in the DTI reference space) were entered into a multiple linear regression model with GA at birth, cortical volume and total brain volume. The partial regression plot in (A) shows the significant association between thalamic volume and thalamic diffusivity. In (B), regions where FA was significantly associated with thalamic diffusivity are shown (FWE-corrected at $p < 0.05$), beyond any associations with GA, PMA at scan, cortical volume and CLD status.

5.5 Discussion

This study demonstrated a significant effect of prematurity on thalamic volume related to specific abnormalities in allied brain structures. These effects were far-reaching, with reductions in the volume of thalamus, hippocampus, orbito-frontal lobe, posterior cingulate cortex and centrum semiovale suggesting that preterm delivery disrupts specific aspects of cerebral development. However, after this general effect was accounted for, a pattern of structural co-variance was observed between the thalamus and particular brain structures, notably in fronto-temporal regions, the cingulate gyrus and hippocampus. This, coupled with the observed association between reduced thalamic and cortical volume together with abnormal thalamic and white matter microstructure suggests the hypothesis that these observations result at least in part from disrupted development of the thalamo-cortical system.

Altered structural brain development has previously been detected in preterm populations as early as term-equivalent age, revealing a combination of cortical alterations and subcortical grey matter loss that accompanies the more commonly described white matter abnormalities (Ajayi-Obe et al. 2000, Inder et al. 2005, Boardman et al. 2006, Kapellou et al. 2006, Thompson et al. 2007). Global cerebral tissue loss, hippocampal reductions and thalamic atrophy have all been described (Inder et al. 2005, Pierson et al. 2007, Thompson et al. 2008, Nagasunder et al. 2011), but independent of severe white matter pathology both deep grey matter growth and cortical development appear significantly altered by term (Boardman et al. 2006, Kapellou et al. 2006). Using DBM, Boardman et al. previously showed significant reductions in the thalamus and lentiform nucleus in comparison to term-born controls, which were significantly greater in association with diffuse white matter injury (Boardman et al. 2006). Thalamic volume loss (in association with diffuse white matter injury) and altered cortical development at term-equivalent age have both been shown to predict neurodevelopment outcome in childhood (Kapellou et al. 2006, Boardman et al. 2010, Rathbone et al. 2011).

The data presented in this chapter confirm that in preterm neonates at term-equivalent age, cortical grey matter and thalamic volume are dependent on the degree of prematurity at birth and are part of a wider developmental pattern of structural alterations. This pattern shows similarity to the neuroanatomical changes seen in ex-preterm adolescents. Using tissue segmentation, Nosarti et al. (Nosarti et al. 2002) reported a significant decrease in cortical grey matter and hippocampal volume compared to age-matched, adolescent controls, and using VBM demonstrated a distributed pattern of cerebral tissue reductions encompassing frontal and temporal regions, including the hippocampus, and subcortical grey matter, including the thalamus, that appeared to mediate neurodevelopmental outcome (Nosarti et al. 2008). Using similar techniques, Nagy et al. reported bilateral grey matter reductions primarily in the temporal lobe, hippocampus and thalamus coupled with reduced FA in the central white matter, assessed with TBSS, at the same age (Nagy et al. 2009). Additionally, a series of studies have demonstrated reduced orbitofrontal volume compared to term-born adolescent controls and reductions in hippocampal and thalamic volume that relate to cognitive performance (Gimenez et al. 2004, Gimenez et al. 2006a, Gimenez et al. 2006b). This pattern is also compatible with histological

evidence from a primate model of preterm birth and neonatal intensive care that found: decreased white matter volume in the temporal, frontal and parietal lobes with relative sparing of the occipital lobe; and tissue loss in the cortex, deep grey matter and hippocampus (Dieni et al. 2004, Loeliger et al. 2006, Loeliger et al. 2009). Coupled with evidence provided in Chapter 4, these data imply that a gestation-dependent pattern of altered brain development comprising widespread micro- and macro-structural disturbances is present by term-equivalent age, and appears to persist beyond childhood and into adolescence.

Beyond the strong association with prematurity, significant co-variations in volume and microstructure were observed in a number of cerebral structures. That anatomically separate regions appear to develop in tandem during this period is not entirely surprising given that functional connectivity, at a systems level, of a number of cortical and subcortical structures is present before term-equivalent age (Fransson et al. 2007, Doria et al. 2010, Smyser et al. 2010). Importantly, a number of the structures shown here to be co-dependent during development are also adversely affected by preterm birth. These results support data suggesting that the neuroanatomical basis for the later sequelae of prematurity develop before the time of normal birth (Rathbone et al. 2011) during the period when the thalamo-cortical system is forming and essential for normal development (Kostovic and Judas 2010).

The hypothesis that disruption of thalamo-cortical development underlies the observed changes would suggest an intimate relationship between grey matter structures and connective white matter tracts. Here, thalamic volume was significantly associated with FA in the internal capsule and the corpus callosum, but subsequent ROI analysis showed that this association only persisted in the internal capsule when cortical volume was also considered. Conversely, cortical volume was only significantly associated with FA in the corpus callosum. Thalamic volume is therefore related to both the microstructure of the thalamic radiations, carrying projection fibres to the cortex, and the volume of the cortex itself. In turn, cortical volume is associated with the microstructure of inter-hemispheric cortico-cortical fibres. It is possible that tissue volume in the thalamus and cortex thus reflects thalamo-cortical connectivity and is dependent on the growth and integrity of connecting white matter tracts.

Reduced thalamo-cortical volume might also reflect reduced cell and axon numbers in component structures. The number of neurons in topographically-connected thalamic and cortical regions is closely related (Stevens 2001) and a large body of histological evidence has determined that both thalamo-cortical and callosal cortico-cortical connections are established by term-equivalent age in humans and other primates (Kostovic and Rakic 1984, LaMantia and Rakic 1990, Kostovic and Jovanov-Milosevic 2006). This process can be interrupted by adverse events: cerebral irradiation in mid-to-late pregnancy leads to parallel neuronal loss in the thalamus and cerebral cortex and volume reduction in the subcortical white matter, indicating the presence of shared developmental trajectories (Schindler et al. 2002, Selemon et al. 2005, Selemon et al. 2009). In addition, reduced thalamic volume was associated with increased mean thalamic diffusivity suggestive of larger extracellular space and compatible with reduced cell density (Beaulieu 2002); and reduced white matter anisotropy with increased radial diffusivity in associated white matter tracts, compatible with reduced axon density. Decreased

thalamic volume, increased thalamic diffusivity and increased white matter radial diffusivity are together compatible with decreased cell numbers in the thalamo-cortical system.

Volpe argues that brain development in preterm infants is ultimately dependent on a combination of destructive and impaired maturational mechanisms (Volpe 2009). Additionally, systemic illness in the neonatal period is an independent risk factor for adverse neurodevelopmental outcome (Short et al. 2003, Miller and Ferriero 2009), and in Chapter 4 chronic lung disease was shown to be associated with decreased FA and increased RD in the cerebral white matter in this cohort. By removing infants with severe, focal lesions such as PVL potential impact of acquired, destructive brain lesions on these observations have been limited and, when factoring in CLD status, the pattern of microstructural covariance between the thalamus and the internal capsule, and the cortex and corpus callosum remained, although the extent of the associations was reduced. As described in Chapter 4, this may imply that the adverse effects associated with systemic illness may potentiate the observed microstructural alterations with subsequent downstream effects on thalamic volume and development of the overlying cortex (Volpe 2009), resulting in the gestation-dependent pattern of brain development described here.

It should be noted that the DBM analyses did not reveal significant associations in the cortex. This was not unexpected: DBM is highly sensitive to local volume change that is spatially consistent across the whole group and thus relies on precise spatial correspondence without reliance on tissue classification and spatial smoothing, however due to the rapid increases in cortical complexity during the neonatal period (Kapellou et al. 2006) and limitations in current image registration techniques for neonates, achieving precise correspondence in cortical regions remains difficult. By combining DBM with cortical segmentations in native image space, it is possible to capture information from the whole brain in this cohort. Similarly, a limitation of using TBSS to investigate thalamo-cortical connectivity is that it provides pointwise comparisons of white matter microstructure that do not account for the orientation of underlying axonal fibres. It is assumed that contiguous voxels contain the same fibre populations and a significant cluster of voxels represent altered microstructural organisation along them. This may not be the case in the presence of more complex fibre configurations, for it is not known which fibre populations contribute to the voxelwise estimate of anisotropy/diffusivity, or the extent to which any observed alterations can be attributed to a population. Specific investigations of the thalamo-cortical system using methods that account for fibre orientation, such as diffusion tractography, could confirm the observations made in this Chapter.

In summary, at term-equivalent age and in the absence of severe white matter injury, preterm infants show a detailed pattern of altered brain structure and microstructure that mirrors changes seen in adolescent ex-preterm infants, and is compatible with disruption of thalamo-cortical development.

Chapter 6

Tractography in Preterm Neonates: Exploring Connectivity

6.1 Introduction

Thalamo-cortical connections are established during the third trimester (Allendoerfer and Shatz 1994, Kostovic and Judas 2010) and almost all cortical regions receive some form of thalamic input (Molnar et al. 2003). During development, cortical organisation and areal specialisation occur according to a strict spatio-temporal schedule (Rakic 1988, Monuki and Walsh 2001) and tracing experiments have established that cortical regions are topographically mapped to corresponding thalamic nuclei (Blakemore and Molnar 1990, Molnar et al. 1998, Scannell et al. 1999).

Due to the timing of key developmental processes, disruption of the thalamo-cortical system is thought to represent a major component of preterm brain injury (Volpe 2009, Kostovic and Judas 2010) and may be a neural substrate for the later cognitive deficits prevalent in this population (Inder et al. 2005, Boardman et al. 2010). In Chapter 5 it was shown that, by term-equivalent age, reduced thalamic volume is associated with reduced cortical volume and altered microstructure in the central white matter in preterm infants. This implies that the relationship between grey matter structures and connective white matter tracts is altered following preterm birth.

Tractography is an *in vivo* technique for inferring connective pathways through the brain based on diffusion MRI. Tractography is commonly used to extract 3-dimensional representations of specific tracts for anatomical comparison (Catani et al. 2002, Wakana et al. 2004), or to examine connectivity between discrete cortical or subcortical regions (Behrens et al. 2003b). The former approach has been successfully applied in neonates to delineate major white matter tracts including the cortico-spinal tracts and corpus callosum (Berman et al. 2005, Partridge et al. 2005, Aeby et al. 2009, de Bruine et al. 2011, Hasegawa et al. 2011, Thompson 2011), and thalamo-cortical pathways in the optic radiations (Bassi et al. 2008). However, no study has used tractography to investigate thalamo-cortical connectivity in a group of preterm infants at term-equivalent age.

Behrens et al. demonstrated how probabilistic tractography can be used to map pathways between the thalamus and the cortex (Behrens et al. 2003b). Using a probabilistic model, multiple streamlines were propagated from a thalamic seed mask, with those that passed through a pre-defined target region

retained. Voxels within the thalamic mask were then clustered according to the likelihood of connection to one of six anatomically-defined cortical regions. Clusters of commonly-connected voxels defined in this way correspond, in part, to the major thalamic nuclei (Morel et al. 1997, Johansen-Berg et al. 2005); appear to have distinct functional roles (Johansen-Berg et al. 2005, Zhang et al. 2010); and share considerable spatial correspondence across adult populations (Johansen-Berg et al. 2005, Traynor et al. 2010). Counsell et al. previously used this technique to map thalamo-cortical connections in children born preterm and demonstrated altered thalamic topography in a 2-year old infant with a unilateral porencephalic cyst (Counsell et al. 2007). Performing tractography-based parcellation in neonatal populations requires a modified processing pipeline (Ball et al. 2011a; see Appendix E) but can produce population-based connectivity maps that correspond well to those defined in adults and to functional maps obtained from paediatric populations (Figure 6.1A; Fair et al. 2010, Traynor et al. 2010). However, individual thalamic maps remain highly variable, both across subjects and across hemispheres (Figure 6.1B).

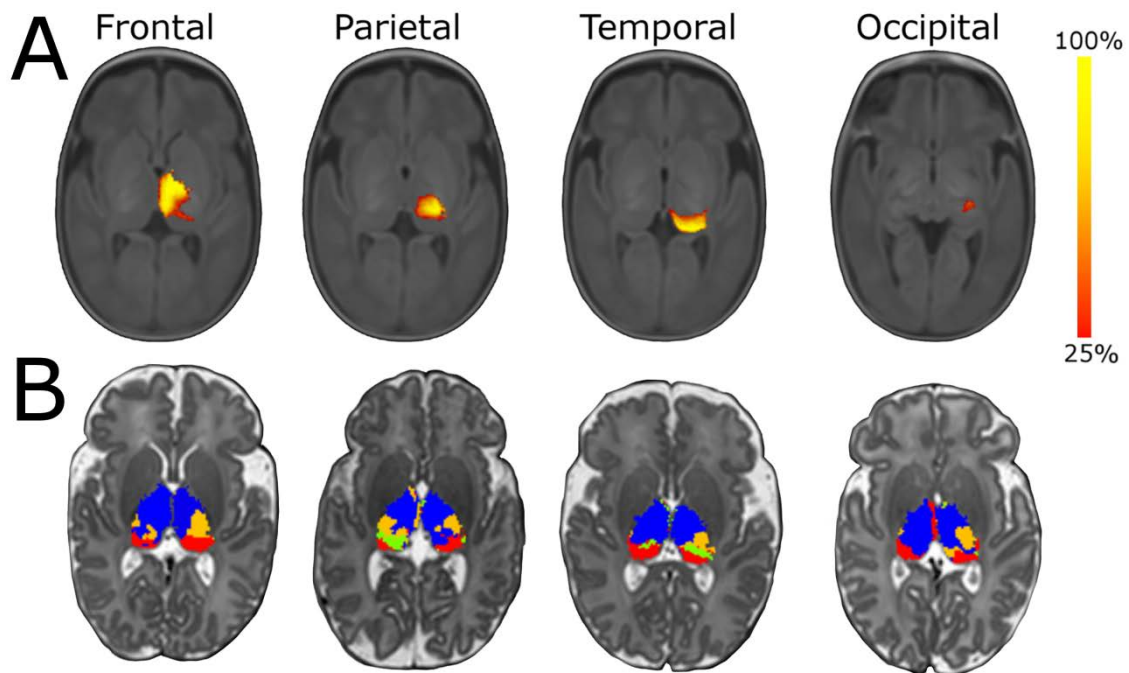


Figure 6.1: Connectivity-based thalamic segmentation in preterm neonates. Probabilistic tractography was used to segment the thalamus in 47 preterm infants at term-equivalent age. Thalamic clusters were defined by maximal connectivity to the frontal (blue voxels), parietal (orange), occipital (green) and temporal (red) cortices. Connectivity maps in (A) show the shared spatial extent of each region across the group. The colour bar indicates the proportion of individual with co-localised parcellations. Four individual connectivity-based parcellations are shown in (B).

Although it is possible to define connections between regions using standard probabilistic tractography algorithms, using these data to quantify structural connectivity can lead to errors in interpretation (Jones and Cercignani 2010). Specifically, calculating the proportion of streamlines reaching a target from the total number of streamlines propagated from a seed does not necessarily represent the

‘connectivity’ of the two regions; a more accurate description would be a measure of confidence that a pathway between them exists (Jones 2008). As such, connection strength calculated in this way is dependent not only on the underlying tissue microstructure but also on the relative size of the seed and target regions, the distance between them and the shape of the connecting pathways (Jones and Cercignani 2010), factors that are particularly pertinent to the current analysis, given the wide variations in cerebral anatomy seen in preterm neonates.

An alternative approach is to estimate connectivity strength from the diffusion anisotropy calculated along the length of the tract (Iturria-Medina et al. 2008, Robinson et al. 2008, Robinson et al. 2010). Scalar measures of diffusional anisotropy, such as FA, reflect the underlying tissue microstructure and are sensitive to the effects of prematurity in neonates (Huppi et al. 1998a, Beaulieu 2002). However, these voxelwise metrics are not suitable for tractographic studies as they are rotationally invariant and do not account for the direction of the underlying fibre trajectories. Instead, local anisotropy *along* tracts can be estimated from the diffusive transfer, or ‘information flow’, between adjacent voxels, and calculated directly from the partial volume (ball-and-stick) model of diffusion at each voxel (Iturria-Medina et al. 2008, Robinson et al. 2010). Importantly, this method provides an estimate of structural connectivity independent of tract length and macrostructural differences between subjects, and is therefore well suited to studying preterm infants.

Previously, this approach has been used to trace connections across the whole brain, defining connectivity between 83 ROI and identifying age-dependent alterations across the network with multivariate statistics (Robinson et al. 2010). Prior to tractography, each region was defined by propagating labels from a set of manually labelled atlases (Hammers et al. 2003, Heckemann et al. 2006; Gousias et al. 2008). Few atlases exist for neonatal populations with such extensive labelling (Shi et al. 2010, Shi et al. 2011) and none as yet exist for preterm neonates. As an alternative to anatomic parcellations, Hagmann et al. split the cortex into between 500 and 4000 small regions of similar surface area to create a dense network of nodes, between which connectivity was estimated (Hagmann et al. 2007, Hagmann et al. 2008). This method allows inter-regional connectivity to be mapped across the whole cortex with relatively high resolution.

Aims

In this Chapter, a novel method for describing thalamo-cortical connectivity in neonates is proposed. By splitting the cortex into small, randomly assigned target regions, and estimating diffusive transfer, or mean anisotropy, along tracts that connect a pre-defined thalamic seed to each target, a topographic map of connectivity between the thalamus and the whole cortex is constructed for each infant. As proof of principle, a comparison between preterm infants at term-equivalent age and term born controls is undertaken, and the effect of prematurity at birth is investigated.

It is hypothesised that thalamo-cortical connectivity will be significantly different in preterm infants at term-equivalent age, and will be adversely affected by increasing prematurity at birth.

6.2 Material and Methods

Ethical permission for this study was granted by the Hammersmith and QCCH Research Ethics Committee. Written parental consent was obtained for each infant.

Subjects

All infants born at less than 36 weeks gestational age (as defined by the last menstrual period) between March 2005 and October 2008 who successfully underwent T_1 - and T_2 -weighted MRI and 32-direction DTI acquisition at term-equivalent age were eligible for inclusion. Infants were excluded if cystic PVL or HPI was apparent on the term-equivalent MRI. All infants were included in the studies described in Chapter 4 and 5.

Forty-seven preterm infants (26 male) underwent successful imaging. The final cohort had a median gestational age of 28^{+3} (range: $23^{+4} - 34^{+6}$) weeks, a median postmenstrual age at scan of 41^{+3} ($38^{+2} - 44^{+1}$) weeks and median birth weight of 1.11 (0.63 – 2.37) kg. No infants received postnatal steroids.

In addition, eighteen term-born infants (7 male) were included to act as controls. Each successfully underwent T_1 - and T_2 -weighted MRI and 32-direction DTI acquisition between October 2006 and February 2011 as part of ongoing studies at QCCH. Median gestational age at birth was 39^{+2} ($36^{+0} - 41^{+6}$) weeks, median age at scan was 41^{+6} ($39^{+0} - 44^{+4}$) weeks and median birth weight was 3.20 (2.68 – 4.20) kg.

Imaging

MRI was performed on a Philips 3-Tesla system (Philips Medical Systems, Netherlands) using an 8-channel phased array head coil. T_1 -weighted and T_2 -weighted fast-spin echo MRI were acquired as described in Chapter 5. Single shot EPI DTI was acquired in the transverse plane in 32 non-collinear directions using the following parameters: TR: 8000 ms; TE: 49 ms; slice thickness: 2 mm; field of view: 224 mm; matrix: 128×128 (voxel size: $1.75 \times 1.75 \times 2$ mm); b -value: 750 seconds/mm²; SENSE factor of 2.

All examinations were supervised by a paediatrician experienced in MRI procedures. Infants were sedated with oral chloral hydrate (25 – 50 mg/kg) prior to scanning and pulse oximetry, temperature and electrocardiography data were monitored throughout. Ear protection was used for each infant, comprising earplugs moulded from a silicone-based putty (President Putty, Coltene Whaledent, Mahwah, NJ) placed in the external ear and neonatal earmuffs (MiniMuffs, Natus Medical Inc, San Carlos, CA).

Tractography

Tractography was performed as described in Robinson et al. (2010). Each infant's diffusion weighted images were affine-registered to the respective non-diffusion weighted image to correct for subject motion and geometric distortions due to eddy currents. Bayesian estimation was used to fit the parameters of a two-compartment partial volume model of diffusion, fitting up to two fibres per voxel,

and distributions on the principal directions of diffusion were generated based on Metropolis Hastings Markov Chain Monte Carlo sampling of the diffusion data using BedpostX (implemented as part of FSL; Behrens et al. 2003a, Behrens et al. 2007).

Streamlines were propagated from a thalamic seed mask and at each step, followed the direction of a sample drawn from the posterior distribution on diffusion direction at a given voxel; the probability of sampling a voxel was given by the weighted proximity of the streamline trajectory to the centre of nearby voxels. Around 500 000 streamlines were propagated from each thalamic seed mask (one mask per cerebral hemisphere), for a total of 2000 steps of 0.5mm in length, tracking stopped when streamlines reached a target region, left the brain mask (or entered CSF), breached a curvature threshold of 0.1 (reduced from the default 0.2) or crossed into the contralateral hemisphere. Regions of CSF were defined by tissue segmentation based on age-specific tissue probability priors (Kuklisova-Murgasova et al. 2011).

In contrast to Behrens et al. (2003a), local diffusion anisotropy was estimated along each streamline that reached a cortical target. This measure incorporates information pertaining to both diffusional anisotropy at each voxel (in a similar way to FA) and fibre coherence between remote regions (Iturria-Medina et al. 2008). Using a modified version of the ProbtrackX algorithm, orientation distribution functions (ODF) were calculated from the partial volume model of diffusion as described in Equation 6.1 (Melie-Garcia et al. 2008):

$$\psi(\theta, \phi) = \frac{1}{N_s} \sum_{k=1}^n \sum_{l=1}^{N_s} f_{kl}^{(\theta, \phi)} \quad [6.1]$$

where n is the total number of fibres, N_s is the total number of Monte Carlo samples drawn from the diffusion data and $f_{kl}^{(\theta, \phi)}$ is the fractional volume of anisotropic diffusion along orientation (θ, ϕ) for iteration l and fibre direction k . The ODF ψ along orientation (θ, ϕ) is equivalent to the probability of diffusion in that direction.

The proportion of the ODF which overlaps between adjacent voxels on the streamline trajectory approximates the probability of diffusive exchange between voxels. Mean anisotropy between connected regions is calculated by averaging the diffusive exchange between adjacent voxels connected by a streamline multiplied by the number of times each voxel is sampled during tractography (Robinson et al. 2010).

In Robinson et al., region-to-region measures of anisotropy were collated into a whole-brain connectivity matrix (Robinson et al. 2010). In the present study, under the prior hypothesis that thalamo-cortical connectivity is vulnerable following preterm birth, tractography was performed only between the thalamic seed and each cortical target region. All streamlines that reached a cortical target were used

to estimate tract anisotropy. Mean thalamo-cortical anisotropy was then mapped back onto each target region to create a cortical map of connectivity (see Figure 6.2).

Cortical parcellation

Cortical tissue segmentation was performed on individual T_2 images as described in Chapter 5 using an expectation-maximisation segmentation method driven by age-specific tissue probability priors followed by an automatic three-step segmentation algorithm to remove mislabeled partial volume voxels at the interface of the grey matter and CSF (Xue et al. 2007, Kuklisova-Murgasova et al. 2011).

Calculating connectivity between the thalamus and every cortical voxel would require significant computational time, and is beyond the capabilities of even a high-end desktop PC. Therefore, it is necessary to group voxels together into regions, the size of which determine the resolution of the connectivity map. Each region needs to be large enough to ensure that a representative number of streamlines pass through it, yet small enough so that the map retains the spatial variation across the cortex at a reasonable resolution (Hagmann et al. 2007). For the purpose of this study, each cortical hemisphere was parcellated into around 500 regions (Left hemisphere: median (range) = 507 (391 – 703); Right hemisphere: median (range) = 505 (386 – 676); see Figure 6.2).

Cortical parcellations were performed using Matlab 7.10 (MathWorks, Natick, MA, USA) with code supplied by Dr. P. Aljabar. Poisson disk sampling describes a method used to randomly place points across a grid, while ensuring that no two placements are within a set distance of each other, producing an evenly distributed but random set of points (Cook 1986, Bridson 2007; Figure 6.2). By defining each voxel in the cortical mask on a 3 dimensional grid, it is possible to use Poisson disk sampling to select a set of evenly distributed centroids, about which other voxels are clustered according to their proximity. This produces a randomly generated set of labels, each with similar size to act as targets for tractography (Figure 6.2). Hemispheres were labelled separately to ensure that no labels incorporated voxels from both.

Unlike Hagmann et al. (2007), this labelling method is not underpinned by an initial anatomic parcellation, therefore it is possible that labelled regions may contain topographically close, but functionally distinct regions or cross over anatomical features such as sulci (see Figure 6.2D). This means that, as each cortical mask is labelled separately, corresponding regions across individuals will not be labelled in the same way. As such, connectivity maps based on a single parcellation are not directly comparable across subjects. To account for this, cortical masks were re-parcellated a number of times to produce a set of connectivity maps for each subject.

Assuming that the labels are distributed evenly and randomly each time, connectivity at each voxel can be estimated from a distribution constructed by performing tractography between the thalamus and each set of cortical labels (Figure 6.3). With enough parcellations, averaging each infant's set of cortical connectivity maps will produce a final map with single voxel resolution.

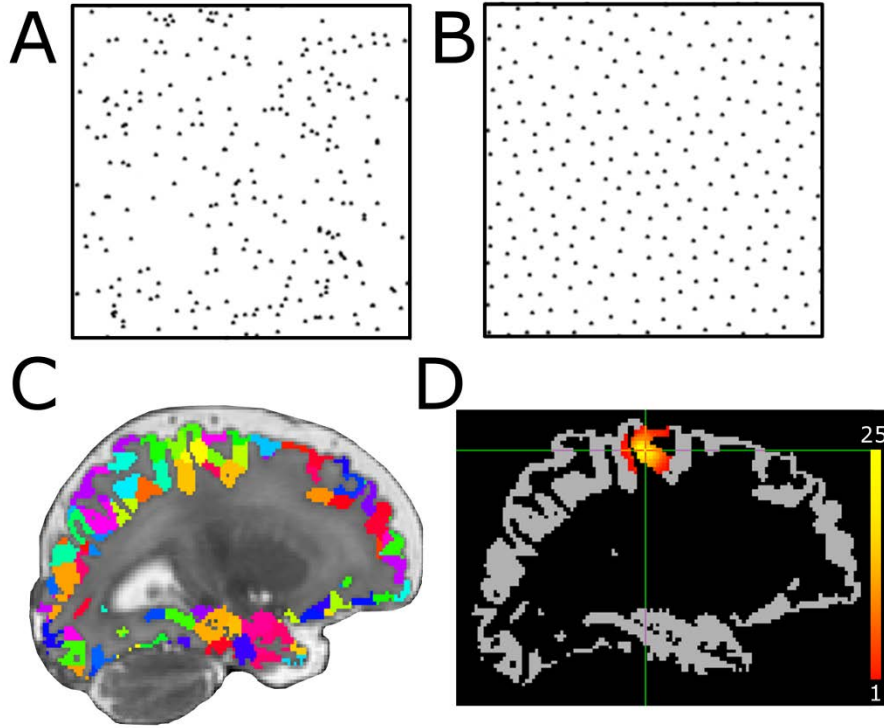


Figure 6.2: Cortical parcellation using Poisson disk sampling. A set of points generated with random sampling (A) and Poisson disk sampling (B). Note the even distribution of points in (B). Labels are generated by clustering voxels about centroids within the cortical mask generated with Poisson disk sampling (C). A single voxel (crosshairs) was chosen to demonstrate the spatial distribution of co-labelled voxels after 25 parcellations (D). The colour bar indicates how often surrounding voxels are clustered within the same labels as the chosen voxel.

Figure 6.3 shows that as few as 10 parcellations can produce an estimate of mean anisotropy at a voxel level which does not differ significantly with additional re-parcellations. However, for this study, 25 were chosen to ensure an accurate estimation of connectivity with reasonable computational demands. To confirm that the connectivity estimates were stable after 25 parcellations, connectivity maps were constructed from 25 and 100 separate parcellations in 10 infants. Each map was transformed into a common reference space and smoothed with a Gaussian kernel (full-width-at-half-maximum (FWHM) = 8mm) and a paired t -test performed across the whole cortex with Randomise. No significant differences between mean anisotropy were detected.

Registration

Each infant's T_1 - and T_2 -weighted and non-diffusion weighted B_0 images were co-registered with IRTK. Although a 6 DOF registration was used to align corresponding T_1 - and T_2 -weighted images, due to geometric distortions present in the EPI-acquired B_0 images, nonlinear registration was used to align each to the corresponding T_2 -weighted image. A manually defined thalamic seed mask (Chapter 5; Figure 5.1) was transformed into the space of each infant's diffusion data via the co-registered T_1 and T_2 images. Similarly, cortical parcellations were transformed from T_2 into diffusion space for tractography, nearest neighbour interpolation was used to preserve mask labelling for both seed and target masks.

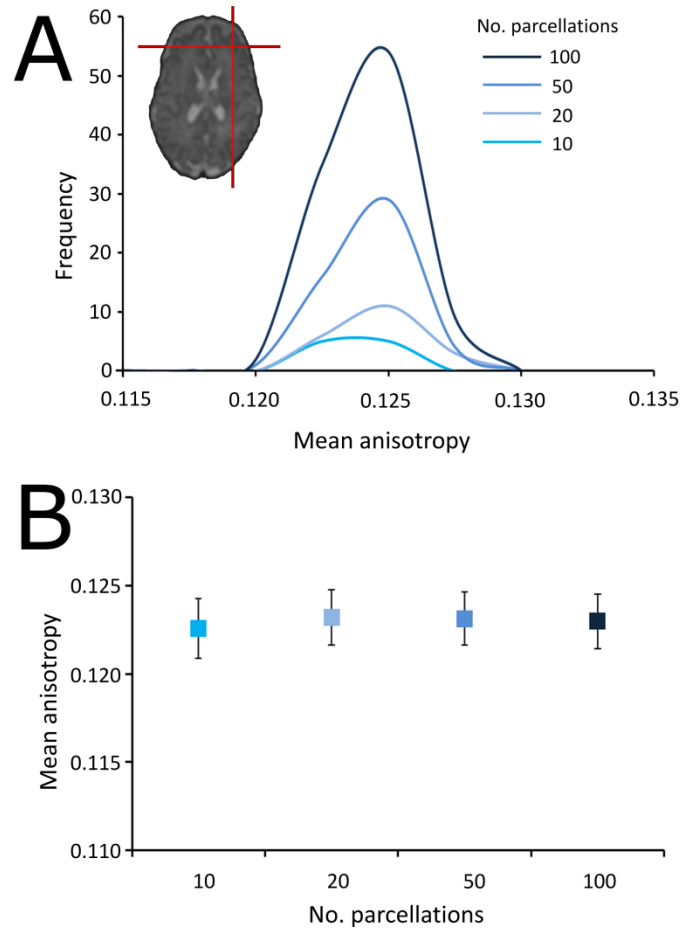


Figure 6.3: Connectivity estimates after repeated parcellations. The left hemispheric cortical mask from a single infant was parcellated and tractography was performed between the thalamus and each labelled region 100 times. Mean tract anisotropy, as an estimate of connectivity, was calculated across the cortex and the distribution of mean anisotropy estimated at a single voxel (crosshairs) from 10, 20, 50 and 100 connectivity maps is shown in (A), mean (\pm SD) anisotropy at this voxel, estimated from each set of maps is shown in (B).

Processing pipeline

Figure 6.4 summarises the processing pipeline used in this Chapter. Cortical segmentations were extracted from each T_2 -weighted image and randomly parcellated 25 times. Each parcellation, along with a thalamic seed mask, was transformed into the individual diffusion space. Probabilistic tractography was performed between the thalamus and each labelled cortical region and the mean anisotropy of the connecting tracts calculated as an estimate of structural connectivity. Twenty-five connectivity maps were constructed by mapping mean anisotropy back onto each cortical region and a final voxelwise map created by averaging connectivity across them. Individual maps were then aligned to a common template, smoothed and merged into a 4D volume for statistical analysis.

For statistical analysis, cortical connectivity maps were transformed into a common reference space. A population-average atlas, constructed from a large ($n=204$) cohort of preterm infants, was used as the template (Serag et al. 2011). Each T_2 -weighted image was aligned with the template using rigid, affine

and nonlinear registration in a coarse-to-fine manner, as described in Chapter 5. A single iteration of nonlinear registration was used.

As previously noted, this method of nonlinear registration does not necessarily ensure precise cortical alignment, particularly if the ensuing transformations are required to be smooth and invertible. To account for residual misalignment in the cortex following registration, the aligned connectivity maps were smoothed with a Gaussian kernel (FWHM = 8 mm) prior to statistical analysis.

Statistical analysis

Voxelwise cross-subject statistical analysis of mean tract anisotropy was performed with Randomise (v2.5). All statistical images were subject to FDR correction for multiple comparisons. Further statistical analysis was performed with SPSS 17.0 (SPSS Inc., Chicago, IL, USA).

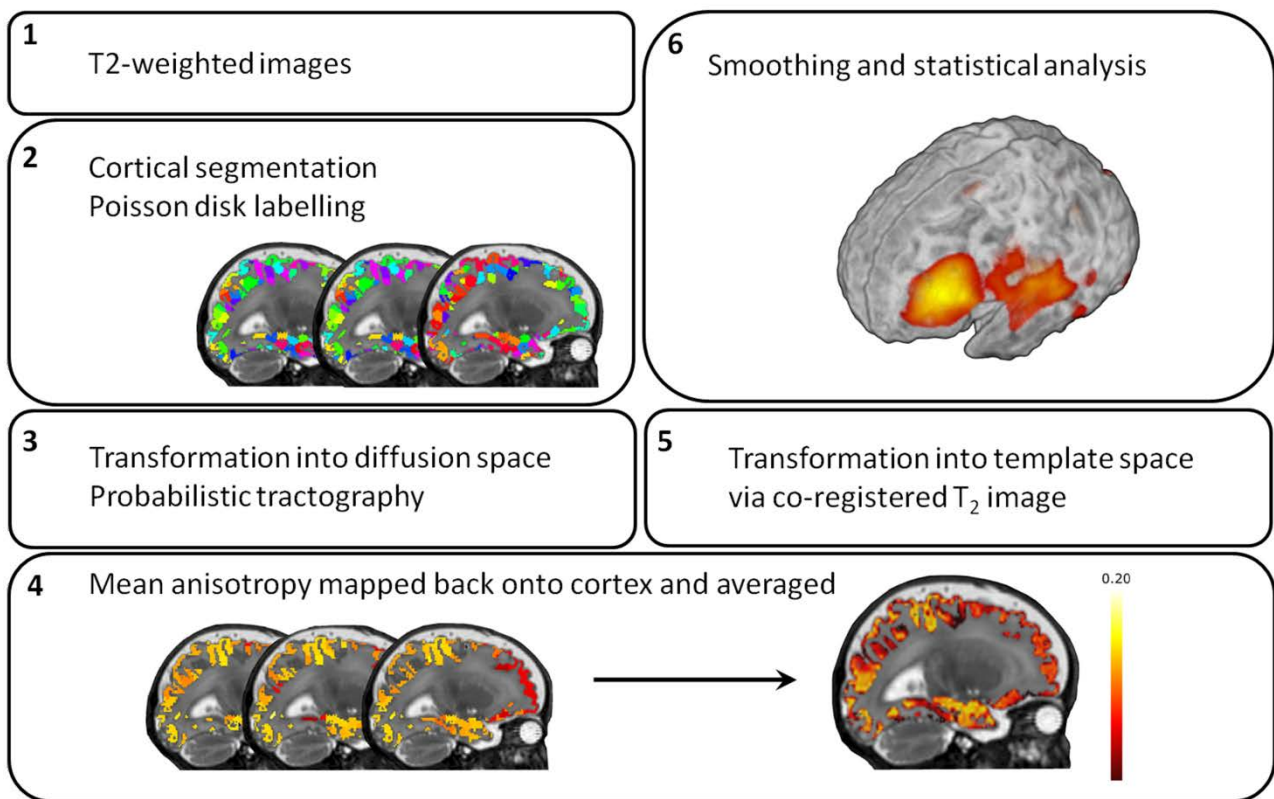


Figure 6.4: Processing pipeline used for assessing thalamo-cortical connectivity in neonates.

6.3 Results: Comparison to Term-Born Controls

Figure 6.5 shows cortical regions with significantly lower connectivity to the thalamus in preterm infants at term-equivalent age compared to term-born controls, as represented by mean anisotropy estimated along connective tracts (FDR-corrected, $p < 0.001$). Connectivity was significantly reduced bilaterally between the thalamus and the lateral frontal cortex. This pattern extended partially into

the insula and into the superior temporal gyrus on the left side. Additionally, large bilateral clusters were seen in the medial wall, including medial supplementary motor areas, and the medial occipital lobe with smaller unilateral clusters in the parahippocampal gyrus, inferior temporal gyrus, temporal-occipital junction and precuneus. Connectivity was not significantly increased in any region in the preterm group. Significant clusters of voxels in three anatomical regions were identified and are shown in Figure 6.6 (medial occipital, green; medial wall, red; frontal, purple); each region was bilaterally represented but manually defined in the left hemisphere only. Within each of these regions, mean anisotropy estimates were extracted from each infant's connectivity map and are shown for preterm and term cohorts in Figure 6.6B. Mean anisotropy was between 15 and 35% greater in term infants. The largest difference was in thalamo-cortical connections to the occipital lobe (Term: mean anisotropy \pm SD = 0.122 ± 0.022 ; Preterm: 0.091 ± 0.017), followed by the frontal (Term: 0.154 ± 0.014 ; Preterm: 0.126 ± 0.013) and medial regions (Term: 0.167 ± 0.023 ; Preterm: 0.144 ± 0.020).

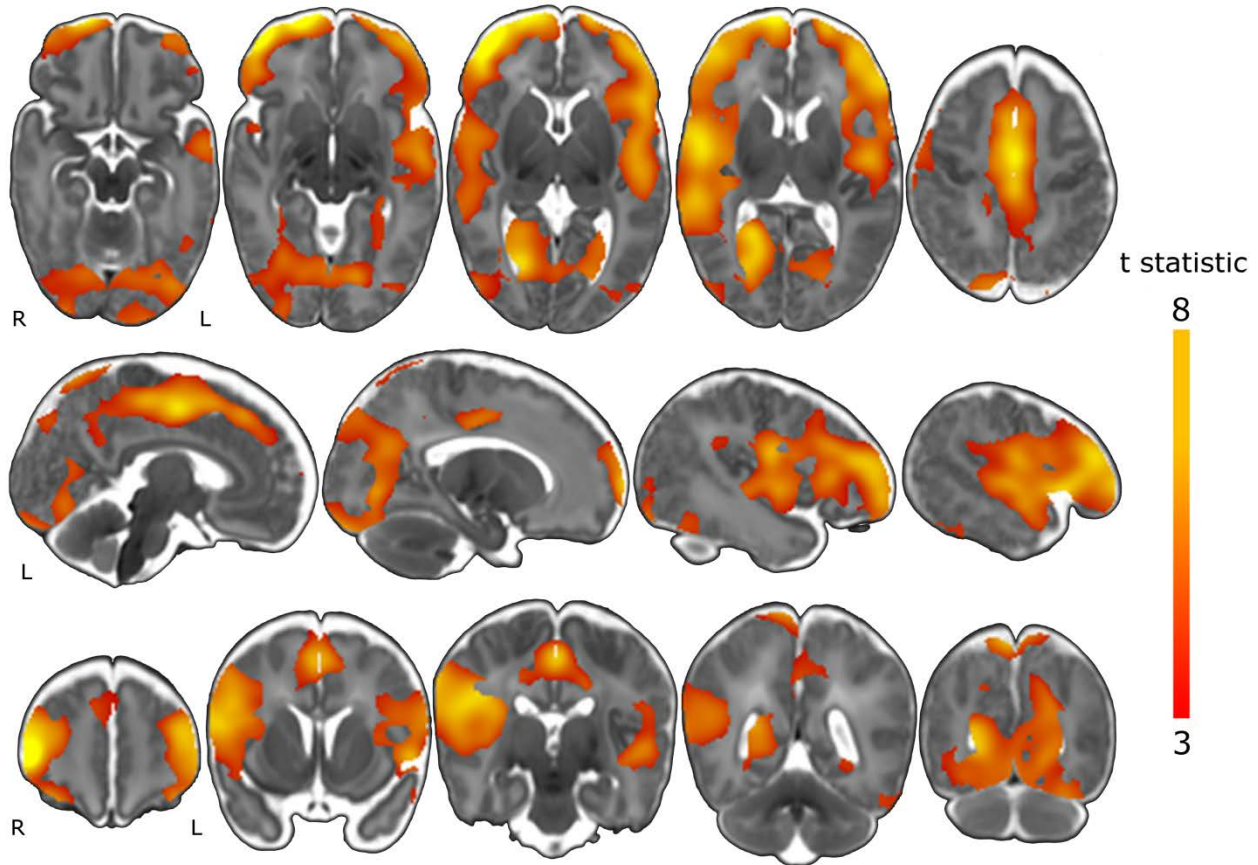


Figure 6.5: Thalamo-cortical anisotropy is significantly lower in preterm infants. Regions of significantly lower thalamo-cortical connectivity in preterm infants, compared to term born controls, are shown. Statistical images are displayed on a population-based T_2 template and are corrected for multiple comparisons at $p < 0.001$ FDR-corrected (colour bar indicates t-statistic).

To visualise the pathways that connect the thalamus to each ROI, standard probabilistic tractography was performed (Behrens et al. 2003a). The thalamic seed and each ROI mask were transformed into individual diffusion space to act as seeds and targets. Tractography was performed by seeding first

from the thalamus, and then from the cortical ROI, the resulting connectivity distributions were combined to give probability maps, where the intensity of each voxel reflects the certainty of it lying on the diffusive pathway from seed to target, or from target to seed. Each map was thresholded to include only voxels with a greater than 5% chance of belonging to a given tract, and binarised to create a tract mask. Each mask was transformed back into the template space and combined to show the spatial extent, across the whole cohort, of tracts connecting the thalamus to each cortical ROI (Figure 6.7).

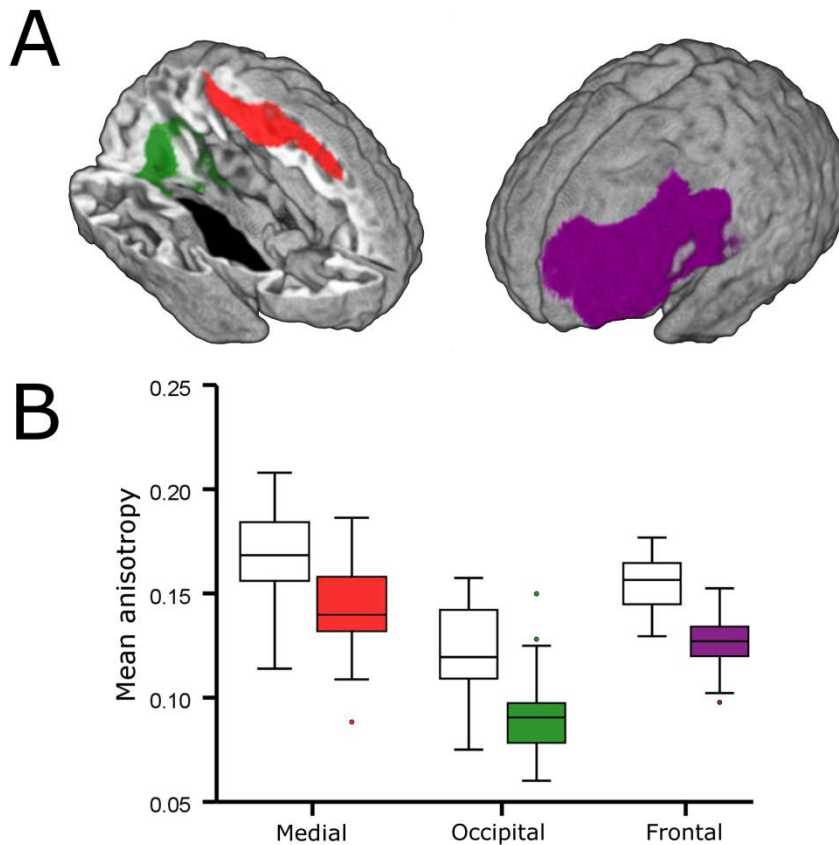


Figure 6.6: Mean anisotropy extracted from three regions-of-interest. Three large clusters identified in Figure 6.5 were manually defined and are shown in (A). For each group, mean anisotropy was extracted from the medial wall (red), medial occipital lobe (green) and frontal lobe (purple) and are plotted in (B). Coloured plots represent the preterm group.

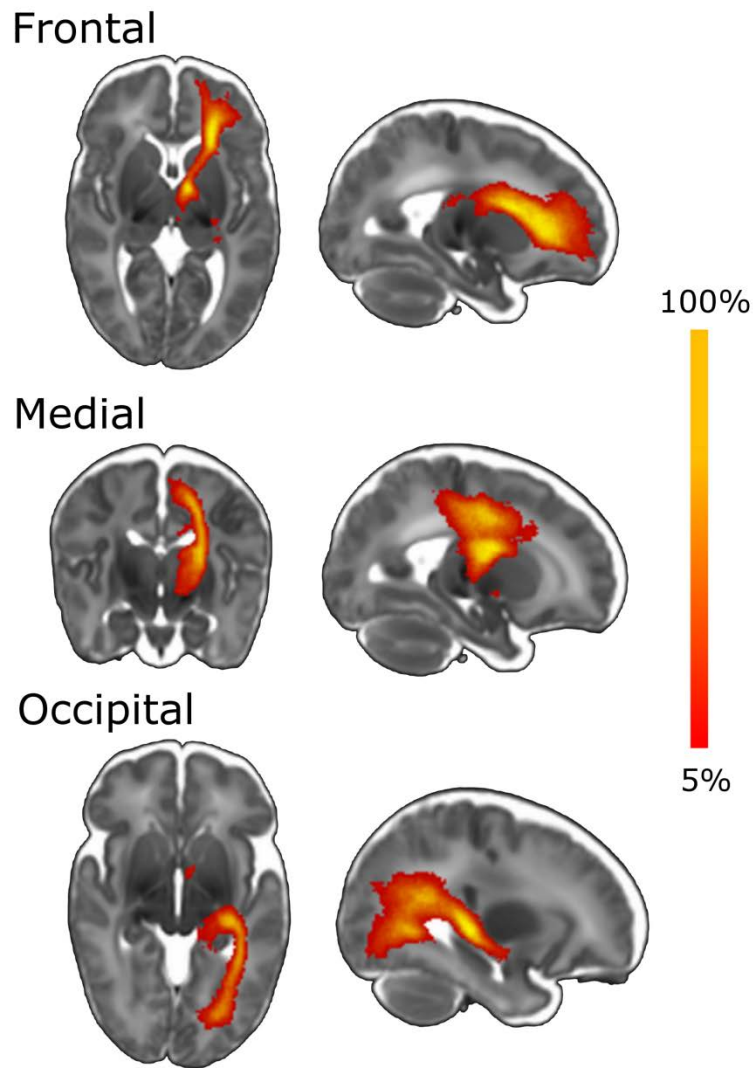


Figure 6.7: Spatial extent of specific thalamo-cortical tracts that appear significantly affected in preterm infants. Tractography was performed in each infant (both term-born and preterm) between the thalamus and each cortical ROI shown in Figure 6.6. Population-average maps, indicating the spatial overlap of each tract across the whole group, are shown overlaid on the template. The colour bar indicates the degree of overlap across the group, thresholded at 5% (i.e. voxels are shown that formed part of the tract in at least 5% of the cohort). Regions are defined as in Figure 6.6. Tractography was performed in the left hemisphere only.

6.4 Results: Effect of Prematurity on Connectivity

Linear regression was performed in the cohort of 47 preterm infants at term-equivalent age to determine if thalamo-cortical connectivity was dependent on gestational age at birth. Figure 6.8 shows regions where a trend-level association between prematurity and connectivity exists (uncorrected $p < 0.01$). Bilateral clusters were seen in the precuneus, orbitofrontal and anterior temporal lobes but these regions did not survive correction for multiple comparisons with FDR.

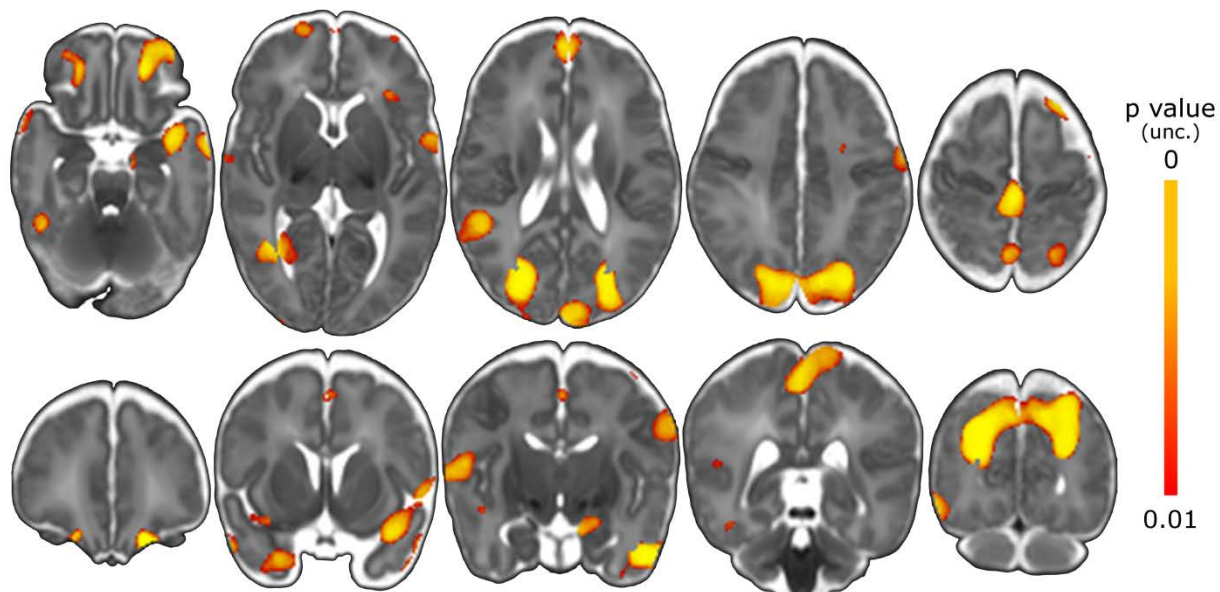


Figure 6.8: Association between thalamo-cortical connectivity and prematurity at birth.

Regions where diminished connectivity to the thalamus was associated with increasing prematurity at birth, after correction for the age of each infant at scan are shown. Images are uncorrected for multiple comparisons, and are shown at voxelwise $p < 0.01$. No regions survived FDR correction.

6.5 Discussion

Using a novel processing pipeline, this study has shown that thalamo-cortical connectivity is significantly diminished in preterm infants compared to term-born controls. Connections between the thalamus and the frontal cortices, supplementary motor areas and medial occipital lobe appear to be most significantly affected, with additional regions identified in the superior temporal and parietal lobes. Performing tractography between three sites of altered connectivity demonstrated that specific thalamo-cortical tracts are disrupted, apparently originating from discrete regions of the thalamus. Although no significant association with gestational age at birth was detected in the preterm cohort, this supports the hypothesis that the thalamo-cortical system is vulnerable following preterm birth. This study represents the first time that thalamo-cortical connectivity has been comprehensively mapped in a neonatal population, and the tractographic framework described represents a novel method for analysing system connectivity that does not rely on atlasing, or manual placement of ROI and can be readily applied to other populations and to investigate other neural systems.

Diffusion imaging enables *in vivo* tracing of neural pathways through the brain and provides complementary evidence to that derived from experimental animal studies, or post mortem histology and dissection (Goldman-Rakic and Porrino 1985, Morel et al. 1997, Scannell et al. 1999, Behrens et al.

2003b). Recently, diffusion tractography has been used to map cortical connections in the human thalamus that mirror histological observations and are reliably reproduced across cohorts (Morel et al. 1997, Behrens et al. 2003b, Johansen-Berg et al. 2005, Traynor et al. 2010). Other studies have exploited diffusion datasets to infer dense structural networks of information flow across the whole brain that are sensitive to aging and disease state (Stam et al. 2007, Hagmann et al. 2008, Rubinov et al. 2009, Robinson et al. 2010). In this Chapter, these approaches were combined and thalamo-cortical connections were mapped using a modified probabilistic tractography algorithm designed to estimate the mean anisotropy along connective paths as measure of structural connectivity (Robinson et al. 2008, Robinson et al. 2010). In addition, a novel method for cortical labelling was employed alongside tissue segmentation and nonlinear registration techniques previously optimised for neonatal analysis (Rueckert et al. 1999, Boardman et al. 2006, Xue et al. 2007). This enabled regional estimates of connectivity to the thalamus to be compared between preterm and term infants across the whole cortex for the first time.

Using DBM, Boardman et al. observed regional tissue loss in the thalamus of preterm infants compared to term-born controls and hypothesised that it reflected a disconnection between the thalamus and cortex in these infants (Boardman et al. 2006). In a later study, this tissue loss was localised to the mediodorsal thalamus and presumed to reflect altered connectivity to the frontal cortex via the anterior thalamic radiations (Boardman et al. 2010). Focal thalamic tissue loss was also accompanied by reduced white matter volume and increased ADC in central corona radiata and centrum semiovale. In Chapter 5, a significant association was described between prematurity and volume in the frontal and temporal lobes that corresponded to thalamic and cortical volume loss. In this Chapter, connectivity between the thalamus and the lateral frontal cortex was shown to be significantly reduced in preterm infants. Subsequent tractography (Figure 6.7) demonstrated that the most likely path of connection between these structures originates from the medial aspect of the thalamus and travels via the anterior thalamic radiation towards the frontal lobe. Connectivity to the medial paracentral gyri, encompassing the supplementary and pre-motor areas, was also significantly decreased. These connections follow the superior thalamic radiation from the lateral portion of the thalamus through the central corona radiata.

Histological evidence from primates shows that the mediodorsal nucleus of the thalamus shares reciprocal projections to the lateral frontal cortex (commonly referred to as the prefrontal cortex), with auxiliary connections to the anterior cingulate, insula and supplementary motor cortex (Tanaka 1976, Goldman-Rakic and Porrino 1985, Russchen et al. 1987). The prefrontal cortex (PFC) is linked with a myriad of high level cognitive and executive functions, including but not limited to working memory, planning and attentional control (Baddeley 1992, Goldman-Rakic 1996, Fuster 2001), damage to which produces an assortment of well described cognitive and behavioural deficits (Stuss and Benson 1984, Stuss and Levine 2002). In ex-preterm adolescents, deficits in executive functions have been reported that are independently associated with altered cerebral structure (Nosarti et al. 2007, Nosarti et al. 2008), and the general poor performance of preterm children in tests of cognitive function are well reported (Rose and Feldman 1996, Harvey et al. 1999, Anderson, et al. 2004, Marlow et al. 2005, Marlow et al. 2007). Similarly, motor and coordination impairments are prevalent, observed in up to

40% of preterm children (Bracewell and Marlow 2002, Foulder-Hughes and Cooke 2003, Goyen and Lui 2009). The supplementary motor areas (SMA) of the medial wall and the more anterior pre-SMA regions are essential for planning and fluent execution of complex movements and are involved in coordinating movements of the hands, and incorporating visual guidance into movement (Goldberg 1985, Tanji 1994, Picard and Strick 1996). Histological studies have revealed that the SMA is connected to the primary motor cortex (Dum and Strick 1991, He et al. 1995) and the pre-SMA to the PFC (Bates and Goldman-Rakic 1993, Luppino et al. 1993). Additionally, both the SMA and pre-SMA receive significant input from the basal ganglia via the ventrolateral nucleus of the thalamus (Schell and Strick 1984, Inase et al. 1999, Sakai et al. 2000, Akkal et al. 2007), as part of a complex motor feedback loop essential for coordinated movement (Goldberg 1985). This agrees with the likely path of projections to significant voxels in the SMA shown in Figure 6.7 that appears to originate in the ventrolateral thalamus (in comparison to the medial aspect of the frontal projections). Altered thalamo-cortical connectivity to the medial premotor areas and the lateral frontal cortex may therefore represent a neural substrate for the complex and overlapping cognitive and motor coordination disorders commonly seen in this population.

In addition to higher level cognitive functions, primary sensory morbidity is also prevalent following preterm birth. The incidence of retinopathy of prematurity increases with prematurity at birth and mild visual impairments have been reported in almost half of extremely preterm infants by 6 years of age (Repka 2002, Austeng et al. 2009, Johnson et al. 2009). In the present study, significant bilateral reductions in thalamo-cortical connectivity were also seen in the medial occipital cortex of preterm infants. The medial occipital cortex is the site of the primary visual cortex V1, and the extrastriate primary association areas, that receive direct innervation from the lateral geniculate nucleus of the thalamus via the optic radiations (see Figure 6.7) (Lund 1988, Felleman and Van Essen 1991), indicating that this pathway could be disrupted in preterm infants. Cortical visual impairment is a leading cause of poor vision in childhood but it is predominantly associated with perinatal hypoxic-ishaemic injury (Repka 2002). Similarly, in preterm infants, PVL is associated with a range of visual impairment including low visual acuity, oculomotor disorders, and reduced visual field, often accompanied by thalamic atrophy (Cioni et al. 1997, Ricci et al. 2006). In the present cohort, no infants had focal parenchymal lesions such as PVL but this does not rule out a lesser maldevelopment of the visual pathways. Both human and animal studies have demonstrated that the connections between the lateral geniculate nucleus and the visual cortices begin to develop around mid-gestation and are established by term-equivalent age (Rakic 1977, Shatz and Rakic 1981, Kostovic and Rakic 1990) and early exposure to the extrauterine environment does not appear to affect this timing (Bourgeois et al. 1989). In contrast, FA in the optic radiations at term-equivalent age is associated with visual function (Bassi et al. 2008), and importantly, it is the rate of development of these pathways, in terms of increasing FA, during the neonatal period that best predicts visual function (Groppa et al. 2009). This indicates that delayed or disrupted maturational processes associated with established neural connections may underlie the reduction in thalamo-cortical connectivity in preterm infants.

Alternatively, the lessened connectivity to the occipital cortex may be suggestive of a confounding technical issue. Due to the high curvature of the optic radiations, particularly through the anterior projection of Meyer's loop, it can be difficult to trace its full extent, even with probabilistic methods (Behrens et al. 2003b, Clatworthy et al. 2010). Reaching the medial wall of the occipital lobe requires streamlines to circumvent the entire lateral horn of the ventricles, which are significantly larger in preterm infants (Inder et al. 2005, Boardman et al. 2007). This may have led to a reduction in streamlines reaching medial occipital targets, or to increased partial volume effects due to the proximity of path trajectories to voxels containing CSF, both of which may have artefactually reduced connectivity scores in the preterm cohort. Further investigation of all the pathways described here, possibly using a traditional ROI-based approach, would be required to confirm the observations made in this Chapter.

As proof of principle, this study has demonstrated that it is possible to describe thalamo-cortical connectivity in the neonate in a manner that is sensitive to the effects of preterm birth. As preliminary work, there are a number of technical considerations to note. A clear limitation is the need for precise alignment of cortical connectivity maps in a common space for statistical analysis. In order to accurately resolve regional differences in thalamo-cortical connectivity, it is necessary to align structurally correspondent regions across individuals. The inherent heterogeneity of the cortical surface coupled with the additional factors of rapid growth during the neonatal period and significantly reduced cortical complexity in preterm infants compared to term born controls present a significant technical challenge (Rademacher et al. 1993, Ajayi-Obe et al. 2000, Kapellou et al. 2006, Xue et al. 2007). In TBSS, a skeletonisation step is performed after nonlinear registration that reduces the confounding effects of misregistration; here, a smoothing kernel of FWHM 8 mm was applied. Smoothing generally serves three functions: increasing signal-to-noise ratio, compensating for misalignment and forcing data towards a normal distribution for parametric statistical analysis and, as previously noted, the choice of smoothing kernel can influence statistical inference and interpretation (Jones and Cercignani 2010). Specifically, smoothing sensitises statistical analysis to the detection of effects with a similar spatial extent to the filter used, thus varying the kernel size can produce different, significant effects (Jones et al. 2005). In this Chapter, multi-scale tests using different kernel sizes were eschewed in preference of a single kernel selected *a priori*. Although larger than kernels previously employed in voxel-based neonatal MR analysis (Lodygensky et al. 2008), 8 mm was selected based on the DBM analysis in Chapter 5 where a relatively widespread pattern of regional covariance was observed and hypothesised to reflect a corresponding pattern of altered thalamo-cortical connectivity. Correspondingly large regions of altered connectivity were observed in preterm infants (Figure 6.5), although this may have come at a cost of spatial resolution and the possible detection of smaller clusters in discrete cortical structures.

In contrast, using the tractographic framework described in this Chapter is advantageous for a number of reasons: the data is modelled using a two-compartment, partial volume model, allowing explicit modelling of up to two fibre populations per voxel with a clinically feasible acquisition scheme (Behrens et al. 2007); the uncertainty of the model is incorporated when tracking, allowing streamlines to be seeded in regions of low anisotropy, such as the deep grey matter, and allowed to continue to the cortex

(Behrens et al. 2003a, Behrens et al. 2003b); mean anisotropy calculated along the length of each tract is weighted both by the underlying microstructural integrity of each voxel passed and the probability of each voxel lying on the connective pathway, ensuring that any alterations in tissue microstructure are attributed to the most likely fibre population (Iturria-Medina et al. 2008, Robinson et al. 2010). In addition, the cortical parcellation methods employed do not depend on the availability or accuracy of a densely labelled anatomical atlas and allow exploratory analysis of thalamo-cortical connectivity without prior hypothesis or selection of regions-of-interest.

Finally, it was hypothesised that connectivity would be associated with increasing prematurity at birth, forming a convergent body of evidence with that presented in Chapter 5. However, no significant associations were observed after correction for multiple comparisons. Uncorrected statistical maps are shown in Figure 6.8, indicating that a trend-level association may exist in some regions, including bilaterally in the precuneus, although given the non-significant effect size these observations may not be robust and are difficult to interpret. It is likely that the lack of significant association is attributable to Type II error due to a lack of statistical power in the relatively small group size ($n = 47$, compared to 71 in Chapter 5, and 93 in Chapter 4). Thirty-two direction diffusion imaging was acquired in less than half of the original cohort, but was required for this study as fewer directions (i.e.: 15) will not support multi-fibre modelling for probabilistic tractography (Behrens et al. 2007). Data collection is ongoing and further investigation with a larger cohort will be conducted.

In conclusion, connectivity in the thalamo-cortical system is significantly reduced in preterm infants by term-equivalent age. This may have consequences for neurodevelopmental outcome in this population.

Chapter 7

Summary

7.1 Conclusions

With the increasing burden of preterm birth on health and economic systems and the poor prognosis of many preterm infants in later life, much attention is focused on defining the early neural substrates of subsequent neurodevelopmental deficits commonly seen in this population. In recent years, studies have shown that up to 75% of preterm infants display diffuse alterations in the developing white matter by term-equivalent age (Dyet et al. 2006). Quantitative MR techniques have revealed that subtle, diffuse microstructural disturbances underlie these changes and may be a symptom of early brain injury (Huppi et al. 1998a, Counsell et al. 2003, Inder et al. 2003, Counsell et al. 2006). In addition, volumetric analyses have detected that regional tissue loss, primarily in the cortical and subcortical grey matter, appears to accompany preterm white matter injury (Inder et al. 1999, Inder et al. 2005, Boardman et al. 2006).

The primary hypothesis of this thesis was that connectivity and growth of developing neural systems is adversely affected by preterm birth, this was tested through the application of multi-subject, multi-modal MRI analysis. In Chapters 4 and 5, widespread microstructural alterations in the cerebral white matter and structural alterations involving both cortical and subcortical grey matter were found to be dependent on the degree of prematurity at birth. Furthermore, thalamic development was shown to be related to discrete microstructural alterations in ascending white matter tracts and growth of a number of connected regions, including the cortex as a whole. In Chapter 6, a combination of probabilistic tractography, image registration and tissue segmentation revealed significant reductions in thalamo-cortical connectivity of preterm infants compared to term born controls. In addition, adverse cerebral development was hypothesised to be associated with specific perinatal risk factors. It was found that chronic lung disease potentiated microstructural disturbances in this population, and neonatal respiratory support requirements were linearly related to white matter development.

Respiratory morbidity is associated with poor cerebral development and cognitive outcome but represents a potentially modifiable neonatal risk factor (Short et al. 2003, Boardman et al. 2007, Anjari et al. 2009). The observed relationship between respiratory morbidity and white matter microstructure is concurrent with evidence of damaging inflammatory pathways associated with systemic illness (Back 2006, Back et al. 2007, Miller and Ferriero 2009) and may provide a possible biomarker for investigating alternative ventilation strategies. Computational MR analysis has already proven

powerful in investigating the efficacy of potential therapeutic strategies in neonates (Porter et al. 2010) and this approach would complement current experimental models (Loeliger et al. 2009, Verney et al. 2010). Indeed, imaging studies are increasingly being employed to support biological and clinical research in the discovery of potential biomarkers, establishing a link between early cerebral disruption and outcome (Ment et al. 2009). The substantial power of the methods described in this thesis could lead to a number of applications including the study of putative neuroprotectants (Limperopoulos 2010), or mapping the influence of specific genetic susceptibilities on preterm cerebral development (Nelson et al. 2005).

The evidence presented in this thesis supports current theories of the injurious mechanisms underpinning preterm brain injury (Volpe 2009). That the thalamo-cortical system was shown to be significantly altered by preterm birth is not to say that other neural systems/connections are not similarly affected. TBSS analysis revealed global changes in white matter microstructure are dependent on prematurity, whereas DBM showed gestation-dependent volumetric change was generally restricted to fronto-temporal regions. Similarly, thalamo-cortical connectivity to the frontal cortices was significantly reduced in preterm infants, as was connectivity to the occipital lobes – a region that appeared relatively spared in DBM analysis. The development of the brain follows a strict spatio-temporal schedule (Yakovlev and Lecours 1967, Chi et al. 1977, Molnar et al. 2003, Kostovic and Jovanov-Milosevic 2006, Bystron et al. 2008) and a number of biological pathways involved in preterm brain injury have been shown to be strictly maturation-dependent (Volpe 2001, Back et al. 2007, Deng 2010). Some of the disparities in the results presented may be due, in part, to the ongoing evolution and varying timescales of the processes that underlie MR-visible structural and microstructural disturbances. Overall, the work presented in this thesis suggests that no single cerebral region or tissue type is affected by preterm birth in isolation.

7.2 Future Work

Below are summarised some possible directions for future study to extend upon the work presented in this thesis.

Functional outcomes

Preterm birth is associated with a wide range of neurodevelopmental deficits, the underlying mechanisms of which are not yet fully understood. The results presented here will be most beneficial to current understanding when described in the context of developmental outcome. Previous studies have demonstrated that alterations to tissue volume and microstructure quantified at term-equivalent age can be predictive of short term measures of developmental performance, and therefore can provide early markers for interventional strategies (Inder et al. 2005, Kapellou et al. 2006, Krishnan et al. 2007, Boardman et al. 2010, Rathbone et al. 2011). Neurodevelopmental assessments are currently being

undertaken for this cohort and future studies will determine how the alterations and associations reported in this thesis influence functional outcome. This will be essential in order for early, quantitative MR analysis to fulfil its substantial potential in the search for early biomarkers of preterm brain injury and the design and implementation of future interventional therapies.

Other perinatal factors

Alongside chronic lung disease, a number of predictors of altered cerebral developmental and/or poor outcome in preterm infants have been identified. Two of the most commonly studied are neonatal infection/inflammation and IUGR. Preterm infants are at significantly increased risk for contracting intrauterine and postnatal infections, often resulting in a systemic inflammatory response, the overall rate of which has not decreased significantly in recent years (Adams-Chapman and Stoll 2006). The link between infection, inflammation and cerebral injury is well described (Volpe 2001, Back et al. 2007) and studies have demonstrated associations between infection, PVL and subsequent neurodevelopmental deficits in preterm infants (Perlman et al. 1996, Leviton et al. 1999, Graham et al. 2004, Shah et al. 2008). Similarly, IUGR is associated with cerebral alterations including lower cerebral volume and reduced cortical complexity, and adverse neurodevelopment (Thompson et al. 2007, Dubois et al. 2008b, Esteban et al. 2010, Torrance et al. 2010, Padilla et al. 2011).

In order to decouple the complex, and often overlapping, influence of the numerous perinatal factors associated with early brain development and preterm birth, large, population-based studies are often most appropriate. With sufficient computing resources, application of the analytical tools and methods described in this thesis in such large cohorts could provide valuable insight into the underlying pathways and developmental interactions of the wide range of often overlapping complications. Furthermore, the availability of such analyses specifically optimised for neonatal cohorts, opens immediate lines of investigation to study the effects of specific perinatal factors such as sepsis and IUGR on the preterm brain without the need for large scale studies.

Improving cortical alignment

Many of the methods used in this thesis to enable quantitative, groupwise analysis of neonatal MRI rely upon image registration and require precise alignment of cerebral structures across an anatomically heterogeneous cohort. As noted in Chapters 5 and 6, cortical registration in this population represents a significant technical challenge.

A number of approaches to neonatal cortical registration have been described: Xue et al. used surface registration to perform longitudinal cortical registration between images obtained in the same infant at three timepoints (Xue et al. 2007). A similar approach was used by Lefèvre et al. (2009). In Hill et al., intersubject cortical registration was performed in a group of healthy term-born controls by extracting cortical surfaces in a semi-automatic fashion and mapping significant sulcal landmarks onto a population-average map with spherical registration (Van Essen 2005, Hill et al. 2010). The additional confounding factors of neonatal analysis – namely the difficulty in producing accurate tissue segmentation and the rapid development of the cortex over a relatively short time means that these methods have so far only been applied in small cohorts. Combining these techniques with those

described in this thesis would allow for more accurate assessment of cortical thickness, to identify regional associations rather than treat the cortex as a whole, and precisely map cortical connectivity across the group.

7.3 Summary

This thesis has presented work quantifying tissue microstructure, volume and connectivity in the developing preterm brain; providing evidence that preterm birth is disruptive to cerebral development on a systems level and results in a complex pattern of regional micro- and macrostructural alterations evident at term-equivalent age. The evidence provided suggests that connected neural structures are affected by preterm birth and future studies into the consequences of prematurity on brain development and the therapeutic effects of any possible future treatment strategies should be considered on a whole-brain level where possible.

References

- Aarnoudse-Moens CS, Weisglas-Kuperus N, van Goudoever JB, Oosterlaan J. 2009. Meta-analysis of neurobehavioral outcomes in very preterm and/or very low birth weight children. *Pediatrics* 124:717-728.
- Adams-Chapman I, Stoll BJ. 2006. Neonatal infection and long-term neurodevelopmental outcome in the preterm infant. *Curr Opin Infect Dis* 19:290-297.
- Aeby A, Liu Y, De Tiege X, Denolin V, David P, Baleriaux D, Kavec M, Metens T, Van Bogaert P. 2009. Maturation of thalamic radiations between 34 and 41 weeks' gestation: A combined voxel-based study and probabilistic tractography with diffusion tensor imaging. *AJNR Am J Neuroradiol* 30:1780-1786.
- Ajayi-Obe M, Saeed N, Cowan FM, Rutherford MA, Edwards AD. 2000. Reduced development of cerebral cortex in extremely preterm infants. *Lancet* 356:1162-1163.
- Akkal D, Dum RP, Strick PL. 2007. Supplementary motor area and presupplementary motor area: Targets of basal ganglia and cerebellar output. *J Neurosci* 27:10659-10673.
- Alexander DC. 2005. Multiple-fiber reconstruction algorithms for diffusion MRI. *Ann N Y Acad Sci* 1064:113-133.
- Aljabar P, Bhatia KK, Murgasova M, Hajnal JV, Boardman JP, Srinivasan L, Rutherford MA, Dyet LE, Edwards AD, Rueckert D. 2008. Assessment of brain growth in early childhood using deformation-based morphometry. *Neuroimage* 39:348-358.
- Allendoerfer KL, Shatz CJ. 1994. The subplate, a transient neocortical structure: Its role in the development of connections between thalamus and cortex. *Annu Rev Neurosci* 17:185-218.
- Allin M, Walshe M, Fern A, Nosarti C, Cuddy M, Rifkin L, Murray R, Rushe T, Wyatt J. 2008. Cognitive maturation in preterm and term born adolescents. *J Neurol Neurosurg Psychiatry* 79:381-386.
- Altaye M, Holland SK, Wilke M, Gaser C. 2008. Infant brain probability templates for MRI segmentation and normalization. *Neuroimage* 43:721-730.
- Ananth CV, Misra DP, Demissie K, Smulian JC. 2001. Rates of preterm delivery among black women and white women in the United States over two decades: An age-period-cohort analysis. *Am J Epidemiol* 154:657-665.
- Andersson JL, Jenkinson M, Smith S. 2007. Non-linear registration aka spatial normalisation. FMRIB Analysis Group Technical Reports TR07JA02. <http://www.fmrib.ox.ac.uk/analysis/techrep>.

- Anderson PJ, Doyle LW, Victorian Infant Collaborative Study Group. 2004. Executive functioning in school-aged children who were born very preterm or with extremely low birth weight in the 1990s. *Pediatrics* 114:50-57.
- Anjari M, Srinivasan L, Allsop JM, Hajnal JV, Rutherford MA, Edwards AD, Counsell SJ. 2007. Diffusion tensor imaging with tract-based spatial statistics reveals local white matter abnormalities in preterm infants. *Neuroimage* 35:1021-1027.
- Anjari M, Counsell SJ, Srinivasan L, Allsop JM, Hajnal JV, Rutherford MA, Edwards AD. 2009. The association of lung disease with cerebral white matter abnormalities in preterm infants. *Pediatrics* 124:268-276.
- Arai Y, Deguchi K, Mizuguchi M, Takashima S. 1995. Expression of beta-amyloid precursor protein in axons of periventricular leukomalacia brains. *Pediatr Neurol* 13:161-163.
- Argyropoulou MI, Xydis V, Drougia A, Argyropoulou PI, Tzoufi M, Bassounas A, Andronikou S, Efremidis SC. 2003. MRI measurements of the pons and cerebellum in children born preterm; associations with the severity of periventricular leukomalacia and perinatal risk factors. *Neuroradiology* 45:730-734.
- Ashburner J, Hutton C, Frackowiak R, Johnsrude I, Price C, Friston K. 1998. Identifying global anatomical differences: Deformation-based morphometry. *Hum Brain Mapp* 6:348-357.
- Ashburner J, Friston KJ. 1999. Nonlinear spatial normalization using basis functions. *Hum Brain Mapp* 7:254-266.
- Ashburner J, Friston KJ. 2000. Voxel-based morphometry--the methods. *Neuroimage* 11:805-821.
- Ashburner J, Friston KJ. 2001. Why voxel-based morphometry should be used. *Neuroimage* 14:1238-1243.
- Ashburner J. 2007. A fast diffeomorphic image registration algorithm. *Neuroimage* 38:95-113.
- Assaf Y, Freidlin RZ, Rohde GK, Basser PJ. 2004. New modeling and experimental framework to characterize hindered and restricted water diffusion in brain white matter. *Magn Reson Med* 52:965-978.
- Austeng D, Kallen KB, Ewald UW, Jakobsson PG, Holmstrom GE. 2009. Incidence of retinopathy of prematurity in infants born before 27 weeks' gestation in Sweden. *Arch Ophthalmol* 127:1315-1319.
- Aylward GP. 2002. Cognitive and neuropsychological outcomes: More than IQ scores. *Ment Retard Dev Disabil Res Rev* 8:234-240.

- Back SA, Luo NL, Borenstein NS, Levine JM, Volpe JJ, Kinney HC. 2001. Late oligodendrocyte progenitors coincide with the developmental window of vulnerability for human perinatal white matter injury. *J Neurosci* 21:1302-1312.
- Back SA, Rivkees SA. 2004. Emerging concepts in periventricular white matter injury. *Semin Perinatol* 28:405-414.
- Back SA. 2006. Perinatal white matter injury: The changing spectrum of pathology and emerging insights into pathogenetic mechanisms. *Ment Retard Dev Disabil Res Rev* 12:129-140.
- Back SA, Luo NL, Mallinson RA, O'Malley JP, Wallen LD, Frei B, Morrow JD, Petito CK, Roberts CT, Murdoch GH, Montine TJ. 2005. Selective vulnerability of preterm white matter to oxidative damage defined by F2-isoprostanes. *Ann Neurol* 58:108-120.
- Back SA, Riddle A, McClure MM. 2007. Maturation-dependent vulnerability of perinatal white matter in premature birth. *Stroke* 38:724-730.
- Bada HS, Korones SB, Perry EH, Arheart KL, Ray JD, Pourcyrous M, Magill HL, Runyan W, Somes GW, Clark FC. 1990. Mean arterial blood pressure changes in premature infants and those at risk for intraventricular hemorrhage. *J Pediatr* 117:607-614.
- Baddeley A. 1992. Working memory. *Science* 255:556-559.
- Bajcsy R, Kovačič S. 1989. Multiresolution elastic matching. *Comput Vis Graph Image Process* 46:1-21.
- Ball G, Counsell SJ, Anjari M, Merchant N, Arichi T, Doria V, Rutherford MA, Edwards AD, Rueckert D, Boardman JP. 2010. An optimised tract-based spatial statistics protocol for neonates: Applications to prematurity and chronic lung disease. *Neuroimage* 53:94-102.
- Ball G, Counsell SJ, Gousias IS, Aljabar P, Hajnal JV, Rueckert D, Edwards AD, Boardman JP. 2011a. Automatic segmentation and parcellation of subcortical white and grey matter using DTI in the preterm neonate. *Proc Int Soc Mag Reson Med* 19:Abstract 2477.
- Ball G, Boardman JP, Rueckert D, Aljabar P, Arichi T, Merchant N, Gousias IS, Edwards AD, Counsell SJ. 2011b. The effect of preterm birth on thalamic and cortical development. *Cereb Cortex*. doi: 10.1093/cercor/bhr176.
- Ballabh P. 2010. Intraventricular hemorrhage in premature infants: Mechanism of disease. *Pediatr Res* 67:1-8.
- Banker BQ, Larroche JC. 1962. Periventricular leukomalacia of infancy. A form of neonatal anoxic encephalopathy. *Arch Neurol* 7:386-410.
- Baraldi E, Filippone M. 2007. Chronic lung disease after premature birth. *N Engl J Med* 357:1946-1955.

- Barrick TR, Charlton RA, Clark CA, Markus HS. 2010. White matter structural decline in normal ageing; a prospective longitudinal study using tract based spatial statistics. *Neuroimage* 51:565-577
- Bassan H, Limperopoulos C, Visconti K, Mayer DL, Feldman HA, Avery L, Benson CB, Stewart J, Ringer SA, Soul JS, Volpe JJ, du Plessis AJ. 2007. Neurodevelopmental outcome in survivors of periventricular hemorrhagic infarction. *Pediatrics* 120:785-792.
- Basser PJ, Mattiello J, LeBihan D. 1994. MR diffusion tensor spectroscopy and imaging. *Biophys J* 66:259-267.
- Basser PJ, Pierpaoli C. 1996. Microstructural and physiological features of tissues elucidated by quantitative-diffusion-tensor MRI. *J Magn Reson B* 111:209-219.
- Bassi L, Ricci D, Volzone A, Allsop JM, Srinivasan L, Pai A, Ribes C, Ramenghi LA, Mercuri E, Mosca F, Edwards AD, Cowan FM, Rutherford MA, Counsell SJ. 2008. Probabilistic diffusion tractography of the optic radiations and visual function in preterm infants at term equivalent age. *Brain* 131:573-582.
- Bassi L, Chew A, Merchant N, Ball G, Ramenghi L, Boardman J, Allsop JM, Doria V, Arichi T, Mosca F, Edwards AD, Cowan FM, Rutherford MA, Counsell SJ. 2011. Diffusion tensor imaging in preterm infants with punctate white matter lesions. *Pediatr Res* 69:561-566.
- Bates JF, Goldman-Rakic PS. 1993. Prefrontal connections of medial motor areas in the rhesus monkey. *J Comp Neurol* 336:211-228.
- Bayley N. 1993. Manual for the Bayley Scales of Infant Development (2nd Ed.). The Psychological Corporation: San Antonio, TX.
- Bayley N. 2006. Bayley Scales of Infant and Toddler Development (3rd Ed.). Harcourt Assessment: San Antonio, TX.
- Bax MC. 1964. Terminology and classification of cerebral palsy. *Dev Med Child Neurol* 6:295-297.
- Bayer SA, Altman J. 2004. The human brain during the third trimester. CRC Press LLC: Boca Raton, FL.
- Beauchamp MH, Thompson DK, Howard K, Doyle LW, Egan GF, Inder TE, Anderson PJ. 2008. Preterm infant hippocampal volumes correlate with later working memory deficits. *Brain* 131:2986-2994.
- Beaulieu C. 2002. The basis of anisotropic water diffusion in the nervous system - a technical review. *NMR Biomed* 15:435-455.
- Beck S, Wojdyla D, Say L, Betran AP, Merialdi M, Requejo JH, Rubens C, Menon R, Van Look PF. 2010. The worldwide incidence of preterm birth: A systematic review of maternal mortality and morbidity. *Bull World Health Organ* 88:31-38.

- Beg MF, Miller MI, Trouvé A, Younes L. 2005. Computing large deformation metric mappings via geodesic flows of diffeomorphisms. *Int J Comput Vis* 61:139-157.
- Behrens TE, Woolrich MW, Jenkinson M, Johansen-Berg H, Nunes RG, Clare S, Matthews PM, Brady JM, Smith SM. 2003a. Characterization and propagation of uncertainty in diffusion-weighted MR imaging. *Magn Reson Med* 50:1077-1088.
- Behrens TE, Johansen-Berg H, Woolrich MW, Smith SM, Wheeler-Kingshott CA, Boulby PA, Barker GJ, Sillery EL, Sheehan K, Ciccarelli O, Thompson AJ, Brady JM, Matthews PM. 2003b. Non-invasive mapping of connections between human thalamus and cortex using diffusion imaging. *Nat Neurosci* 6:750-757.
- Behrens TE, Berg HJ, Jbabdi S, Rushworth MF, Woolrich MW. 2007. Probabilistic diffusion tractography with multiple fibre orientations: What can we gain? *Neuroimage* 34:144-155.
- Behrman RE, Butler AS. 2007. Preterm birth: Causes, consequences, and prevention. National Academies Press: Washington, D.C.
- Bell JE, Becher JC, Wyatt B, Keeling JW, McIntosh N. 2005. Brain damage and axonal injury in a Scottish cohort of neonatal deaths. *Brain* 128:1070-1081.
- Benes FM. 1989. Myelination of cortical-hippocampal relays during late adolescence. *Schizophr Bull* 15:585-593.
- Bergouignan L, Chupin M, Czechowska Y, Kinkingnehun S, Lemogne C, Le Bastard G, Lepage M, Garnerio L, Colliot O, Fossati P. 2009. Can voxel based morphometry, manual segmentation and automated segmentation equally detect hippocampal volume differences in acute depression? *Neuroimage* 45:29-37.
- Berman JI, Mukherjee P, Partridge SC, Miller SP, Ferriero DM, Barkovich AJ, Vigneron DB, Henry RG. 2005. Quantitative diffusion tensor MRI fiber tractography of sensorimotor white matter development in premature infants. *Neuroimage* 27:862-871.
- Bhatia KK, Aljabar P, Boardman JP, Srinivasan L, Murgasova M, Counsell SJ, Rutherford MA, Hajnal J, Edwards AD, Rueckert D. 2007. Groupwise combined segmentation and registration for atlas construction. *Med Image Comput Comput Assist Interv* 10:532-540.
- Bhutta AT, Cleves MA, Casey PH, Cradock MM, Anand KJ. 2002. Cognitive and behavioral outcomes of school-aged children who were born preterm: A meta-analysis. *JAMA* 288:728-737.
- Blakemore C, Molnar Z. 1990. Factors involved in the establishment of specific interconnections between thalamus and cerebral cortex. *Cold Spring Harb Symp Quant Biol* 55:491-504.
- Bloch F, Hansen WW, Packard M. 1946. Nuclear induction. *Phys Rev* 69:127.

- Blondel B, Kaminski M. 2002. Trends in the occurrence, determinants, and consequences of multiple births. *Semin Perinatol* 26:239-249.
- Boardman JP, Counsell SJ, Rueckert D, Kapellou O, Bhatia KK, Aljabar P, Hajnal J, Allsop JM, Rutherford MA, Edwards AD. 2006. Abnormal deep grey matter development following preterm birth detected using deformation-based morphometry. *Neuroimage* 32:70-78.
- Boardman JP, Counsell SJ, Rueckert D, Hajnal JV, Bhatia KK, Srinivasan L, Kapellou O, Aljabar P, Dyet LE, Rutherford MA, Allsop JM, Edwards AD. 2007. Early growth in brain volume is preserved in the majority of preterm infants. *Ann Neurol* 62:185-192.
- Boardman JP, Craven C, Valappil S, Counsell SJ, Dyet LE, Rueckert D, Aljabar P, Rutherford MA, Chew AT, Allsop JM, Cowan F, Edwards AD. 2010. A common neonatal image phenotype predicts adverse neurodevelopmental outcome in children born preterm. *Neuroimage* 52:409-414.
- Bookstein FL. 1989. Principal warps: Thin-plate splines and the decomposition of deformations. *IEEE Trans Pattern Anal Mach Intell* 11:567-585.
- Bookstein FL. 2001. "Voxel-based morphometry" should not be used with imperfectly registered images. *Neuroimage* 14:1454-1462.
- Botting N, Powls A, Cooke RW, Marlow N. 1997. Attention deficit hyperactivity disorders and other psychiatric outcomes in very low birthweight children at 12 years. *J Child Psychol Psychiatry* 38:931-941.
- Bourgeois JP, Jastreboff PJ, Rakic P. 1989. Synaptogenesis in visual cortex of normal and preterm monkeys: Evidence for intrinsic regulation of synaptic overproduction. *Proc Natl Acad Sci U S A* 86:4297-4301.
- Bracewell M, Marlow N. 2002. Patterns of motor disability in very preterm children. *Ment Retard Dev Disabil Res Rev* 8:241-248.
- Breslau N, DelDotto JE, Brown GG, Kumar S, Ezhuthachan S, Hufnagle KG, Peterson EL. 1994. A gradient relationship between low birth weight and IQ at age 6 years. *Arch Pediatr Adolesc Med* 148:377-383.
- Breslau N, Chilcoat H, DelDotto J, Andreski P, Brown G. 1996. Low birth weight and neurocognitive status at six years of age. *Biol Psychiatry* 40:389-397.
- Bridson R. 2007. Fast poisson disk sampling in arbitrary dimensions. In *ACM SIGGRAPH 2007 Sketches & Applications*. ACM Press, 22.
- Bullmore E, Sporns O. 2009. Complex brain networks: Graph theoretical analysis of structural and functional systems. *Nat Rev Neurosci* 10:186-198.

- Bystron I, Blakemore C, Rakic P. 2008. Development of the human cerebral cortex: Boulder committee revisited. *Nat Rev Neurosci* 9:110-122.
- Callaghan WM, MacDorman MF, Rasmussen SA, Qin C, Lackritz EM. 2006. The contribution of preterm birth to infant mortality rates in the United States. *Pediatrics* 118:1566-1573.
- Cardenas VA, Boxer AL, Chao LL, Gorno-Tempini ML, Miller BL, Weiner MW, Studholme C. 2007. Deformation-based morphometry reveals brain atrophy in frontotemporal dementia. *Arch Neurol* 64:873-877.
- Catani M, Howard RJ, Pajevic S, Jones DK. 2002. Virtual in vivo interactive dissection of white matter fasciculi in the human brain. *Neuroimage* 17:77-94.
- Ceccarelli A, Rocca MA, Pagani E, Falini A, Comi G, Filippi M. 2009. Cognitive learning is associated with gray matter changes in healthy human individuals: A tensor-based morphometry study. *Neuroimage* 48:585-589.
- Chahboune H, Ment LR, Stewart WB, Rothman DL, Vaccarino FM, Hyder F, Schwartz ML. 2009. Hypoxic injury during neonatal development in murine brain: Correlation between in vivo DTI findings and behavioral assessment. *Cereb Cortex* 19:2891-2901.
- Chandiramani M, Shennan A. 2006. Preterm labour: Update on prediction and prevention strategies. *Curr Opin Obstet Gynecol* 18:618-624.
- Chen Y, Guo W, Zeng Q, He G, Vemuri B, Liu Y. 2004. Recovery of intra-voxel structure from HARD DWI. *ISBI: Nano to Macro* 1:1028-1031.
- Cheong JL, Thompson DK, Wang HX, Hunt RW, Anderson PJ, Inder TE, Doyle LW. 2009. Abnormal white matter signal on MR imaging is related to abnormal tissue microstructure. *AJNR Am J Neuroradiol* 30:623-628.
- Chi JG, Dooling EC, Gilles FH. 1977. Gyral development of the human brain. *Ann Neurol* 1:86-93.
- Christensen GE, Rabbitt RD, Miller MI. 1996. Deformable templates using large deformation kinematics. *IEEE Trans Image Process* 5:1435-1447.
- Chung MK, Worsley KJ, Paus T, Cherif C, Collins DL, Giedd JN, Rapoport JL, Evans AC. 2001. A unified statistical approach to deformation-based morphometry. *Neuroimage* 14:595-606.
- Ciccarelli O, Catani M, Johansen-Berg H, Clark C, Thompson A. 2008. Diffusion-based tractography in neurological disorders: Concepts, applications, and future developments. *Lancet Neurol* 7:715-727.
- Cioni G, Fazzi B, Coluccini M, Bartalena L, Boldrini A, van Hof-van Duin J. 1997. Cerebral visual impairment in preterm infants with periventricular leukomalacia. *Pediatr Neurol* 17:331-338.

- Clatworthy PL, Williams GB, Acosta-Cabronero J, Jones SP, Harding SG, Johansen-Berg H, Baron J-. 2010. Probabilistic tractography of the optic radiations – An automated method and anatomical validation. *Neuroimage* 49:2001-2012.
- Conturo TE, Lori NF, Cull TS, Akbudak E, Snyder AZ, Shimony JS, McKinstry RC, Burton H, Raichle ME. 1999. Tracking neuronal fiber pathways in the living human brain. *Proc Natl Acad Sci U S A* 96:10422-10427.
- Cook RL. 1986. Stochastic sampling in computer graphics. *ACM Trans Graph* 5:51-72.
- Cooke RW, Foulder-Hughes L, Newsham D, Clarke D. 2004. Ophthalmic impairment at 7 years of age in children born very preterm. *Arch Dis Child Fetal Neonatal Ed* 89:249-53.
- Counsell SJ, Allsop JM, Harrison MC, Larkman DJ, Kennea NL, Kapellou O, Cowan FM, Hajnal JV, Edwards AD, Rutherford MA. 2003. Diffusion-weighted imaging of the brain in preterm infants with focal and diffuse white matter abnormality. *Pediatrics* 112:1-7.
- Counsell SJ, Shen Y, Boardman JP, Larkman DJ, Kapellou O, Ward P, Allsop JM, Cowan FM, Hajnal JV, Edwards AD, Rutherford MA. 2006. Axial and radial diffusivity in preterm infants who have diffuse white matter changes on magnetic resonance imaging at term-equivalent age. *Pediatrics* 117:376-386.
- Counsell SJ, Dyet LE, Larkman DJ, Nunes RG, Boardman JP, Allsop JM, Fitzpatrick J, Srinivasan L, Cowan FM, Hajnal JV, Rutherford MA, Edwards AD. 2007. Thalamo-cortical connectivity in children born preterm mapped using probabilistic magnetic resonance tractography. *Neuroimage* 34:896-904.
- Counsell SJ, Edwards AD, Chew AT, Anjari M, Dyet LE, Srinivasan L, Boardman JP, Allsop JM, Hajnal JV, Rutherford MA, Cowan FM. 2008. Specific relations between neurodevelopmental abilities and white matter microstructure in children born preterm. *Brain* 131:3201-3208.
- Crowther CA, Hiller JE, Doyle LW, Haslam RR, Australasian Collaborative Trial of Magnesium Sulphate (ACTOMg SO₄) Collaborative Group. 2003. Effect of magnesium sulfate given for neuroprotection before preterm birth: A randomized controlled trial. *JAMA* 290:2669-2676.
- Crum WR, Griffin LD, Hill DL, Hawkes DJ. 2003. Zen and the art of medical image registration: Correspondence, homology, and quality. *Neuroimage* 20:1425-1437.
- Crum WR, Hartkens T, Hill DL. 2004. Non-rigid image registration: Theory and practice. *Br J Radiol* 77:140-53.
- de Bruine FT, van Wezel-Meijler G, Leijser LM, van den Berg-Huysmans AA, van Steenis A, van Buchem MA, van der Grond J. 2011. Tractography of developing white matter of the internal capsule and corpus callosum in very preterm infants. *Eur Radiol* 21:538-547.

- de Haan M, Bauer PJ, Georgieff MK, Nelson CA. 2000. Explicit memory in low-risk infants aged 19 months born between 27 and 42 weeks of gestation. *Dev Med Child Neurol* 42:304-312.
- de Vries LS, Eken P, Groenendaal F, van Haastert IC, Meiners LC. 1993. Correlation between the degree of periventricular leukomalacia diagnosed using cranial ultrasound and MRI later in infancy in children with cerebral palsy. *Neuropediatrics* 24:263-268.
- de Vries LS, Rademaker KJ, Groenendaal F, Eken P, van Haastert IC, Vandertop WP, Gooskens R, Meiners LC. 1998. Correlation between neonatal cranial ultrasound, MRI in infancy and neurodevelopmental outcome in infants with a large intraventricular haemorrhage with or without unilateral parenchymal involvement. *Neuropediatrics* 29:180-188.
- de Vries LS, Groenendaal F, van Haastert IC, Eken P, Rademaker KJ, Meiners LC. 1999. Asymmetrical myelination of the posterior limb of the internal capsule in infants with periventricular haemorrhagic infarction: An early predictor of hemiplegia. *Neuropediatrics* 30:314-319.
- de Vries LS, Roelants-van Rijn AM, Rademaker KJ, Van Haastert IC, Beek FJ, Groenendaal F. 2001. Unilateral parenchymal haemorrhagic infarction in the preterm infant. *Eur J Paediatr Neurol* 5:139-149.
- de Vries LS, Van Haastert IL, Rademaker KJ, Koopman C, Groenendaal F. 2004. Ultrasound abnormalities preceding cerebral palsy in high-risk preterm infants. *J Pediatr* 144:815-820.
- Deipolyi AR, Mukherjee P, Gill K, Henry RG, Partridge SC, Veeraraghavan S, Jin H, Lu Y, Miller SP, Ferriero DM, Vigneron DB, Barkovich AJ. 2005. Comparing microstructural and macrostructural development of the cerebral cortex in premature newborns: Diffusion tensor imaging versus cortical gyration. *Neuroimage* 27:579-586.
- Delobel-Ayoub M, Arnaud C, White-Koning M, Casper C, Pierrat V, Garel M, Burguet A, Roze JC, Matis J, Picaud JC, Kaminski M, Larroque B, EPIPAGE Study Group. 2009. Behavioral problems and cognitive performance at 5 years of age after very preterm birth: The EPIPAGE study. *Pediatrics* 123:1485-1492.
- Deng W. 2010. Neurobiology of injury to the developing brain. *Nat Rev Neurol* 6:328-336.
- Dieni S, Inder T, Yoder B, Briscoe T, Camm E, Egan G, Denton D, Rees S. 2004. The pattern of cerebral injury in a primate model of preterm birth and neonatal intensive care. *J Neuropathol Exp Neurol* 63:1297-1309.
- Doria V, Beckmann CF, Arichi T, Merchant N, Groppo M, Turkheimer FE, Counsell SJ, Murgasova M, Aljabar P, Nunes RG, Larkman DJ, Rees G, Edwards AD. 2010. Emergence of resting state networks in the preterm human brain. *Proc Natl Acad Sci U S A* 107:20015-20020.

- Douaud G, Gaura V, Ribeiro MJ, Lethimonnier F, Maroy R, Verny C, Krystkowiak P, Damier P, Bachoud-Levi AC, Hantraye P, Remy P. 2006. Distribution of grey matter atrophy in Huntington's disease patients: A combined ROI-based and voxel-based morphometric study. *Neuroimage* 32:1562-1575.
- Douaud G, Jbabdi S, Behrens TE, Menke RA, Gass A, Monsch AU, Rao A, Whitcher B, Kindlmann G, Matthews PM, Smith S. 2011. DTI measures in crossing-fibre areas: Increased diffusion anisotropy reveals early white matter alteration in MCI and mild Alzheimer's disease. *Neuroimage* 55:880-890.
- Doyle LW, Anderson PJ. 2010. Adult outcome of extremely preterm infants. *Pediatrics* 126:342-351.
- Drobyshevsky A, Song SK, Gamkrelidze G, Wyrwicz AM, Derrick M, Meng F, Li L, Ji X, Trommer B, Beardsley DJ, Luo NL, Back SA, Tan S. 2005. Developmental changes in diffusion anisotropy coincide with immature oligodendrocyte progression and maturation of compound action potential. *J Neurosci* 25:5988-5997.
- Dubois J, Benders M, Cachia A, Lazeyras F, Ha-Vinh Leuchter R, Sizonenko SV, Borradori-Tolsa C, Mangin JF, Huppi PS. 2008a. Mapping the early cortical folding process in the preterm newborn brain. *Cereb Cortex* 18:1444-1454.
- Dubois J, Benders M, Borradori-Tolsa C, Cachia A, Lazeyras F, Ha-Vinh Leuchter R, Sizonenko SV, Warfield SK, Mangin JF, Huppi PS. 2008b. Primary cortical folding in the human newborn: An early marker of later functional development. *Brain* 131:2028-2041.
- Dudink J, Lequin M, van Pul C, Buijs J, Conneman N, van Goudoever J, Govaert P. 2007. Fractional anisotropy in white matter tracts of very-low-birth-weight infants. *Pediatr Radiol* 37:1216-1223.
- Dudink J, Buijs J, Govaert P, van Zwol AL, Conneman N, van Goudoever JB, Lequin M. 2010. Diffusion tensor imaging of the cortical plate and subplate in very-low-birth-weight infants. *Pediatr Radiol* 40:1397-1404.
- Dum RP, Strick PL. 1991. The origin of corticospinal projections from the premotor areas in the frontal lobe. *J Neurosci* 11:667-689.
- Dyet LE, Kennea N, Counsell SJ, Maalouf EF, Ajayi-Obe M, Duggan PJ, Harrison M, Allsop JM, Hajnal J, Herlihy AH, Edwards B, Laroche S, Cowan FM, Rutherford MA, Edwards AD. 2006. Natural history of brain lesions in extremely preterm infants studied with serial magnetic resonance imaging from birth and neurodevelopmental assessment. *Pediatrics* 118:536-548.
- Eikenes L, Lohaugen GC, Brubakk AM, Skranes J, Haberg AK. 2011. Young adults born preterm with very low birth weight demonstrate widespread white matter alterations on brain DTI. *Neuroimage* 54:1774-1785.

- Einstein A. 1905. On the motion of small particles suspended in liquids at rest required by the molecular-kinetic theory of heat. *Ann Phys* 322:549-560.
- Esteban FJ, Padilla N, Sanz-Cortes M, de Miras JR, Bargallo N, Villoslada P, Gratacos E. 2010. Fractal-dimension analysis detects cerebral changes in preterm infants with and without intrauterine growth restriction. *Neuroimage* 53:1225-1232.
- Fair DA, Bathula D, Mills KL, Dias TG, Blythe MS, Zhang D, Snyder AZ, Raichle ME, Stevens AA, Nigg JT, Nagel BJ. 2010. Maturing thalamo-cortical functional connectivity across development. *Front Syst Neurosci* 4:10.
- Fazzi E, Orcesi S, Caffi L, Ometto A, Rondini G, Telesca C, Lanzi G. 1994. Neurodevelopmental outcome at 5-7 years in preterm infants with periventricular leukomalacia. *Neuropediatrics* 25:134-139.
- Felleman DJ, Van Essen DC. 1991. Distributed hierarchical processing in the primate cerebral cortex. *Cereb Cortex* 1:1-47.
- Ferrant M, Nabavi A, Macq B, Black PM, Jolesz FA, Kikinis R, Warfield SK. 2002. Serial registration of intraoperative MR images of the brain. *Med Image Anal* 6:337-359.
- Fonov V, Evans AC, Botteron K, Almli CR, McKinstry RC, Collins DL, Brain Development Cooperative Group. 2011. Unbiased average age-appropriate atlases for pediatric studies. *Neuroimage* 54:313-327.
- Foulder-Hughes LA, Cooke RW. 2003. Motor, cognitive, and behavioural disorders in children born very preterm. *Dev Med Child Neurol* 45:97-103.
- Fransson P, Skiold B, Horsch S, Nordell A, Blennow M, Lagercrantz H, Aden U. 2007. Resting-state networks in the infant brain. *Proc Natl Acad Sci U S A* 104:15531-15536.
- Friston KJ, Ashburner J, Frith CD, Poline J-, Heather JD, Frackowiak RSJ. 1995. Spatial registration and normalization of images. *Hum Brain Mapp* 3:165-189.
- Fuster JM. 2001. The prefrontal cortex--an update: Time is of the essence. *Neuron* 30:319-333.
- Gardner MO, Goldenberg RL, Cliver SP, Tucker JM, Nelson KG, Copper RL. 1995. The origin and outcome of preterm twin pregnancies. *Obstet Gynecol* 85:553-557.
- Gaser C, Volz HP, Kiebel S, Riehemann S, Sauer H. 1999. Detecting structural changes in whole brain based on nonlinear deformations-application to schizophrenia research. *Neuroimage* 10:107-113.
- Gaser C, Nenadic I, Buchsbaum BR, Hazlett EA, Buchsbaum MS. 2001. Deformation-based morphometry and its relation to conventional volumetry of brain lateral ventricles in MRI. *Neuroimage* 13:1140-1145.

- Gaser C, Nenadic I, Volz HP, Buchel C, Sauer H. 2004. Neuroanatomy of "hearing voices": A frontotemporal brain structural abnormality associated with auditory hallucinations in schizophrenia. *Cereb Cortex* 14:91-96.
- Ghosh A, Antonini A, McConnell SK, Shatz CJ. 1990. Requirement for subplate neurons in the formation of thalamo-cortical connections. *Nature* 347:179-181.
- Gilles FH, Shankle W, Dooling EC. 1983. Myelinated tracts: Growth patterns. In: Gilles FH, Leviton A, Dooling EC (Eds.). *The developing human brain: Growth and epidemiologic neuropathology*. John Wright: Boston, MA.
- Gimenez M, Junque C, Narberhaus A, Caldu X, Salgado-Pineda P, Bargallo N, Segarra D, Botet F. 2004. Hippocampal gray matter reduction associates with memory deficits in adolescents with history of prematurity. *Neuroimage* 23:869-877.
- Gimenez M, Junque C, Narberhaus A, Botet F, Bargallo N, Mercader JM. 2006a. Correlations of thalamic reductions with verbal fluency impairment in those born prematurely. *Neuroreport* 17:463-466.
- Gimenez M, Junque C, Vendrell P, Narberhaus A, Bargallo N, Botet F, Mercader JM. 2006b. Abnormal orbitofrontal development due to prematurity. *Neurology* 67:1818-1822.
- Gimenez M, Miranda MJ, Born AP, Nagy Z, Rostrup E, Jernigan TL. 2008. Accelerated cerebral white matter development in preterm infants: A voxel-based morphometry study with diffusion tensor MR imaging. *Neuroimage* 41:728-734.
- Giorgio A, Santelli L, Tomassini V, Bosnell R, Smith S, De Stefano N, Johansen-Berg H. 2010a. Age-related changes in grey and white matter structure throughout adulthood. *Neuroimage* 51:943-951.
- Giorgio A, Watkins KE, Chadwick M, James S, Winmill L, Douaud G, De Stefano N, Matthews PM, Smith SM, Johansen-Berg H, James AC. 2010b. Longitudinal changes in grey and white matter during adolescence. *Neuroimage* 49:94-103.
- Goldberg G. 1985. Supplementary motor area structure and function: Review and hypotheses. *Behav Brain Sci* 8:567-588.
- Goldenberg RL, Culhane JF, Iams JD, Romero R. 2008. Epidemiology and causes of preterm birth. *Lancet* 371:75-84.
- Goldman-Rakic PS, Porrino LJ. 1985. The primate mediodorsal (MD) nucleus and its projection to the frontal lobe. *J Comp Neurol* 242:535-560.

- Goldman-Rakic PS. 1996. The prefrontal landscape: Implications of functional architecture for understanding human mentation and the central executive. *Philos Trans R Soc Lond B Biol Sci* 351:1445-1453.
- Gong G, He Y, Concha L, Lebel C, Gross DW, Evans AC, Beaulieu C. 2009. Mapping anatomical connectivity patterns of human cerebral cortex using in vivo diffusion tensor imaging tractography. *Cereb Cortex* 19:524-536.
- Good CD, Johnsrude IS, Ashburner J, Henson RN, Friston KJ, Frackowiak RS. 2001. A voxel-based morphometric study of ageing in 465 normal adult human brains. *Neuroimage* 14:21-36.
- Good CD, Scahill RI, Fox NC, Ashburner J, Friston KJ, Chan D, Crum WR, Rossor MN, Frackowiak RS. 2002. Automatic differentiation of anatomical patterns in the human brain: Validation with studies of degenerative dementias. *Neuroimage* 17:29-46.
- Gousias IS, Rueckert D, Heckemann RA, Dyet LE, Boardman JP, Edwards AD, Hammers A. 2008. Automatic segmentation of brain MRIs of 2-year-olds into 83 regions of interest. *Neuroimage* 40:672-84
- Goyen TA, Lui K, Woods R. 1998. Visual-motor, visual-perceptual, and fine motor outcomes in very-low-birthweight children at 5 years. *Dev Med Child Neurol* 40:76-81.
- Goyen TA, Lui K. 2009. Developmental coordination disorder in "apparently normal" schoolchildren born extremely preterm. *Arch Dis Child* 94:298-302.
- Grachev ID, Berdichevsky D, Rauch SL, Heckers S, Kennedy DN, Caviness VS, Alpert NM. 1999. A method for assessing the accuracy of intersubject registration of the human brain using anatomic landmarks. *Neuroimage* 9:250-268.
- Graham EM, Holcroft CJ, Rai KK, Donohue PK, Allen MC. 2004. Neonatal cerebral white matter injury in preterm infants is associated with culture positive infections and only rarely with metabolic acidosis. *Am J Obstet Gynecol* 191:1305-1310.
- Groenendaal F, Termote JU, van der Heide-Jalving M, van Haastert IC, de Vries LS. 2010. Complications affecting preterm neonates from 1991 to 2006: What have we gained? *Acta Paediatr* 99:354-358.
- Grosso M, Counsell SJ, Merchant N, Doria V, Arichi T, Ricci D, Bassi L, Mosca F, Ramenghi LA, Cowan FM, Rutherford M, Edwards AD. 2009. Visual function and postnatal development of white matter microstructure in the optic radiations in preterm infants. *Acta Paediatr* 98:24.
- Gupta RK, Hasan KM, Trivedi R, Pradhan M, Das V, Parikh NA, Narayana PA. 2005. Diffusion tensor imaging of the developing human cerebrum. *J Neurosci Res* 81:172-178.

- Guzzetta F, Shackelford GD, Volpe S, Perlman JM, Volpe JJ. 1986. Periventricular intraparenchymal echodensities in the premature newborn: Critical determinant of neurologic outcome. *Pediatrics* 78:995-1006.
- Hack M, Flannery DJ, Schluchter M, Cartar L, Borawski E, Klein N. 2002. Outcomes in young adulthood for very-low-birth-weight infants. *N Engl J Med* 346:149-157.
- Hagberg B, Hagberg G, Olow I, von Wendt L. 1996. The changing panorama of cerebral palsy in Sweden. VII. prevalence and origin in the birth year period 1987-90. *Acta Paediatr* 85:954-960.
- Hagmann P, Kurant M, Gigandet X, Thiran P, Wedeen VJ, Meuli R, Thiran JP. 2007. Mapping human whole-brain structural networks with diffusion MRI. *PLoS One* 2:e597.
- Hagmann P, Cammoun L, Gigandet X, Meuli R, Honey CJ, Wedeen VJ, Sporns O. 2008. Mapping the structural core of human cerebral cortex. *PLoS Biol* 6:e159.
- Hajnal JV, Saeed N, Soar EJ, Oatridge A, Young IR, Bydder GM. 1995. A registration and interpolation procedure for subvoxel matching of serially acquired MR images. *J Comput Assist Tomogr* 19:289-296.
- Hajnal J, Hawkes DJ, Hill DL. 2001. Medical image registration. CRC Press LLC: Boca Raton, FL.
- Hambleton G, Wigglesworth JS. 1976. Origin of intraventricular haemorrhage in the preterm infant. *Arch Dis Child* 51:651-659.
- Hammers A, Allom R, Koepp MJ, Free SL, Myers R, Lemieux L, Mitchell TN, Brooks DJ, Duncan JS. 2003. Three-dimensional maximum probability atlas of the human brain, with particular reference to the temporal lobe. *Hum Brain Mapp* 19:224-247.
- Han Z, Yang X, Landman B A, Gore JC, Dawant BM. 2011. Effects of nonrigid registrations on DBM analysis using SSD model. *Proc Int Soc Mag Reson Med* 19: Abstract 4278.
- Hansen BM et al. 2004. Perinatal risk factors of adverse outcome in very preterm children: A role of initial treatment of respiratory insufficiency? *Acta Paediatr* 93:185-189.
- Hard AL, Niklasson A, Svensson E, Hellstrom A. 2000. Visual function in school-aged children born before 29 weeks of gestation: A population-based study. *Dev Med Child Neurol* 42:100-105.
- Harvey JM, O'Callaghan MJ, Mohay H. 1999. Executive function of children with extremely low birthweight: A case control study. *Dev Med Child Neurol* 41:292-297.
- Hasegawa T, Yamada K, Morimoto M, Morioka S, Tozawa T, Isoda K, Murakami A, Chiyonobu T, Tokuda S, Nishimura A, Nishimura T, Hosoi H. 2011. Development of corpus callosum in preterm infants is affected by the prematurity: In vivo assessment of diffusion tensor imaging at term-equivalent age. *Pediatr Res* 69:249-254.

- Hassan SS, Romero R, Berry SM, Dang K, Blackwell SC, Treadwell MC, Wolfe HM. 2000. Patients with an ultrasonographic cervical length ≤ 15 mm have nearly a 50% risk of early spontaneous preterm delivery. *Am J Obstet Gynecol* 182:1458-1467.
- Hatten ME. 1999. Central nervous system neuronal migration. *Annu Rev Neurosci* 22:511-539.
- Haynes RL, Billiards SS, Borenstein NS, Volpe JJ, Kinney HC. 2008. Diffuse axonal injury in periventricular leukomalacia as determined by apoptotic marker fractin. *Pediatr Res* 63:656-661.
- He SQ, Dum RP, Strick PL. 1995. Topographic organization of corticospinal projections from the frontal lobe: Motor areas on the medial surface of the hemisphere. *J Neurosci* 15:3284-3306.
- Health and Social Care Information Centre. 2010. NHS maternity statistics, 2009-2010. <http://www.hesonline.nhs.uk/Ease/servlet/ContentServer?siteID=1937&categoryID=1475>. (Accessed: June 2011).
- Heckemann RA, Hajnal JV, Aljabar P, Rueckert D, Hammers A. 2006. Automatic anatomical brain MRI segmentation combining label propagation and decision fusion. *Neuroimage* 33:115-126.
- Herrmann K, Antonini A, Shatz CJ. 1994. Ultrastructural evidence for synaptic interactions between thalamo-cortical axons and subplate neurons. *Eur J Neurosci* 6:1729-1742.
- Hill DL, Batchelor PG, Holden M, Hawkes DJ. 2001. Medical image registration. *Phys Med Biol* 46:1-45.
- Hill J, Dierker D, Neil J, Inder T, Knutsen A, Harwell J, Coalson T, Van Essen D. 2010. A surface-based analysis of hemispheric asymmetries and folding of cerebral cortex in term-born human infants. *J Neurosci* 30:2268-2276.
- Hille ET, Weisglas-Kuperus N, van Goudoever JB, Jacobusse GW, Ens-Dokkum MH, de Groot L, Wit JM, Geven WB, Kok JH, de Kleine MJ, Kollee LA, Mulder AL, van Straaten HL, de Vries LS, van Weissenbruch MM, Verloove-Vanhorick SP, Dutch Collaborative POPS 19 Study Group. 2007. Functional outcomes and participation in young adulthood for very preterm and very low birth weight infants: The dutch project on preterm and small for gestational age infants at 19 years of age. *Pediatrics* 120:e587-95.
- Holden M, Schnabel JA, Hill DL. 2002. Quantification of small cerebral ventricular volume changes in treated growth hormone patients using nonrigid registration. *IEEE Trans Med Imaging* 21:1292-1301.
- Holmstrom G, el Azazi M, Kugelberg U. 1999. Ophthalmological follow up of preterm infants: A population based, prospective study of visual acuity and strabismus. *Br J Ophthalmol* 83:143-150.

- Horbar JD, Badger GJ, Carpenter JH, Fanaroff AA, Kilpatrick S, LaCorte M, Phibbs R, Soll RF, Members of the Vermont Oxford Network. 2002. Trends in mortality and morbidity for very low birth weight infants, 1991-1999. *Pediatrics* 110:143-151.
- Hosey T, Williams G, Ansorge R. 2005. Inference of multiple fiber orientations in high angular resolution diffusion imaging. *Magn Reson Med* 54:1480-1489.
- Huddy CL, Johnson A, Hope PL. 2001. Educational and behavioural problems in babies of 32-35 weeks gestation. *Arch Dis Child Fetal Neonatal Ed* 85:F23-8.
- Huntley M. 1996. The griffiths mental development scales: From birth to 2 years (revised). Association for Research in Infant and Child Development (ARICD).
- Huppi PS, Maier SE, Peled S, Zientara GP, Barnes PD, Jolesz FA, Volpe JJ. 1998a. Microstructural development of human newborn cerebral white matter assessed in vivo by diffusion tensor magnetic resonance imaging. *Pediatr Res* 44:584-590.
- Huppi PS, Warfield S, Kikinis R, Barnes PD, Zientara GP, Jolesz FA, Tsuji MK, Volpe JJ. 1998b. Quantitative magnetic resonance imaging of brain development in premature and mature newborns. *Ann Neurol* 43:224-235.
- Inase M, Tokuno H, Nambu A, Akazawa T, Takada M. 1999. Corticostriatal and corticosubthalamic input zones from the presupplementary motor area in the macaque monkey: Comparison with the input zones from the supplementary motor area. *Brain Res* 833:191-201.
- Inder TE, Huppi PS, Warfield S, Kikinis R, Zientara GP, Barnes PD, Jolesz F, Volpe JJ. 1999. Periventricular white matter injury in the premature infant is followed by reduced cerebral cortical gray matter volume at term. *Ann Neurol* 46:755-760.
- Inder TE, Wells SJ, Mogridge NB, Spencer C, Volpe JJ. 2003. Defining the nature of the cerebral abnormalities in the premature infant: A qualitative magnetic resonance imaging study. *J Pediatr* 143:171-179.
- Inder TE, Warfield SK, Wang H, Huppi PS, Volpe JJ. 2005. Abnormal cerebral structure is present at term in premature infants. *Pediatrics* 115:286-294.
- Indredavik MS, Vik T, Heyerdahl S, Kulseng S, Fayers P, Brubakk AM. 2004. Psychiatric symptoms and disorders in adolescents with low birth weight. *Arch Dis Child Fetal Neonatal Ed* 89:F445-50.
- Iturria-Medina Y, Sotero RC, Canales-Rodriguez EJ, Aleman-Gomez Y, Melie-Garcia L. 2008. Studying the human brain anatomical network via diffusion-weighted MRI and graph theory. *Neuroimage* 40:1064-1076.
- Jansons KM, Alexander DC. 2003. Persistent angular structure: New insights from diffusion MRI data. *Inf Process Med Imaging* 18:672-683.

- Jenkinson M, Smith S. 2001. A global optimisation method for robust affine registration of brain images. *Med Image Anal* 5:143-156.
- Jessen KR, Mirsky R. 1991. Schwann cell precursors and their development. *Glia* 4:185-194.
- Jezzard P, Barnett AS, Pierpaoli C. 1998. Characterization of and correction for eddy current artifacts in echo planar diffusion imaging. *Magn Reson Med* 39:801-812.
- Johansen-Berg H, Behrens TE, Sillery E, Ciccarelli O, Thompson AJ, Smith SM, Matthews PM. 2005. Functional-anatomical validation and individual variation of diffusion tractography-based segmentation of the human thalamus. *Cereb Cortex* 15:31-39.
- Johnson HJ, Christensen GE. 2002. Consistent landmark and intensity-based image registration. *IEEE Trans Med Imaging* 21:450-461.
- Johnson S, Fawke J, Hennessy E, Rowell V, Thomas S, Wolke D, Marlow N. 2009. Neurodevelopmental disability through 11 years of age in children born before 26 weeks of gestation. *Pediatrics* 124:e249-57.
- Jones DK, Simmons A, Williams SC, Horsfield MA. 1999. Non-invasive assessment of axonal fiber connectivity in the human brain via diffusion tensor MRI. *Magn Reson Med* 42:37-41.
- Jones DK, Symms MR, Cercignani M, Howard RJ. 2005. The effect of filter size on VBM analyses of DT-MRI data. *Neuroimage* 26:546-554.
- Jones DK. 2008. Studying connections in the living human brain with diffusion MRI. *Cortex* 44:936-952.
- Jones DK, Cercignani M. 2010. Twenty-five pitfalls in the analysis of diffusion MRI data. *NMR Biomed* 23:803-820.
- Joshi SH, Cabeen RP, Joshi AA, Woods RP, Narr KL, Toga AW. 2010. Diffeomorphic sulcal shape analysis for cortical surface registration. *Proc IEEE Comput Soc Conf Comput Vis Pattern Recognit* 13-18 June:475-482.
- Judas M, Rados M, Jovanov-Milosevic N, Hrabac P, Stern-Padovan R, Kostovic I. 2005. Structural, immunocytochemical, and MR imaging properties of periventricular crossroads of growing cortical pathways in preterm infants. *AJNR Am J Neuroradiol* 26:2671-2684.
- Kapellou O, Counsell SJ, Kennea N, Dyet L, Saeed N, Stark J, Maalouf E, Duggan P, Ajayi-Obe M, Hajnal J, Allsop JM, Boardman J, Rutherford MA, Cowan F, Edwards AD. 2006. Abnormal cortical development after premature birth shown by altered allometric scaling of brain growth. *PLoS Med* 3:e265.
- Kaufman A, Kaufman N. 1983. Kaufmann Assessment Battery for Children (K-ABC). American Guidance Service: Circle Pines, MN.

- Kaukola T, Perhomaa M, Vainionpää L, Tolonen U, Jauhiainen J, Paakko E, Hallman M. 2009a. Apparent diffusion coefficient on magnetic resonance imaging in pons and in corona radiata and relation with the neurophysiologic measurement and the outcome in very preterm infants. *Neonatology* 97:15-21.
- Kaukola T, Kapellou O, Laroche S, Counsell SJ, Dyet LE, Allsop JM, Edwards AD. 2009b. Severity of perinatal illness and cerebral cortical growth in preterm infants. *Acta Paediatr* 98:990-995.
- Kennedy KM, Erickson KI, Rodrigue KM, Voss MW, Colcombe SJ, Kramer AF, Acker JD, Raz N. 2009. Age-related differences in regional brain volumes: A comparison of optimized voxel-based morphometry to manual volumetry. *Neurobiol Aging* 30:1657-1676.
- Kjems U, Strother SC, Anderson J, Law I, Hansen LK. 1999. Enhancing the multivariate signal of [15O] water PET studies with a new nonlinear neuroanatomical registration algorithm. *IEEE Trans Med Imaging* 18:306-319.
- Klein A, Andersson J, Ardekani BA, Ashburner J, Avants B, Chiang MC, Christensen GE, Collins DL, Gee J, Hellier P, Song JH, Jenkinson M, Lepage C, Rueckert D, Thompson P, Vercauteren T, Woods RP, Mann JJ, Parsey RV. 2009. Evaluation of 14 nonlinear deformation algorithms applied to human brain MRI registration. *Neuroimage* 46:786-802.
- Kochunov P, Lancaster JL, Thompson P, Woods R, Mazziotta J, Hardies J, Fox P. 2001. Regional spatial normalization: Toward an optimal target. *J Comput Assist Tomogr* 25:805-816.
- Kostovic I, Rakic P. 1984. Development of prestriate visual projections in the monkey and human fetal cerebrum revealed by transient cholinesterase staining. *J Neurosci* 4:25-42.
- Kostovic I, Goldman-Rakic PS. 1983. Transient cholinesterase staining in the mediodorsal nucleus of the thalamus and its connections in the developing human and monkey brain. *J Comp Neurol* 219:431-447.
- Kostovic I. 1990. Structural and histochemical reorganization of the human prefrontal cortex during perinatal and postnatal life. *Prog Brain Res* 85:223-39.
- Kostovic I, Rakic P. 1990. Developmental history of the transient subplate zone in the visual and somatosensory cortex of the macaque monkey and human brain. *J Comp Neurol* 297:441-470.
- Kostovic I, Judas M. 2002. Correlation between the sequential ingrowth of afferents and transient patterns of cortical lamination in preterm infants. *Anat Rec* 267:1-6.
- Kostovic I, Jovanov-Milosevic N. 2006. The development of cerebral connections during the first 20-45 weeks' gestation. *Semin Fetal Neonatal Med* 11:415-422.
- Kostovic I, Judas M. 2010. The development of the subplate and thalamo-cortical connections in the human foetal brain. *Acta Paediatr* 99:1119-1127.

- Krishnan ML, Dyet LE, Boardman JP, Kapellou O, Allsop JM, Cowan F, Edwards AD, Rutherford MA, Counsell SJ. 2007. Relationship between white matter apparent diffusion coefficients in preterm infants at term-equivalent age and developmental outcome at 2 years. *Pediatrics* 120:e604-9.
- Kuklisova-Murgasova M, Aljabar P, Srinivasan L, Counsell SJ, Doria V, Serag A, Gousias IS, Boardman JP, Rutherford MA, Edwards AD, Hajnal JV, Rueckert D. 2011. A dynamic 4D probabilistic atlas of the developing brain. *Neuroimage* 54:2750-2763.
- LaMantia AS, Rakic P. 1990. Axon overproduction and elimination in the corpus callosum of the developing rhesus monkey. *J Neurosci* 10:2156-2175.
- Larroque B, Marret S, Ancel PY, Arnaud C, Marpeau L, Supernant K, Pierrat V, Roze JC, Matis J, Cambonie G, Burguet A, Andre M, Kaminski M, Breart G, EPIPAGE Study Group. 2003. White matter damage and intraventricular hemorrhage in very preterm infants: The EPIPAGE study. *J Pediatr* 143:477-483.
- Lauterbur PC. 1973. Image formation by induced local interactions: Examples employing nuclear magnetic resonance. *Nature* 242:190-191.
- Lawn JE, Wilczynska-Ketende K, Cousens SN. 2006. Estimating the causes of 4 million neonatal deaths in the year 2000. *Int J Epidemiol* 35:706-718.
- Le Bihan D, Breton E, Lallemand D, Grenier P, Cabanis E, Laval-Jeantet M. 1986. MR imaging of intravoxel incoherent motions: Application to diffusion and perfusion in neurologic disorders. *Radiology* 161:401-407.
- Le Bihan D, Poupon C, Amadon A, Lethimonnier F. 2006. Artifacts and pitfalls in diffusion MRI. *J Magn Reson Imaging* 24:478-488.
- Lefebvre F, Mazurier E, Tessier R. 2005. Cognitive and educational outcomes in early adulthood for infants weighing 1000 grams or less at birth. *Acta Paediatr* 94:733-740.
- Lefèvre J, Leroy F, Khan S, Dubois J, Huppi P, Baillet S, Mangin J. 2009. Identification of growth seeds in the neonate brain through surfacic Helmholtz decomposition. *Inf Process Med Imaging* 21:252-263.
- Lehmann TM, Gonner C, Spitzer K. 1999. Survey: Interpolation methods in medical image processing. *IEEE Trans Med Imaging* 18:1049-1075.
- Leijser LM, de Bruine FT, Steggerda SJ, van der Grond J, Walther FJ, van Wezel-Meijler G. 2009. Brain imaging findings in very preterm infants throughout the neonatal period: Part I. incidences and evolution of lesions, comparison between ultrasound and MRI. *Early Hum Dev* 85:101-109.

- Leow AD, Yanovsky I, Chiang MC, Lee AD, Klunder AD, Lu A, Becker JT, Davis SW, Toga AW, Thompson PM. 2007. Statistical properties of jacobian maps and the realization of unbiased large-deformation nonlinear image registration. *IEEE Trans Med Imaging* 26:822-832.
- Leow AD et al. 2009. Alzheimer's disease neuroimaging initiative: A one-year follow up study using tensor-based morphometry correlating degenerative rates, biomarkers and cognition. *Neuroimage* 45:645-655.
- Lepore N, Brun C, Pennec X, Chou YY, Lopez OL, Aizenstein HJ, Becker JT, Toga AW, Thompson PM. 2007. Mean template for tensor-based morphometry using deformation tensors. *Med Image Comput Comput Assist Interv* 10:826-833.
- Leviton A, Paneth N, Reuss ML, Susser M, Allred EN, Dammann O, Kuban K, Van Marter LJ, Pagano M, Hegyi T, Hiatt M, Sanocka U, Shahrvivar F, Abiri M, Disalvo D, Doubilet P, Kairam R, Kazam E, Kirpekar M, Rosefeld D, Schonfeld S, Share J, Collins M, Genest D, Shen-Schwarz S, Developmental Epidemiology Network Investigators. 1999. Maternal infection, fetal inflammatory response, and brain damage in very low birth weight infants. *Pediatr Res* 46:566-575.
- Lichtenberger EO. 2005. General measures of cognition for the preschool child. *Ment Retard Dev Disabil Res Rev* 11:197-208.
- Ligam P, Haynes RL, Folkerth RD, Liu L, Yang M, Volpe JJ, Kinney HC. 2009. Thalamic damage in periventricular leukomalacia: Novel pathologic observations relevant to cognitive deficits in survivors of prematurity. *Pediatr Res* 65:524-529.
- Limperopoulos C. 2010. Pediatrics: neuroprotective effects of erythropoietin in preterm infants. *Nat Rev Neurol* 6:301-302
- Lin Y, Okumura A, Hayakawa F, Kato K, Kuno T, Watanabe K. 2001. Quantitative evaluation of thalami and basal ganglia in infants with periventricular leukomalacia. *Dev Med Child Neurol* 43:481-485.
- Lind A, Parkkola R, Lehtonen L, Munck P, Maunu J, Lapinleimu H, Haataja L, PIPARI Study Group. 2011. Associations between regional brain volumes at term-equivalent age and development at 2 years of age in preterm children. *Pediatr Radiol* 41:953-961.
- Linder N, Haskin O, Levit O, Klinger G, Prince T, Naor N, Turner P, Karmazyn B, Sirota L. 2003. Risk factors for intraventricular hemorrhage in very low birth weight premature infants: A retrospective case-control study. *Pediatrics* 111:e590-5.
- Liu Y, Baleriaux D, Kavec M, Metens T, Absil J, Denolin V, Pardou A, Avni F, Van Bogaert P, Aeby A. 2010. Structural asymmetries in motor and language networks in a population of healthy preterm neonates at term equivalent age: A diffusion tensor imaging and probabilistic tractography study. *Neuroimage* 51:783-788.

- Lockwood CJ, Senyei AE, Dische MR, Casal D, Shah KD, Thung SN, Jones L, Deligdisch L, Garite TJ. 1991. Fetal fibronectin in cervical and vaginal secretions as a predictor of preterm delivery. *N Engl J Med* 325:669-674.
- Lockwood CJ, Toti P, Arcuri F, Paidas M, Buchwalder L, Krikun G, Schatz F. 2005. Mechanisms of abruption-induced premature rupture of the fetal membranes: Thrombin-enhanced interleukin-8 expression in term decidua. *Am J Pathol* 167:1443-1449.
- Lodygensky GA, Seghier ML, Warfield SK, Tolsa CB, Sizonenko S, Lazeyras F, Huppi PS. 2008. Intrauterine growth restriction affects the preterm infant's hippocampus. *Pediatr Res* 63:438-443.
- Loeliger M, Inder T, Cain S, Ramesh RC, Camm E, Thomson MA, Coalson J, Rees SM. 2006. Cerebral outcomes in a preterm baboon model of early versus delayed nasal continuous positive airway pressure. *Pediatrics* 118:1640-1653.
- Loeliger M, Inder TE, Shields A, Dalitz P, Cain S, Yoder B, Rees SM. 2009. High-frequency oscillatory ventilation is not associated with increased risk of neuropathology compared with positive pressure ventilation: A preterm primate model. *Pediatr Res* 66:545-550.
- Lu PH, Thompson PM, Leow A, Lee GJ, Lee A, Yanovsky I, Parikshak N, Khoo T, Wu S, Geschwind D, Bartzokis G. 2011. Apolipoprotein E genotype is associated with temporal and hippocampal atrophy rates in healthy elderly adults: A tensor-based morphometry study. *J Alzheimers Dis* 23:433-442.
- Lund JS. 1988. Anatomical organization of macaque monkey striate visual cortex. *Annu Rev Neurosci* 11:253-288.
- Luoma L, Herrgard E, Martikainen A, Ahonen T. 1998. Speech and language development of children born at < or = 32 weeks' gestation: A 5-year prospective follow-up study. *Dev Med Child Neurol* 40:380-387.
- Luppino G, Matelli M, Camarda R, Rizzolatti G. 1993. Corticocortical connections of area F3 (SMA-proper) and area F6 (pre-SMA) in the macaque monkey. *J Comp Neurol* 338:114-140.
- Lyttelton O, Boucher M, Robbins S, Evans A. 2007. An unbiased iterative group registration template for cortical surface analysis. *Neuroimage* 34:1535-1544.
- Maalouf EF, Duggan PJ, Rutherford MA, Counsell SJ, Fletcher AM, Battin M, Cowan F, Edwards AD. 1999. Magnetic resonance imaging of the brain in a cohort of extremely preterm infants. *J Pediatr* 135:351-357.
- Maalouf EF, Duggan PJ, Counsell SJ, Rutherford MA, Cowan F, Azzopardi D, Edwards AD. 2001. Comparison of findings on cranial ultrasound and magnetic resonance imaging in preterm infants. *Pediatrics* 107:719-727.

- Maas LC, Mukherjee P, Carballido-Gamio J, Veeraraghavan S, Miller SP, Partridge SC, Henry RG, Barkovich AJ, Vigneron DB. 2004. Early laminar organization of the human cerebrum demonstrated with diffusion tensor imaging in extremely premature infants. *Neuroimage* 22:1134-1140.
- Maes F, Collignon A, Vandermeulen D, Marchal G, Suetens P. 1997. Multimodality image registration by maximization of mutual information. *IEEE Trans Med Imaging* 16:187-198.
- Maguire EA, Gadian DG, Johnsrude IS, Good CD, Ashburner J, Frackowiak RS, Frith CD. 2000. Navigation-related structural change in the hippocampi of taxi drivers. *Proc Natl Acad Sci U S A* 97:4398-4403.
- Mansfield P. 1977. Multi-planar image formation using NMR spin echoes. *J Phys C: Solid State Phys* 10:L55.
- Marin-Padilla M. 1997. Developmental neuropathology and impact of perinatal brain damage. II: White matter lesions of the neocortex. *J Neuropathol Exp Neurol* 56:219-235.
- Marin-Padilla M. 1999. Developmental neuropathology and impact of perinatal brain damage. III: Gray matter lesions of the neocortex. *J Neuropathol Exp Neurol* 58:407-429.
- Marlow N, Wolke D, Bracewell MA, Samara M, EPICure Study Group. 2005. Neurologic and developmental disability at six years of age after extremely preterm birth. *N Engl J Med* 352:9-19.
- Marlow N, Hennessy EM, Bracewell MA, Wolke D, EPICure Study Group. 2007. Motor and executive function at 6 years of age after extremely preterm birth. *Pediatrics* 120:793-804.
- Marsland S, Twining CJ. 2004. Constructing diffeomorphic representations for the groupwise analysis of nonrigid registrations of medical images. *IEEE Trans Med Imaging* 23:1006-1020.
- Martinussen M, Flanders DW, Fischl B, Busa E, Lohaugen GC, Skranes J, Vangberg TR, Brubakk AM, Haraldseth O, Dale AM. 2009. Segmental brain volumes and cognitive and perceptual correlates in 15-year-old adolescents with low birth weight. *J Pediatr* 155:848-853.e1.
- Maunu J, Lehtonen L, Lapinleimu H, Matomaki J, Munck P, Rikalainen H, Parkkola R, Haataja L, PIPARI Study Group. 2011. Ventricular dilatation in relation to outcome at 2 years of age in very preterm infants: A prospective Finnish cohort study. *Dev Med Child Neurol* 53:48-54.
- McCarton CM, Brooks-Gunn J, Wallace IF, Bauer CR, Bennett FC, Bernbaum JC, Broyles RS, Casey PH, McCormick MC, Scott DT, Tyson J, Tonascia J, Meinert CL. 1997. Results at age 8 years of early intervention for low-birth-weight premature infants. the infant health and development program. *JAMA* 277:126-132.

- McKinstry RC, Mathur A, Miller JH, Ozcan A, Snyder AZ, Schefft GL, Almli CR, Shiran SI, Conturo TE, Neil JJ. 2002. Radial organization of developing preterm human cerebral cortex revealed by non-invasive water diffusion anisotropy MRI. *Cereb Cortex* 12:1237-1243.
- McQuillen PS, Sheldon RA, Shatz CJ, Ferriero DM. 2003. Selective vulnerability of subplate neurons after early neonatal hypoxia-ischemia. *J Neurosci* 23:3308-3315.
- Melie-Garcia L, Canales-Rodriguez EJ, Aleman-Gomez Y, Lin CP, Iturria-Medina Y, Valdes-Hernandez PA. 2008. A bayesian framework to identify principal intravoxel diffusion profiles based on diffusion-weighted MR imaging. *Neuroimage* 42:750-770.
- Ment LR, Hirtz D, Huppi PS. 2009. Imaging biomarkers of outcome in the developing preterm brain. *Lancet Neurol* 8:1042-1055.
- Miller RH. 2002. Regulation of oligodendrocyte development in the vertebrate CNS. *Prog Neurobiol* 67:451-467.
- Miller SP, Vigneron DB, Henry RG, Bohland MA, Ceppi-Cozzio C, Hoffman C, Newton N, Partridge JC, Ferriero DM, Barkovich AJ. 2002. Serial quantitative diffusion tensor MRI of the premature brain: Development in newborns with and without injury. *J Magn Reson Imaging* 16:621-632.
- Miller SP, Ferriero DM. 2009. From selective vulnerability to connectivity: Insights from newborn brain imaging. *Trends Neurosci* 32:496-505.
- Molnar Z, Adams R, Blakemore C. 1998. Mechanisms underlying the early establishment of thalamo-cortical connections in the rat. *J Neurosci* 18:5723-5745.
- Molnar Z, Higashi S, Lopez-Bendito G. 2003. Choreography of early thalamo-cortical development. *Cereb Cortex* 13:661-669.
- Monuki ES, Walsh CA. 2001. Mechanisms of cerebral cortical patterning in mice and humans. *Nat Neurosci* 4:1199-1206.
- Morel A, Magnin M, Jeanmonod D. 1997. Multiarchitectonic and stereotactic atlas of the human thalamus. *J Comp Neurol* 387:588-630.
- Mori S, Crain BJ, Chacko VP, van Zijl PC. 1999. Three-dimensional tracking of axonal projections in the brain by magnetic resonance imaging. *Ann Neurol* 45:265-269.
- Mori S, Kaufmann WE, Davatzikos C, Stieltjes B, Amodei L, Fredericksen K, Pearlson GD, Melhem ER, Solaiyappan M, Raymond GV, Moser HW, van Zijl PC. 2002. Imaging cortical association tracts in the human brain using diffusion-tensor-based axonal tracking. *Magn Reson Med* 47:215-223.
- Mori S, van Zijl PC. 2002. Fiber tracking: Principles and strategies - a technical review. *NMR Biomed* 15:468-480.

- Moseley ME, Cohen Y, Kucharczyk J, Mintorovitch J, Asgari HS, Wendland MF, Tsuruda J, Norman D. 1990. Diffusion-weighted MR imaging of anisotropic water diffusion in cat central nervous system. *Radiology* 176:439-445.
- Mukherjee P, Miller JH, Shimony JS, Philip JV, Nehra D, Snyder AZ, Conturo TE, Neil JJ, McKinstry RC. 2002. Diffusion-tensor MR imaging of gray and white matter development during normal human brain maturation. *AJNR Am J Neuroradiol* 23:1445-1456.
- Nagasunder AC, Kinney HC, Bluml S, Tavaré CJ, Rosser T, Gilles FH, Nelson MD, Panigrahy A. 2011. Abnormal microstructure of the atrophic thalamus in preterm survivors with periventricular leukomalacia. *AJNR Am J Neuroradiol* 32:185-191.
- Nagy Z, Westerberg H, Skare S, Andersson JL, Lilja A, Flodmark O, Fernell E, Holmberg K, Bohm B, Forssberg H, Lagercrantz H, Klingberg T. 2003. Preterm children have disturbances of white matter at 11 years of age as shown by diffusion tensor imaging. *Pediatr Res* 54:672-679.
- Nagy Z, Ashburner J, Andersson J, Jbabdi S, Draganski B, Skare S, Bohm B, Smedler AC, Forssberg H, Lagercrantz H. 2009. Structural correlates of preterm birth in the adolescent brain. *Pediatrics* 124:e964-72.
- Nakamura Y, Okudera T, Fukuda S, Hashimoto T. 1990. Germinal matrix hemorrhage of venous origin in preterm neonates. *Hum Pathol* 21:1059-1062.
- Neil JJ, Shiran SI, McKinstry RC, Schefft GL, Snyder AZ, Almli CR, Akbudak E, Aronovitz JA, Miller JP, Lee BC, Conturo TE. 1998. Normal brain in human newborns: Apparent diffusion coefficient and diffusion anisotropy measured by using diffusion tensor MR imaging. *Radiology* 209:57-66.
- Nelson KB, Dambrosia JM, Iovannisci DM, Cheng S, Grether JK, Lammer E. 2005. Genetic polymorphisms and cerebral palsy in very preterm infants. *Pediatr Res* 57:494-499
- Nichols TE, Holmes AP. 2002. Nonparametric permutation tests for functional neuroimaging: A primer with examples. *Hum Brain Mapp* 15:1-25.
- Nosarti C, Al-Asady MH, Frangou S, Stewart AL, Rifkin L, Murray RM. 2002. Adolescents who were born very preterm have decreased brain volumes. *Brain* 125:1616-1623.
- Nosarti C, Giouroukou E, Micali N, Rifkin L, Morris RG, Murray RM. 2007. Impaired executive functioning in young adults born very preterm. *J Int Neuropsychol Soc* 13:571-581.
- Nosarti C, Giouroukou E, Healy E, Rifkin L, Walshe M, Reichenberg A, Chitnis X, Williams SC, Murray RM. 2008. Grey and white matter distribution in very preterm adolescents mediates neurodevelopmental outcome. *Brain* 131:205-217.
- Odegard TN, Farris EA, Ring J, McColl R, Black J. 2009. Brain connectivity in non-reading impaired children and children diagnosed with developmental dyslexia. *Neuropsychologia* 47:1972-1977.

- Offidani C, Pomini F, Caruso A, Ferrazzani S, Chiarotti M, Fiori A. 1995. Cocaine during pregnancy: A critical review of the literature. *Minerva Ginecol* 47:381-390.
- Olsen P, Laara E, Rantakallio P, Jarvelin MR, Sarpola A, Hartikainen AL. 1995. Epidemiology of preterm delivery in two birth cohorts with an interval of 20 years. *Am J Epidemiol* 142:1184-1193.
- Ordidge RJ, Mansfield P, Coupland RE. 1981. Rapid biomedical imaging by NMR. *Br J Radiol* 54:850-855.
- Padilla N, Falcon C, Sanz-Cortes M, Figueras F, Bargallo N, Crispi F, Eixarch E, Arranz A, Botet F, Gratacos E. 2011. Differential effects of intrauterine growth restriction on brain structure and development in preterm infants: A magnetic resonance imaging study. *Brain Res* 1382:98-108.
- Papile LA, Burstein J, Burstein R, Koffler H. 1978. Incidence and evolution of subependymal and intraventricular hemorrhage: A study of infants with birth weights less than 1,500 gm. *J Pediatr* 92:529-534.
- Parker GJ, Alexander DC. 2005. Probabilistic anatomical connectivity derived from the microscopic persistent angular structure of cerebral tissue. *Philos Trans R Soc Lond B Biol Sci* 360:893-902.
- Partridge SC, Mukherjee P, Henry RG, Miller SP, Berman JI, Jin H, Lu Y, Glenn OA, Ferriero DM, Barkovich AJ, Vigneron DB. 2004. Diffusion tensor imaging: Serial quantitation of white matter tract maturity in premature newborns. *Neuroimage* 22:1302-1314.
- Partridge SC, Mukherjee P, Berman JI, Henry RG, Miller SP, Lu Y, Glenn OA, Ferriero DM, Barkovich AJ, Vigneron DB. 2005. Tractography-based quantitation of diffusion tensor imaging parameters in white matter tracts of preterm newborns. *J Magn Reson Imaging* 22:467-474.
- Perkins L, Hughes E, Srinivasan L, Allsop J, Glover A, Kumar S, Fisk N, Rutherford M. 2008. Exploring cortical subplate evolution using magnetic resonance imaging of the fetal brain. *Dev Neurosci* 30:211-220.
- Perlman JM, Risser R, Broyles RS. 1996. Bilateral cystic periventricular leukomalacia in the premature infant: Associated risk factors. *Pediatrics* 97:822-827.
- Peterson BS, Anderson AW, Ehrenkranz R, Staib LH, Tageldin M, Colson E, Gore JC, Duncan CC, Makuch R, Ment LR. 2003. Regional brain volumes and their later neurodevelopmental correlates in term and preterm infants. *Pediatrics* 111:939-948.
- Petrou S, Eddama O, Mangham L. 2011. A structured review of the recent literature on the economic consequences of preterm birth. *Arch Dis Child Fetal Neonatal Ed* 96:F225-32.
- Pfeiffer SE, Warrington AE, Bansal R. 1993. The oligodendrocyte and its many cellular processes. *Trends Cell Biol* 3:191-197.

- Picard N, Strick PL. 1996. Motor areas of the medial wall: A review of their location and functional activation. *Cereb Cortex* 6:342-353.
- Pierpaoli C, Basser PJ. 1996. Toward a quantitative assessment of diffusion anisotropy. *Magn Reson Med* 36:893-906.
- Pierson CR, Folkerth RD, Billiards SS, Trachtenberg FL, Drinkwater ME, Volpe JJ, Kinney HC. 2007. Gray matter injury associated with periventricular leukomalacia in the premature infant. *Acta Neuropathol* 114:619-631.
- Pluim JP, Maintz JB, Viergever MA. 2003. Mutual-information-based registration of medical images: A survey. *IEEE Trans Med Imaging* 22:986-1004.
- Porter EJ, Counsell SJ, Edwards AD, Allsop J, Azzopardi D. 2010. Tract-based spatial statistics of magnetic resonance images to assess disease and treatment effects in perinatal asphyxial encephalopathy. *Pediatr Res* 68:205-209.
- Purcell EM, Torrey HC, Pound RV. 1946. Resonance absorption by nuclear magnetic moments in a solid. *Phys Rev* 69:37-38.
- Rabi II, Zacharias JR, Millman S, Kusch P. 1938. A new method of measuring nuclear magnetic moment. *Phys Rev* 53:318.
- Rademacher J, Caviness VS, Steinmetz H, Galaburda AM. 1993. Topographical variation of the human primary cortices: Implications for neuroimaging, brain mapping, and neurobiology. *Cereb Cortex* 3:313-329.
- Rakic P. 1977. Prenatal development of the visual system in rhesus monkey. *Philos Trans R Soc Lond B Biol Sci* 278:245-260.
- Rakic P. 1988. Specification of cerebral cortical areas. *Science* 241:170-176.
- Rathbone R, Counsell SJ, Kapellou O, Dyet L, Kennea N, Hajnal JV, Allsop JM, Cowan FM, Edwards AD. 2011. Perinatal cortical growth and childhood neurocognitive abilities. *Neurology*. In press.
- Repka MX. 2002. Ophthalmological problems of the premature infant. *Ment Retard Dev Disabil Res Rev* 8:249-257.
- Resch B, Vollaard E, Maurer U, Haas J, Rosegger H, Muller W. 2000. Risk factors and determinants of neurodevelopmental outcome in cystic periventricular leucomalacia. *Eur J Pediatr* 159:663-670.
- Ricci D, Anker S, Cowan F, Pane M, Gallini F, Luciano R, Donvito V, Baranello G, Cesarini L, Bianco F, Rutherford M, Romagnoli C, Atkinson J, Braddick O, Guzzetta F, Mercuri E. 2006. Thalamic atrophy in infants with PVL and cerebral visual impairment. *Early Hum Dev* 82:591-595.

- Robinson EC, Valstar M, Hammers A, Ericsson A, Edwards AD, Rueckert D. 2008. Multivariate statistical analysis of whole brain structural networks obtained using probabilistic tractography. *Med Image Comput Comput Assist Interv* 11:486-493.
- Robinson EC, Hammers A, Ericsson A, Edwards AD, Rueckert D. 2010. Identifying population differences in whole-brain structural networks: A machine learning approach. *Neuroimage* 50:910-919.
- Robinson S, Li Q, Dechant A, Cohen ML. 2006. Neonatal loss of gamma-aminobutyric acid pathway expression after human perinatal brain injury. *J Neurosurg* 104:396-408.
- Roelants-van Rijn AM, Groenendaal F, Beek FJ, Eken P, van Haastert IC, de Vries LS. 2001. Parenchymal brain injury in the preterm infant: Comparison of cranial ultrasound, MRI and neurodevelopmental outcome. *Neuropediatrics* 32:80-89.
- Rogers B, Msall M, Owens T, Guernsey K, Brody A, Buck G, Hudak M. 1994. Cystic periventricular leukomalacia and type of cerebral palsy in preterm infants. *J Pediatr* 125:S1-8.
- Rohlfing T, Sullivan EV, Pfefferbaum A. 2006. Deformation-based brain morphometry to track the course of alcoholism: Differences between intra-subject and inter-subject analysis. *Psychiatry Res* 146:157-170.
- Rohr K, Stiehl HS, Sprengel R, Buzug TM, Weese J, Kuhn MH. 2001. Landmark-based elastic registration using approximating thin-plate splines. *IEEE Trans Med Imaging* 20:526-534.
- Roizen JD, Asada M, Tong M, Tai HH, Muglia LJ. 2008. Preterm birth without progesterone withdrawal in 15-hydroxyprostaglandin dehydrogenase hypomorphic mice. *Mol Endocrinol* 22:105-112.
- Romero R, Gomez R, Chaiworapongsa T, Conoscenti G, Kim JC, Kim YM. 2001. The role of infection in preterm labour and delivery. *Paediatr Perinat Epidemiol* 15:41-56.
- Roosendaal SD, Geurts JJ, Vrenken H, Hulst HE, Cover KS, Castelijns JA, Pouwels PJ, Barkhof F. 2009. Regional DTI differences in multiple sclerosis patients. *Neuroimage* 44:1397-1403.
- Rose J, Mirmiran M, Butler EE, Lin CY, Barnes PD, Kermoian R, Stevenson DK. 2007. Neonatal microstructural development of the internal capsule on diffusion tensor imaging correlates with severity of gait and motor deficits. *Dev Med Child Neurol* 49:745-750.
- Rose SA, Feldman JF. 1996. Memory and processing speed in preterm children at eleven years: A comparison with full-terms. *Child Dev* 67:2005-2021.
- Rose SE, Hatzigeorgiou X, Strudwick MW, Durbridge G, Davies PS, Colditz PB. 2008. Altered white matter diffusion anisotropy in normal and preterm infants at term-equivalent age. *Magn Reson Med* 60:761-767.
- Rosenbaum P. 2006. Classification of abnormal neurological outcome. *Early Hum Dev* 82:167-171.

- Rouse DJ, Hirtz DG, Thom E, Varner MW, Spong CY, Mercer BM, Iams JD, Wapner RJ, Sorokin Y, Alexander JM, Harper M, Thorp JM, Ramin SM, Malone FD, Carpenter M, Miodovnik M, Moawad A, O'Sullivan MJ, Peaceman AM, Hankins GD, Langer O, Caritis SN, Roberts JM, Eunice Kennedy Shriver NICHD Maternal-Fetal Medicine Units Network. 2008. A randomized, controlled trial of magnesium sulfate for the prevention of cerebral palsy. *N Engl J Med* 359:895-905.
- Rubinov M, Knock SA, Stam CJ, Micheloyannis S, Harris AW, Williams LM, Breakspear M. 2009. Small-world properties of nonlinear brain activity in schizophrenia. *Hum Brain Mapp* 30:403-416.
- Rueckert D, Sonoda LI, Hayes C, Hill DL, Leach MO, Hawkes DJ. 1999. Nonrigid registration using free-form deformations: Application to breast MR images. *IEEE Trans Med Imaging* 18:712-721.
- Rueckert D, Frangi AF, Schnabel JA. 2003. Automatic construction of 3-D statistical deformation models of the brain using nonrigid registration. *IEEE Trans Med Imaging* 22:1014-1025.
- Rueckert D, Aljabar P, Heckemann RA, Hajnal JV, Hammers A. 2006. Diffeomorphic registration using B-splines. *Med Image Comput Comput Assist Interv* 9:702-709.
- Rushe TM, Rifkin L, Stewart AL, Townsend JP, Roth SC, Wyatt JS, Murray RM. 2001. Neuropsychological outcome at adolescence of very preterm birth and its relation to brain structure. *Dev Med Child Neurol* 43:226-233.
- Russchen FT, Amaral DG, Price JL. 1987. The afferent input to the magnocellular division of the mediodorsal thalamic nucleus in the monkey, *macaca fascicularis*. *J Comp Neurol* 256:175-210.
- Saigal S, Hoult LA, Streiner DL, Stoskopf BL, Rosenbaum PL. 2000. School difficulties at adolescence in a regional cohort of children who were extremely low birth weight. *Pediatrics* 105:325-331.
- Saigal S, den Ouden L, Wolke D, Hoult L, Paneth N, Streiner DL, Whitaker A, Pinto-Martin J. 2003. School-age outcomes in children who were extremely low birth weight from four international population-based cohorts. *Pediatrics* 112:943-950.
- Sakai ST, Stepniewska I, Qi HX, Kaas JH. 2000. Pallidal and cerebellar afferents to pre-supplementary motor area thalamo-cortical neurons in the owl monkey: A multiple labeling study. *J Comp Neurol* 417:164-180.
- Sakuma H, Nomura Y, Takeda K, Tagami T, Nakagawa T, Tamagawa Y, Ishii Y, Tsukamoto T. 1991. Adult and neonatal human brain: Diffusional anisotropy and myelination with diffusion-weighted MR imaging. *Radiology* 180:229-233.
- Sarkar S, Bhagat I, Dechert R, Schumacher RE, Donn SM. 2009. Severe intraventricular hemorrhage in preterm infants: Comparison of risk factors and short-term neonatal morbidities between grade 3 and grade 4 intraventricular hemorrhage. *Am J Perinatol* 26:419-424.

- Scannell JW, Burns GA, Hilgetag CC, O'Neil MA, Young MP. 1999. The connectional organization of the cortico-thalamic system of the cat. *Cereb Cortex* 9:277-299.
- Schell G, Strick P. 1984. The origin of thalamic inputs to the arcuate premotor and supplementary motor areas. *J Neurosci* 4:539-560.
- Schindler MK, Wang L, Selemon LD, Goldman-Rakic PS, Rakic P, Csernansky JG. 2002. Abnormalities of thalamic volume and shape detected in fetally irradiated rhesus monkeys with high dimensional brain mapping. *Biol Psychiatry* 51:827-837.
- Schnabel JA, Rueckert D, Quist M, Blackall JM, Castellano-Smith AD, Hartkens T, Penney GP, Hall WA, Liu H, Truwit CL, Gerritsen FA, Hill DLG, Hawkes DJ. 2001. A generic framework for non-rigid registration based on non-uniform multi-level free-form deformations. *Med Image Comput Comput Assist Interv* 8:573-581.
- Scholz J, Klein MC, Behrens TE, Johansen-Berg H. 2009. Training induces changes in white-matter architecture. *Nat Neurosci* 12:1370-1371.
- Selemon LD, Wang L, Nebel MB, Csernansky JG, Goldman-Rakic PS, Rakic P. 2005. Direct and indirect effects of fetal irradiation on cortical gray and white matter volume in the macaque. *Biol Psychiatry* 57:83-90.
- Selemon LD, Begovic A, Rakic P. 2009. Selective reduction of neuron number and volume of the mediodorsal nucleus of the thalamus in macaques following irradiation at early gestational ages. *J Comp Neurol* 515:454-464.
- Serag A, Aljabar P, Counsell SJ, Boardman JP, Hajnal JV, Rueckert D. 2011. Construction of a 4D atlas of the developing brain using non-rigid registration. *ISBI: Nano to Macro* 1:1532-1535.
- Shah DK, Anderson PJ, Carlin JB, Pavlovic M, Howard K, Thompson DK, Warfield SK, Inder TE. 2006. Reduction in cerebellar volumes in preterm infants: Relationship to white matter injury and neurodevelopment at two years of age. *Pediatr Res* 60:97-102.
- Shah DK, Doyle LW, Anderson PJ, Bear M, Daley AJ, Hunt RW, Inder TE. 2008. Adverse neurodevelopment in preterm infants with postnatal sepsis or necrotizing enterocolitis is mediated by white matter abnormalities on magnetic resonance imaging at term. *J Pediatr* 153:170-5, 175.e1.
- Shatz CJ, Rakic P. 1981. The genesis of efferent connections from the visual cortex of the fetal rhesus monkey. *J Comp Neurol* 196:287-307.
- Sherlock RL, Anderson PJ, Doyle LW, Victorian Infant Collaborative Study Group. 2005. Neurodevelopmental sequelae of intraventricular haemorrhage at 8 years of age in a regional cohort of ELBW/very preterm infants. *Early Hum Dev* 81:909-916.

- Shi L, Wang D, Chu WC, Burwell RG, Freeman BJ, Heng PA, Cheng JC. 2009. Volume-based morphometry of brain MR images in adolescent idiopathic scoliosis and healthy control subjects. *AJNR Am J Neuroradiol* 30:1302-1307.
- Shi F, Yap PT, Fan Y, Gilmore JH, Lin W, Shen D. 2010. Construction of multi-region-multi-reference atlases for neonatal brain MRI segmentation. *Neuroimage* 51:684-693.
- Shi F, Yap PT, Wu G, Jia H, Gilmore JH, Lin W, Shen D. 2011. Infant brain atlases from neonates to 1- and 2-year-olds. *PLoS One* 6:e18746.
- Short EJ, Klein NK, Lewis BA, Fulton S, Eisengart S, Kerckmar C, Baley J, Singer LT. 2003. Cognitive and academic consequences of bronchopulmonary dysplasia and very low birth weight: 8-year-old outcomes. *Pediatrics* 112:e359.
- Simon TJ, Ding L, Bish JP, McDonald-McGinn DM, Zackai EH, Gee J. 2005. Volumetric, connective, and morphologic changes in the brains of children with chromosome 22q11.2 deletion syndrome: An integrative study. *Neuroimage* 25:169-180.
- Skiold B, Horsch S, Hallberg B, Engstrom M, Nagy Z, Mosskin M, Blennow M, Aden U. 2010. White matter changes in extremely preterm infants, a population-based diffusion tensor imaging study. *Acta Paediatr* 99:842-849.
- Skranes J, Lohaugen GC, Martinussen M, Indredavik MS, Dale AM, Haraldseth O, Vangberg TR, Brubakk AM. 2009. White matter abnormalities and executive function in children with very low birth weight. *Neuroreport* 20:263-266.
- Slattery MM, Morrison JJ. 2002. Preterm delivery. *Lancet* 360:1489-1497.
- Smith SM, Jenkinson M, Woolrich MW, Beckmann CF, Behrens TE, Johansen-Berg H, Bannister PR, De Luca M, Drobnjak I, Flitney DE, Niazy RK, Saunders J, Vickers J, Zhang Y, De Stefano N, Brady JM, Matthews PM. 2004. Advances in functional and structural MR image analysis and implementation as FSL. *Neuroimage* 23 Suppl 1:S208-19.
- Smith SM, Jenkinson M, Johansen-Berg H, Rueckert D, Nichols TE, Mackay CE, Watkins KE, Ciccarelli O, Cader MZ, Matthews PM, Behrens TE. 2006. Tract-based spatial statistics: Voxelwise analysis of multi-subject diffusion data. *Neuroimage* 31:1487-1505.
- Smith SM, Nichols TE. 2009. Threshold-free cluster enhancement: Addressing problems of smoothing, threshold dependence and localisation in cluster inference. *Neuroimage* 44:83-98.
- Smith VC, Zupancic JA, McCormick MC, Croen LA, Greene J, Escobar GJ, Richardson DK. 2005. Trends in severe bronchopulmonary dysplasia rates between 1994 and 2002. *J Pediatr* 146:469-473.

- Smyser CD, Inder TE, Shimony JS, Hill JE, Degnan AJ, Snyder AZ, Neil JJ. 2010. Longitudinal analysis of neural network development in preterm infants. *Cereb Cortex* 20:2852-2862.
- Sporns O, Tononi G, Kotter R. 2005. The human connectome: A structural description of the human brain. *PLoS Comput Biol* 1:e42.
- Srinivasan L, Allsop J, Counsell SJ, Boardman JP, Edwards AD, Rutherford M. 2006. Smaller cerebellar volumes in very preterm infants at term-equivalent age are associated with the presence of supratentorial lesions. *AJNR Am J Neuroradiol* 27:573-579.
- Srinivasan L, Dutta R, Counsell SJ, Allsop JM, Boardman JP, Rutherford MA, Edwards AD. 2007. Quantification of deep gray matter in preterm infants at term-equivalent age using manual volumetry of 3-Tesla magnetic resonance images. *Pediatrics* 119:759-765.
- Stam CJ, Jones BF, Nolte G, Breakspear M, Scheltens P. 2007. Small-world networks and functional connectivity in Alzheimer's disease. *Cereb Cortex* 17:92-99.
- Steer P. 2005. The epidemiology of preterm labour. *BJOG: Int J Obs Gyn* 112:1-3.
- Stehling MJ, Howseman AM, Ordidge RJ, Chapman B, Turner R, Coxon R, Glover P, Mansfield P, Coupland RE. 1989. Whole-body echo-planar MR imaging at 0.5 T. *Radiology* 170:257-263.
- Stejskal EO, Tanner JE. 1965. Spin diffusion measurements: Spin echoes in the presence of a time-dependent field gradient. *J Chem Phys* 42:288-292.
- Stevens CF. 2001. An evolutionary scaling law for the primate visual system and its basis in cortical function. *Nature* 411:193-195.
- Stewart AL, Rifkin L, Amess PN, Kirkbride V, Townsend JP, Miller DH, Lewis SW, Kingsley DP, Moseley IF, Foster O, Murray RM. 1999. Brain structure and neurocognitive and behavioural function in adolescents who were born very preterm. *Lancet* 353:1653-1657.
- Strogatz SH. 2001. Exploring complex networks. *Nature* 410:268-276.
- Studholme C, Hill DL, Hawkes DJ. 1996. Automated 3-D registration of MR and CT images of the head. *Med Image Anal* 1:163-175.
- Studholme C, Hill DLG, Hawkes DJ. 1999. An overlap invariant entropy measure of 3D medical image alignment. *Pattern Recognit* 32:71-86.
- Stuss DT, Benson DF. 1984. Neuropsychological studies of the frontal lobes. *Psychol Bull* 95:3-28.
- Stuss DT, Levine B. 2002. Adult clinical neuropsychology: Lessons from studies of the frontal lobes. *Annu Rev Psychol* 53:401-433.

- Subsol G, Roberts N, Doran M, Thirion JP, Whitehouse GH. 1997. Automatic analysis of cerebral atrophy. *Magn Reson Imaging* 15:917-927.
- Takagi T, Nakamura M, Yamada M, Hikishima K, Momoshima S, Fujiyoshi K, Shibata S, Okano HJ, Toyama Y, Okano H. 2009. Visualization of peripheral nerve degeneration and regeneration: Monitoring with diffusion tensor tractography. *Neuroimage* 44:884-892.
- Takashima S, Tanaka K. 1978. Microangiography and vascular permeability of the subependymal matrix in the premature infant. *Can J Neurol Sci* 5:45-50.
- Tanaka J, Duke. 1976. Thalamic projections of the dorsomedial prefrontal cortex in the rhesus monkey (*macaca mulatta*). *Brain Res* 110:21-38.
- Tanji J. 1994. The supplementary motor area in the cerebral cortex. *Neurosci Res* 19:251-268.
- Tanner SF, Ramenghi LA, Ridgway JP, Berry E, Saysell MA, Martinez D, Arthur RJ, Smith MA, Levene MI. 2000. Quantitative comparison of intrabrain diffusion in adults and preterm and term neonates and infants. *AJR Am J Roentgenol* 174:1643-1649.
- Taylor HG, Klein N, Minich NM, Hack M. 2000. Middle-school-age outcomes in children with very low birthweight. *Child Dev* 71:1495-1511.
- Thompson DK, Warfield SK, Carlin JB, Pavlovic M, Wang HX, Bear M, Kean MJ, Doyle LW, Egan GF, Inder TE. 2007. Perinatal risk factors altering regional brain structure in the preterm infant. *Brain* 130:667-677.
- Thompson DK, Wood SJ, Doyle LW, Warfield SK, Lodygensky GA, Anderson PJ, Egan GF, Inder TE. 2008. Neonate hippocampal volumes: Prematurity, perinatal predictors, and 2-year outcome. *Ann Neurol* 63:642-651.
- Thompson DK, Inder TE, Faggian N, Johnston L, Warfield SK, Anderson PJ, Doyle LW, Egan GF. 2011. Characterization of the corpus callosum in very preterm and full-term infants utilizing MRI. *Neuroimage* 55:479-490.
- Thompson PM, Toga AW. 1996. A surface-based technique for warping three-dimensional images of the brain. *IEEE Trans Med Imaging* 15:402-417.
- Thompson PM, Giedd JN, Woods RP, MacDonald D, Evans AC, Toga AW. 2000. Growth patterns in the developing brain detected by using continuum mechanical tensor maps. *Nature* 404:190-193.
- Thompson PM, Hayashi KM, de Zubicaray G, Janke AL, Rose SE, Semple J, Herman D, Hong MS, Dittmer SS, Doddrell DM, Toga AW. 2003. Dynamics of gray matter loss in Alzheimer's disease. *J Neurosci* 23:994-1005.

- Tobi EW, Heijmans BT, Kremer D, Putter H, Delemarre-van de Waal HA, Finken MJ, Wit JM, Slagboom PE. 2011. DNA methylation of IGF2, GNASAS, INSIGF and LEP and being born small for gestational age. *Epigenetics* 6:171-176.
- Toga AW, Thompson PM. 2001. The role of image registration in brain mapping. *Image Vis Comput* 19:3-24.
- Torrance HL, Bloemen MC, Mulder EJ, Nikkels PG, Derks JB, de Vries LS, Visser GH. 2010. Predictors of outcome at 2 years of age after early intrauterine growth restriction. *Ultrasound Obstet Gynecol* 36:171-177.
- Tosun D, Dabbs K, Caplan R, Siddarth P, Toga A, Seidenberg M, Hermann B. 2011. Deformation-based morphometry of prospective neurodevelopmental changes in new onset paediatric epilepsy. *Brain* 134:1003-1014.
- Tournier JD, Calamante F, Gadian DG, Connelly A. 2004. Direct estimation of the fiber orientation density function from diffusion-weighted MRI data using spherical deconvolution. *Neuroimage* 23:1176-1185.
- Traynor C, Heckemann RA, Hammers A, O'Muircheartaigh J, Crum WR, Barker GJ, Richardson MP. 2010. Reproducibility of thalamic segmentation based on probabilistic tractography. *Neuroimage* 52:69-85.
- Trivedi R, Gupta RK, Husain N, Rathore RK, Saksena S, Srivastava S, Malik GK, Das V, Pradhan M, Sarma MK, Pandey CM, Narayana PA. 2009. Region-specific maturation of cerebral cortex in human fetal brain: Diffusion tensor imaging and histology. *Neuroradiology* 51:567-576.
- Trouvé A. 1998. Diffeomorphisms groups and pattern matching in image analysis. *Int J Comput Vis* 28:213-221.
- Tuch DS, Reese TG, Wiegell MR, Makris N, Belliveau JW, Wedeen VJ. 2002. High angular resolution diffusion imaging reveals intravoxel white matter fiber heterogeneity. *Magn Reson Med* 48:577-582.
- Tuch DS, Reese TG, Wiegell MR, Wedeen VJ. 2003. Diffusion MRI of complex neural architecture. *Neuron* 40:885-895.
- Tuch DS. 2004. Q-ball imaging. *Magn Reson Med* 52:1358-1372.
- Unser M. 1999. Splines: A perfect fit for signal and image processing. *IEEE Signal Processing Mag* 16:22-38.

- Vadillo-Ortega F, Sadowsky DW, Haluska GJ, Hernandez-Guerrero C, Guevara-Silva R, Gravett MG, Novy MJ. 2002. Identification of matrix metalloproteinase-9 in amniotic fluid and amniochorion in spontaneous labor and after experimental intrauterine infection or interleukin-1 beta infusion in pregnant rhesus monkeys. *Am J Obstet Gynecol* 186:128-138.
- van Essen DC. 2005. A population-average, landmark- and surface-based (PALS) atlas of human cerebral cortex. *Neuroimage* 28:635-662.
- van Haastert IC, de Vries LS, Eijssermans MJ, Jongmans MJ, Helders PJ, Gorter JW. 2008. Gross motor functional abilities in preterm-born children with cerebral palsy due to periventricular leukomalacia. *Dev Med Child Neurol* 50:684-689.
- van Haastert IC, Groenendaal F, Uiterwaal CS, Termote JU, van der Heide-Jalving M, Eijssermans MJ, Gorter JW, Helders PJ, Jongmans MJ, de Vries LS. 2011. Decreasing incidence and severity of cerebral palsy in prematurely born children. *J Pediatr* 159:86-91.e1.
- van Kooij BJM, Counsell SJ, Ball G, van Haastert IC, Benders M, de Vries LS, Groenendaal F. 2011. Neonatal tract-based spatial statistics findings and outcome in preterm infants. *Am J Neuroradiol*. In press.
- Verney C, Rees S, Biran V, Thompson M, Inder T, Gressens P. 2010. Neuronal damage in the preterm baboon: Impact of the mode of ventilatory support. *J Neuropathol Exp Neurol* 69:473-482.
- Vohr BR, Ment LR. 1996. Intraventricular hemorrhage in the preterm infant. *Early Hum Dev* 44:1-16.
- Vohr BR, Wright LL, Poole WK, McDonald SA. 2005. Neurodevelopmental outcomes of extremely low birth weight infants <32 weeks' gestation between 1993 and 1998. *Pediatrics* 116:635-643.
- Volpe JJ. 1996. Subplate neurons--missing link in brain injury of the premature infant? *Pediatrics* 97:112-113.
- Volpe JJ. 2001. Neurobiology of periventricular leukomalacia in the premature infant. *Pediatr Res* 50:553-562.
- Volpe JJ. 2005. Encephalopathy of prematurity includes neuronal abnormalities. *Pediatrics* 116:221-225.
- Volpe JJ. 2009. Brain injury in premature infants: A complex amalgam of destructive and developmental disturbances. *Lancet Neurol* 8:110-124.
- Volpe JJ, Kinney HC, Jensen FE, Rosenberg PA. 2011. The developing oligodendrocyte: Key cellular target in brain injury in the premature infant. *Int J Dev Neurosci* 29:423-440.

- Vuadens F, Benay C, Crettaz D, Gallot D, Sapin V, Schneider P, Bienvenut WV, Lemery D, Quadroni M, Dastugue B, Tissot JD. 2003. Identification of biologic markers of the premature rupture of fetal membranes: Proteomic approach. *Proteomics* 3:1521-1525.
- Wakana S, Jiang H, Nagae-Poetscher LM, van Zijl PC, Mori S. 2004. Fiber tract-based atlas of human white matter anatomy. *Radiology* 230:77-87.
- Wakana S, Caprihan A, Panzenboeck MM, Fallon JH, Perry M, Gollub RL, Hua K, Zhang J, Jiang H, Dubey P, Blitz A, van Zijl P, Mori S. 2007. Reproducibility of quantitative tractography methods applied to cerebral white matter. *Neuroimage* 36:630-644.
- Wedeen VJ, Hagmann P, Tseng WY, Reese TG, Weisskoff RM. 2005. Mapping complex tissue architecture with diffusion spectrum magnetic resonance imaging. *Magn Reson Med* 54:1377-1386.
- Weisenfeld NI, Warfield SK. 2009. Automatic segmentation of newborn brain MRI. *Neuroimage* 47:564-572.
- Wells WM, Viola P, Atsumi H, Nakajima S, Kikinis R. 1996. Multi-modal volume registration by maximization of mutual information. *Med Image Anal* 1:35-51.
- Westby Wold SH, Sommerfelt K, Reigstad H, Ronnestad A, Medbo S, Farstad T, Kaaresen PI, Stoen R, Leversen KT, Irgens LM, Markestad T. 2009. Neonatal mortality and morbidity in extremely preterm small for gestational age infants: A population based study. *Arch Dis Child Fetal Neonatal Ed* 94:F363-7.
- Wilke M, Holland SK, Altaye M, Gaser C. 2008. Template-O-matic: A toolbox for creating customized pediatric templates. *Neuroimage* 41:903-913.
- Wilson-Costello D, Friedman H, Minich N, Siner B, Taylor G, Schluchter M, Hack M. 2007. Improved neurodevelopmental outcomes for extremely low birth weight infants in 2000-2002. *Pediatrics* 119:37-45.
- Wimberger DM, Roberts TP, Barkovich AJ, Prayer LM, Moseley ME, Kucharczyk J. 1995. Identification of "premyelination" by diffusion-weighted MRI. *J Comput Assist Tomogr* 19:28-33.
- Wood NS, Marlow N, Costeloe K, Gibson AT, Wilkinson AR. 2000. Neurologic and developmental disability after extremely preterm birth. EPICure study group. *N Engl J Med* 343:378-384.
- Woods RP, Mazziotta JC, Cherry SR. 1993. MRI-PET registration with automated algorithm. *J Comput Assist Tomogr* 17:536-546.
- Wright IC, McGuire PK, Poline JB, Traverso JM, Murray RM, Frith CD, Frackowiak RS, Friston KJ. 1995. A voxel-based method for the statistical analysis of gray and white matter density applied to schizophrenia. *Neuroimage* 2:244-252.

- Xue H, Srinivasan L, Jiang S, Rutherford M, Edwards AD, Rueckert D, Hajnal JV. 2007. Automatic segmentation and reconstruction of the cortex from neonatal MRI. *Neuroimage* 38:461-477.
- Yakovlev PI, Lecours AR. 1967. The myelogenetic cycles of regional maturation of the brain. In: Minkowski A (Ed.). *Regional Development of the Brain in Early Life*. Blackwell, Oxford, UK.
- Yanovsky I, Leow AD, Lee S, Osher SJ, Thompson PM. 2009. Comparing registration methods for mapping brain change using tensor-based morphometry. *Med Image Anal* 13:679-700.
- Yeo BT, Sabuncu MR, Vercauteren T, Ayache N, Fischl B, Golland P. 2010. Spherical demons: Fast diffeomorphic landmark-free surface registration. *IEEE Trans Med Imaging* 29:650-668.
- Zacharia A, Zimine S, Lovblad KO, Warfield S, Thoeny H, Ozdoba C, Bossi E, Kreis R, Boesch C, Schroth G, Huppi PS. 2006. Early assessment of brain maturation by MR imaging segmentation in neonates and premature infants. *AJNR Am J Neuroradiol* 27:972-977.
- Zhang D, Snyder AZ, Shimony JS, Fox MD, Raichle ME. 2010. Noninvasive functional and structural connectivity mapping of the human thalamo-cortical system. *Cereb Cortex* 20:1187-1194.

Appendix A

MR Pulse Sequences

Outlined below are examples of three common pulse sequences used for MR acquisition: gradient-echo, spin-echo and pulsed gradient spin-echo.

Gradient-echo

In gradient-echo MRI (Figure A.1), a RF pulse is applied coincident with a slice-select gradient (G_z) to selectively excite protons in one section along the z-axis. Position within the slice is identified by repeating phase- (G_y) and frequency (G_x) -encoding at multiple phase magnitudes. Brief dephasing gradients are applied prior to signal readout to ensure that spins rephase midway through the application of G_x – producing the ‘gradient echo’ – represented by an oscillating MR signal. Image contrast is achieved by altering the time between consecutive RF excitations pulses (TR) and between the RF excitation pulse and signal readout (TE).

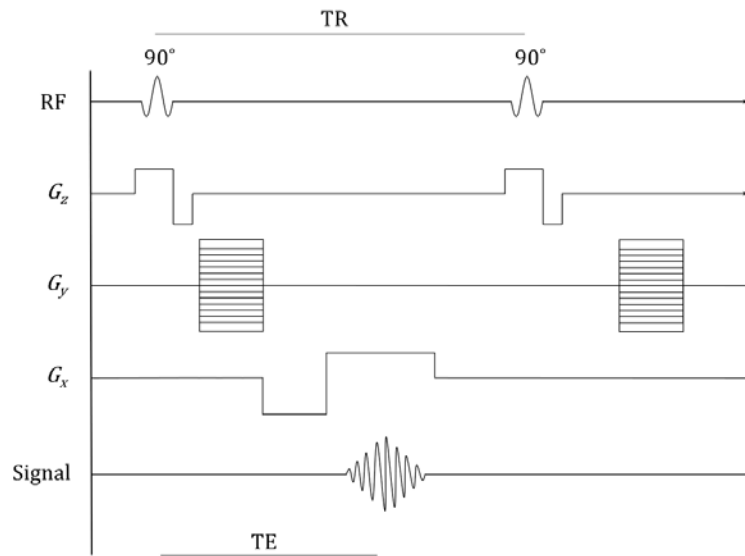


Figure A.1: Gradient-echo pulse sequence.

Spin-echo

In spin-echo acquisitions (Figure A.2), the dephasing spins are re-phased with the application of an additional 180° RF pulse applied at time t , prior to frequency-encoding and signal readout. This allows for a longer TR and full recovery of longitudinal magnetisation before the next excitation pulse.

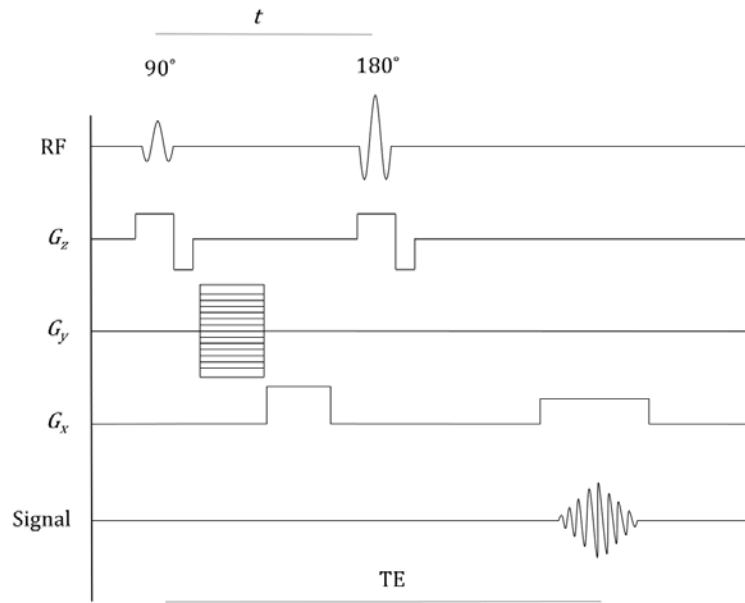


Figure A.2: Spin-echo pulse sequence.

Pulsed gradient spin-echo

To sensitise MR signal intensity to diffusion, two spatially-varying diffusion gradients (G_D) with gradient strength G , duration δ and spaced Δ apart are applied either side of a 180° RF pulse. Stationary spins are refocused by the phase-shift induced by the second gradient. Spins moving due to diffusion are not completely refocused, resulting in MR signal attenuation.

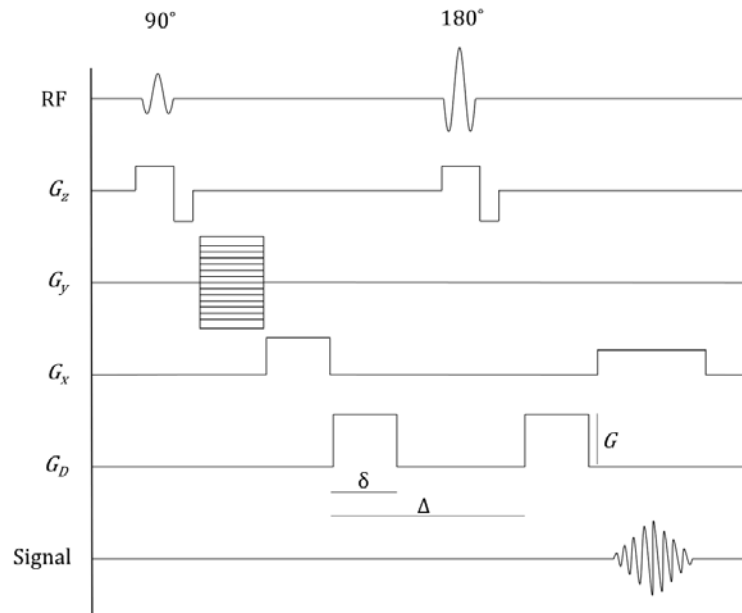


Figure A.3: Pulsed gradient spin-echo sequence.

Appendix B

Deformation-Based Morphometry: Analyses

B.1 Effect of Target Choice

To demonstrate the robust nature of the DBM processing pipeline used in Chapter 5, an additional population-based template was produced using a different subjects's T_1 -weighted image as the starting point. Each T_1 image was aligned to the alternative target image (GA = 27⁺⁰ weeks; PMA at scan = 41⁺⁰ weeks) using 6 DOF linear registration, followed by 12 DOF affine registration, and an intensity-average template produced. Two iterations of affine, followed by nonlinear registrations were then performed, updating the template after each (see Chapter 5; Figure 5.3). Figure B.1 compares the regional associations between prematurity at birth and tissue volume at term-equivalent age determined using the original and alternative targets.

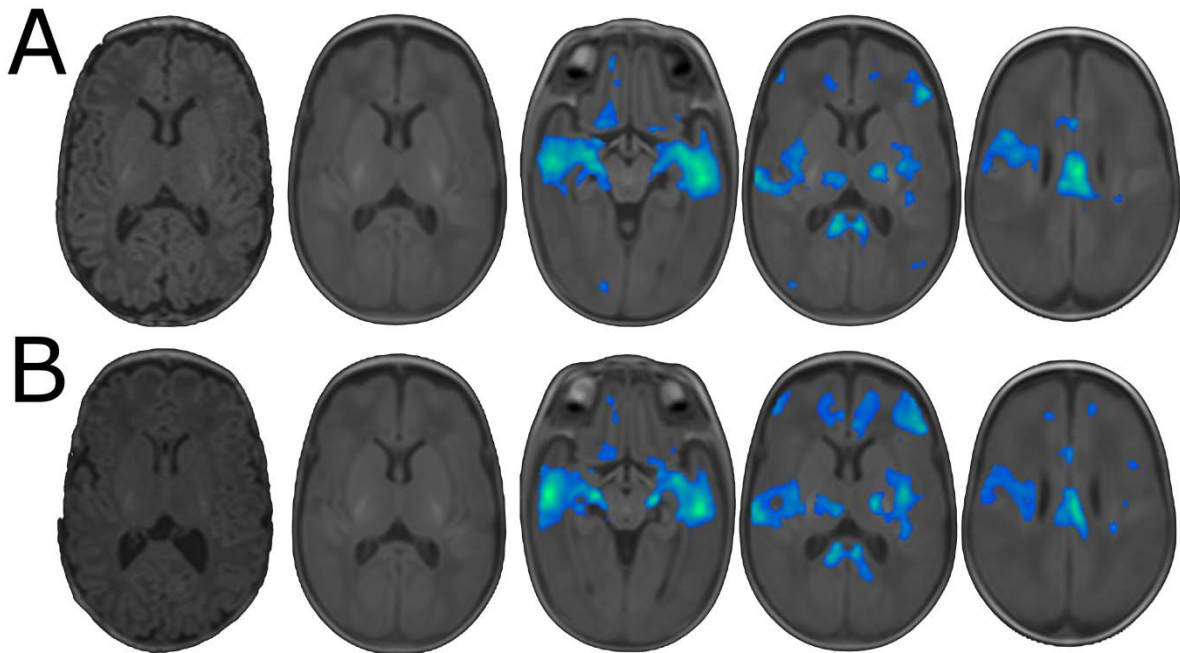


Figure B.1: DBM analysis is robust to target choice. T_1 -weighted images were registered to the original (A) or an alternative (B) target (shown in first column) according to the DBM processing pipeline. The final DBM templates are shown in the second column. Statistical analysis (presented in Chapter 5; Figure 5.5) shows the regional associations between GA at birth and the Jacobian determinant, corrected for the age of each infant at scan, after registration to each template. Images are shown FDR-corrected at $p < 0.01$.

B.2 Effect of Increasing Registration Iterations

In Chapter 5, two iterations of nonlinear registration followed by intensity-averaging were performed in the final analysis pipeline prior to statistical analysis. Figure B.2 shows the statistical associations reported in Chapter 5 (Figure 5.5) after one, two and three iterations of nonlinear registration, with analysis performed on the Jacobians derived from the deformations of the first, second and third set of registrations respectively. The results do not change significantly after three, compared to two iterations.

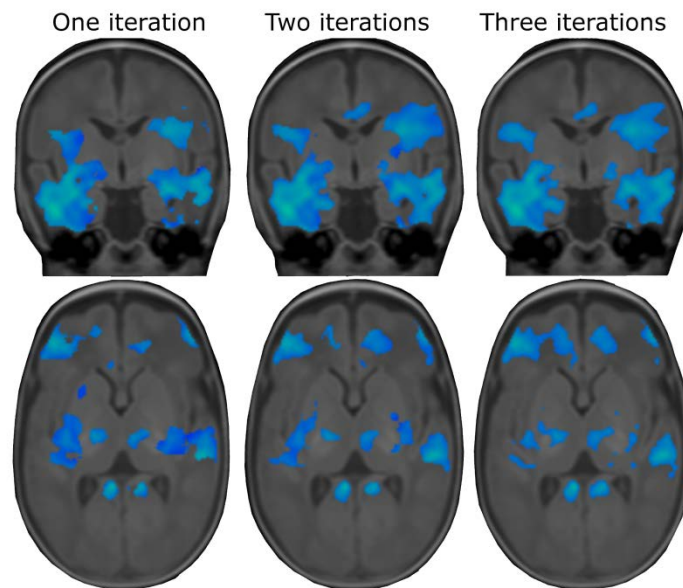


Figure B.2: Performing further iterations of nonlinear registration when constructing the final DBM template does not significantly alter the resulting statistical associations. Regions where the Jacobian determinant was significantly related to GA at birth, after correcting for the age of each infant at scan are shown (FDR-corrected, $p < 0.01$). All results are overlaid on the DBM template used in Chapter 5 (i.e.: constructed from two iterations of registration) for comparison.

Appendix C

An Optimised Tract-Based Spatial Statistics Protocol for Neonates: Applications to Prematurity and Chronic Lung Disease

Ball, G., Counsell, S.J., Anjari, M., Merchant, N., Arichi, T., Doria, V., Rutherford, M.A., Edwards, A.D, Rueckert, D. & Boardman, J.P.

NeuroImage (2010). 53:1, 984-102



Contents lists available at ScienceDirect

NeuroImage

journal homepage: www.elsevier.com/locate/ynimg

An optimised tract-based spatial statistics protocol for neonates: Applications to prematurity and chronic lung disease

Gareth Ball^a, Serena J. Counsell^a, Mustafa Anjari^a, Nazakat Merchant^{a,b}, Tomoki Arichi^{a,b},
Valentina Doria^{a,b}, Mary A. Rutherford^a, A. David Edwards^{a,b}, Daniel Rueckert^c, James P. Boardman^{a,d,*}

^a Institute of Clinical Sciences, Imperial College and MRC Clinical Sciences Centre, Hammersmith Hospital, London, UK

^b Division of Neonatology, Imperial College Healthcare NHS Trust, London, UK

^c Department of Computing, Imperial College London, London, UK

^d Simpson Centre for Reproductive Health, Royal Infirmary of Edinburgh, UK

ARTICLE INFO

Article history:

Received 29 December 2009

Revised 18 May 2010

Accepted 19 May 2010

Available online 25 May 2010

ABSTRACT

Preterm birth is associated with altered white matter microstructure, defined by metrics derived from diffusion tensor imaging (DTI). Tract-based spatial statistics (TBSS) is a useful tool for investigating developing white matter using DTI, but standard TBSS protocols have limitations for neonatal studies. We describe an optimised TBSS protocol for neonatal DTI data, in which registration errors are reduced. As chronic lung disease (CLD) is an independent risk factor for abnormal white matter development, we investigate the effect of this condition on white matter anisotropy and diffusivity using the optimised protocol in a proof of principle experiment.

DTI data were acquired from 93 preterm infants (48 male) with a median gestational age at birth of 28^{+5}_{-2} (23^{+4}_{-2} – 35^{+2}_{-2}) weeks at a median postmenstrual age at scan of 41^{+4}_{-4} (38^{+1}_{-1} – 46^{+6}_{-6}) weeks. Nineteen infants developed CLD, defined as requiring supplemental oxygen at 36 weeks postmenstrual age. TBSS was modified to include an initial low degrees-of-freedom linear registration step and a second registration to a population-average FA map.

The additional registration steps reduced global misalignment between neonatal fractional anisotropy (FA) maps. Infants with CLD had significantly increased radial diffusivity (RD) and significantly reduced FA within the centrum semiovale, corpus callosum and inferior longitudinal fasciculus ($p < 0.05$) compared to their peers, controlling for degree of prematurity and age at scan.

The optimised TBSS protocol improved reliability for neonatal DTI analysis. These data suggest that potentially modifiable respiratory morbidity is associated with widespread altered white matter microstructure in preterm infants at term-equivalent age.

© 2010 Elsevier Inc. All rights reserved.

Introduction

The incidence of preterm birth is increasing, and it is associated with a high prevalence of neurocognitive impairment in childhood (Delobel-Ayoub et al., 2009; Marlow et al., 2005) and adverse functional consequences that appear to persist into adolescence and early adulthood (Aarnoudse-Moens et al., 2009; Hille et al., 2007; Rushe et al., 2001). The perinatal factors that underlie abnormal brain development are not fully understood; however, respiratory illness is implicated because CLD is a risk factor for neurodevelopmental impairment independent of the degree of prematurity at birth (Hansen et al., 2004; Short et al., 2003; Westby Wold et al., 2009).

Diffusion tensor imaging (DTI) can provide voxelwise, scalar measures of water diffusion within the brain that reflect the underlying tissue microstructure (Basser et al., 1994; Basser and Pierpaoli, 1996). Low water diffusivity and high fractional anisotropy are characteristic of well-developed, myelinated white matter tracts, and are altered in experimental models of dysmyelination and neonatal white matter injury (Song et al., 2005; Wang et al., 2009). Compared with term-born controls, decreases in fractional anisotropy and increases in diffusivity have been observed within the white matter of preterm infants (Cheong et al., 2009; Counsell et al., 2006; Huppi et al., 1998; Miller et al., 2002; Partridge et al., 2004). These alterations are dependent on the degree of prematurity at birth (Anjari et al., 2007) and closely linked to neurodevelopmental outcome at 2 years corrected age (Counsell et al., 2008; Krishnan et al., 2007).

Most analyses of neonatal DTI have employed regions of interest (ROI) selected *a priori* to measure diffusion parameters directly in

* Corresponding author. Hammersmith House, Hammersmith Campus, Imperial College London, DuCane Road, London, W12 0HS, UK.
E-mail address: j.boardman@imperial.ac.uk (J.P. Boardman).

native diffusion tensor images (Cheong et al., 2009; Counsell et al., 2006; Kaukola et al., 2009; Partridge et al., 2004). Although this technique avoids computationally demanding image registration and offers a valid method to infer groupwise variation in white matter development, it remains subjective and manually intensive and does not easily allow for comparisons across many subjects. Tract-based spatial statistics (TBSS) is a powerful tool for studies of the adult brain that improves the sensitivity, objectivity and interpretability of multi-subject DTI analysis (Smith et al., 2006). TBSS achieves this through carefully tuned alignment of fractional anisotropy maps to a standard-space template, followed by projection of individual data onto a skeletonised representation of major white matter tracts common to the group for voxelwise analysis.

Neonatal DTI data are of lower resolution and contrast compared to adult data, and these differences together with relatively wide variations in brain size and complexity within neonatal populations pose technical challenges to DTI processing tools including TBSS. In previous work we have overcome some of these challenges by using a representative, individual FA map as a study-specific template (Anjari et al., 2007, 2009); however, registration between neonatal FA maps can still fail (Bassi et al., 2008). In addition, registration within TBSS has been empirically optimized for accurate alignment to a group-average map that is distinctly different in both contrast and smoothness to an individual FA map.

The primary aim of this study was to improve the reliability of TBSS in neonates by implementing two modifications: the inclusion of an initial low degrees-of-freedom linear registration to improve global alignment between neonatal FA maps and a second registration to a population-average FA map to produce accurate projection of individual data on a skeleton for subsequent multi-subject analysis of white matter diffusivity and anisotropy.

As a secondary aim, using the optimised TBSS protocol, we investigated the association between prematurity, CLD and white matter microstructure in a cohort of preterm infants imaged at term-equivalent age.

Materials and methods

Ethical permission for this study was granted by the Hammersmith and Queen Charlotte's and Chelsea Research Ethics Committee. Written parental consent was obtained for each infant.

Subjects

Infants were recruited from the Neonatal Intensive Care Unit at Queen Charlotte's and Chelsea Hospital (QCCH). All infants born at less than 36 weeks gestational age and who successfully underwent 15-direction DTI at term-equivalent age between March 2005 and October 2008 were eligible for inclusion. Infants were excluded if cystic periventricular leukomalacia or haemorrhagic parenchymal infarction was apparent on the term-equivalent MRI. Forty-seven infants were included in a previously reported study of CLD (Anjari et al., 2009).

Ninety-three preterm infants (48 male) underwent successful DTI. The cohort had a median (range) gestational age of 28^{+5} (23^{+4} – 35^{+2}) weeks, median (range) birth weight of 1.10 (0.63–3.71) kg, and a median (range) postmenstrual age at scan of 41^{+4} (38^{+1} – 46^{+6}) weeks. Seventy infants (75%) were treated with a full course of antenatal steroids, defined as the mother receiving the last dose of steroid at least 12 hours before birth; none received postnatal steroids. Twenty-nine infants (31%) received mechanical ventilation for a median (range) 2 (1–33) days, and additional ventilatory support was provided with nasal continuous positive airway pressure (nCPAP) and oxygen supplementation. Across the whole cohort, the median (range) time spent receiving any form of respiratory support was 18 (0–116) days. According to standard practice at QCCH, prophylactic surfactant on

the labour ward was administered to all infants born at less than 30 weeks gestational age. Nineteen infants had CLD, defined by the need for respiratory support at 36 weeks postmenstrual age.

Imaging

MRI was performed on a Philips 3-Tesla system (Philips Medical Systems, Netherlands) using an 8-channel phased array head coil. The 3D MP-RAGE and high-resolution T2-weighted fast spin echo images were obtained before diffusion tensor imaging. Single-shot EPI DTI was acquired in the transverse plane in 15 non-collinear directions using the following parameters: repetition time (TR): 8000 ms; echo time (TE): 49 ms; slice thickness: 2 mm; field of view: 224 mm; matrix: 128×128 (voxel size: $1.75 \times 1.75 \times 2$ mm³); *b* value: 750 s/mm². Data were acquired with a SENSE factor of 2, and the scanning time for the sequence was 5 minutes.

All examinations were supervised by a paediatrician experienced in MRI procedures. Infants were sedated with oral chloral hydrate (25–50 mg/kg) prior to scanning and pulse oximetry, temperature and electrocardiography data were monitored throughout. Ear protection was used for each infant, comprising earplugs moulded from a silicone-based putty (President Putty, Coltene Whaledent, Mahwah, NJ) placed in the external ear and neonatal earmuffs (MiniMuffs, Natus Medical Inc, San Carlos, CA).

Data analysis

Preprocessing

DTI analysis was performed using FMRIB's Diffusion Toolbox (FDT v2.0) and Tract-Based Spatial Statistics (TBSS v1.2) as implemented in FMRIB's Software Library (FSL v4.1; www.fmrib.ox.ac.uk/fsl; Smith et al., 2004). Each infant's diffusion weighted images were registered to their *b* = 0 image and corrected for differences in spatial distortion due to eddy currents. Images were brain extracted using Brain Extraction Tool (BET v2.1) and diffusion tensors calculated voxelwise, using a simple least squares fit of the tensor model to the diffusion data. From this, the tensor eigenvalues, describing the diffusion strength in the primary, secondary and tertiary diffusion directions, and fractional anisotropy maps were calculated.

Image registration

Prior to warping, individual fractional anisotropy maps were aligned to each other with an initial 12 degrees-of-freedom (DOF) affine registration using FMRIB's Linear Registration Tool (FLIRT v5.5; default parameters). To achieve accurate spatial alignment, fractional anisotropy maps were then registered using FMRIB's Non-Linear Registration Tool (FNIRT v1.0; parameters as defined in FA_2_FMRIB58_1mm configuration file). This is the default TBSS process and has been optimised for the registration of adult FA maps to the FMRIB58 FA standard-space image, constructed from 58 FA maps acquired from healthy adults aged 20–50 years. This approach is not suitable for the neonatal population; therefore, a study-specific target image was chosen.

To identify an appropriate individual FA map to act as a study-specific target, every subject's FA map was registered to the map of every other subject. Each warp field (final resolution: $8.75 \times 8.75 \times 10$ mm³) was summarized by a score representing the mean square spline coefficients of displacement across 3 dimensions and the target image was chosen as the one with the minimum mean displacement score from all other subjects in the group, thus deemed to be the most 'typical' image of the group. Using the optimized registration method, the chosen target image was from an infant born at 33^{+2} weeks gestation and imaged at 38^{+2} postmenstrual weeks. The summary mean displacement score \pm SD between the target and all other images was 0.76 ± 0.32 .

Registration optimisation

Two additional registration steps were added to the original protocol. Firstly, to reduce the number of failed registrations obtained using the standard TBSS protocol, an additional 6 DOF linear registration (default parameters) was performed prior to 12 DOF registration and warping. Following the initial linear registration, the image was transformed according to the estimated transformation matrix, and 12 DOF registration performed between the transformed image and the intended target. Both the 6 DOF and 12 DOF registration matrices were then concatenated and entered as an initial estimate for nonlinear warping. To compare both linear registration protocols, every subject's FA map was linearly registered to the map of every other subject using both protocols, resulting in 8556 transformations (after excluding self-to-self registrations). As a measure of similarity, the volumetric difference between every linearly transformed FA map and the intended target FA map was calculated. After successful linear registration, global differences in image scale are normalised and both the linearly transformed image and target image are of similar volume.

Secondly, after nonlinear registration of all images to the intended target image, estimated warps, including both linear and nonlinear transform, were applied to the original images to bring them into spatial correspondence. From these images, an average FA map in the target space was produced. A second iteration of linear and nonlinear registrations was then performed between the original images and the average FA map, and an average FA map, FA skeleton and projected, skeletonised data set was produced from the aligned images for statistical analysis.

Voxelwise analysis

Individual FA maps were aligned into the target space and upsampled to $1 \times 1 \times 1 \text{ mm}^3$ voxel size using the previously estimated warps. An average FA map was created and thinned by perpendicular non-maximum suppression to generate a mean FA skeleton to represent the centre of all white matter tracts common to the group. This skeleton was thresholded at $\text{FA} > 0.15$ and manually cleaned to include the major white matter pathways but exclude cerebral sinuses and cerebrospinal fluid artefactually represented in the skeleton. Individual FA, axial diffusivity – the magnitude of the principle vector of the diffusion tensor, λ_1 – and radial diffusivity –

the mean magnitude of the transverse vectors, $(\lambda_2 + \lambda_3)/2$ – data were then projected onto this skeleton prior to statistical analysis.

Voxelwise cross-subject statistical analysis was performed with Randomise (v2.1) using univariate linear modelling in the form of a general linear model. The effect of CLD on radial diffusivity (RD), axial diffusivity (AD) and FA was investigated. Infants with CLD had a significantly lower mean gestational age at birth ($\text{CLD}: 26.26 \pm 1.62$ weeks; No CLD: 29.74 ± 2.84 weeks; t -test, $p < 0.001$) and significantly higher postmenstrual age at scan ($\text{CLD}: 42.13 \pm 1.98$ weeks; No CLD: 41.33 ± 1.42 weeks; t -test, $p < 0.05$) than infants without CLD so gestational age at birth and postmenstrual age at scan were included in all statistical models as covariates. In addition, a linear regression was performed to investigate the relationship between length of respiratory support and white matter diffusion parameters, correcting for gestational age at birth and postmenstrual age at scan. All images were subject to family-wise error (FWE) correction for multiple comparisons following threshold-free cluster enhancement (TFCE; Smith and Nichols, 2009) and are shown at $p < 0.05$.

Statistical analysis was performed using SPSS 16.0 (SPSS Inc., Chicago, IL, USA).

Results

Registration optimisation

Introducing an additional linear registration

Fig. 1A shows the mean warp displacement scores that summarise transformations between each subject's FA map ($n = 93$) and the map of every other subject using a 12 DOF linear registration followed by nonlinear registration. For each target, a column of scores summarises transformations to every other FA map.

Mean displacement scores greater than 10 (mean = 1.42, range = 0–19.52) were present after registration to 29 out of 93 targets (31.2%). Fig. 1C demonstrates how summary displacement scores of different magnitudes are represented in warped FA maps. Four separate images were registered to the same target (Fig. 1C, right) and the estimated transformation applied in each case, displayed with its summary score. Large displacement scores represent registrations that have globally failed to align the image to the intended target. Applying a 6 DOF linear registration prior to 12 DOF linear registration

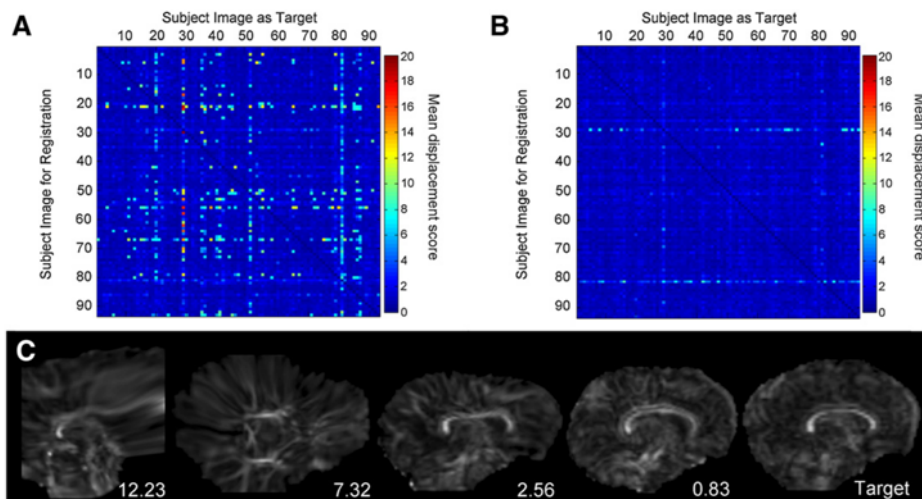


Fig. 1. Matrices showing mean warp displacement scores as a summary of linear and nonlinear transformations between every subject's FA map. (A) Using original registration parameters of a 12 DOF linear registration followed by nonlinear registration. (B) Using an initial 6 DOF linear registration before 12 DOF linear and nonlinear registration. (C) Example images obtained by registering 4 separate images to a target image (right) displayed with summary displacement scores of each transformation.

significantly reduced mean displacement scores across the whole group (mean = 1.11, range = 0–9.30; Fig. 1B). The symmetric nature of the matrix in Fig. 1B indicates that two FA maps in particular (from subject 29 and subject 81) required large displacements to bring them into alignment with several other images. Visual inspection of the original data sets revealed that both infants were plagiocephalic, a condition characterised by an asymmetrical lateral distortion of the skull.

Applying an additional 6 DOF registration improved alignment in registrations that failed but was not detrimental to registrations that were successful using the original protocol. Fig. 2 shows two example registrations to the same target (right column) using the original protocol: one that failed (top row; mean displacement score = 6.41) and one that was successful (bottom row; mean displacement score = 0.65). Registration with the modified protocol resulted in accurate anatomical alignment in both cases, improving the registration that failed initially (top row; modified mean displacement score = 0.61) but with a similar outcome to the successful registration (bottom row; modified mean displacement score = 0.52).

The global misalignment resulting from nonlinear registration (Figs. 1C and 2) is likely secondary to failure in the initial linear registration, as opposed to the relatively small local deformations normally performed during nonlinear registration. Poor global alignment would be expected to result in overcompensation by the nonlinear registration tool in an attempt to realign the two images and would consequently create a warp field with large mean displacement score. To test this hypothesis, each FA map was linearly registered to every other map. 8556 linear registrations (excluding self-to-self registrations) were performed with a single 12 DOF step resulting in a median volumetric difference between transformed images and their intended targets of 28.4 cm³ (interquartile range, 8.6–51.4 cm³). With an additional 6 DOF registration, the median difference in volume was 12.7 cm³ (interquartile range, 8.0–17.7 cm³). Fig. 3 displays the difference in volume (cm³) between each transformed FA map and their intended target following a 12 DOF registration and both 6 DOF and 12 DOF registrations. Of the 12 DOF transformations, 2327 (27.2%) produced final volumetric differences larger than the maximum produced through the two-step process, indicating large scaling errors in the single 12 DOF linear transformation.

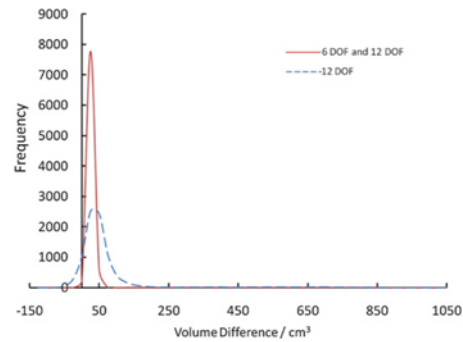


Fig. 3. Frequency histogram showing the volume difference in cm³ between transformed images and their intended target images following linear registration. Linear registration comprised a single 12 DOF linear registration (dashed line, range: −112.8 to 1027.4 cm³) or a 6 DOF followed by a 12 DOF registration (solid line, range: −15.2 to 48.7 cm³).

Using an average FA map as a target

To parallel TBSS analysis in adults, the effect of registration and projection of individual neonatal FA data onto the average FA map instead of an individual FA map was investigated. Fig. 4 shows voxelwise standard deviation of FA across the group calculated after co-registration of all images to the chosen target (A) and registration to the subsequent average FA map (B). Higher standard deviation is visible in several regions including the genu and splenium of the corpus callosum and corticospinal tracts (A; black arrows) after registration to the individual FA map. To quantify the effect of the increased variance on the skeletonisation and projection step of the TBSS protocol, Fig. 5 shows a Bland–Altman plot of individual FA values extracted from the intersection of both skeletonised data sets. Projected FA was significantly higher across the whole skeleton after registration to the average FA map (paired *t*-test; *p* < 0.01).

Optimised registration pipeline

To summarise, Fig. 6 shows the optimised pipeline for TBSS preprocessing of neonatal DTI data. After the registration of every subject's FA map to each other, using two linear registration steps

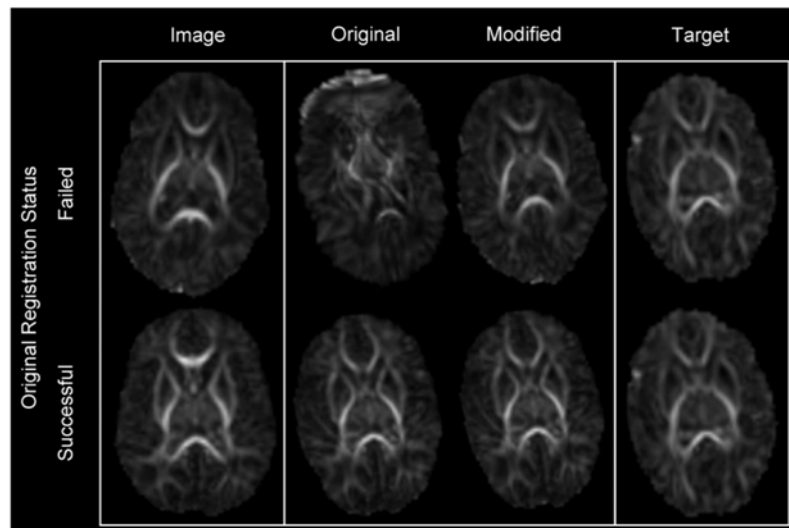


Fig. 2. Example registrations between source images (left) and target (right) using the original and modified registration protocols. The central panel shows both a failed and a successful registration before and after modification of the protocol.

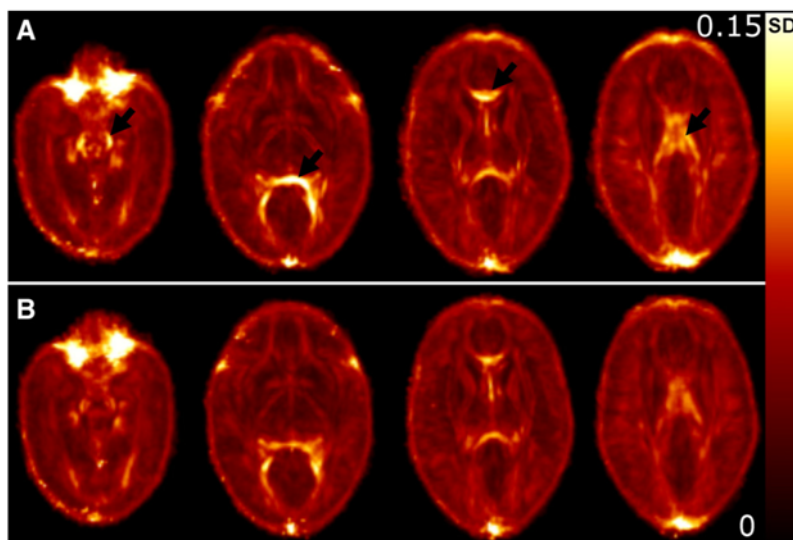


Fig. 4. Standard deviation in FA across the group following registration to an individual FA map (A) and the subsequent average FA map (B). Black arrowheads indicate where standard deviation was greater after registration to the individual map. Colour bar indicates SD.

prior to nonlinear registration, the target described with minimum mean warp displacement score is chosen as the most 'typical' image, the chosen target. The estimated transformations are then applied to each image to align them in the target space and an average FA map is created, the mean FA map. A second set of registrations is completed to register every individual FA map to the mean FA map. The aligned images are then used to create another mean FA map and a mean FA skeleton that are passed into voxelwise statistical analysis.

Investigating respiratory morbidity in preterm infants

Chronic lung disease

Using the modified TBSS protocol, we investigated the relationship between the need for prolonged respiratory support during the neonatal period and white matter microstructure. RD was significantly increased (A) and FA significantly decreased (B) in infants with CLD (FWE-corrected for multiple comparisons, $p < 0.05$), correcting for both gestational age and the postmenstrual age of the infant at scan (Fig. 7). Increases in AD failed to reach significance after correction for multiple comparisons. RD is significantly increased bilaterally in the

inferior longitudinal fasciculus (ILF), internal capsule and centrum semiovale and in the left external capsule and corpus callosum, including the genu and the splenium. Increased RD corresponds to regions of significantly decreased FA, seen in the ILF, left external capsule, centrum semiovale and corpus callosum. Mean RD and FA data were extracted from significant voxels and are shown in Table 1. On average RD was increased by 6.0% and FA decreased by 6.4% in infants with CLD.

Length of respiratory support

Fig. 8 shows regions where AD (A), RD (B) and FA (C) were linearly associated with the length of respiratory support received across the whole cohort (FWE-corrected for multiple comparisons, $p < 0.05$), after correcting for both the gestational age at birth and the age of the infant at scan. Increasing AD was found in the centrum semiovale, corpus callosum and internal and external capsules. Increases in RD appeared more widespread, incorporating most of the white matter skeleton and in many regions, surviving at a threshold of $p < 0.01$ corrected. Decreasing FA was observed across the skeleton and corresponded to regions of increasing RD and, to a lesser extent, increasing AD. To demonstrate these relationships, individual data were extracted from significant voxels in each statistic image and plotted in partial correlation plots showing the relationship between respiratory support and AD (D; $\beta = 0.67$, $r^2 = 0.23$), RD (E; $\beta = 0.55$, $r^2 = 0.20$) and FA (F; $\beta = -0.53$, $r^2 = 0.19$) after correcting for gestational age and age at scan.

Confounding variables: prematurity and age at imaging

Fig. 9 shows widespread linear associations between FA, RD and AD and the postmenstrual age of each infant at imaging (A) and increasing prematurity at birth (E, corrected for age at imaging). Within these regions, increasing postmenstrual age was significantly associated with increasing FA (B: $r = 0.67$, $p < 0.001$), decreasing RD (C: $r = -0.63$, $p < 0.001$) and decreasing AD (D: $r = -0.46$, $p < 0.001$). Decreased prematurity at birth was significantly associated with increased FA (partial correlation: F, $\beta = 0.50$, $p < 0.001$), decreased RD (G: $\beta = -0.43$, $p < 0.001$) and, to a lesser extent, decreased AD (H: $\beta = -0.24$, $p < 0.05$) at term-equivalent age after correction for postmenstrual age at imaging.

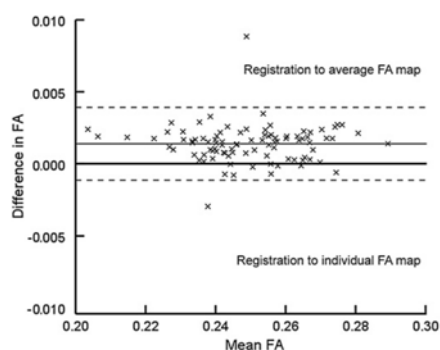


Fig. 5. Bland–Altman plot showing higher projected FA across the mean skeleton following registration to a mean FA map compared to registration to an individual FA map. Median difference in FA and 95% confidence intervals are shown with solid and dotted lines.

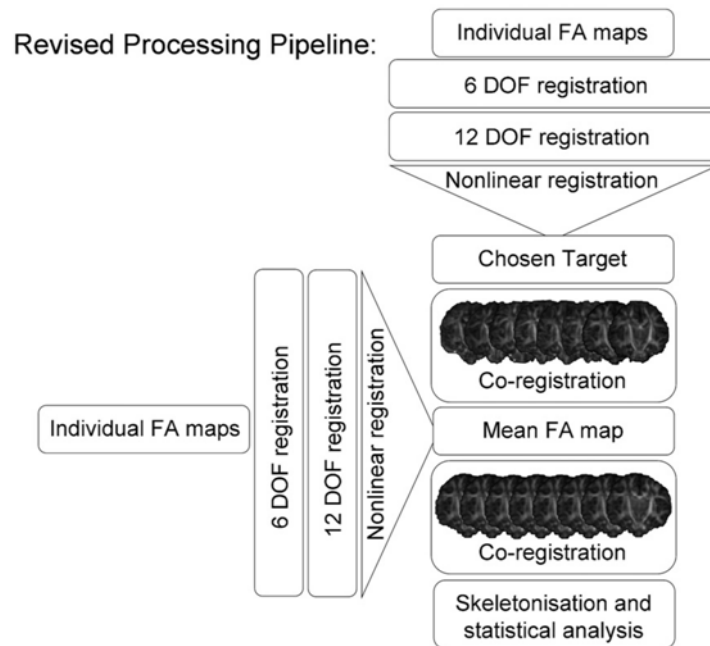


Fig. 6. Revised processing pipeline for use in TBSS analysis of neonatal diffusion data sets.

Discussion

We have demonstrated that, through modification of the existing TBSS pipeline, it is possible to reliably and precisely co-register neonatal DTI data. We have used this method to demonstrate a strong association between potentially modifiable respiratory morbidity and global alterations in white matter anisotropy and diffusivity in preterm infants.

The advantages of using TBSS for analysis of diffusion data are that it provides an objective, sensitive and clearly interpretable method for multi-subject, whole-brain diffusion data analysis. Central to the

method is the need for accurate spatial alignment of individual data sets through linear and nonlinear registration. Neonatal diffusion data sets are frequently of lower resolution compared with adult data and have relatively poor signal to noise. In addition there are large increases in brain volume and complexity during the neonatal period that present technical challenges for this process. We have shown that introducing an additional low DOF registration step prior to nonlinear registration improves global alignment between neonatal FA maps. This method requires minimal extra processing time, it does not require alterations to the default parameters of the nonlinear registration tool FNIRT, which has been optimised specifically for

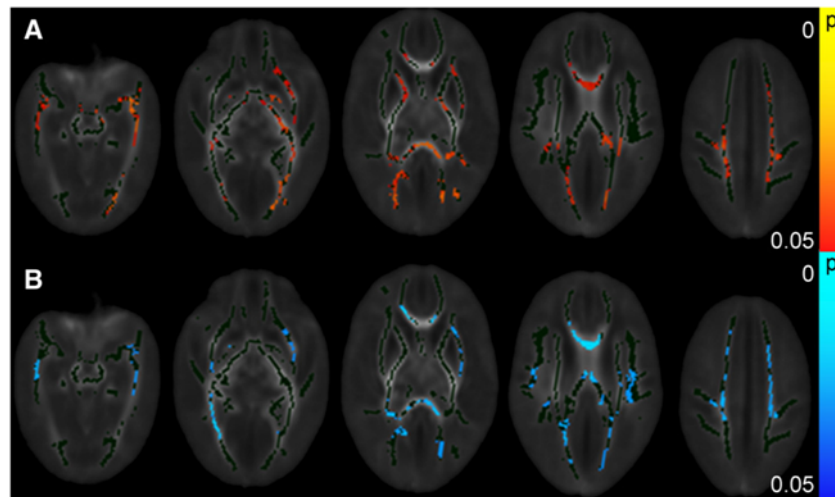


Fig. 7. Chronic lung disease is associated with significantly increased RD (A) and decreased FA (B) but not AD, independent of both gestational age at birth and postmenstrual age at scan. (FWE-corrected, $p < 0.05$; colour bars indicate p -value). The mean FA skeleton is shown in dark green.

Table 1
Mean RD and FA data extracted from voxels significantly associated with CLD, showing increased RD and decreased FA in infants with chronic lung disease, after correction for gestational age at birth and postmenstrual age at scan.

Group	n	RD		FA	
		Mean	SD	Mean	SD
Chronic lung disease	19	0.00124	0.00006	0.264	0.027
No chronic lung disease	74	0.00117	0.00008	0.282	0.019

DTI data, and does not adversely affect registrations that were successful using the default protocol.

Prior experience informs us that co-registration of neonatal FA maps can result in poorly aligned data sets that prevent meaningful statistical analysis and may result in individual data sets being removed from studies (Bassi et al., 2008). Using the modified protocol, registrations between FA maps were improved. By improving the

reliability of neonatal registration, we can remove the need to exclude data sets based solely on the inability to register them. To demonstrate, two FA maps proved particularly problematic for the registration procedure. Both of these were from plagiocephalic infants – a condition likely to have had an adverse outcome on image registration – and transformations between these maps and others were summarised by relatively large mean displacement scores (maximum = 9.03) using the optimised protocol. However, large displacements were not readily detected by visual inspection of the transformed images after registration to the chosen target for subsequent analysis. In addition, summarising the warps between individuals in this way (Figs. 1A and B) proved an excellent method to augment individual image inspection and detect possibly confounding anatomical features that may cause registration to fail.

The second modification required a second set of registrations between each individual FA map and the average FA map created from

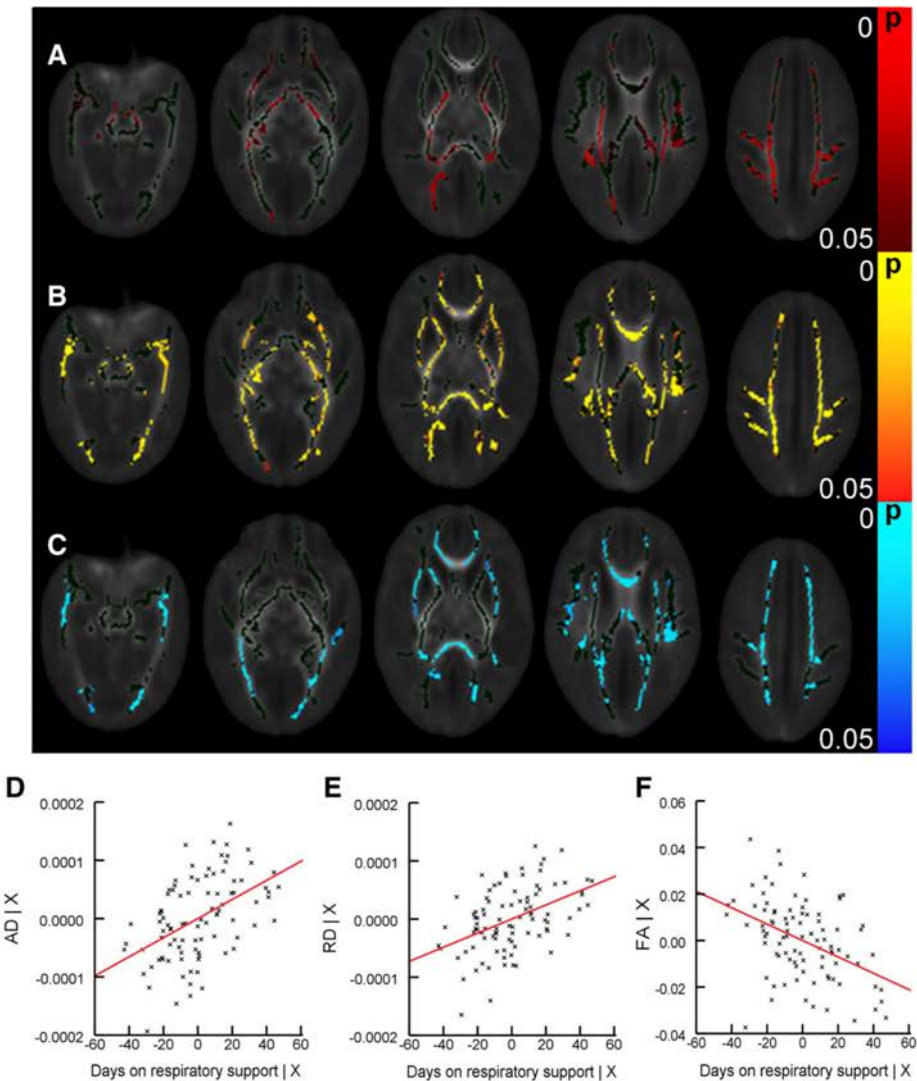


Fig. 8. Increased length of neonatal respiratory support is associated with increasing axial diffusivity (A) and radial diffusivity (B) and decreasing FA (C) in preterm infants, independent of gestational age at birth and postmenstrual age at scan (FWE-corrected, $p < 0.05$; colour bars indicate p -value). The mean FA skeleton is shown in dark green. Partial regression plots showing the linear relationship between respiratory support and AD (D), RD (E) and FA (F) in data extracted from significant voxels in A, B and C, corrected for gestational age at birth and postmenstrual age at scan. Key: AD | X = residuals of AD given the regression model; RD | X = residuals of RD given the model; FA | X = residuals of FA given the model; Days on respiratory support | X = residuals in length of respiratory support given the model.

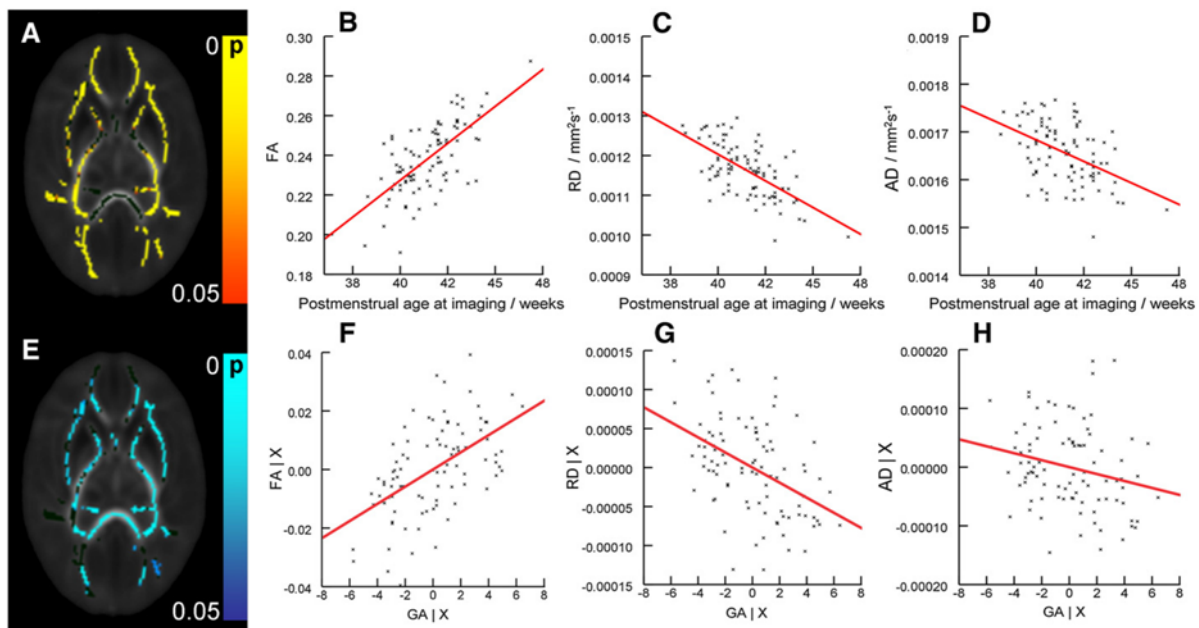


Fig. 9. Association between white matter microstructure, age at imaging and gestational age at birth. Panels A and E show, in a mid-axial slice, regions where increased FA was significantly associated with age at imaging (A) and length of gestation (E, corrected for age at imaging). FA, RD and AD within these regions are plotted in panels B, C and D (age at imaging) and F, G and H (gestational age), respectively. Images are FWE-corrected at $p < 0.05$ (colour bars indicate p -value). The mean FA skeleton is shown in both images in dark green. Key: FA | X = residuals of FA given the model; RD | X = residuals of RD given the model; AD | X = residuals of AD given the regression model; GA | X = residuals in length of gestation given the model.

the initial registrations to the chosen target. This was implemented to parallel a typical adult TBSS analysis, where individual FA maps are aligned to a standard space, population-based template. Although registration to the individual and average maps produced good and very similar mean FA maps and mean FA skeletons, there appeared to be greater variance in voxelwise FA after registration to the individual target, indicating that the co-registration of data was more variable. Subsequently, we demonstrated significantly higher projected FA from individual data sets onto the group skeleton after registration to the average target. The skeletonisation process within TBSS is designed to overcome some residual misalignment between subjects after the initial nonlinear registration (Smith et al., 2006), but this may signify that less precise registration to the individual FA map had an adverse effect on the subsequent data projection. As noted by Good et al. (2001), it is typically advantageous in structural MRI studies to use a population-specific target rather than a generic template or individual image. Indeed, the benefits of population-average targets in volumetric studies of paediatric cohorts have been well described elsewhere (Aljabar et al., 2008; Altaye et al., 2008; Wilke et al., 2008). We believe the present study is the first to demonstrate quantifiable improvements in DTI analysis through the use of an average, study-specific template in TBSS.

Although the increase in mean FA proved to be small and the computational time required for data processing was effectively doubled, we believe that this is an important step to incorporate for studies requiring a subject-specific target, particularly those involving paediatric or neonatal cohorts. TBSS is designed to project individual data from the centre of white matter tracts onto the mean skeleton and due to the nature of the relationship between FA and tissue microstructure, it is likely that the higher skeleton FA better represents the tract centre in these individuals (Basser and Pierpaoli, 1996).

The secondary aim of this study was to use the modified registration method to further investigate the association between white matter microstructural development and respiratory morbidity

in preterm neonates. We found that CLD was associated with increased RD and decreased FA and that a global pattern of altered AD, RD and FA was linearly associated with the length of respiratory support needed, even in the absence of CLD. Recently, TBSS has been used successfully to demonstrate the association between prematurity and chronic lung disease on fractional anisotropy in preterm infants (Anjari et al., 2007, 2009). Specifically, alterations in FA in the left inferior longitudinal fasciculus were observed in infants with CLD, independent of prematurity (Anjari et al., 2009). Here we have demonstrated widespread associations between increasing prematurity at birth and postmenstrual age at imaging and altered white matter microstructure at term-equivalent age. After regressing out these strong effects, we have demonstrated a more widespread association of CLD on both FA and RD incorporating not just the inferior longitudinal fasciculus bilaterally but also the corpus callosum and centrum semiovale. We propose that these observations are due to the refined registration method in the optimised protocol, a larger experimental cohort and to methods of statistical inference that do not rely on arbitrary cluster thresholding (Smith and Nichols, 2009).

Experimental evidence suggests that FA is primarily dependent on axonal thickness, density and myelination (Sakuma et al., 1991; Takagi et al., 2009). At term-equivalent age, within the telencephalon, only the posterior limb of the internal capsule displays histological evidence of myelination (Yakovlev and Lecours, 1967). Most regions with observed alterations in this study are likely to be at a stage of premyelination, characterised by various processes including axonal widening and packing and association with immature oligodendroglia (Jessen and Mirsky, 1991; Wimberger et al., 1995). Experimentally, the appearance and association of precursor oligodendroglia are enough to induce anisotropy in white matter in a process primarily driven by changes in radial diffusivity (Drobyshevsky et al., 2005). In a primate model of premature birth, prolonged exposure to ventilation is associated with adverse cerebral outcomes including reduced oligodendroglia number, volume loss and white matter injury,

regardless of the type of ventilation used (Loeliger et al., 2006), and we and others have found that CLD is a risk factor for global reductions in brain size at term-equivalent age (Boardman et al., 2007; Thompson et al., 2007). Our findings are consistent with clinical, imaging and experimental data that suggest an association between respiratory disease and abnormal brain development (Anjari et al., 2009; Chahboune et al., 2009; Short et al., 2003).

In conclusion, we have presented a modified TBSS protocol for improved reliability in the analysis of neonatal DTI data sets. Respiratory morbidity is a potentially modifiable factor that appears to be associated with adverse brain development in preterm infants.

Acknowledgments

We are grateful for support from the Imperial College Healthcare Comprehensive Biomedical Research Centre Funding Scheme, the Medical Research Council (UK), the Academy of Medical Sciences, The Health Foundation and the Philips Medical Systems for research grant support. We thank the families who took part in the study and our colleagues in the Neonatal Intensive Care Unit at Hammersmith Hospital.

References

- Aarnoudse-Moens, C.S., Weisglas-Kuperus, N., van Goudoever, J.B., Oosterlaan, J., 2009. Meta-analysis of neurobehavioral outcomes in very preterm and/or very low birth weight children. *Pediatrics* 124 (2), 717–728.
- Aljabar, P., Bhatia, K.K., Murgasova, M., Hajnal, J.V., Boardman, J.P., Srinivasan, L., Rutherford, M.A., Dyet, L.E., Edwards, A.D., Rueckert, D., 2008. Assessment of brain growth in early childhood using deformation-based morphometry. *NeuroImage* 39 (1), 348–358.
- Altaye, M., Holland, S.K., Wilke, M., Gaser, C., 2008. Infant brain probability templates for MRI segmentation and normalization. *NeuroImage* 43 (4), 721–730.
- Anjari, M., Srinivasan, L., Allsop, J.M., Hajnal, J.V., Rutherford, M.A., Edwards, A.D., Counsell, S.J., 2007. Diffusion tensor imaging with tract-based spatial statistics reveals local white matter abnormalities in preterm infants. *NeuroImage* 35 (3), 1021–1027.
- Anjari, M., Counsell, S.J., Srinivasan, L., Allsop, J.M., Hajnal, J.V., Rutherford, M.A., Edwards, A.D., 2009. The association of lung disease with cerebral white matter abnormalities in preterm infants. *Pediatrics* 124 (1), 268–276.
- Basser, P.J., Pierpaoli, C., 1996. Microstructural and physiological features of tissues elucidated by quantitative-diffusion-tensor MRI. *J. Magn. Reson. B* 111 (3), 209–219.
- Basser, P.J., Mattiello, J., LeBihan, D., 1994. Estimation of the effective self-diffusion tensor from the NMR spin echo. *J. Magn. Reson. B* 103 (3), 247–254.
- Bassi, L., Ricci, D., Volzone, A., Allsop, J.M., Srinivasan, L., Pai, A., Ribes, C., Ramenghi, L.A., Mercuri, E., Mosca, F., et al., 2008. Probabilistic diffusion tractography of the optic radiations and visual function in preterm infants at term equivalent age. *Brain* 131 (Pt 2), 573–582.
- Boardman, J.P., Counsell, S.J., Rueckert, D., Hajnal, J.V., Bhatia, K.K., Srinivasan, L., Kapellou, O., Aljabar, P., Dyet, L.E., Rutherford, M.A., et al., 2007. Early growth in brain volume is preserved in the majority of preterm infants. *Ann. Neurol.* 62 (2), 185–192.
- Chahboune, H., Ment, L.R., Stewart, W.B., Rothman, D.L., Vaccarino, F.M., Hyder, F., Schwartz, M.L., 2009. Hypoxic injury during neonatal development in murine brain: Correlation between in vivo DTI findings and behavioral assessment. *Cereb. Cortex* 19 (12), 2891–2901.
- Cheong, J.L., Thompson, D.K., Wang, H.X., Hunt, R.W., Anderson, P.J., Inder, T.E., Doyle, L.W., 2009. Abnormal white matter signal on MR imaging is related to abnormal tissue microstructure. *AJNR. Am. J. Neuroradiol.* 30 (3), 623–628.
- Counsell, S.J., Shen, Y., Boardman, J.P., Larkman, D.J., Kapellou, O., Ward, P., Allsop, J.M., Cowan, F.M., Hajnal, J.V., Edwards, A.D., et al., 2006. Axial and radial diffusivity in preterm infants who have diffuse white matter changes on magnetic resonance imaging at term-equivalent age. *Pediatrics* 117 (2), 376–386.
- Counsell, S.J., Edwards, A.D., Chew, A.T., Anjari, M., Dyet, L.E., Srinivasan, L., Boardman, J.P., Allsop, J.M., Hajnal, J.V., Rutherford, M.A., et al., 2008. Specific relations between neurodevelopmental abilities and white matter microstructure in children born preterm. *Brain* 131 (Pt 12), 3201–3208.
- Delobel-Ayoub, M., Arnaud, C., White-Koning, M., Casper, C., Pierrat, V., Garel, M., Burguet, A., Roze, J.C., Matis, J., Picaud, J.C., et al., 2009. Behavioral problems and cognitive performance at 5 years of age after very preterm birth: the EPIPAGE study. *Pediatrics* 123 (6), 1485–1492.
- Drobyshevsky, A., Song, S.K., Gamkrelidze, G., Wyrciw, A.M., Derrick, M., Meng, F., Li, L., Ji, X., Trommer, B., Beardsley, D.J., et al., 2005. Developmental changes in diffusion anisotropy coincide with immature oligodendrocyte progression and maturation of compound action potential. *J. Neurosci.* 25 (25), 5988–5997.
- Good, C.D., Johnsrude, I.S., Ashburner, J., Henson, R.N., Friston, K.J., Frackowiak, R.S., 2001. A voxel-based morphometric study of ageing in 465 normal adult human brains. *NeuroImage* 14 (1 Pt 1), 21–36.
- Hansen, B.M., Hoff, B., Uldall, P., Greisen, G., Kamper, J., Djernes, B., Hertel, J., Christensen, M.F., Andersen, E., Lillquist, K., et al., 2004. Perinatal risk factors of adverse outcome in very preterm children: A role of initial treatment of respiratory insufficiency? *Acta Paediatr.* 93 (2), 185–189.
- Hille, E.T., Weisglas-Kuperus, N., van Goudoever, J.B., Jacobus, G.W., Ens-Dokkum, M. H., de Groot, L., Wit, J.M., Geven, W.B., Kok, J.H., de Kleine, M.J., et al., 2007. Functional outcomes and participation in young adulthood for very preterm and very low birth weight infants: The Dutch project on preterm and small for gestational age infants at 19 years of age. *Pediatrics* 120 (3), e587–e595.
- Huppi, P.S., Maier, S.E., Peled, S., Zientara, G.P., Barnes, P.D., Jolesz, F.A., Volpe, J.J., 1998. Microstructural development of human newborn cerebral white matter assessed in vivo by diffusion tensor magnetic resonance imaging. *Pediatr. Res.* 44 (4), 584–590.
- Jessen, K.R., Mirsky, R., 1991. Schwann cell precursors and their development. *Glia* 4 (2), 185–194.
- Kaukola, T., Perhoma, M., Vainionpää, L., Tolonen, U., Jauhainen, J., Paakko, E., Hallman, M., 2009. Apparent diffusion coefficient on magnetic resonance imaging in pons and in corona radiata and relation with the neurophysiologic measurement and the outcome in very preterm infants. *Neonatology* 97 (1), 15–21.
- Krishnan, M.L., Dyet, L.E., Boardman, J.P., Kapellou, O., Allsop, J.M., Cowan, F., Edwards, A.D., Rutherford, M.A., Counsell, S.J., 2007. Relationship between white matter apparent diffusion coefficients in preterm infants at term-equivalent age and developmental outcome at 2 years. *Pediatrics* 120 (3), e604–e609.
- Loeliger, M., Inder, T., Cain, S., Ramesh, R.C., Camm, E., Thomson, M.A., Coalson, J., Rees, S.M., 2006. Cerebral outcomes in a preterm baboon model of early versus delayed nasal continuous positive airway pressure. *Pediatrics* 118 (4), 1640–1653.
- Marlow, N., Wolke, D., Bracewell, M.A., Samara, M., EPIPAGE Study Group, 2005. Neurologic and developmental disability at six years of age after extremely preterm birth. *N. Engl. J. Med.* 352 (1), 9–19.
- Miller, S.P., Vigneron, D.B., Henry, R.G., Bohland, M.A., Ceppi-Cozzio, C., Hoffman, C., Newton, N., Partridge, J.C., Ferriero, D.M., Barkovich, A.J., 2002. Serial quantitative diffusion tensor MRI of the premature brain: Development in newborns with and without injury. *J. Magn. Reson. Imaging* 16 (6), 621–632.
- Partridge, S.C., Mukherjee, P., Henry, R.G., Miller, S.P., Berman, J.I., Jin, H., Lu, Y., Glenn, O. A., Ferriero, D.M., Barkovich, A.J., et al., 2004. Diffusion tensor imaging: serial quantitation of white matter tract maturity in premature newborns. *NeuroImage* 22 (3), 1302–1314.
- Rushe, T.M., Rifkin, L., Stewart, A.L., Townsend, J.P., Roth, S.C., Wyatt, J.S., Murray, R.M., 2001. Neuropsychological outcome at adolescence of very preterm birth and its relation to brain structure. *Dev. Med. Child Neurol.* 43 (4), 226–233.
- Sakuma, H., Nomura, Y., Takeda, K., Tagami, T., Nakagawa, T., Tamagawa, Y., Ishii, Y., Tsukamoto, T., 1991. Adult and neonatal human brain: diffusional anisotropy and myelination with diffusion-weighted MR imaging. *Radiology* 180 (1), 229–233.
- Short, E.J., Klein, N.K., Lewis, B.A., Fulton, S., Eisengart, S., Kercmar, C., Baley, J., Singer, L. T., 2003. Cognitive and academic consequences of bronchopulmonary dysplasia and very low birth weight: 8-year-old outcomes. *Pediatrics* 112 (5), e359.
- Smith, S.M., Nichols, T.E., 2009. Threshold-free cluster enhancement: addressing problems of smoothing, threshold dependence and localisation in cluster inference. *NeuroImage* 44 (1), 83–98.
- Smith, S.M., Jenkinson, M., Woolrich, M.W., Beckmann, C.F., Behrens, T.E., Johansen-Berg, H., Bannister, P.R., De Luca, M., Drobnjak, I., Flitney, D.E., et al., 2004. Advances in functional and structural MR image analysis and implementation as FSL. *NeuroImage* 23 (Suppl 1), S208–S219.
- Smith, S.M., Jenkinson, M., Johansen-Berg, H., Rueckert, D., Nichols, T.E., Mackay, C.E., Watkins, K.E., Ciccarelli, O., Cader, M.Z., Matthews, P.M., et al., 2006. Tract-based spatial statistics: voxelwise analysis of multi-subject diffusion data. *NeuroImage* 31 (4), 1487–1505.
- Song, S.K., Yoshino, J., Le, T.Q., Lin, S.J., Sun, S.W., Cross, A.H., Armstrong, R.C., 2005. Demyelination increases radial diffusivity in corpus callosum of mouse brain. *NeuroImage* 26 (1), 132–140.
- Takagi, T., Nakamura, M., Yamada, M., Hikishima, K., Momoshima, S., Fujiyoshi, K., Shibata, S., Okano, H.J., Toyama, Y., Okano, H., 2009. Visualization of peripheral nerve degeneration and regeneration: Monitoring with diffusion tensor tractography. *NeuroImage* 44 (3), 884–892.
- Thompson, D.K., Warfield, S.K., Carlin, J.B., Pavlovic, M., Wang, H.X., Bear, M., Kean, M.J., Doyle, L.W., Egan, G.F., Inder, T.E., 2007. Perinatal risk factors altering regional brain structure in the preterm infant. *Brain* 130 (Pt 3), 667–677.
- Wang, S., Wu, E.X., Cai, K., Lau, H.F., Cheung, P.T., Khong, P.L., 2009. Mild hypoxic-ischemic injury in the neonatal rat brain: longitudinal evaluation of white matter using diffusion tensor MR imaging. *AJNR. Am. J. Neuroradiol.* 30 (10), 1907–1913.
- Westby Wold, S.H., Sommerfelt, K., Reigstad, H., Ronnestad, A., Medbo, S., Farstad, T., Kaarens, P.L., Stoen, R., Lervens, K.T., Irgens, L.M., et al., 2009. Neonatal mortality and morbidity in extremely preterm small for gestational age infants: a population based study. *Arch. Dis. Child. Fetal Neonatal Ed.* 94 (5), F363–F367.
- Wilke, M., Holland, S.K., Altaye, M., Gaser, C., 2008. Template-O-matic: a toolbox for creating customized pediatric templates. *NeuroImage* 41 (3), 903–913.
- Wimberger, D.M., Roberts, T.P., Barkovich, A.J., Prayer, L.M., Moseley, M.E., Kucharczyk, J., 1995. Identification of “premyelination” by diffusion-weighted MRI. *J. Comput. Assist. Tomogr.* 19 (1), 28–33.
- Yakovlev, P.L., Lecours, A.R., 1967. The myelogenetic cycles of regional maturation of the brain. In: Minkowski, A. (Ed.), *Regional Development of the Brain in Early Life*. Blackwell, Oxford, pp. 3–69.

Appendix D

The Effect of Preterm Birth on Thalamic and Cortical Development

Ball, G., Boardman, J.P., Rueckert, D., Aljabar, P., Arichi, T., Merchant, N., Gousias, I.S., Edwards, A.D. & Counsell, S.J.

Cerebral Cortex (2011). DOI:10.1093/cercor/bhr0176

The Effect of Preterm Birth on Thalamic and Cortical Development

Gareth Ball¹, James P. Boardman^{1,2}, Daniel Rueckert³, Paul Aljabar³, Tomoki Arichi^{1,4}, Nazakat Merchant^{1,4}, Ioannis S. Gousias¹, A. David Edwards^{1,4} and Serena J. Counsell¹

¹Centre for the Developing Brain, Imperial College London and MRC Clinical Sciences Centre, Hammersmith Hospital, London W12 0NN, UK, ²Simpson Centre for Reproductive Health, Royal Infirmary of Edinburgh, Edinburgh EH16 4SA, UK, ³Biomedical Image Analysis Group, Department of Computing, Imperial College London, London SW7 2AZ, UK and ⁴Division of Neonatology, Imperial College Healthcare NHS Trust, London W12 0HS, UK

Address correspondence to Serena J. Counsell, Robert Steiner MR Unit, Imaging Sciences Department, Imperial College London, Hammersmith Hospital, DuCane Road, London W12 0HS, UK. Email: serena.counsell@imperial.ac.uk

Preterm birth is a leading cause of cognitive impairment in childhood and is associated with cerebral gray and white matter abnormalities. Using multimodal image analysis, we tested the hypothesis that altered thalamic development is an important component of preterm brain injury and is associated with other macro- and microstructural alterations. T_1 - and T_2 -weighted magnetic resonance images and 15-direction diffusion tensor images were acquired from 71 preterm infants at term-equivalent age. Deformation-based morphometry, Tract-Based Spatial Statistics, and tissue segmentation were combined for a nonsubjective whole-brain survey of the effect of prematurity on regional tissue volume and microstructure. Increasing prematurity was related to volume reduction in the thalamus, hippocampus, orbitofrontal lobe, posterior cingulate cortex, and centrum semiovale. After controlling for prematurity, reduced thalamic volume predicted: lower cortical volume; decreased volume in frontal and temporal lobes, including hippocampus, and to a lesser extent, parietal and occipital lobes; and reduced fractional anisotropy in the corticospinal tracts and corpus callosum. In the thalamus, reduced volume was associated with increased diffusivity. This demonstrates a significant effect of prematurity on thalamic development that is related to abnormalities in allied brain structures. This suggests that preterm delivery disrupts specific aspects of cerebral development, such as the thalamocortical system.

Keywords: brain development, deformation-based morphometry, DTI, cortex, TBSS, thalamus

Introduction

Preterm birth is rapidly emerging as a leading cause of neurodevelopmental impairment in childhood. With advances in neonatal intensive care, mortality has decreased considerably but there is a high prevalence of cognitive and behavioral deficits in up to 50% of surviving preterm infants in childhood (Marlow et al. 2005; Delobel-Ayoub et al. 2009). Understanding the neural substrates for impairment in this population is essential for designing mechanistic and therapeutic studies and may provide further insight into the development of systems that underlie human cognition.

Evidence from in vivo magnetic resonance imaging (MRI) studies has identified a number of cerebral abnormalities in preterm populations thought to reflect disturbances of key developmental processes during the neonatal period. The incidence of severe pathology such as periventricular leukomalacia (PVL) has declined (Horbar et al. 2002; Wilson-Costello et al. 2007); however, diffuse white matter changes in the

absence of more obvious focal lesions are now the most common abnormality detected by conventional MR imaging. Diffusion tensor imaging (DTI) has revealed diffuse microstructural disturbances in the developing white matter that are dependent on the degree of prematurity at birth and correlated to short-term measures of neurodevelopmental outcome (Huppi et al. 1998; Counsell et al. 2006; Anjari et al. 2007; Krishnan et al. 2007; Ball et al. 2010). In addition, early systemic illness, in the form of chronic lung disease (CLD), has been shown to further exacerbate these alterations and impact negatively on outcome (Short et al. 2003; Anjari et al. 2007; Ball et al. 2010).

Morphometric MR studies have identified cortical disturbances developing before term-equivalent age (Ajayi-Obe et al. 2000; Inder et al. 2005; Kapellou et al. 2006), and widespread cerebral tissue loss is common in the presence of PVL and characterized pathologically by neuronal loss and gliosis (Inder et al. 2005; Pierson et al. 2007; Thompson et al. 2007; Ligam et al. 2009). These observations support the concept of an “encephalopathy of prematurity,” a complex of white and gray matter abnormalities that includes disruptions to the thalamocortical system with linked disturbances in the development and function of thalamic nuclei, topographically related cortical regions and connecting white matter tracts (Volpe 2009).

Indeed, even in the absence of severe focal white matter pathology, the subcortical gray matter and, in particular, the thalamus appears specifically vulnerable following preterm birth (Boardman et al. 2006; Srinivasan et al. 2007). Volumetric deficits in the thalamus also appear to be dependent on prematurity at birth and associated with poor functional outcome (Inder et al. 2005; Boardman et al. 2010). Transient developmental processes that underlie thalamocortical connectivity occur during a critical window for vulnerability following preterm birth and disruption of these processes may result in complex cerebral abnormalities (Allendoerfer and Shatz 1994; Volpe 2009; Kostovic and Judas 2010). Here, we examine the thalamocortical system of preterm infants at term-equivalent age, testing the hypothesis that tissue loss in the thalamus is associated with changes in the associated cortical gray matter and macro- and microstructural alterations in the cerebral white matter containing thalamocortical tracts.

Materials and Methods

Ethical permission for this study was granted by the Hammersmith and Queen Charlotte's and Chelsea Hospital (QCH) Research Ethics Committee. Written parental consent was obtained for each infant.

© The Authors 2011. Published by Oxford University Press.

This is an Open Access article distributed under the terms of the Creative Commons Attribution Non-Commercial License (<http://creativecommons.org/licenses/by-nc/2.5>), which permits unrestricted non-commercial use, distribution, and reproduction in any medium, provided the original work is properly cited.

Subjects

Infants were recruited from the Neonatal Intensive Care Unit at QCCH. All infants born at less than 36 weeks gestational age (as defined by the last menstrual period) between March 2005 and October 2008 who successfully underwent T_1 - and T_2 -weighted MRI and 15-direction DTI acquisition at term-equivalent age were eligible for inclusion. Infants were excluded if cystic PVL or haemorrhagic parenchymal infarction was apparent on the term-equivalent MRI. Forty-eight infants (67.6%) had evidence of diffuse and excessive high signal intensity (DEHSI) on T_2 -weighted scans; 8 infants (11.3%) had evidence of punctuate white matter lesions.

Seventy-four preterm infants (42 male) underwent successful imaging; 3 infants were removed prior to statistical analysis due to unsatisfactory alignment to the reference template. The final cohort of 71 did not differ from the original cohort in gestational age, age at scan, birth weight, or gender. The final cohort (41 male) had a median gestational age of $28 + 5$ (range: $23 + 4$ to $35 + 2$) weeks, a median postmenstrual age at scan of $41 + 5$ ($38 + 1$ to $44 + 4$) weeks and median birth weight of 1.11 (0.63–2.87) kg. No infants received postnatal steroids. Across the whole cohort, the median (range) time spent receiving any form of respiratory support was 17 (0–116) days. Fifteen infants had CLD, defined by the need for respiratory support at 36 weeks postmenstrual age. All infants were included in a previously reported study optimizing Tract-Based Spatial Statistics (TBSS) for neonates and examining the effects of prematurity and CLD (Ball et al. 2010).

Imaging

MRI was performed on a Philips 3 T system (Philips Medical Systems, Netherlands) using an 8-channel phased array head coil. T_1 -weighted MRI was acquired using: repetition time (TR): 17 ms; echo time (TE): 4.6 ms; flip angle 13° ; slice thickness: 1.6 mm; field of view: 210 mm; matrix: 256×256 (voxel size: $0.82 \times 0.82 \times 0.8$ mm). T_2 -weighted fast-spin echo MRI was acquired using: TR: 8670 ms; TE: 160 ms; flip angle 90° ; slice thickness 2 mm; field of view: 220 mm; matrix: 256×256 (voxel size: $0.86 \times 0.86 \times 1$ mm). Single-shot echo planar DTI was acquired in 15 noncollinear directions (TR: 8000 ms; TE: 49 ms; slice thickness: 2 mm; field of view: 224 mm; matrix: 128×128 (voxel size: $1.75 \times 1.75 \times 2$ mm); b value: 750 s/mm²; SENSE factor of 2). All examinations were supervised by a pediatrician experienced in MRI procedures. Infants were sedated with oral chloral hydrate (25–50 mg/kg) prior to scanning and pulse oximetry, temperature and electrocardiography data were monitored throughout. Ear protection was used for each infant, comprising earplugs molded from a silicone-based putty (President Putty, Coltene Whaledent, Mahwah, NJ) placed in the external ear and neonatal earmuffs (MiniMuffs, Natus Medical Inc., San Carlos, CA).

Data Analysis

Thalamic Segmentation

The manual placement of regions of interest (ROI) on individual MR images can be subjective and manually intensive and does not easily allow for comparisons across large groups. To avoid this, a single bilateral thalamic mask was manually drawn on the final reference template according to anatomical borders previously described (Srinivasan et al. 2007) (Fig. 1B; for details of template construction, see Deformation-Based Morphometry). The high spatial correspondence between each T_1 image and the reference template following nonlinear registration precluded the need to manually place thalamic masks on individual T_1 images. Individual thalamic volume could be estimated by scaling the reference mask volume by the mean Jacobian determinant (a voxelwise measure of volume change between each image and the template, described below) calculated within the mask. To validate, manual thalamic segmentation was performed on T_1 images from 10 randomly selected infants, thalamic volumes measured manually and volumes estimated from the mean Jacobian were consistent (mean difference and limits of agreement = 0.29 ± 1.43 ; intraclass coefficient = 0.89, $P < 0.001$).

Cortical Segmentation

Cortical segmentation was performed on individual T_2 images using methods specifically optimized for neonatal tissue segmentation (for an example segmentation, see Fig. 1C). Images were initially segmented using an expectation-maximization segmentation method driven by age-specific coregistered tissue probability priors obtained from a 4D probabilistic neonatal atlas (Kuklisova-Murgasova et al. 2011). In addition, an automatic 3-step segmentation algorithm was used to remove mislabeled partial volume voxels at the interface of the gray matter and cerebrospinal fluid (Xue et al. 2007).

Deformation-Based Morphometry

Deformation based morphometry (DBM) does not require tissue segmentation or classification and can be used to localize regional variations in tissue volume. The key step is to achieve precise spatial correspondence between each subject's image and a reference template through image registration. The output of each registration is a 3D deformation field representing transformations between each image and the final template. Voxelwise volume change induced by the transformation between each image and the template can be characterized by the determinant of the Jacobian operator applied to the transformation at any given point in the template space, referred to here as the Jacobian. Statistical groupwise analysis of the Jacobian reveals structural volume relative to the group template in an objective voxelwise manner (Ashburner et al. 1998; Rueckert et al. 2003).

After bias correction (FMRIB's Automated Segmentation Tool; FAST v4.1), each MR image was aligned to a chosen target image (gestational age = $28 + 5$ weeks; postmenstrual age at scan = $42 + 0$ weeks) using linear registration. A reference template was created by taking an intensity average of the aligned images. Each MR image was then aligned to the reference template using a high dimensional registration algorithm based on cubic B-splines (Rueckert et al. 1999, 2003) and averaged to form a second reference template. The nonlinear registration was carried out with successive control point spacing of 20, 10, 5, and 2.5 mm using normalised mutual information as the similarity metric and the bending energy of the deformation as the smoothness penalty (Gousias et al. 2010). A final set of registrations were performed with the second reference template as the target (Fig. 2). A qualitative evaluation of the alignment accuracy of the transformed images with the template was made before individual deformation fields were used to calculate volume changes. The average intensity template generated from the final set of registrations is shown in Figure 1A.

Voxelwise cross-subject statistical analysis of volume relative to the template, represented by the Jacobian, was performed with Randomise (v2.5) as implemented in FMRIB's Software Library (Smith et al. 2004) (FSL v4.1; www.fmrib.ox.ac.uk/fsl). All statistical images were subject to false discovery rate (FDR) correction for multiple comparisons.

Tract-Based Spatial Statistics

DTI analysis was performed using FMRIB's Diffusion Toolbox (FDT v2.0) and Tract-Based Spatial Statistics (Smith et al. 2006) (TBSS v1.2). From each data set, the tensor eigenvalues, λ_1 , λ_2 , and λ_3 , describing the diffusion strength in the primary, secondary, and tertiary diffusion directions, and fractional anisotropy maps were calculated. Individual fractional anisotropy (FA) maps were aligned into a common reference space and a mean FA skeleton, representing the center of all white matter tracts common to the group, was generated using a method optimized for neonatal DTI analysis (Ball et al. 2010). The calculated values of FA, axial diffusivity—the magnitude of λ_1 —and radial diffusivity—the mean magnitude of λ_2 and λ_3 —were then projected onto this skeleton. Nonparametric permutation-based statistical analysis was performed with Randomise; all diffusion statistics were subject to familywise error (FWE) correction for multiple comparisons following threshold-free cluster enhancement (Smith and Nichols 2009) and are shown at $P < 0.05$.

Statistical Analysis

Further statistical analysis with multiple linear regression was performed with SPSS 17.0 (SPSS Inc., Chicago, IL). In addition to explanatory variables of interest, gestational age at birth, postmenstrual

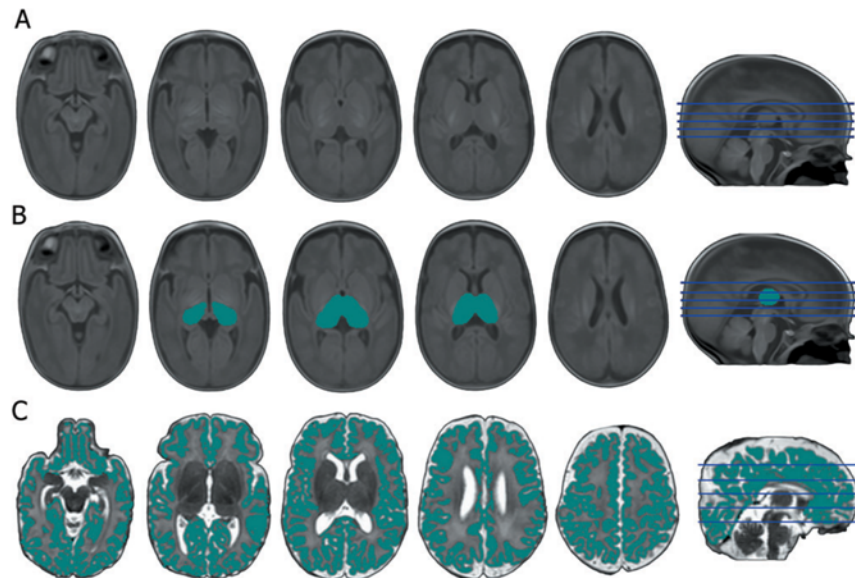


Figure 1. Final reference template and thalamic and cortical segmentations. The final average intensity template is shown in (A), the clarity of the subcortical structures and cortical differentiation indicates the accurate alignment of individual images. The mean Jacobian determinant within the mask shown in (B) represents the relative volume change between the template and each image and was used to represent thalamic volume across the cohort. A representative example of cortical gray matter segmentation is shown in (C).

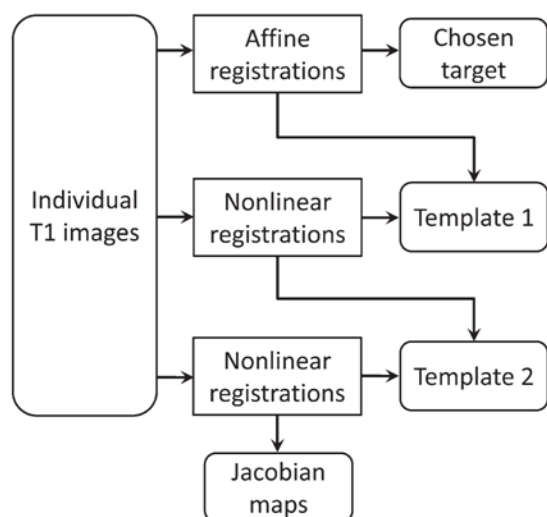


Figure 2. DBM processing pipeline. After preprocessing, T_1 images are affinely aligned to an arbitrarily chosen target MR image and averaged to produce a reference template. Two subsequent iterations of nonlinear registration and template construction produce the final transformations used for analysis.

age at scan, CLD status, and total brain volume were entered into the regression models where stated, partial r values are reported.

Results

Regional Brain Volume and Prematurity at Birth

Mean total cortical gray matter volume was 158 (\pm 26.6) ml. Both cortical gray matter volume and mean thalamic Jacobian (representing thalamic volume) were significantly associated

with gestational age at birth, entered into the regression model with the age of each infant at scan (cortical volume: partial r = 0.37, P = 0.002; thalamic: partial r = 0.40, P = 0.001; Fig. 3).

DBM was used to locate other brain regions where tissue volume was associated with degree of prematurity at birth. Linear regression revealed significant localized associations between tissue volume (represented voxelwise by the Jacobian) and gestational age at birth (Fig. 4; FDR-corrected for multiple comparisons at P < 0.01; minimum t -statistic = 2.98). Increasing prematurity was associated with a bilateral pattern of reduced volume present at term-equivalent age and encompassing the anterior temporal lobes, including the hippocampus, the orbitofrontal lobe, and posterior cingulate cortex and extending into the centrum semiovale. Within the deep gray matter, the relationship was most prominent in the thalamus. In addition, discrete clusters were observed in the midbrain and cerebellum. DBM also revealed that increasing prematurity was associated with increasing extra-cerebral CSF, but this did not pass correction for multiple comparisons.

Thalamocortical Development after Preterm Birth

Cortical volume was significantly associated with mean thalamic Jacobian, entered into the regression model with total brain tissue volume (partial r = 0.32, P = 0.007; Fig. 3C). This association remained significant when also including gestational age at birth (partial r = 0.31, P = 0.009).

After correcting for the effects of prematurity and removing volume change due to individual differences in global brain scaling, DBM revealed significant volumetric covariance between the thalamus and subcortical cerebral tissue (Fig. 5; FDR-corrected P < 0.001, minimum t -statistic = 3.25). A bilateral pattern was observed comprising white and gray matter proximal to the thalamus and extending into the frontal and temporal lobes, including the hippocampus, through the centrum semiovale into the parietal lobe and, to a lesser

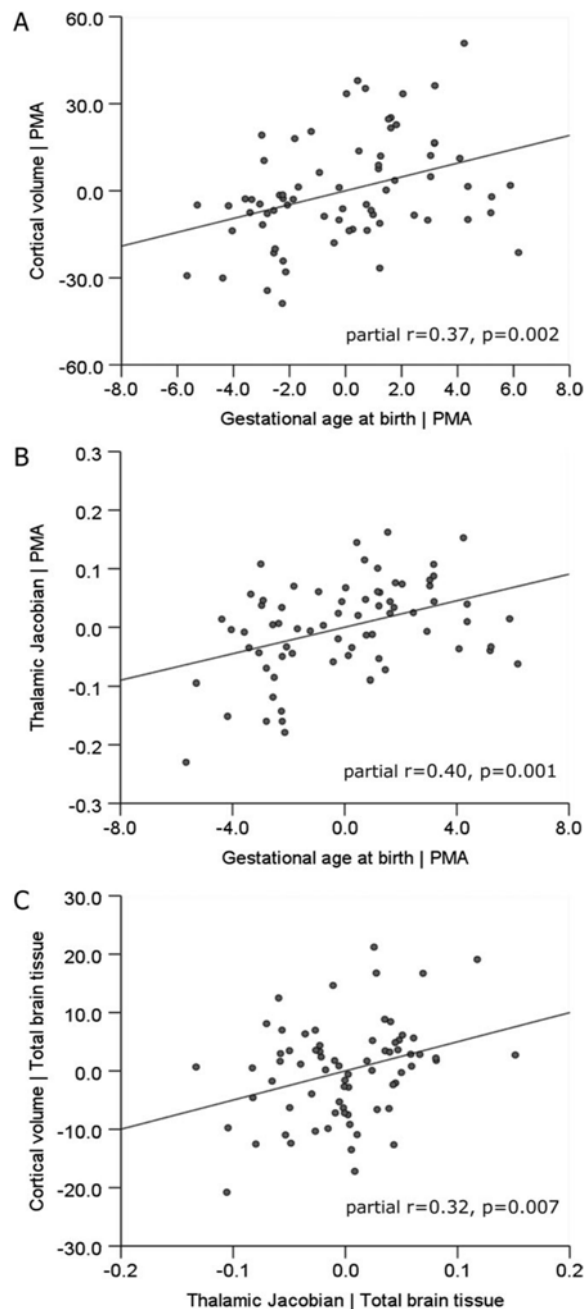


Figure 3. Cortical gray matter volume is correlated with prematurity at birth and thalamic volume at term-equivalent age. Partial regression plots show significant associations between cortical gray matter volume and gestational age at birth (A) and mean thalamic Jacobian (representing thalamic volume) and gestational age (B), after correction of each measure for the postmenstrual age at scan (PMA) of each infant. Shown in (C) is the significant association between cortical volume and thalamic Jacobian, after correction of each for total cerebral tissue volume.

extent, into periventricular white matter in the occipital lobes. This pattern remained highly significant when also covarying for total cortical volume (Supplementary Fig. 1).

In addition to the observed structural associations, TBSS was used to identify where white matter microstructure was associated with thalamic and cortical volume. Increasing thalamic volume at term-equivalent age was significantly associated with FA in the posterior limb of the internal capsule and corpus callosum (including the splenium) after correction for degree of prematurity at birth and the age of each infant when scanned (FWE-corrected for multiple comparison, $P < 0.05$; Fig. 6). Within these regions, linear regression showed that decreasing thalamic volume was independently associated with increasing radial diffusivity (partial $r = -0.34$, $P = 0.004$) but not with axial diffusivity (partial $r = 0.008$) when entered into a model with gestational age at birth and age at scan.

Cortical volume was significantly associated with FA in the posterior corpus callosum after correction for degree of prematurity at birth and age at scan ($P < 0.05$, Fig. 7). In these regions, only radial diffusivity was significantly associated with cortical volume (partial $r = -0.29$, $P = 0.014$; axial diffusivity: partial $r = 0.15$, $P = 0.21$) independent of gestational age and age at scan. Both thalamic and cortical associations remained significant when also correcting for CLD status (Supplementary Fig. 2; CLD defined as requiring respiratory support at 36 weeks postmenstrual age). To investigate the interaction of thalamic and cortical associations with white matter microstructure, a secondary ROI analysis was performed. FA values were extracted from masks in the posterior limb of the internal capsule and posterior corpus callosum (Supplementary Fig. 3). In the internal capsule, FA was significantly associated with thalamic (partial $r = 0.35$, $P = 0.003$) but not cortical volume (partial $r = -0.13$, $P = 0.29$) when both metrics were entered into linear regression alongside gestational age and age at scan (Supplementary Fig. 3A). Conversely, FA in the posterior corpus callosum was significantly associated with cortical volume (partial $r = 0.26$, $P = 0.034$) but not with thalamic volume (partial $r = 0.07$, $P = 0.36$; Supplementary Fig. 3B).

Finally, to determine how reduced thalamic volume is reflected by the underlying tissue microstructure, mean diffusivity (mean magnitude of λ_1 , λ_2 , and λ_3) was extracted from each infant's DTI using a thalamic mask transformed onto the DTI reference template. Linear regression revealed that smaller thalamic volume was associated with increased mean thalamic diffusivity when entered into a model with gestational age at birth, total brain volume, and cortical volume (Fig. 8; partial $r = -0.395$, $P = 0.001$). TBSS analysis revealed that thalamic diffusivity was significantly associated with FA in the internal capsule, after correction for degree of prematurity, age at scan, cortical volume, and CLD status (Fig. 8B; FWE-corrected $P < 0.05$).

Discussion

These data showed a significant effect of prematurity on thalamic volume related to specific abnormalities in allied brain structures. The effects of prematurity were far-reaching, with reductions in the volume of thalamus, hippocampus, orbito-frontal lobe, posterior cingulate cortex, and centrum semiovale that suggest preterm delivery disrupts specific aspects of cerebral development. However, after this general effect was accounted for, a pattern of structural covariance was observed between the thalamus and particular brain structures, notably in frontotemporal regions, cingulate gyrus, and hippocampus. The observed relation between reduced thalamic and total

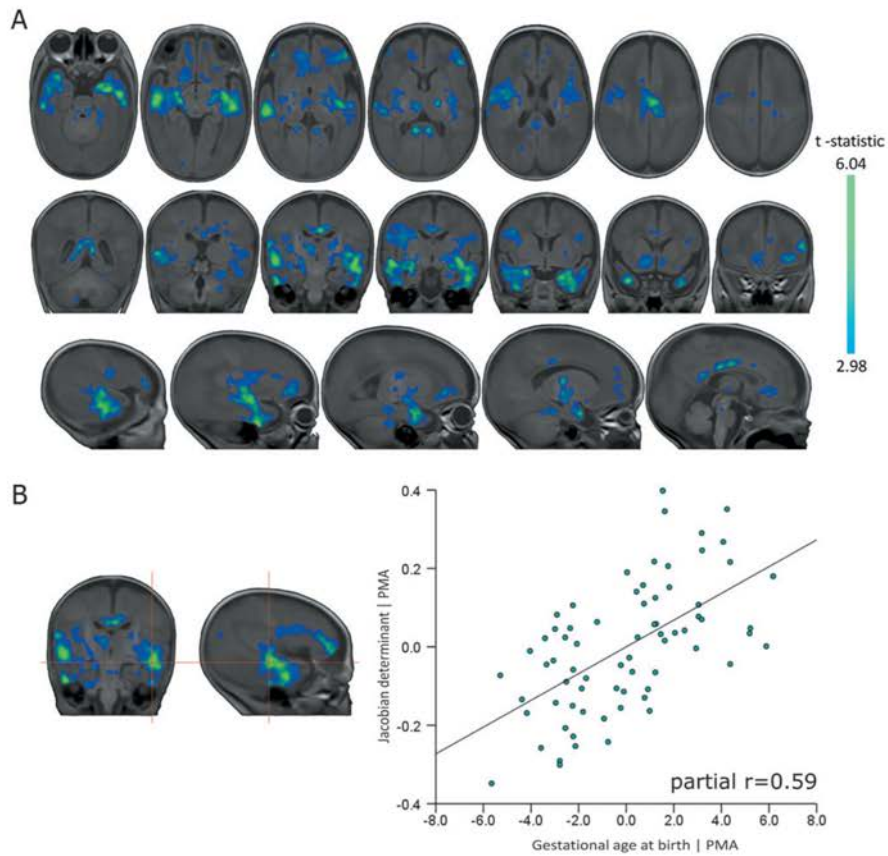


Figure 4. Regional associations between brain tissue volume and prematurity at birth. Regions where tissue volume is significantly associated with gestational age at birth after correcting for the age of each infant at scan are shown in (A). Statistical images are corrected for multiple comparisons at $P < 0.01$ FDR-corrected (color bar indicates t -statistic). To illustrate this relationship, the Jacobian determinant, representing volume change relative to the reference template, at the site of the maximum t -statistic (red crosshairs; $t = 6.04$), was entered into a multiple linear regression with gestational age at birth and age at scan. The partial regression plot (B) shows the relationship between Jacobian and gestational age at birth.

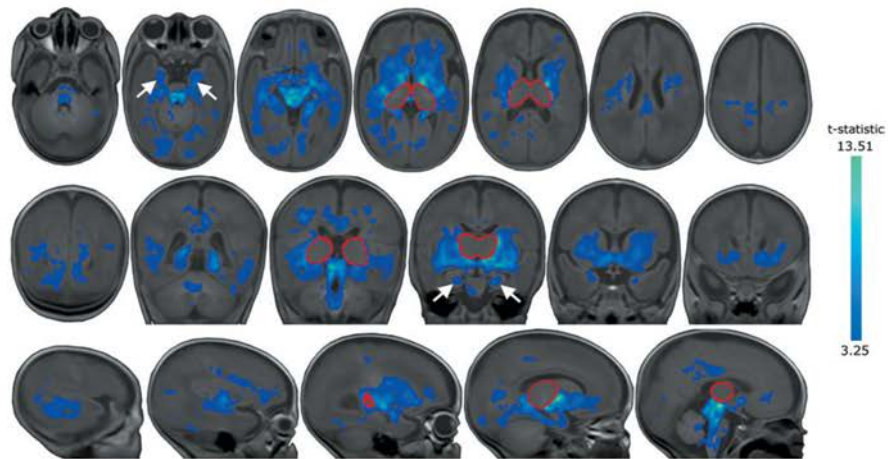


Figure 5. Regional associations between brain tissue volume and thalamic volume at term-equivalent age. Regions where cerebral tissue volume significantly covaried with mean thalamic Jacobian (calculated within the region circled in red). Arrows indicate the hippocampi, statistical images are corrected for multiple comparisons at $P < 0.001$ FDR-corrected (color bar indicates t -statistic).

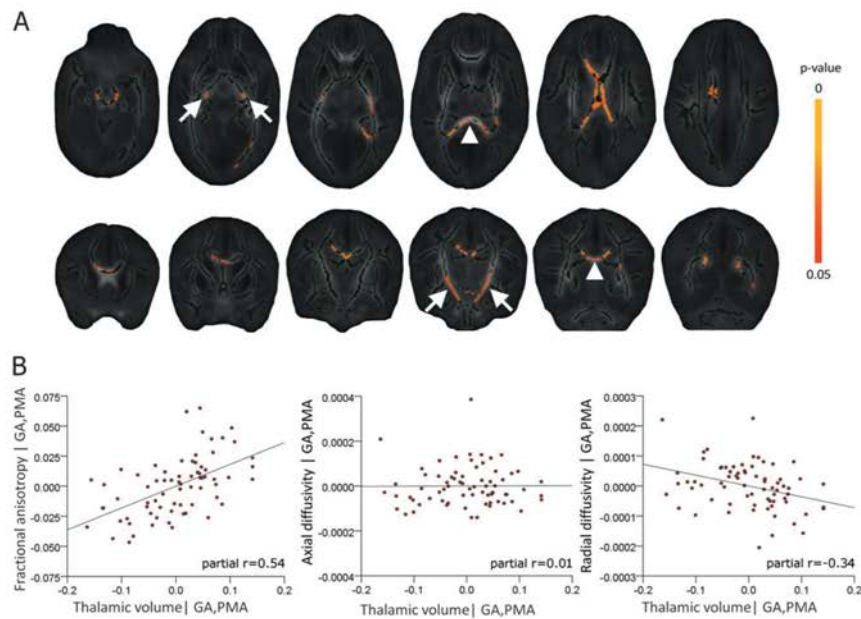


Figure 6. Thalamic volume is associated with white matter microstructure. Regions where fractional anisotropy is significantly associated with thalamic volume, beyond any common association with prematurity at birth and age at imaging, are shown in (A). These regions include the posterior limb of the internal capsule (arrows) and the corpus callosum (arrowheads). Images are FWE-corrected at $P < 0.05$ (color bar indicates P value), the mean FA skeleton is shown in dark green. Partial regression plots of the relationship between thalamic volume and mean FA, axial diffusivity (AD), and radial diffusivity (RD) extracted from each significant voxel identified in (A) and entered into linear regression with gestational age and age at scan are shown in (B).

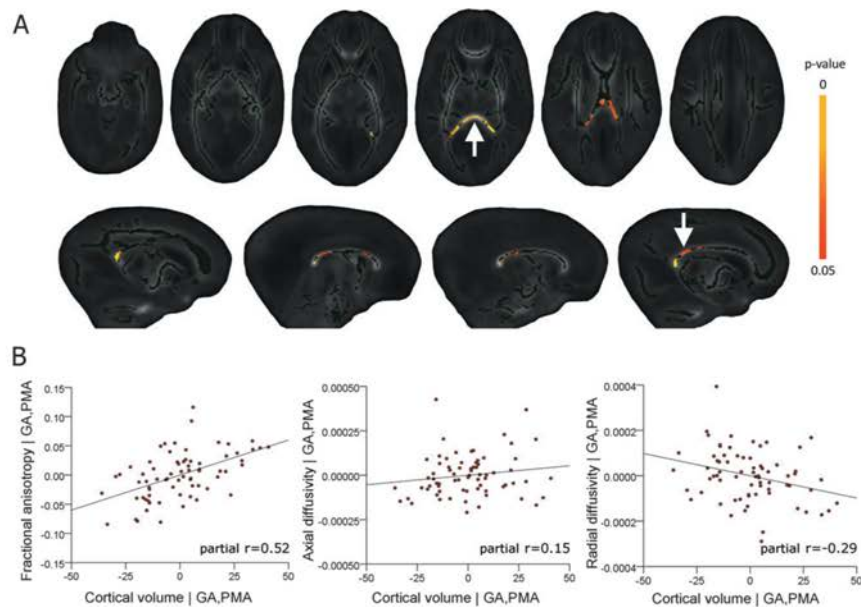


Figure 7. Cortical volume is associated with white matter microstructure. Fractional anisotropy in the posterior corpus callosum (A; arrow, bottom row) including the splenium (A; arrow, top row) is significantly associated with cortical volume, after correction for prematurity at birth and age at imaging. Images are shown as in Figure 6. Cortical volume and mean FA, AD, and RD extracted from each significant voxel identified in (A) were entered into linear regression with gestational age at birth (GA) and age at scan (PMA). Partial regression plots of the relationship between cortical volume and FA, AD and RD, after correction for gestational age and age at scan are shown in (B).

cerebral cortical volume together with abnormal thalamic and white matter microstructure suggests the hypothesis that these observations result at least in part from disrupted development of the thalamocortical system.

Previously, altered brain development at term-equivalent age has been detected in preterm infants (Volpe 2009). Studies using tissue segmentation reported that reduced cortical and deep gray matter volumes correlated to neurodevelopmental

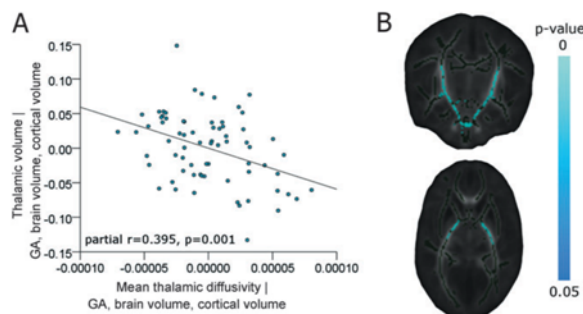


Figure 8. Thalamic diffusivity is associated with thalamic volume and FA in the internal capsule. Thalamic volume (estimated from the mean Jacobian) and mean thalamic diffusivity (estimated from a thalamic mask placed in the DTI reference space) were entered into a multiple linear regression model with gestational age at birth (GA), cortical volume, and total brain volume. The partial regression plot in (A) shows the significant association between thalamic volume and thalamic diffusivity. In (B), regions where FA was significantly associated with thalamic diffusivity are shown (FWE-corrected at $P < 0.05$), beyond any associations with GA, PMA, cortical volume, and CLD status.

disability at 1 year (Inder et al. 2005) and that reduced cortical surface area predicts neurocognitive abilities at 2 and 6 years (Kapellou et al. 2006; Rathbone et al. 2011). Effects on specific brain structures have been reported, including reduced volume of the hippocampi, although it was not clear if this predicted neurological function independently of white matter pathology (Thompson et al. 2008). Thalamic atrophy and microstructural change have been seen in association with white matter damage (Pierson et al. 2007; Nagasunder et al. 2011), and studies using DBM have shown that the thalamus is specifically vulnerable after preterm birth, particularly in association with white matter pathology (Boardman et al. 2006). Furthermore, a pattern of injury that includes thalamic volume loss and microstructural change in white matter is associated with neurodevelopmental outcome in early childhood (Boardman et al. 2010).

The more detailed pattern of structural covariation reported here shows similarity to the neuroanatomical changes seen in ex-preterm adolescents (Nosarti et al. 2002, 2008; Gimenez et al. 2004; Gimenez, Junque, Narberhaus, et al. 2006; Gimenez, Junque, Vendrell, et al. 2006; Martinussen et al. 2009; Nagy et al. 2009) and is consistent with the development of functional connectivity observed by resting state functional MRI (fMRI) during this period (Fransson et al. 2007; Doria et al. 2010; Smyser et al. 2010). This pattern is also compatible with histological evidence from a primate model of preterm birth and neonatal intensive care that found: decreased white matter volume in the temporal, frontal, and parietal lobes with relative sparing of the occipital lobe and tissue loss in the cortex, deep gray matter, and hippocampi (Dieni et al. 2004; Loeliger et al. 2006, 2009). These results support data suggesting that the neuroanatomical basis for the later sequelae of prematurity develop before the time of normal birth (Rathbone et al. 2011) during the period when the thalamocortical system is forming and essential for normal development (Kostovic and Judas 2010).

The hypothesis that disruption of thalamocortical development underlies the observed changes would suggest an intimate relationship between gray matter structures and connective white matter tracts. We observed that thalamic volume was

significantly associated with FA in the internal capsule and the corpus callosum, but subsequent ROI analysis showed that this association only persisted in the internal capsule when cortical volume was also considered. Conversely, cortical volume was only significantly associated with FA in the corpus callosum. Thalamic volume is therefore related to both the microstructure of the thalamic radiations, carrying projection fibers to the cortex, and the volume of the cortex itself. In turn, cortical volume is associated with the microstructure of interhemispheric corticocortical fibers. It is possible that tissue volume in the thalamus and cortex thus reflects thalamocortical connectivity and is dependent on the growth and integrity of connecting white matter tracts.

Reduced thalamocortical volume might also reflect reduced cell and axon numbers in component structures. The number of neurons in topographically connected thalamic and cortical regions is closely related (Stevens 2001) and a large body of histological evidence has determined that both thalamocortical and callosal corticocortical connections are established by term-equivalent age in humans and other primates (Kostovic and Rakic 1984; LaMantia and Rakic 1990; Kostovic and Jovanov-Milosevic 2006). This process can be interrupted by adverse events: cerebral irradiation in mid-to-late pregnancy leads to parallel neuronal loss in the thalamus and cerebral cortex and volume reduction in the subcortical white matter indicating the presence of shared developmental trajectories (Schindler et al. 2002; Selemon et al. 2005, 2009). We found reduced thalamic volume in association with increased mean thalamic diffusivity suggestive of larger extracellular space and compatible with reduced cell density (Beaulieu 2002) and reduced white matter anisotropy with increased radial diffusivity compatible with reduced axon density in associated white matter tracts. Decreased thalamic volume, increased thalamic diffusivity, and increased white matter radial diffusivity are together compatible with decreased cell numbers in the thalamocortical system.

Volpe (2009) argues that brain development in preterm infants is ultimately dependent on a combination of destructive and impaired maturational mechanisms. Here, by removing infants with severe focal lesions such as PVL, we have limited the potential impact of acquired destructive brain lesions on our observations; however, 67% of the cohort had some evidence of DEHSI, thought to reflect diffuse white matter injury possible due to ischemic or hypoxic pathways (Counsell et al. 2003, 2006). Defining normal white matter in the preterm population with conventional MRI is a subjective process; however, by using diffusion metrics such as FA and radial diffusivity (RD), we are able to perform an objective analysis of white matter integrity to capture more fully the spectrum of white matter abnormality present in this population. Additionally, converging evidence suggests that systemic illness in the neonatal period increases the risk of injury and adverse neurodevelopmental outcome (Miller and Ferriero 2009) and we have previously shown in this cohort that CLD is associated with decreased FA and increased RD in the cerebral white matter (Anjari et al. 2009; Ball et al. 2010). Factoring in the presence of CLD status, the pattern of microstructural covariance between the thalamus and the internal capsule and the cortex and corpus callosum remained, although the extent of the associations was reduced. This indicates that numerous injurious processes associated with preterm birth and systemic illness and mediated through inflammatory or excitotoxic

pathways (Arai et al. 1995; Back et al. 2005; Bell et al. 2005; Robinson et al. 2006; Ligam et al. 2009) may potentiate the observed structural and microstructural covariations, possibly with subsequent downstream effects on thalamic volume and development of the overlying cortex (Volpe 2009), resulting in the gestation-dependent pattern of brain development described here. Further investigation during the early neonatal period and longitudinal follow-up of this cohort may help elucidate the nature and evolution of maldevelopment in white matter, deep gray matter, and cerebrum as a whole in this population.

It should be noted that the DBM analyses did not reveal significant associations in the cortex. This was not unexpected: DBM is highly sensitive to local volume change that is spatially consistent across the whole group and thus relies on precise spatial correspondence without reliance on tissue classification and spatial smoothing, however due to the rapid increases in cortical complexity during the neonatal period (Kapellou et al. 2006) and limitations in current image registration techniques for neonates, achieving precise correspondence in cortical regions remains difficult. By combining DBM with cortical segmentations in native image space, we were still able to capture information from the whole brain in this cohort.

In summary, we have shown that at term-equivalent age and in the absence of severe white matter injury, preterm infants show a detailed pattern of altered brain structure and microstructure that mirror changes seen in adolescent ex-preterm infants and are compatible with disruption of thalamocortical development.

Supplementary Material

Supplementary material can be found at: <http://www.cercor.oxfordjournals.org/>

Notes

We are grateful for support from the Imperial College Healthcare Comprehensive Biomedical Research Centre Funding Scheme, the Medical Research Council (UK), the Academy of Medical Sciences, The Health Foundation and Philips Medical Systems for research grant support. We thank the families who took part in the study and our colleagues in the Neonatal Intensive Care Unit at QCCH. *Conflict of Interest*: None declared.

References

- Ajayi-Obe M, Saeed N, Cowan FM, Rutherford MA, Edwards AD. 2000. Reduced development of cerebral cortex in extremely preterm infants. *Lancet*. 356:1162–1163.
- Allendoerfer KL, Shatz CJ. 1994. The subplate, a transient neocortical structure: its role in the development of connections between thalamus and cortex. *Annu Rev Neurosci*. 17:185–218.
- Anjari M, Counsell SJ, Srinivasan L, Allsop JM, Hajnal JV, Rutherford MA, Edwards AD. 2009. The association of lung disease with cerebral white matter abnormalities in preterm infants. *Pediatrics*. 124:268–276.
- Anjari M, Srinivasan L, Allsop JM, Hajnal JV, Rutherford MA, Edwards AD, Counsell SJ. 2007. Diffusion tensor imaging with tract-based spatial statistics reveals local white matter abnormalities in preterm infants. *Neuroimage*. 35:1021–1027.
- Arai Y, Deguchi K, Mizuguchi M, Takashima S. 1995. Expression of beta-amyloid precursor protein in axons of periventricular leukomalacia brains. *Pediatr Neurol*. 13:161–163.
- Ashburner J, Hutton C, Frackowiak R, Johnsrude I, Price C, Friston K. 1998. Identifying global anatomical differences: deformation-based morphometry. *Hum Brain Mapp*. 6:348–357.
- Back SA, Luo NL, Mallinson RA, O'Malley JP, Wallen LD, Frei B, Morrow JD, Petito CK, Roberts CT, Jr, Murdoch GH, et al. 2005. Selective vulnerability of preterm white matter to oxidative damage defined by F2-isoprostanes. *Ann Neurol*. 58:108–120.
- Ball G, Counsell SJ, Anjari M, Merchant N, Arichi T, Doria V, Rutherford MA, Edwards AD, Rueckert D, Boardman JP. 2010. An optimised tract-based spatial statistics protocol for neonates: applications to prematurity and chronic lung disease. *Neuroimage*. 53:94–102.
- Beaulieu C. 2002. The basis of anisotropic water diffusion in the nervous system—a technical review. *NMR Biomed*. 15:435–455.
- Bell JE, Becher JC, Wyatt B, Keeling JW, McIntosh N. 2005. Brain damage and axonal injury in a Scottish cohort of neonatal deaths. *Brain*. 128:1070–1081.
- Boardman JP, Counsell SJ, Rueckert D, Kapellou O, Bhatia KK, Aljabar P, Hajnal J, Allsop JM, Rutherford MA, Edwards AD. 2006. Abnormal deep grey matter development following preterm birth detected using deformation-based morphometry. *Neuroimage*. 32:70–78.
- Boardman JP, Craven C, Valappil S, Counsell SJ, Dyet LE, Rueckert D, Aljabar P, Rutherford MA, Chew AT, Allsop JM, et al. 2010. A common neonatal image phenotype predicts adverse neurodevelopmental outcome in children born preterm. *Neuroimage*. 52:409–414.
- Counsell SJ, Allsop JM, Harrison MC, Larkman DJ, Kennea NL, Kapellou O, Cowan FM, Hajnal JV, Edwards AD, Rutherford MA. 2003. Diffusion-weighted imaging of the brain in preterm infants with focal and diffuse white matter abnormality. *Pediatrics*. 112:1–7.
- Counsell SJ, Shen Y, Boardman JP, Larkman DJ, Kapellou O, Ward P, Allsop JM, Cowan FM, Hajnal JV, Edwards AD, et al. 2006. Axial and radial diffusivity in preterm infants who have diffuse white matter changes on magnetic resonance imaging at term-equivalent age. *Pediatrics*. 117:376–386.
- Delobel-Ayoub M, Arnaud C, White-Koning M, Casper C, Pierrat V, Garel M, Burguet A, Roze JC, Matis J, Picaud JC, et al. 2009. Behavioral problems and cognitive performance at 5 years of age after very preterm birth: the EPIPAGE study. *Pediatrics*. 123:1485–1492.
- Dieni S, Inder T, Yoder B, Briscoe T, Camm E, Egan G, Denton D, Rees S. 2004. The pattern of cerebral injury in a primate model of preterm birth and neonatal intensive care. *J Neuropathol Exp Neurol*. 63:1297–1309.
- Doria V, Beckmann CF, Arichi T, Merchant N, Groppo M, Turkheimer FE, Counsell SJ, Murgasova M, Aljabar P, Nunes RG, et al. 2010. Emergence of resting state networks in the preterm human brain. *Proc Natl Acad Sci U S A*. 107:20015–20020.
- Fransson P, Skjold B, Horsch S, Nordell A, Blennow M, Lagercrantz H, Aden U. 2007. Resting-state networks in the infant brain. *Proc Natl Acad Sci U S A*. 104:15531–15536.
- Gimenez M, Junque C, Narberhaus A, Botet F, Bargallo N, Mercader JM. 2006. Correlations of thalamic reductions with verbal fluency impairment in those born prematurely. *Neuroreport*. 17:463–466.
- Gimenez M, Junque C, Narberhaus A, Caldu X, Salgado-Pineda P, Bargallo N, Segarra D, Botet F. 2004. Hippocampal gray matter reduction associates with memory deficits in adolescents with history of prematurity. *Neuroimage*. 23:869–877.
- Gimenez M, Junque C, Vendrell P, Narberhaus A, Bargallo N, Botet F, Mercader JM. 2006. Abnormal orbitofrontal development due to prematurity. *Neurology*. 67:1818–1822.
- Gousias IS, Hammers A, Heckemann RA, Counsell SJ, Dyet LE, Boardman JP, Edwards AD, Rueckert D. 2010. Atlas selection strategy for automatic segmentation of pediatric brain MRIs into 83 ROIs. In: *Imaging Systems and Techniques (IST)*, 2010 IEEE International Conference on. p. 290–293. doi: 10.1109/IST.2010.5548493.
- Horbar JD, Badger GJ, Carpenter JH, Fanaroff AA, Kilpatrick S, LaCorte M, Phibbs R, Soll RF. Members of the Vermont Oxford Network. 2002. Trends in mortality and morbidity for very low birth weight infants, 1991–1999. *Pediatrics*. 110:143–151.

- Huppi PS, Maier SE, Peled S, Zientara GP, Barnes PD, Jolesz FA, Volpe JJ. 1998. Microstructural development of human newborn cerebral white matter assessed in vivo by diffusion tensor magnetic resonance imaging. *Pediatr Res*. 44:584-590.
- Inder TE, Warfield SK, Wang H, Huppi PS, Volpe JJ. 2005. Abnormal cerebral structure is present at term in premature infants. *Pediatrics*. 115:286-294.
- Kapellou O, Counsell SJ, Kennea N, Dyet L, Saeed N, Stark J, Maalouf E, Duggan P, Ajayi-Obe M, Hajnal J, et al. 2006. Abnormal cortical development after premature birth shown by altered allometric scaling of brain growth. *PLoS Med*. 3:e265.
- Kostovic I, Jovanov-Milosevic N. 2006. The development of cerebral connections during the first 20-45 weeks' gestation. *Semin Fetal Neonatal Med*. 11:415-422.
- Kostovic I, Judas M. 2010. The development of the subplate and thalamocortical connections in the human foetal brain. *Acta Paediatr*. 99:1119-1127.
- Kostovic I, Rakic P. 1984. Development of prestriate visual projections in the monkey and human fetal cerebrum revealed by transient cholinesterase staining. *J Neurosci*. 4:25-42.
- Krishnan ML, Dyet LE, Boardman JP, Kapellou O, Allsop JM, Cowan F, Edwards AD, Rutherford MA, Counsell SJ. 2007. Relationship between white matter apparent diffusion coefficients in preterm infants at term-equivalent age and developmental outcome at 2 years. *Pediatrics*. 120:e604-e609.
- Kuklisova-Murgasova M, Aljabar P, Srinivasan L, Counsell SJ, Doria V, Serag A, Gousias IS, Boardman JP, Rutherford MA, Edwards AD, et al. 2011. A dynamic 4D probabilistic atlas of the developing brain. *Neuroimage*. 54:2750-2763.
- LaMantia AS, Rakic P. 1990. Axon overproduction and elimination in the corpus callosum of the developing rhesus monkey. *J Neurosci*. 10:2156-2175.
- Ligam P, Haynes RL, Folkerth RD, Liu L, Yang M, Volpe JJ, Kinney HC. 2009. Thalamic damage in periventricular leukomalacia: novel pathologic observations relevant to cognitive deficits in survivors of prematurity. *Pediatr Res*. 65:524-529.
- Loeliger M, Inder T, Cain S, Ramesh RC, Camm E, Thomson MA, Coalson J, Rees SM. 2006. Cerebral outcomes in a preterm baboon model of early versus delayed nasal continuous positive airway pressure. *Pediatrics*. 118:1640-1653.
- Loeliger M, Inder TE, Shields A, Dalitz P, Cain S, Yoder B, Rees SM. 2009. High-frequency oscillatory ventilation is not associated with increased risk of neuropathology compared with positive pressure ventilation: a preterm primate model. *Pediatr Res*. 66:545-550.
- Marlow N, Wolke D, Bracewell MA, Samara M. EPIcure Study Group. 2005. Neurologic and developmental disability at six years of age after extremely preterm birth. *N Engl J Med*. 352:9-19.
- Martinussen M, Flanders DW, Fischl B, Busa E, Lohaugen GC, Skranes J, Vangberg TR, Brubakk AM, Haraldseth O, Dale AM. 2009. Segmental brain volumes and cognitive and perceptual correlates in 15-year-old adolescents with low birth weight. *J Pediatr*. 155:848-853.e1.
- Miller SP, Ferriero DM. 2009. From selective vulnerability to connectivity: insights from newborn brain imaging. *Trends Neurosci*. 32:496-505.
- Nagander AC, Kinney HC, Bluml P, Tavaré CJ, Rosser T, Gilles FH, Nelson MD, Panigrahy A. 2011. Abnormal microstructure of the atrophic thalamus in preterm survivors with periventricular leukomalacia. *AJNR Am J Neuroradiol*. 32:185-191.
- Nagy Z, Ashburner J, Andersson J, Jbabdi S, Draganski B, Skare S, Bohm B, Smedler AC, Forsberg H, Lagercrantz H. 2009. Structural correlates of preterm birth in the adolescent brain. *Pediatrics*. 124:e964-e972.
- Nosarti C, Al-Asady MH, Frangou S, Stewart AL, Rifkin L, Murray RM. 2002. Adolescents who were born very preterm have decreased brain volumes. *Brain*. 125:1616-1623.
- Nosarti C, Giouroukou E, Healy E, Rifkin L, Walshe M, Reichenberg A, Chitnis X, Williams SC, Murray RM. 2008. Grey and white matter distribution in very preterm adolescents mediates neurodevelopmental outcome. *Brain*. 131:205-217.
- Pierson CR, Folkerth RD, Billiards SS, Trachtenberg FL, Drinkwater ME, Volpe JJ, Kinney HC. 2007. Gray matter injury associated with periventricular leukomalacia in the premature infant. *Acta Neuropathol*. 114:619-631.
- Rathbone R, Counsell SJ, Kapellou O, Dyet L, Kennea N, Hajnal JV, Allsop JM, Cowan FM, Edwards AD. Forthcoming 2011. Perinatal cortical growth and childhood neurocognitive abilities. *Neurology*.
- Robinson S, Li Q, Dechant A, Cohen ML. 2006. Neonatal loss of gamma-aminobutyric acid pathway expression after human perinatal brain injury. *J Neurosurg*. 104:396-408.
- Rueckert D, Frangi AF, Schnabel JA. 2003. Automatic construction of 3-D statistical deformation models of the brain using nonrigid registration. *IEEE Trans Med Imaging*. 22:1014-1025.
- Rueckert D, Sonoda LI, Hayes C, Hill DL, Leach MO, Hawkes DJ. 1999. Nonrigid registration using free-form deformations: application to breast MR images. *IEEE Trans Med Imaging*. 18:712-721.
- Schindler MK, Wang L, Selemon LD, Goldman-Rakic PS, Rakic P, Csernansky JG. 2002. Abnormalities of thalamic volume and shape detected in fetally irradiated rhesus monkeys with high dimensional brain mapping. *Biol Psychiatry*. 51:827-837.
- Selemon LD, Begovic A, Rakic P. 2009. Selective reduction of neuron number and volume of the mediodorsal nucleus of the thalamus in macaques following irradiation at early gestational ages. *J Comp Neurol*. 515:454-464.
- Selemon LD, Wang L, Nebel MB, Csernansky JG, Goldman-Rakic PS, Rakic P. 2005. Direct and indirect effects of fetal irradiation on cortical gray and white matter volume in the macaque. *Biol Psychiatry*. 57:83-90.
- Short EJ, Klein NK, Lewis BA, Fulton S, Eisengart S, Kercsma C, Baley J, Singer LT. 2003. Cognitive and academic consequences of bronchopulmonary dysplasia and very low birth weight: 8-year-old outcomes. *Pediatrics*. 112:e359.
- Smith SM, Jenkinson M, Johansen-Berg H, Rueckert D, Nichols TE, Mackay CE, Watkins KE, Ciccarelli O, Cader MZ, Matthews PM, et al. 2006. Tract-based spatial statistics: voxelwise analysis of multi-subject diffusion data. *Neuroimage*. 31:1487-1505.
- Smith SM, Jenkinson M, Woolrich MW, Beckmann CF, Behrens TE, Johansen-Berg H, Bannister PR, De Luca M, Drobnjak I, Flitney DE, et al. 2004. Advances in functional and structural MR image analysis and implementation as FSL. *Neuroimage*. 23(Suppl 1):S208-S219.
- Smith SM, Nichols TE. 2009. Threshold-free cluster enhancement: addressing problems of smoothing, threshold dependence and localisation in cluster inference. *Neuroimage*. 44:83-98.
- Smyser CD, Inder TE, Shimony JS, Hill JE, Degnan AJ, Snyder AZ, Neil JJ. 2010. Longitudinal analysis of neural network development in preterm infants. *Cereb Cortex*. 20:2852-2862.
- Srinivasan L, Dutta R, Counsell SJ, Allsop JM, Boardman JP, Rutherford MA, Edwards AD. 2007. Quantification of deep gray matter in preterm infants at term-equivalent age using manual volumetry of 3-Tesla magnetic resonance images. *Pediatrics*. 119:759-765.
- Stevens CF. 2001. An evolutionary scaling law for the primate visual system and its basis in cortical function. *Nature*. 411:193-195.
- Thompson DK, Warfield SK, Carlin JB, Pavlovic M, Wang HX, Bear M, Kean MJ, Doyle LW, Egan GF, Inder TE. 2007. Perinatal risk factors altering regional brain structure in the preterm infant. *Brain*. 130:667-677.
- Thompson DK, Wood SJ, Doyle LW, Warfield SK, Lodygensky GA, Anderson PJ, Egan GF, Inder TE. 2008. Neonate hippocampal volumes: prematurity, perinatal predictors, and 2-year outcome. *Ann Neurol*. 63:642-651.
- Volpe JJ. 2009. Brain injury in premature infants: a complex amalgam of destructive and developmental disturbances. *Lancet Neurol*. 8:110-124.
- Wilson-Costello D, Friedman H, Minich N, Siner B, Taylor G, Schluchter M, Hack M. 2007. Improved neurodevelopmental outcomes for extremely low birth weight infants in 2000-2002. *Pediatrics*. 119:37-45.
- Xue H, Srinivasan L, Jiang S, Rutherford M, Edwards AD, Rueckert D, Hajnal JV. 2007. Automatic segmentation and reconstruction of the cortex from neonatal MRI. *Neuroimage*. 38:461-477.

Appendix E

Automatic Segmentation and Parcellation of Subcortical White and Grey Matter using DTI in the Preterm Neonate

Ball, G., Counsell, S.J., Gousias, I.G., Aljabar, P., Hajnal, J.V., Rueckert, D., Edwards, A.D. & Boardman, J.P.

Proc. Intl. Soc. Mag. Reson. Med. 19 (2011). Montreal, Abstract 2477

Abstract also accepted for presentation at the Pediatric Academic Societies (PAS) meeting, Denver 2011

Automatic segmentation and parcellation of subcortical white and grey matter using DTI in the preterm neonate

G. Ball¹, S. J. Counsell¹, I. S. Gousias¹, P. Aljabar², J. V. Hajnal¹, D. Rueckert², A. D. Edwards^{1,3}, and J. P. Boardman^{1,4}

¹Imperial College London and MRC Clinical Sciences Centre, London, United Kingdom, ²Department of Computing, Imperial College London, London, United Kingdom, ³Division of Neonatology, Imperial College Healthcare NHS Trust, London, United Kingdom, ⁴Simpson Centre for Reproductive Health, Royal Infirmary of Edinburgh, Edinburgh, United Kingdom

Background

Tractography-based segmentation is a method for mapping structural connectivity in the brain¹ that is both highly reliable and corresponds well to cytoarchitectonic atlases². Preterm birth is a leading cause of cognitive impairment in childhood, and is associated with a spectrum of structural brain abnormalities, most commonly characterised by white matter disturbance thought to arise from aberrant thalamo-cortical and cortico-cortical connectivity^{3,4}. Although tractography-based segmentation has revealed disturbances in thalamo-cortical connectivity in preterm infants at 2 years of age⁵ it is not yet feasible to objectively and reliably perform this technique in neonates without a subjective and time-consuming process of manually labelling the cortex. Using a combination of atlas-based parcellation, tissue segmentation and multi-modal imaging, we aimed to implement a fully-automated pipeline for tractography-based segmentation in preterm neonates for objective, noninvasive mapping of connectivity in major subcortical structures.

Methods

43 preterm infants (median gestational age = 28⁺³; range = 23⁺⁴ – 34⁺⁶) underwent 3-Tesla 32-direction DTI acquisition at term-equivalent age. T1-weighted (MP-RAGE) and T2-weighted (FSE with overlapping slices) anatomical images volumes were also obtained for each subject. Cortical segmentation was performed for the T2-weighted images using an expectation-maximisation approach⁶ with age-appropriate tissue priors from a four-dimensional neonatal atlas⁷. Extracted cortices were parcellated by propagating four large, anatomically-defined cortical labels (frontal, parietal, occipital and temporal) from a population-based, neonatal anatomical atlas using non-rigid registration with the individual T1-weighted images as targets^{8,9}. Labelled cortical segmentations were passed into individual DTI space as target masks for tractography (see Fig. 1). In addition the same non-rigid registration method was used to automatically label the whole thalamus and corpus callosum in each subject. Each DTI dataset was processed with FSL¹⁰; streamlines were propagated from the thalamus and corpus callosum seed masks, which were then parcellated into sub-regions according to the maximal connectivity to each cortical area.

Results

Both the thalamus and corpus callosum were successfully parcellated in all subjects. We identified distinct thalamic and callosal subregions that closely mirror those previously observed in adults and older preterm infants^{1,5,11}. Figure 1B shows population maps of both thalamic (left side shown) and callosal subregions after transformation into a common reference space. Across the cohort, a large spatial overlap (indicated by yellow) was seen in the frontal, parietal and temporal subregions of the thalamus and in frontal and parietal subregions of the corpus callosum demonstrating the robust nature of this technique.

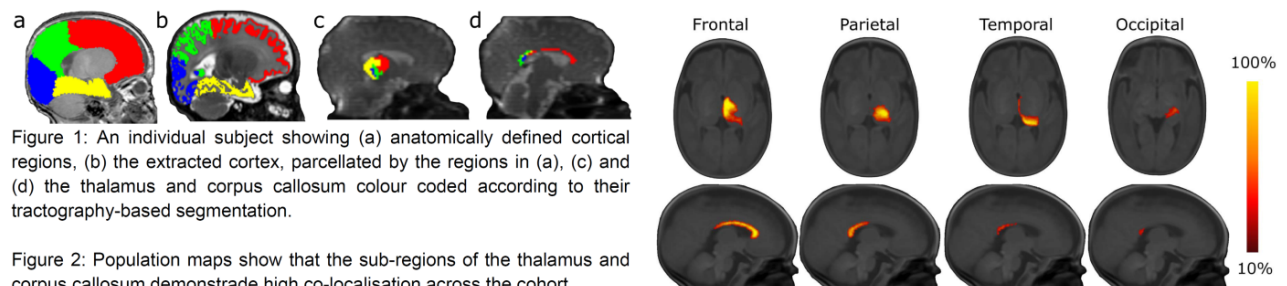


Figure 1: An individual subject showing (a) anatomically defined cortical regions, (b) the extracted cortex, parcellated by the regions in (a), (c) and (d) the thalamus and corpus callosum colour coded according to their tractography-based segmentation.

Figure 2: Population maps show that the sub-regions of the thalamus and corpus callosum demonstrate high co-localisation across the cohort.

Conclusion

We demonstrate, using a multi-modal, fully automated processing pipeline, that tractography-based segmentation provides a reliable, non-invasive tool for mapping structural connectivity in the neonate. We propose that this technique will provide a tool for the future study of brain development in preterm infants to further elucidate the nature of aberrant connectivity thought to underlie the common neurocognitive impairment in this population.

References

1. Behrens, T. *et al. Nat. Neurosci.* **6** 750-757 (2003)
2. Johansen-Berg, H. *et al. Cereb. Cortex* **15** 31-39 (2005)
3. Marlow, N. *et al. N. Engl. J. Med.* **352**, 9-19 (2005)
4. Volpe, J. J. *Lancet Neurol.* **8**, 110-124 (2009)
5. Counsell, S.J. *et al. Neuroimage* **34** 896-904 (2007)
6. Van Leemput, K. *et al. IEEE Trans Med Imaging* **18** 885-896 (1999)
7. Kuklisova-Murgasova, M. *et al. Neuroimage* (2010)
8. Gousias, I.S. *et al. Acta Paed.* **98** 146-147 (2009)
9. Gousias, I.S. *et al. (IST), IEEE* (2010)
10. Smith, S. M. *et al. Neuroimage* **31**, 1487-1505 (2006)
11. Huang, H. *et al. Neuroimage* **26**, 195-205 (2005)